

# **Microfluidic methods for Single Cell analysis in clinically relevant samples**

Ksenia Katsanovskaja

Doctor of Philosophy

Institute of Chemical Biology, Department of Chemistry

Imperial College London

2020



# Abstract

Single cell protein analysis has the potential to comprehensively profile cellular heterogeneity advancing the understanding of cell function, disease progression and drug development. Although it is a possible contributor to the discovery of novel therapy, the protein mapping on the individual cell basis is complex and poses challenges. For example, cancer is a heterogeneous disease which analysis using conventional bulk methods can potentially conceal a dangerous population like Circulating Tumour Cells (CTCs). Analysis of CTCs can only be reliably attained using single cell technologies. The Microfluidic Affinity Capture (MAC) chip is a tool that was developed in our group to study cellular heterogeneity by measuring protein abundance in single cells. Another problem in analysing cancer cells is the difficulty in obtaining samples in a non-invasive manner. This thesis reports on attempts to obtain, concentrate and analyse CTCs from blood using a composite MAC-based device.

The ability to analyse single cells has advantages beyond the potential for analysing heterogeneity. Chronic Obstructive Pulmonary Disease (COPD) is a heterogeneous illness that is characterised by a chronic inflammation. Although the immune response in COPD requires investigation, it is complicated by a lack of biomarkers and methods to non-invasively collect samples. The ability to obtain and effectively analyse precious and scarce biomaterial from lungs, is greatly advantageous for both diagnosis and tracking of COPD. Here, we report on a workflow to achieve this using sputum from negative control volunteers and COPD+ patients.

Also, we describe the establishment of a novel MAC chip assay targeting FOXO3 protein which is involved in regulation of processes like tumour suppression, inflammation and senescence. Therefore, it has a biomarker potential to monitor and study diseases like cancer and COPD. We developed the protocol to analyse Forkhead box 3 (FOXO3) protein expression in nasal cells from healthy donor samples that were retrieved with a non-invasive tool (NASAM, nasal synthetic absorptive matrix). Nasal cavity is a front line of exposure to inhaled pernicious substances and, it is speculated to reflect anomalous bioprocesses in lungs preceding respiratory disease development and progression. This study provides the first-time quantification of FOXO3 protein in single cells from nasal samples. This work shows the analytical capacity of the MAC chip to study cellular heterogeneity and quantify important biomarkers in single cells of clinically relevant material.

# Declaration of originality

All work presented here is my own with the following exceptions:

- MAC chip designs were engineered by Dr Alastair Magness and Dr Ali Salehi-Reyhani
- Different flow regime methods testing for CTCs isolation with microtube was performed in collaboration with Celia Cheung
- Single molecule localization and counting algorithms were written in Fiji software by Dr Alastair Magness
- Active and total FOXO1 MAC assay was established by Dr John Simpson
- The ZSTK474 treatment of Toledo cells was implemented in collaboration with Suhuur Osman
- Sputum samples were collected in collaboration with Prof Peter Barnes' group NHLI, imperial College London

# Declaration of Copyright

The copyright of this thesis rests with the author and is made available under a Creative Commons Attribution Non-Commercial No Derivatives licence. Researchers are free to copy, distribute or transmit the thesis on the condition that they attribute it, that they do not use it for commercial purposes and that they do not alter, transform or build upon it. For any reuse or redistribution, researchers must make clear to others the licence terms of this work

# Acknowledgements

I would like to thank my supervisors, Prof. David Klug and Prof. Keith Willison, for giving me this opportunity to submerge myself into the world of science and research.

Among the challenges I faced during my research, the most difficult one was to say 'Goodbye' to my new friends and colleagues when they finally became doctors or found a job. Surely the pain was slightly alleviated by the post-viva or farewell drunk faces but still it is a truly sad moment. I said 'Goodbye' to many of you my dear friends and now it is my turn to leave this place. I thank you all, soldiers! However, my special thanks go to Dr MaDness, Jimbo, Suhur and Ryan who helped a lot with my writing and not only. Also, I would like to thank animals and donors without whom this research could not be done and to whom this thesis is devoted.

I want to thank my family who asked me on a daily basis what I've been doing in the labs and how many pages I have written. Dad definitely did not miss a day asking one or another of these questions. You are a great support to me, and I miss you very much. Roman, thank you for everything mate. Your cheerful, bald and smooth head shared the most important moments of my life. Man, you are greater than Alexander the Great!

# Table of contents

<b>Abstract</b> .....	<b>3</b>
<b>Declaration of originality</b> .....	<b>4</b>
<b>Declaration of Copyright</b> .....	<b>4</b>
<b>Acknowledgements</b> .....	<b>5</b>
<b>List of abbreviations</b> .....	<b>11</b>
<b>List of Figures</b> .....	<b>13</b>
<b>List of Tables</b> .....	<b>15</b>
<b>Chapter 1. Introduction</b> .....	<b>16</b>
1.1    What is single cell proteomics and why it is important to study? .....	16
1.1.1    Characterisation of cellular heterogeneity .....	18
1.1.1.1    Microfluidic Affinity Capture based chip .....	20
1.1.1.2    Microtube device.....	21
1.2    Chronic Obstructive Pulmonary Disease .....	21
1.3    Thesis overview .....	21
1.4    The introduction to the single cell analysis with the Microfluidic Affinity Capture chip .....	22
1.4.1    The antibodies mechanism of action in microspot assay .....	26
1.4.2    Microarray production .....	30
1.4.3    TIRF imaging.....	32
1.4.4    Image processing .....	33
1.4.4.1    Single molecule counting and image analysis.....	34
1.4.4.2    Image processing workflow and algorithms .....	35
1.4.4.3    Non-congested algorithm .....	35
1.4.4.3.1    Baseline Noise Offset compensation for non-congested data .....	37
1.4.4.3.2    PSF estimation.....	37
1.4.4.3.3    Single molecule fitting and counting.....	38
1.4.4.4    Analysis of congested images .....	39
1.5    Conclusion .....	40
<b>Chapter 2. Microfluidic Methods for Single Cell and Single Molecule Analysis of Circulating Tumour Cells in Blood</b> .....	<b>42</b>
2.1    The aim of the study.....	42
2.2    Metastasis.....	44
2.2.1    Epithelial mesenchymal transition (EMT).....	44
2.2.2    The process of invasion by steps .....	45
2.2.3    Existing methods for CTCs isolation and analysis .....	46
2.2.3.1    Label-free isolation .....	46
2.2.3.2    Positive selection strategy .....	47

2.2.3.3	Negative selection strategy .....	48
2.3	Methods and materials .....	49
2.3.1	Spinning top MAC chip fabrication.....	49
2.3.1.1	Spinning top chip design.....	50
2.3.1.2	Design fabrication.....	50
2.3.1.3	Chip production .....	52
2.3.2	Capture microtubes preparation.....	52
2.3.2.1	White blood cells (WBC)-depletion tube production.....	53
2.3.2.2	Microtubes set-up.....	54
2.3.3	Samples preparation.....	55
2.3.3.1	Polystyrene beads sample .....	55
2.3.3.2	Model cell line samples.....	55
2.3.3.3	Spiked blood samples.....	56
2.3.3.3.1	Blood sample processing.....	56
2.3.3.3.1.1	Isolation of peripheral blood mononuclear cells using Ficoll-Paque™.....	56
2.3.3.3.1.2	Red Blood Cells (RBC) lysis.....	58
2.3.4	The CTCs isolation experimental overview.....	59
2.3.4.1	CTCs capturing and purification.....	59
2.4	Results and discussion.....	60
2.4.1	Method development for MCF7 cell capture from cellular solution.....	60
2.4.2	Isolation of MCF7 cancer cells from model blood samples.....	61
2.4.2.1	WBC-depletion tube introduction .....	63
2.4.2.2	Elution.....	64
2.4.3	Validation of spinning top chip methodology with polystyrene beads .....	67
2.4.3.1	MCF7 cells enrichment on the spinning top chip.....	68
2.4.4	Incorporation of microtubes and spinning chip to isolate MCF7 from model blood samples .....	70
2.4.4.1	Spinning top with debris filter.....	71
2.5	Conclusion .....	73
<b>Chapter 3. A microfluidic capture affinity assay development for FOXO3 protein.....</b>		<b>76</b>
3.1	Why is it important to study FOXO3? .....	76
3.1.1	FOXO transcription factors .....	76
3.1.1.1	Properties of FOXO3 .....	78
3.2	Methods and Materials.....	79
3.2.1	Experimental overviews .....	79
3.2.2	Chip preparation .....	82
3.2.2.1	Design fabrication.....	82
3.2.2.2	Slide preparation .....	82
3.2.2.2.1	Coverslip functionalisation and passivation.....	82

3.2.2.2.2	Slide printing.....	84
3.2.2.2.2.1	Primary antibodies biotinylation.....	85
3.2.2.2.2.2	Microarray production.....	85
3.2.2.3	Aligning and storing.....	86
3.2.3	Devices filling and cell handling .....	87
3.2.3.1	Samples analysed with the Open chip.....	87
3.2.3.2	Samples analysed with the MAC chip .....	89
3.2.3.2.1	Background and standards solutions .....	89
3.2.3.2.2	Cell culturing and handling for analysis.....	89
3.2.3.3	Readout and data acquisition .....	89
3.3	Results and Discussions .....	90
3.3.1	Capturing agents' spots morphology analysis .....	91
3.3.2	Background analysis.....	92
3.3.3	Assays performance comparison using FOXO3 recombinant protein.....	93
3.3.4	Single cell analysis using MAC chip.....	95
3.3.5	Open chip experiments with cellular lysate .....	97
3.3.6	Finding the reason for the failure to develop the FOXO3 assay .....	99
3.3.6.1	Microarrayed agents' composition influence.....	99
3.3.6.2	Effect of capturing agents' dilution in MAC chip platform .....	101
3.3.6.3	Printing buffers comparison.....	102
3.3.6.4	Effect of detection antibody concentration .....	105
3.3.6.5	The effect of immobilised antibody biotinylation on the assay performance .....	106
3.3.7	Calibration curve with CA7/D1 assay .....	107
3.4	Conclusion .....	108
<b>Chapter 4. The MAC assay validation and FOXO3 protein quantification in single cells.....</b>		<b>110</b>
4.1	Aim of the study.....	110
4.2	FOXOs regulation.....	110
4.2.1	Phosphorylation .....	111
4.2.2	Acetylation.....	112
4.2.3	Ubiquitylation .....	112
4.3	Methods and Materials.....	113
4.3.1	Cell culturing and handling.....	113
4.3.2	FOXO modulation with ZSTK474 .....	114
4.3.3	HOECHST staining .....	114
4.3.4	Chemical lysis.....	115
4.3.5	Analysis platforms .....	115
4.4	Results.....	115
4.4.1	Different cell lines analysis with the CA7/D1 .....	115



4.4.2	Drug perturbation experiments with H1975 .....	117
4.4.2.1	Optical lysis efficiency testing .....	119
4.4.2.2	The response uniqueness hypothesis testing .....	120
4.4.3	Chemical lysis methods testing.....	122
4.4.3.1	Incubation time determination for chemical lysis .....	131
4.4.3.2	Optically and chemically derived single cell lysates analysis for FOXO3 expression .....	134
4.4.4	Calibration curve with chemical lysis buffer addition .....	136
4.5	Conclusion .....	137
<b>Chapter 5. Measuring of FOXOs expression in clinical samples.....</b>		<b>140</b>
5.1	The aim of the study.....	140
5.2	Overview of Chronic Obstructive Pulmonary Disease.....	141
5.2.1	Causes of COPD .....	141
5.2.1.1	Host factors .....	142
5.2.1.2	Environmental factors .....	143
5.2.2	Pathology, pathogenesis, pathophysiology of COPD .....	143
5.2.2.1	Pathogenesis.....	143
5.2.2.1.1	Chronic inflammation.....	143
5.2.2.1.2	Oxidative stress .....	144
5.2.2.1.3	Accelerated ageing .....	144
5.2.2.1.4	Protease-antiprotease imbalance .....	145
5.2.2.2	Pathophysiology of COPD.....	145
5.2.2.2.1	Chronic bronchitis.....	145
5.2.2.2.2	Obstructive bronchiolitis .....	146
5.2.2.2.3	Emphysema .....	146
5.2.3	Diagnosis .....	147
5.2.4	Treatment.....	147
5.2.5	Markers.....	147
5.3	Methods for sampling .....	148
5.3.1	Lower respiratory tract sampling .....	148
5.3.1.1	Sputum analysis .....	149
5.3.2	Upper respiratory tract sampling .....	149
5.3.2.1	Nasal sampling.....	150
5.3.2.2	Spontaneous sampling.....	150
5.3.2.3	Nasal lavage .....	150
5.3.2.4	Nasopharyngeal aspiration .....	151
5.3.2.5	Nasal absorption.....	151
5.4	Method and Materials .....	153
5.4.1	Working solution preparation for FOXO1 and FOXO3 assays .....	153

5.4.2	Samples and processing.....	153
5.4.2.1	Sputum sample collection, storing and handling.....	153
5.4.2.2	Nasal sampling.....	154
5.4.2.2.1	Participants recruitment.....	154
5.4.2.2.2	Study Approval .....	155
5.4.2.2.3	Inclusion and Exclusion Criteria .....	155
5.4.2.2.4	Study Design .....	155
5.4.2.2.5	Nasosorption.....	155
5.4.2.2.6	Nasal samples processing .....	156
5.4.3	Analysis platform.....	157
5.4.4	On-chip cell sorting .....	157
5.4.4.1	Cells counting .....	159
5.4.5	Statistical analysis.....	159
5.4.5.1	Linear discriminant analysis .....	159
5.5	Results and Discussion.....	161
5.5.1	Sputum cells analysis.....	161
5.5.1.1	Statistical analysis .....	163
5.5.2	Nasal Samples analysis.....	164
5.5.2.1	Optimisation of the nasal sample protocol .....	165
5.5.2.2	Evaluation of FOXO3 level in epithelial and CD3+ T-cells .....	166
5.5.2.3	Statistical analysis.....	168
5.5.2.4	FOXO3 expression classification by gender.....	170
5.6	Conclusion .....	171
<b>Chapter 6. Conclusion and future work .....</b>		<b>174</b>
6.1	Conclusion .....	174
6.2	Future work.....	176
6.2.1	Strategies for MAC chip analysis improvement .....	176
6.2.2	Alternative ways for CTCs interrogation.....	179
6.2.3	Directions for further COPD research .....	180
6.3	Summary.....	181
<b>References .....</b>		<b>183</b>
<b>Appendix A: Volunteer recruitment.....</b>		<b>195</b>
<b>Appendix B: Consent forms.....</b>		<b>196</b>
<b>Appendix C: Participant information sheet .....</b>		<b>197</b>

# List of abbreviations

Akt	protein kinase B
APTES	(3-Aminopropyl)triethoxysilane
ASMI	Average Single Molecule Intensity analysis
BNO	Baseline Noise Offset
BSA	Bovine Serum Albumin
CA	Capturing Agent
COLD	Cryogenic Optical Localization in Three Dimensions
COPD	Chronic Obstructive Pulmonary Disease
CTC	Circulating Tumour Cells
D	Detection Agent
DMEM	Dulbecco's Modified Eagle's Medium
ELISA	Enzyme Linked Immunosorbent Assay
ELF	Epithelial Lining Fluid
EMCCD	Electron multiplying charged coupled device Epithelial
EMT	Epithelial Mesenchymal Transition
EpCAM	Epithelial-cell adhesion molecules
FACS	fluorescence-activated cell sorting
FBS	Fetal bovine serum
FFC	Fluorescence flow cytometry
FKH	Forkhead domain of FOXO
FLISA	fluorescence-linked immunosorbent assay
FOXO	forkhead box protein O
H1975	lung adenocarcinoma cell line
IGF-1	insulin-like growth factor
IRE	insulin response element
IRS	Insulin receptor substrate
LDA	Linear Discriminant Analysis
LOD	Limit of Detection

MAC	Microfluidic Affinity Capture chip
MCF7	Human breast adenocarcinoma cell line
MDA-MB-231	Epithelial human breast cancer cell line
MLF	Mucosal Lining Fluid
MNC	Mononuclear Cells
NASAM	nasosorption tool
NSCLC	Non-small cell lung carcinoma
PALM	Photoactivated localization microscopy
PBS	Phosphate Buffered Saline
PDMS	Polydimethyl Siloxane
PEG	Polyethylene Glycol
PI3K	Phosphoinositide 3-kinase
PTM	Post-translational modifications
RBC	Red Blood Cells
RIPA	Radio Immuno Precipitation Assay buffer
RPMI	Roswell Park Memorial Institute Medium
SIRT	Sirtuin protein
SMLM	Single Molecule Localisation Microscopy
SSC	saline-sodium citrate buffer
STED	Stimulated emission depletion
STORM	Stochastic optical reconstruction microscopy
TGF- $\beta$	Transforming growth factor beta
TIRF	Total Internal Reflection Fluorescence
TNF	Tumor Necrosis Factor
Toledo	diffuse large cell lymphoma
TRAIL	TNF-related apoptosis-inducing ligand
WBC	White Blood Cells
ZSTK474	pan-class PI3K inhibitor

# List of Figures

Figure 1	The protein expression measured in bulk sample.....	17
Figure 2	A schematic for previous MAC chip design.....	23
Figure 3	A diagram of optical configuration for experimental setup.....	24
Figure 4	The currently exploited MAC chip platform design.....	25
Figure 5	The graphical representation of sorting and selecting the cells of interest.....	25
Figure 6	A schematic of the released analyte binding.....	27
Figure 7	Fractional occupancy of antibody binding site.....	29
Figure 8	Basic steps for microarray production with contact pin printing.....	31
Figure 9	Comparison between epifluorescence and TIRF microscopy.....	33
Figure 10	The three types of images could be obtained from experiments using the MAC chip.....	34
Figure 11	Non-congested images processing and analysis algorithm.....	36
Figure 12	Gaussian approximation of the Airy pattern.....	38
Figure 13	Congested images processing and analysis algorithm.....	40
Figure 14	The mechanism of metastasis.....	45
Figure 15	Trapping of synthetic beads by Guan traps.....	49
Figure 16	Spinning top chip design.....	50
Figure 17	Microfluidic mould production diagram.....	51
Figure 18	The inner surface of the functionalised tube.....	54
Figure 19	Microtubing set-up.....	55
Figure 20	Layers formation with Ficoll-Paque™ density gradient centrifugation.....	58
Figure 21	Average percentage of cell recovery by program.....	61
Figure 22	Captured cells number from spiked blood samples processed by RBC lysis and Ficoll.....	63
Figure 23	Captured cells purity from spiked blood sample by capturing microtubing.....	64
Figure 24	Eluted cells recovery.....	66
Figure 25	The polystyrene beads trapped by the Guan trap.....	68
Figure 26	The trapped MCF7 cells after the flow rate reduction on the spinning top chip.....	69
Figure 27	MCF7 cell clusters occupied the Guan traps on the spinning top chip.....	70
Figure 28	The images of clogged Guan by cells.....	71
Figure 29	The design of the modified spinning top chip.....	73
Figure 30	Schematic representation of FOXO proteins.....	77
Figure 31	Open chip experimental workflow.....	79
Figure 32	MAC chip experiments workflow.....	80
Figure 33	The microarray for Open chip and MAC chip.....	86
Figure 34	The custom-built alignment rig.....	87
Figure 35	Example of the Open chip utilization.....	88
Figure 36	The experimental set-up configuration.....	90
Figure 37	Mean single molecule counts of recovered FOXO3 recombinant protein by CA1-CA5 capturing agents with D1 detection antibody.....	95
Figure 38	FOXO3 level evaluation in MCF7, H1975 and Toledo with CA2/D1 and CA3/D197.....	99
Figure 39	Testing of different assay systems with cellular lysate on Open chip.....	99
Figure 40	The CA4 microspot morphology at different antibody/printing buffer ratios.....	101
Figure 41	H1975 single cell analysis on the MAC chip platform using different CA5 dilutions with D1 antibody.....	102
Figure 42	The comparison of ArrayIt and 3×SSC/1.5M buffers for CA5 and CA8.....	103
Figure 43	The comparison of FOXO3 expression in H1975 cells with CA5 and CA8.....	104

Figure 44 FOXO3 level measuring in H1975 cells with D1 at different concentrations.....	106
Figure 45 Biotinylation effect on CA6 and CA7 performance for single cell analysis .....	107
Figure 46 FOXO3 protein calibration curve for CA7/D1 assay .....	108
Figure 47 The FOXO3 expression measured from single cells of different cell lines.....	116
Figure 48 The H1975 response to the 2 and 15 hrs-long drug treatment.....	118
Figure 49 HOECHST stained H1975 cell pre-lysis and post-lysis.....	120
Figure 50 Active FOXO1 and FOXO3 measured in Toledo single cells upon 2 hrs of treatment with 10 $\mu$ M ZSTK474.....	122
Figure 51 Challenge to couple chemical lysis with the MAC chip.....	124
Figure 52 The FOXO3 signal comparison from optically or chemically lysed H1975 .....	129
Figure 53 The signal comparison between empty and chambers with single H1975 cells....	131
Figure 54 Schematic of the two different lysis approaches .....	133
Figure 55 Comparison of signal kinetics from optically and chemically lysed cells.....	134
Figure 56 The FOXO3 protein signal in different cell lines obtained with optical and chemical lysis .....	135
Figure 57 Comparison of two FOXO3 calibration curves obtained with and without 1 $\times$ RIPA lysis buffer addition. ....	137
Figure 58 Schematic of Nasosorption <sup>TM</sup> FX-i .....	156
Figure 59 The diagram of the sample collection procedure.....	156
Figure 60 Morphology of T cells and epithelial cells from sputum samples.....	158
Figure 61 The signal distribution of two populations for features X1 and X2.....	159
Figure 62 FOXO3 and FOXO1 expression in cells of COPD and healthy donors.....	163
Figure 63 The frame of the main channel with sputum and eluted nasal samples.....	165
Figure 64 The healthy baseline for FOXO3 expression in epithelial and CD3+ T cells sourced from nasal MLF of 7 donors.....	168
Figure 65 The FOXO3 expression in healthy epithelial and T-cells resolved by gender using LDA .....	171
Figure 66 MAC chip experiments to quantify free and bound FOXO3 protein in single cells	178

# List of Tables

Table 1 Tested flow programs for the MCF7 cells trapping .....	61
Table 2 The list of the tested capturing agents to establish the FOXO3 assay .....	84
Table 3 The physical parameters of the microarrayed spots for different capturing agents ....	92
Table 4 The mean background signal with standard deviation for 10 spots of each tested capturing agent (CA1-CA5) with detection agents (D1 and D2) in Open chip experiments .....	93
Table 5 The mean of background and analyte binding signal for CA5 and CA8 using ArrayIt and 3xSSC/1.5M betaine buffers .....	104
Table 6 The exploited reagents for the FOXO1 and FOXO3 assays.....	115
Table 7 The protocols for chemical lysis methods.....	126
Table 8 The methods investigated for the nasal MLF sample processing characterised by the mean cellular count in the main channel .....	165
Table 9 Single molecule mean value of FOXO3 in Epithelial and CD3+ T-cells per sample	168

# Chapter 1. Introduction

## 1.1 What is single cell proteomics and why it is important to study?

A cell discovery in 1665<sup>1</sup> brought to the Cell Theory formulation that was postulated by Schleiden and Schwann with contribution from Remak and Virchow<sup>2</sup>. One of the tenets of the modern cell theory states that “a cell is a fundamental unit of structure and function in organisms”<sup>2</sup>.

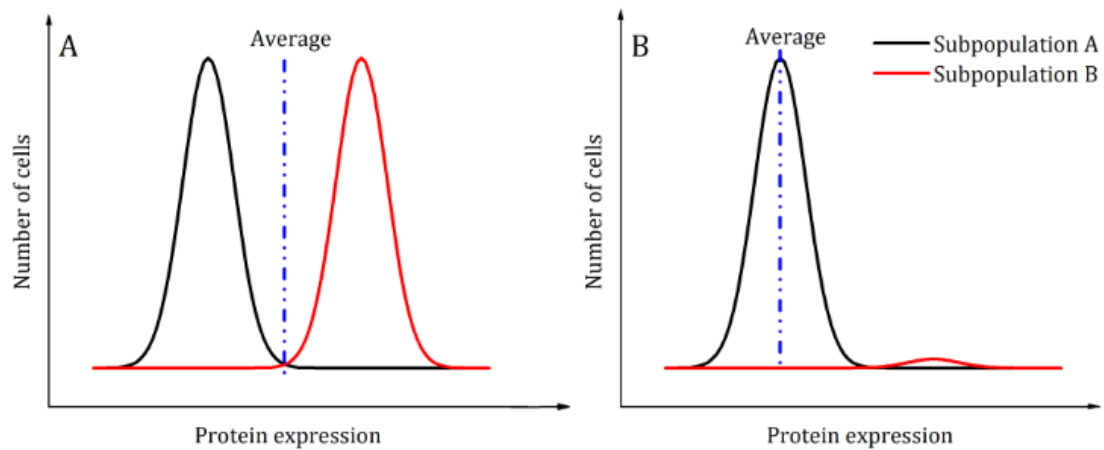
Therefore, the rationale to study a single cell stems from the cell theory itself implying that to understand the biology of multicellular organisms like humans, we must study the underlying single cells and their functions. Human physiology is governed by normal cellular functions and intercellular interactions. However, the mutations in the cells can disrupt these processes<sup>3</sup>. Although cells of the same organism are genetically identical, their phenotypes vary because each cell regulates its own program of gene expression which is stochastic in nature. Phenotypic traits or variations are largely determined by environmental factors which play a central role in evolution and adaptation<sup>4</sup>. Thus, the accumulating evidence suggests that cell-to-cell variability is unlikely arbitrary<sup>5-7</sup>.

Cellular heterogeneity is a ubiquitous feature of biological systems that originates from the stochastic nature of molecular interactions. Elowitz et al defined two types of noise: extrinsic, that is controlled by fluctuations of proteins, and intrinsic, that is characterized by stochasticity of gene expression<sup>8</sup>. Molecular stochasticity or noise induces individual transcription programs that give rise to heterogeneous cellular phenotypes. The phenotypically different cells are subsequently instructed and selected by inter- and intracellular signaling leading to the formation of tissues, organs and organisms. The molecular noise is an essential component of cellular machinery to provide robustness of a biological system in fluctuating environment<sup>7</sup>.

However, cellular heterogeneity may also reflect a pathological mutation that a cell underwent upon exposure to harmful environment. For example, mutations in BRCA1 and BRCA2 genes are accompanied by deficiency of transcription-coupled repair of DNA and a lack of functional proteins that trigger the cell cycle arrest in the G2 phase leading to breast and ovarian cancer development<sup>9</sup>. Additionally, the cellular heterogeneity may result in drug-tolerance of cells that is nearly universal in patients with cancer. Cancer is a heterogeneous disease that is composed of a diverse collection of cells responding to the administered



treatment differently. In almost all cases, cancer gradually develops resistance to the treatment which it was initially responsive to. This occurs because cancer cells dynamically evolve and adapt to the environment causing formation of a phenotypically divergent population that is immune to applied drug and conferred with highly proliferative and invasive signatures<sup>10</sup>. The therapy-unresponsive cells cause the disease recurrence, progression and metastasis. The underlying cause of resistance was related to the genetic instabilities which gave rise to cancer subpopulation capable of evading the effect of the treatment <sup>10</sup>. Therefore, it is essential to study the cancer dynamics comprehensively. However, the conventional bulk population analysis produces an average estimate of the cell-related information masking the cellular heterogeneity and neglecting the cell-to-cell variability in sensitivity to specific treatments, Figure 1A <sup>11</sup>.



**Figure 1** The protein expression measured in bulk sample where A) two distinctive populations are equally represented. The obtained average result fails to reflect the protein level in any of the populations. B) two distinctive populations are not-equally represented. The measured average masks the population of lower abundance. Obtained from <sup>12</sup>

Another advantage of the cellular analysis using individual cells is its suitability to study rare cells like Circulating Tumour Cells (CTCs). CTCs are a rare subset of dangerous cancer cells endowed with migratory and invasive properties that are present in low quantity in liquid biopsies of patients with metastatic cancers. Typically, there is only a handful of CTCs in the bloodstream of ill subjects which is accounted for one to ten CTCs per  $10^8$  mononuclear lymphocytes. In traditional bulk-cell approaches, the average protein expression results are obtained analysing a heterogeneous sample that in addition to CTCs comprise a considerable number of white blood cells (WBCs). The WBCs contamination is often a cause to obscure the

underrepresented and extremely dangerous CTCs in a clinical sample inevitably leading to false-negative result, Figure 1B<sup>13</sup>. While deconvoluting the complex nature of CTCs with bulk-cell analysis was found largely ineffective, single-cell strategies are capable to target cellular heterogeneity of CTCs providing a foundation for liquid biopsy in the clinic<sup>13</sup>. The methods to extract CTCs from liquid biopsy is further described in section 2.2.3.

Clinical samples collected via, for instance, bronchoscopy are only available in small quantities to avoid inflicting damage to a vital organ that organism would be incapable of recovering from. The insufficient sample amount is frequently a limiting factor for the important information extraction using bulk-cell methods. To satisfy a minimal quantity requirement for the sample to be characterised using bulk approaches, the researchers are compelled to deploy sample pre-handling procedures like dilution. Dilution reduces the concentration of screened analytes challenging the detection of those present in low levels. Therefore, there is a need for alternative approaches that are capable to analyse a minute quantity samples like sputum, nasosorption, tissue biopsy. Unlike conventional methods, some of the single cell resolution approaches are relatively sample size insensitive and enable analysis of clinical samples as small as 20  $\mu\text{L}$ .

Additional motivation for single cell analysis is to determine of how many cells you need before the average properties give a sufficiently good representation of the mean or median to be able to use that value in interpretation of data.

The single cell -omics allow analysis of biochemical processes occurring in single cells that emanate from molecular stochasticity or ‘noise’ and can be related to the cellular heterogeneity. Moreover, single cell resolution has become one of the most powerful tools to comprehensively understand and statistically interpret cell-to-cell variability in rare cells and samples with limited quantity.

### **1.1.1 Characterisation of cellular heterogeneity**

The single cell -omics has attracted attention in recent years leading to development of analytical tools including single cell isolation, sequencing assays, flow cytometry and mass spectrometry (MS). Understanding of underlying molecular changes and cell behavior on the individual basis can foster accurate disease diagnosis creating a favourable environment for personalized medicine<sup>11</sup>. Though the methods emerged for single cell gene expression profiling realized the sensitive detection of low-frequency genetic alteration<sup>14</sup>, the technologies to

screen protein level and modifications in a single cell regime have been missing. Protein are, however, accurate indicators of environmental sensing and signaling networks directly reflecting physiological and pathological changes in the organism <sup>15</sup>. Proteins generation in single cells occurs in stochastic bursts <sup>16</sup> which variation in their copy number provide an essential ground for clinical practice and many medical treatment <sup>17</sup>. Thus, single cell proteomics has become a critical and powerful tool to investigate cell biology and heterogeneity.

It is more difficult to access protein information of a single cell due to several technical intricacies <sup>18</sup>: 1) proteins are present in low abundance and encapsulated within a small volume of a single cell <sup>19</sup> 2) proteins are expressed in a wide dynamic range <sup>16</sup> 3) the lack of controllable amplification methods as in nucleic acid analysis for related proteomics counterpart.

Currently, the most widely deployed techniques for the single- cell proteomics are flow cytometry, enzyme-linked immunospot and microfluidic based technologies <sup>20</sup>.

Fluorescence flow cytometry (FFC) or fluorescence-activated cell sorting (FACS) is a widely utilized method for single-cell phenotyping and protein analysis. The technique facilitates a high-throughput screening of 10-17 different proteins simultaneously using fluorescently tagged antibody specific to the target protein. However, the exploitation of multiple fluorescent dyes causes the spectral overlap challenging the protein information retrieval <sup>21</sup>. Furthermore, to monitor intracellular proteins, fixation procedures have to be undertaken prior to the analysis which precludes studying protein-protein interactions, measuring metabolites and monitoring protein activity which require living cell assays. The FACS method also requires a minimum of  $10^4$  cells in suspension which is often infeasible to obtain for many clinical samples <sup>16,21</sup>. Also, the rapid fluid flow in the machine creates mechanical stress to cells deforming and lysing them.

Mass cytometry (CyTOF) is an alternative single-cell protein analysis technology that exploits antibodies labelled with metal isotopes. Unlike fluorescent tags, the metal conjugates have minimal signal overlap which enables a concurrent measurement of 40+ proteins within single cell <sup>20</sup>. However, in addition to large requirement for input material ( $>10^6$  cells) akin to flow cytometry, the considerable loss of a sample has been observed while introducing the specimen into the CyTOF analyser <sup>22</sup>.

Microfluidics, also known as ‘Lab-on-a-chip’, is a rapidly evolving field that resulted in the emergence of numerous different platforms. The microfluidic devices feature designs of miniaturised fluidic channels that allow manipulating and controlling fluids at micron or submicron dimensions. The miniaturisation of a chemical lab has become attractive in single-cell research due to a low requirement for sample and reagents amounts to carry out analysis, the manufacturing of the microfluidic designs is cheap and often in-house performed, the platforms may be customised and integrated to allow cell sorting, optical trapping, lysis and etc. The representative microfluidic-based tools that have been developed to specifically address the cellular heterogeneity at a single-cell proteomics level are microengraving, single-cell western blot, single-cell barcode chips <sup>6,16</sup>.

#### **1.1.1.1 Microfluidic Affinity Capture based chip**

Microfluidic Affinity Capture Chip or MAC chip is a development from our research group that has first been used to probe for p53 protein evaluation in single cells of different human cell lines <sup>23</sup>. The MAC chip exploits an ELISA based immunoassay format that is miniaturised within a nanoliter-scale volume thus, enabling highly sensitive detection of proteins expressed individual cells with a high dynamic range <sup>23,24</sup>. The MAC approach is flexible and can be customised for specific experimental and analytical purposes to enable detection of different proteins or multiple proteins simultaneously. The group has studied various proteins at a single cell level including p53, phosphorylated-p53, FOXO1, FOXO3, c-jun, phosphorylated-c-jun and AP-1. Careful calibration of the MAC platform can often provide access to the absolute quantity of the analysed protein which ensures more accurate understanding of cell-to-cell variability, cell behavior and fate decision taking <sup>24</sup>. The MAC platform can be coupled with various peripheral technologies like optical traps, cavitation wave lysis and surface acoustic wave lysis methods to manipulate, sort and lyse cells on chip <sup>23</sup>.

The MAC platform has already been applied to count proteins in clinical samples. The p53 and phospho-p53 levels were concurrently assessed in single cells from disaggregated tumour samples <sup>24</sup>. Also, the platform allowed discrimination of healthy and COPD+ individuals based on c-jun and FOXOs expression in T- and epithelial cells from lower respiratory tract.

The device has an extremely low minimal requirement for the cell numbers and sample size which is highly satisfactory for working with rare cells and precious samples analyses.

### **1.1.1.2 Microtube device**

Microtube device is a microfluidics-based tool that utilizes functionalised lumen to selectively capture rare cells like CTCs from non-solid biological tissue. Liquid biopsy is a revolutionary technique that offers a non-invasive insight into biochemical processes behind cancer and metastasis progression potentiating personalized medicine development and novel therapy discovery<sup>25</sup>. Although the CTCs isolation and analysis is not an easy task to achieve, the microtube method was demonstrated by King's group to extract circulating tumour cells (CTCs) from patients with metastatic cancer<sup>26,27</sup>. The device facilitates surface customisation to assist in pursuing the research goals<sup>25,27,28</sup>. Due to its high flexibility for surface functionalization, the technology could potentially be effectively employed as a positive and negative selection method to either isolate the target cells or alternatively reduce the level of unwanted cells in a sample. The tool integration with other technologies enables to implement of a downstream analysis of captured cells. The cell recovery from a sample is accomplished with high purity via sample perfusion through the surface-coated tubing at a laminar flow<sup>26,29</sup>. This technique is appealing for clinical studies because of its ability to enrich the underrepresented CTCs from diluted blood samples and buffy coats<sup>25</sup>.

## **1.2 Chronic Obstructive Pulmonary Disease**

Chronic obstructive pulmonary disease or COPD is a complex respiratory condition which embraces a set of diseases that are characterised by chronic inflammation, abnormal immune response, airflow irreversible structural changes and impaired gas exchange<sup>30</sup>. Due to the poor understanding of the illness, the causative factors of the condition development and treatment to completely stop the disease remain largely undiscovered<sup>30</sup>. It is partially because of the reliable biomarkers absence and the lack of non-invasive sampling techniques (that are simple to operate and result in pure samples) that would facilitate a routine monitoring of the COPD development and treatment effectiveness<sup>30</sup>. The COPD topic is further discussed in detail in section 5.2.

## **1.3 Thesis overview**

This research aimed at applying MAC chip technology to characterise cellular variability at a protein copy number level in clinically-relevant or -derived material. The thesis focusing

on cells obtained from upper and lower respiratory tract and circulating tumour cells isolated from the blood samples.

The Chapter 2 is devoted to the attempt to isolate and analyse CTCs from blood samples using a composite set-up that combines functionalised microtubes and MAC-based spinning top chip. The CTC was a subject of scrutiny for many research groups which analysis is hindered by cell-to-cell variability and scarcity of the cells in a highly heterogeneous blood matrix. In this chapter we tried to address the challenges related to the CTCs study to implement protein profiling in a single cell regime.

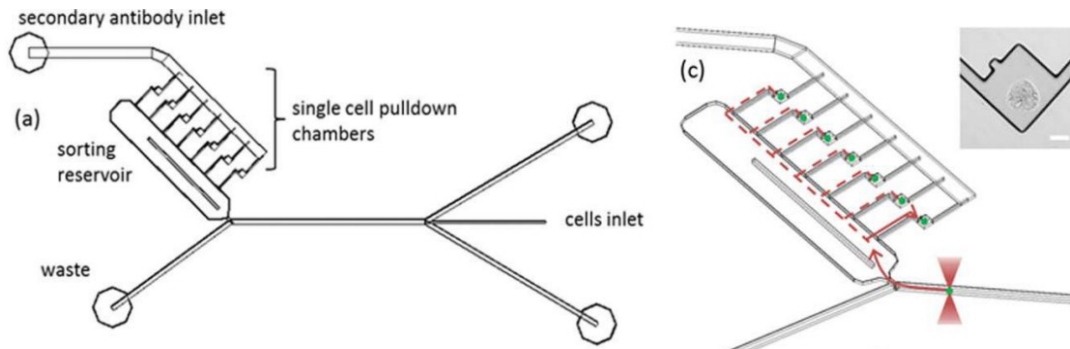
Although there is a lack of reliable biomarkers for COPD characterisation and progression, the FOXO proteins were speculated to be involved in pathological biochemical processes underlying the disease. It has been previously discovered that FOXO3 is a transcription factor that regulates the program of genes activation and inhibition during oxidation, ageing and cells differentiation. Thus, these findings became an overarching motivation for the MAC FOXO3 assay development. The FOXO3 assay incorporation into the MAC platform, its testing, validation and optimisation are described in Chapter 3 and 4.

The COPD is a complex disease which biological mechanisms, despite the endeavours, is yet to be fully understood. The illness is characterized by chronic inflammation and pulmonary function decline which is accompanied with acute immune response and hypersecretion. The expectorated sputum was collected by collaborators in NHLI (Imperial College London) and undergone the FOXO analysis on the MAC chip platform which methods and results are discussed in the Chapter 5. Additionally, this section covers the elaboration of protocol for FOXO3 analysis in non-invasively sourced nasal samples. It was attempted to investigate the potential of nasal sampling as an alternative candidate to sputum for monitoring the COPD progression, diagnosis and treatment.

## **1.4 The introduction to the single cell analysis with the Microfluidic Affinity Capture chip**

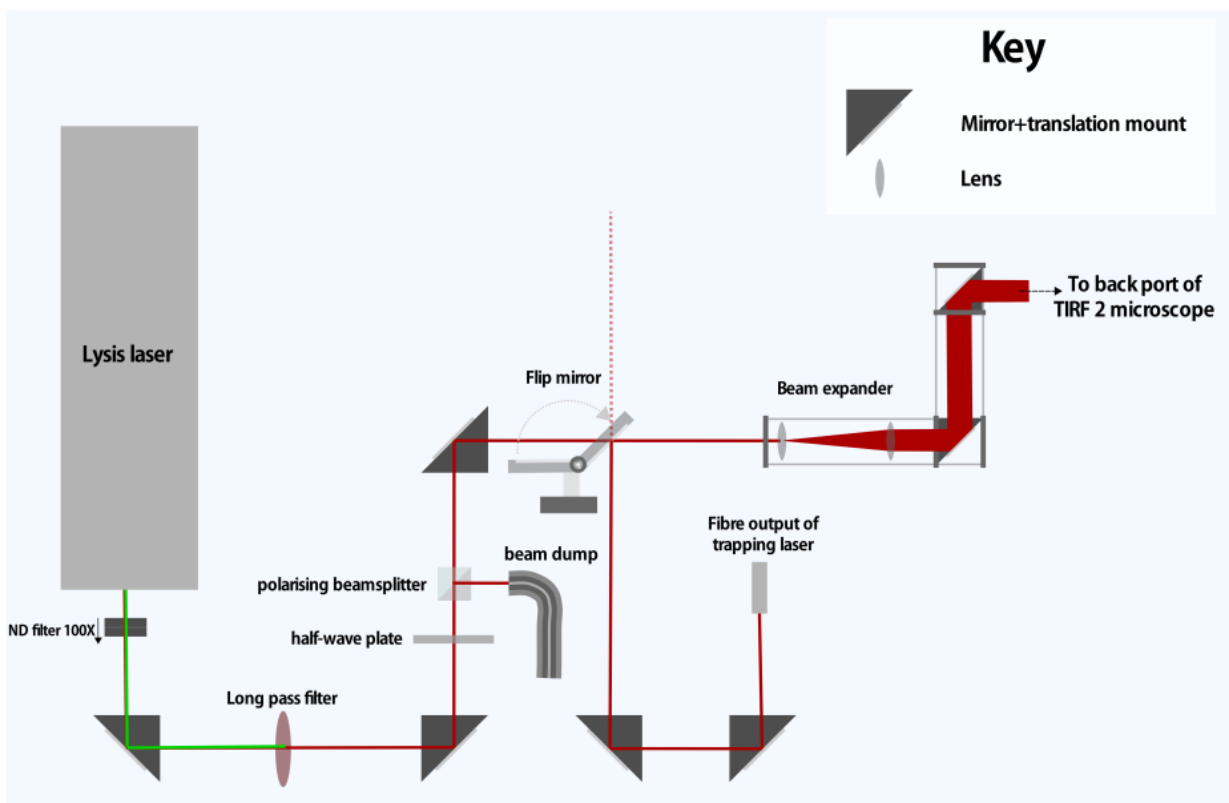
MAC chip or Microfluidic Affinity Capture chip is a single-molecule-sensitive microarray biosensor that enables quantitative assessment of proteins expression at a single cell level in a nanoliter environment. This technology was developed by Klug research group and was first introduced in 2011 by Salehi-Reyhani et al <sup>31,32</sup>. In the early studies, the MAC

platform has been successfully exploited to measure the GFP copy number in genetically modified colon cancer cells and tumour suppressor p53 protein in MDA-MB-438 breast cancer cell line<sup>31</sup>. The schematic of the platform at a time of publication is depicted on Figure 2.



**Figure 2 a) a schematic for previous MAC chip design which consisted of cell inlet, cellular reservoir, analytical chambers, secondary inlet and waste reservoir b) optical trapping of single cells into analytical chambers of the MAC chip. Scale bar =100 μm. Adapted from <sup>31</sup>**

The MAC chip mechanism of action is based on FLISA assay (fluorescence-linked immunosorbent assay) principles that are adapted to a microfluidic environment. The device uses optical tweezers to manipulate cells and laser-induced lysis to release cellular proteins (Figure 3). The bound protein fraction readout is implemented with coupled fluorescent TIRF to directly measure protein content in single cells.

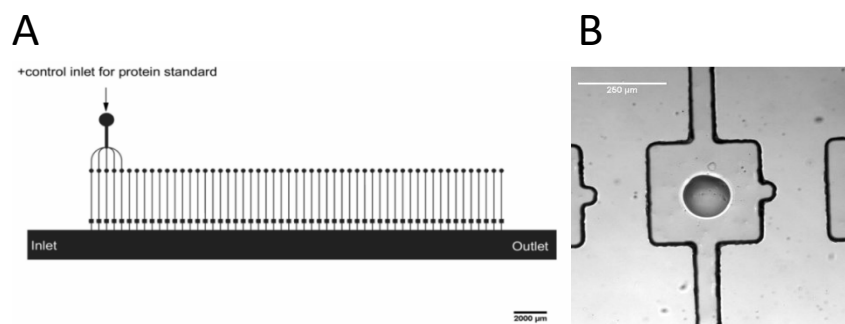


**Figure 3** A diagram of optical configuration for experimental setup which describes coupling of lysis and trapping lasers with TIRF microscope.

Although the working concept remained unaltered, the MAC chip device underwent significant structural modifications since 2011<sup>24</sup>. The structure of the device that was used in the current research is shown in Figure 4.

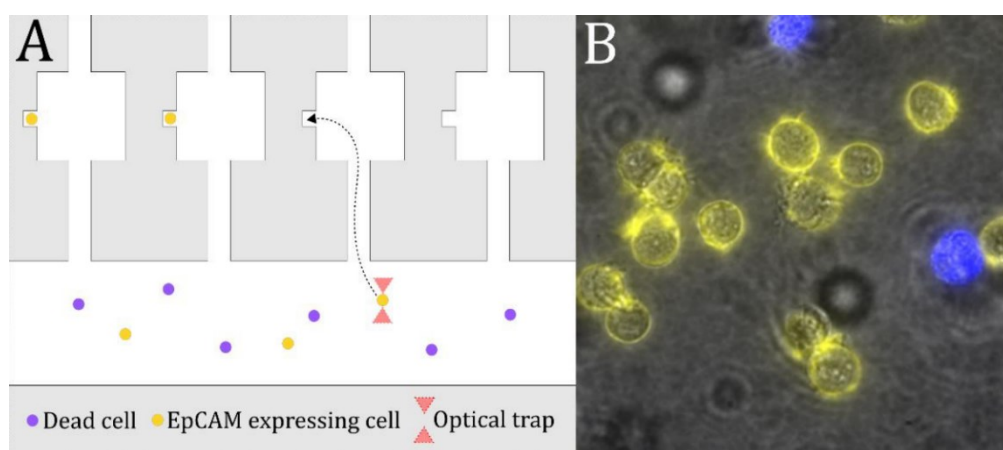
The design of the platform consists of a main channel and 55 perpendicular capillaries leading to individual analysis chambers (300x300  $\mu\text{m}$  or 190x190 $\mu\text{m}$ ). However, only 50 of analysis chambers contain microarrayed immunosorbent spots situated in the center of the compartments and used for single cell analysis. The remaining five chambers are intentionally left spotless to further exploit for flattening the image in the image processing procedure. The inlet and outlet orifices at both ends of the main channel provide sample loading and withdrawal ports, respectively (Figure 4).





**Figure 4 A) The currently exploited MAC chip platform design. Scale bar=2000μm. B) Analysis chamber with microarrayed immunospot. Scale bar=200μm. The image is obtained from <sup>24</sup>**

The unique feature of the MAC chip is its ability to provide a quantitative data on proteins expression in single cells. Thus, Burgin et al has shown that the device could be applied for absolute quantification of p53 protein in BE and MCF7 cancer cell lines<sup>23</sup>. Moreover, the MAC chip has been demonstrated to be an effective platform for clinical sample analysis to address biomedical questions. Magness and Squires et al implemented a simultaneous analysis of p53 and phospho-p53 in single cells from disaggregated colon cancer xenografts <sup>24</sup>. Additionally, the authors elaborated a protocol that enables on-chip analysis and sorting (Figure 5) of live cells from clinical matrix containing considerable amount of biological debris and dead cells <sup>24</sup>.



**Figure 5 A) The graphical representation of sorting and selecting target cells from heterogeneous samples like disaggregated colon cancer on a MAC chip B) Surface marker based cells of the interest selection demonstrated in MCF7 cells: yellow EpCAM+ cells; violet Dead cells. The image was retrieved from <sup>24</sup>**

Also, the research group has contributed to the understanding of chronic obstructive pulmonary disease (COPD) by using the MAC chip for protein analysis in cells from sputum of the healthy and ill individuals. The expression of FOXOs and c-Jun proteins have been measured in epithelial and CD3+ T-cells which levels have been found to differ between individuals with and without the disease. The attempts to analyse the FOXO1 and FOXO3 in sputum samples were also addressed in this work and will be further discussed in Chapter 5.

The MAC chip technology has been developed to address problems that are frequently encountered in the analysis of clinically relevant biomaterial at a single cell level. The advantages of using the MAC chip device for clinical samples are following:

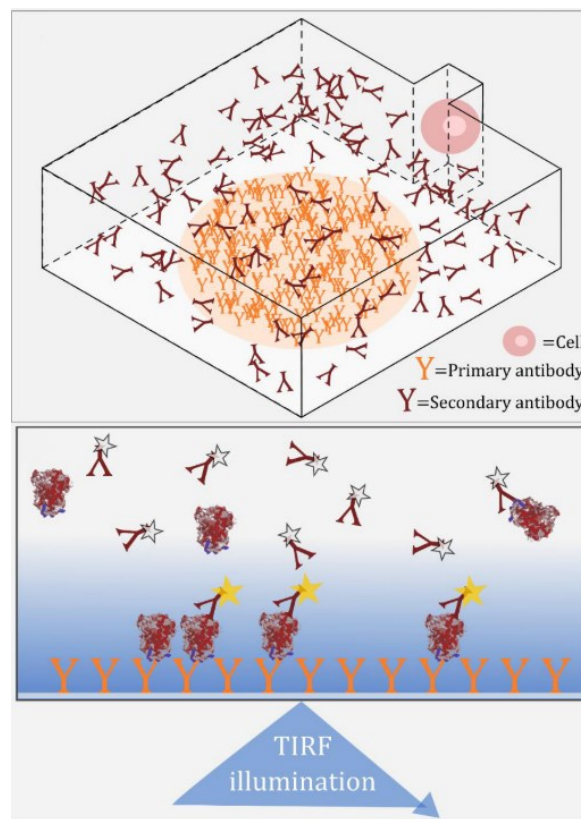
- There is no minimum cell number requirement to perform MAC chip analysis which is, therefore, suitable for analysis of rare cells in clinical material like CTCs.
- The biosensor can be applied for a scarce or precious biomaterial amount that are frequently obtained by less invasive methods like nasosorption
- It enables on-chip sorting and selection of viable and morphologically defined cells or cells expressing specific surface biomarkers.
- There is no need for cell fixation, the cells are viable till the certain point of analysis
- It is a label-free technology because the proteins are not required to be pre-labeled to conduct the analyses
- It enables the retrospective data calibration to quantify an absolute protein copy number in single cells <sup>24</sup>.

These qualities make MAC chip a useful tool for diagnostic and prognostic purposes, treatment efficacy tracking and protein-protein interaction studies.

#### **1.4.1 The antibodies mechanism of action in microspot assay**

The MAC chip is a microarray biosensor which mechanism of action is based on sandwich FLISA (fluorescence-linked immunosorbent assay) principles but in a nanolitre environment. Each analysis chamber of the device contains an immobilised capturing microspot which, upon the single cell lysis, becomes exposed to the mixture of ruptured cell contents and fluorescently labeled detecting agent, Figure 6.

Since the lysis is implemented in the cubicle of the analysis chamber, the distribution of the target analyte immediately after lysis within the volume of the structure is not homogeneous and therefore, the propagation of the released compounds from the ruptured cells through medium is a diffusion driven process that occurs with intrinsic concentration gradient. Protein diffusion in a fluid is a time dependent process where particles' stochastic movement towards the lower gradient is governed by Brownian motion <sup>33</sup>. Whilst in transit, protein epitopes are recognised and sensed by the antibodies present in the solution. Assuming the protein of interest is suspended in the solution it is first recognised and then bound by the detection antibody. Diffusing, the formed complex reaches the immobilised capture agent's range of action entailing a subsequent formation of trimolecular complex or so-called sandwich on the chip's surface. This complex formation requires time to reach thermodynamic equilibrium which duration is in the range of 0.5-3hr depending on the analyte structure, concentration, assay reagents and experimental conditions.



**Figure 6 top: The analysis chamber pre-cellular lysis bottom: A schematic of the released analyte binding by the capturing and detection agents forming a trimolecular complex which signal is subsequently imaged with TIRF. The image adapted from <sup>12</sup>**

The “sensors” binding to the analyte is based on a simple model of the law of mass action. The model assumes that the binding is reversible, and the rate of the reaction is directly proportional to the product concentration. Also, it implies that when the system is in equilibrium the ratio between the concentration of reactants and products is constant <sup>34</sup>.

The sandwich complex formation in the MAC chip can be subdivided into two steps: detection antibody-antigen duplex formation and this complex binding to the primary antibody spot,

*Equation 1 and Equation 2.*



where  $[D]$ ,  $[An]$  and  $[C]$  are the concentrations of detection antibody, analyte and capturing antibody, respectively,  $[DAn]$  and  $[DAnC]$  are the concentrations of detection antibody-analyte and detection-analyte-capturing antibody complexes,  $k_{on}$  and  $k_{off}$  are the rates for forward and backward reactions

At equilibrium the rate of complex formation is equal to the rate of the complex dissociation:

$$k_{on} \times [D] \times [An] \leftrightarrow k_{off} \times [DAn] \quad \text{Equation 3}$$

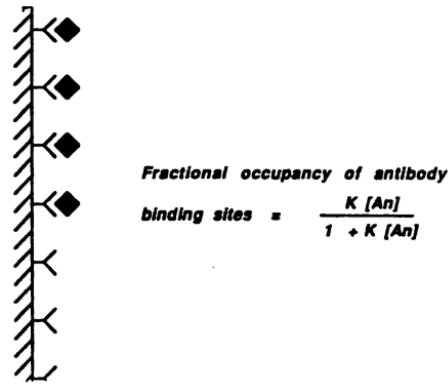
$$k_{on} \times [DAn] \times [C] \leftrightarrow k_{off} \times [DAnC] \quad \text{Equation 4}$$

And therefore, the association constants,  $K_a$  and dissociation constants,  $K_d$  are:

$$K_{a1} = \frac{k_{on1}}{k_{off1}} = \frac{[DAn]}{[D] \times [An]}; K_{d1} = \frac{k_{off1}}{k_{on1}} = \frac{[D] \times [An]}{[DAn]}; \quad \text{Equation 5}$$

$$K_{a2} = \frac{k_{on2}}{k_{off2}} = \frac{[DAnC]}{[DAn] \times [C]}; K_{d2} = \frac{k_{off2}}{k_{on2}} = \frac{[DAn] \times [C]}{[DAnC]}; \quad \text{Equation 6}$$

The analyte tends to occupy only a fraction of the available antibody binding sites at equilibrium (Figure 7) which in conventional immunoassays would lead to a depletion of the analyte in the surrounding environment <sup>35</sup>.



**Figure 7 The immunoassay principle of “antibody binding site occupancy”. Fractional occupancy of antibody binding sites correlates with concentration of analyte that the microspot has been exposed to. [An]=concentration of the analyte and K is a complex association constant. Taken from <sup>36</sup>**

However, microspot immunoassays utilise antibody amounts far smaller than the conventional ones implying that the assay is performed with a number of antibodies so small that it can be confined in a microspot. Since the immobilised molecule number is small, the fraction of analyte bound to the antibody spot results in negligible disturbance of the analyte concentration in the medium, such assays are called ambient analyte regime assay <sup>35,36</sup>.

In the MAC chip experiments, the TIRFM readout of the primary antibody spot reveals the fractional coverage of the receptor by analyte which is dependent on the analyte concentration. The fractional occupancy of the antibody in ambient analyte immunoassays is independent of sample volume and antibody concentration <sup>35-37</sup>. However, it is correlated with the analyte concentration. The analyte adsorption by the antibody can be described using Langmuir adsorption model <sup>38</sup>. The model is based on the following assumptions:

- The analyte is adsorbed in a monolayer
- All sites are equivalent, and the surface is uniform and without defects
- The binding site holds only one analyte molecule
- There is no interaction between adjacent molecules

The fractional coverage  $\theta$  of immobilised antibody by analyte at equilibrium is given by:

$$\theta = \frac{N_{\text{occupied}}}{N_{\text{total}}} \quad \text{Equation 7}$$

where  $N_{\text{occupied}}$  and  $N_{\text{total}}$  are numbers for occupied and total binding sites, respectively.

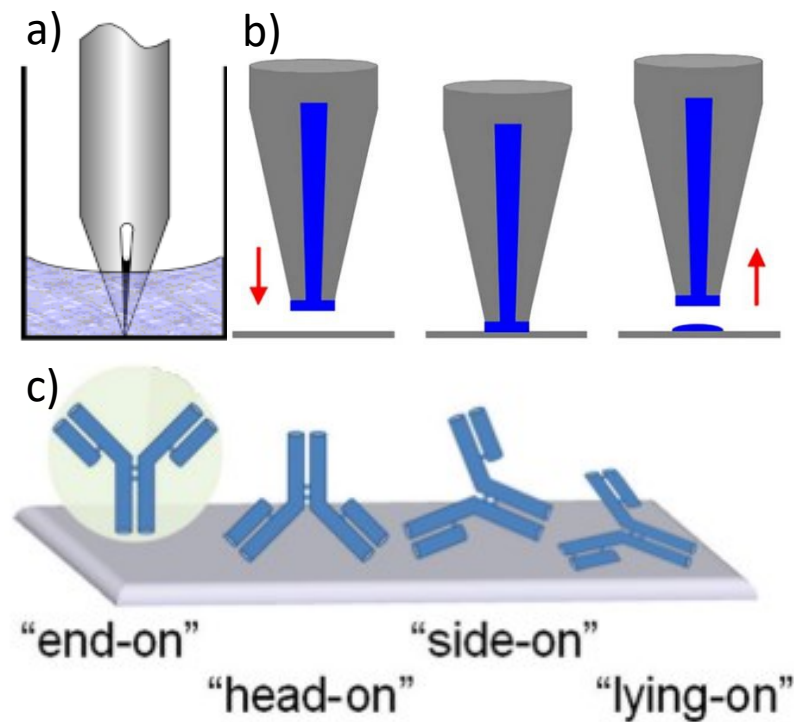
Thus, combining *Equations 5, 6 and 7* gives the fractional occupancy of the microarrayed antibody by detection antibody-analyte complex which directly correlates with the analyte concentration:

$$\theta = \frac{[DAnC]}{[C]} = \frac{K[DA_n]}{1 + K[DA_n]} \quad \text{Equation 8}$$

### 1.4.2 Microarray production

Bio-microarrays have had a marked impact in understanding of bioprocesses in living organisms through the high-throughput measurements of gene expression levels, DNA sequence genotyping, protein expression mapping and pretein-protein-interaction study<sup>39</sup>. Microarrays are 2D arrangements of biomaterials that are delivered to the substrates with specific tools<sup>40</sup>. There are different techniques emerged to the market that enable bio-microspots fabrication for biological research, including genomics, proteomics, and cell analysis<sup>40,41</sup>. The methods are basically categorised as non- and contact printing. The non-contact spot formation techniques include photochemistry-based methods, laser writing, electrospray deposition and inkjet technologies. Although the contact microarraying methods exist in a relatively narrow diversity, they appear to be more preferable microsorbens fabrication techniques due to its advantages<sup>40</sup>.

The contact pin printing and microstamping form arrays by a direct contact between print device and the substrate which result in uniform microspots with high positional accuracy and spot morphological reproducibility. In this research, the microarrays were fabricated using a contact pin printing because this method has a low requirement for printing sample volume and a good control of the transferred sample amount. The printing mechanism of contact pin printing is based on the surface tension and adhesion, Figure 8 a and b.



**Figure 8 Basic steps for microarray production with contact pin printing: a) the pin is plunged into the well and filled with the sample via capillary force, b) the sample is delivered via direct pin contact onto a planar substrate forming a microarray of biomaterial spots. c) The orientation of deposited material, such as antibodies, onto the planar substrate. The images were adapted from<sup>42,43</sup>**

The pin was dipped into a microwell to load the sample by the means of the capillary action. The pin's tip, being covered with a thin layer of a sample, contacted the planar surface leaving a spot behind when the pin travelled upwards and the strong adhesive force of the substrate pulled the droplet off the pin's end. The immobilisation of the deposited biomaterial on the solid support occurs via physical adsorption. Although this method is the simplest way to attach the microarrayed compounds, the orientation of the active binding sites is yet uncontrollable and random. The most favourable position for the microarrayed agent is referred as "end-on", however, various substrate orientations should be assumed during the spotting process such as "head-on", "side-on", "lying-on"<sup>43</sup>, Figure 8 c.

### 1.4.3 TIRF imaging

Total internal reflection fluorescence (TIRF) microscopy is widely used in single molecule spectroscopy and visualisation because it enables observation of states, kinetics and patterns of fluorescently labelled molecules <sup>44,45</sup>.

With TIRF microscopy, the light illuminates fluorophores in the sample medium very close to a refractive surface (<150nm) without exciting fluorescence from regions farther from the surface <sup>45</sup>. The primary advantage of this feature is improved signal-to-noise ratio which is frequently a limiting factor for microarray sensitivity in a single molecule regime. The thin excitation zone, called evanescent wave, decays exponentially in intensity with the distance away from coverslip surface. The evanescent field is an electromagnetic field that occurs when light beam, propagating media of different refractive indices and incident at high angle  $\theta$ , is totally internally reflected rather than refracted. The evanescent field formation and light total internal reflection is observed at and above critical angle  $\theta_c$  <sup>45</sup>.

The critical angle  $\theta_c$  depends on refractive indices of different media and is described by Snell's Law:

$$\theta_c = \sin^{-1}\left(\frac{n_1}{n_2}\right) \quad \text{Equation 9}$$

Where  $\theta_c$  is a critical angle,  $n_1$  and  $n_2$  are refractive indices for different media.

At angles outside the critical angle all the light is reflected; however, some proportion of energy penetrates through the interface forming an evanescent wave that decays exponentially with perpendicular distance from an interface, governed by the following equation:

$$I_z = I_0 e^{-\frac{z}{d}} \quad \text{Equation 10}$$

with  $I_z$  the intensity of evanescent field in the distance of  $z$  from the interface,  $I_0$  is laser intensity at interface,  $d$  is the penetration depth <sup>46</sup>.



For example, epifluorescence allows light to penetrate through the entirety of the sample, whereas the illumination of fluorophores floating in the solution far away from the microspot does not occur in TIRF. Therefore, the TIRF excitation field exponential decay eliminates the noise caused by the excess of fluorophores significantly removed from the interface, Figure 9 <sup>46</sup>.

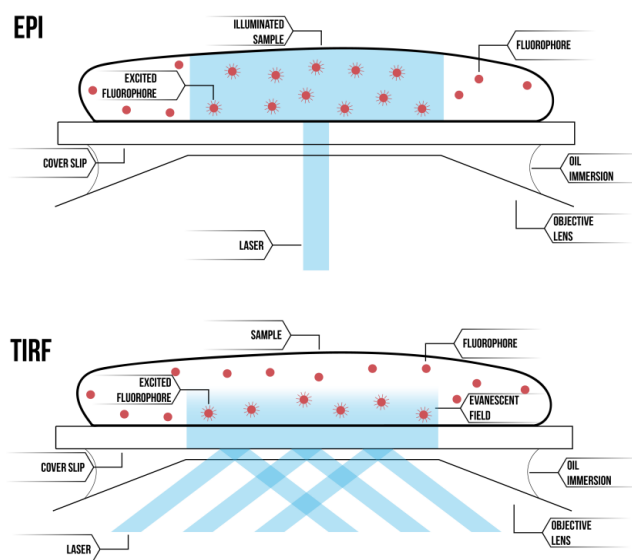


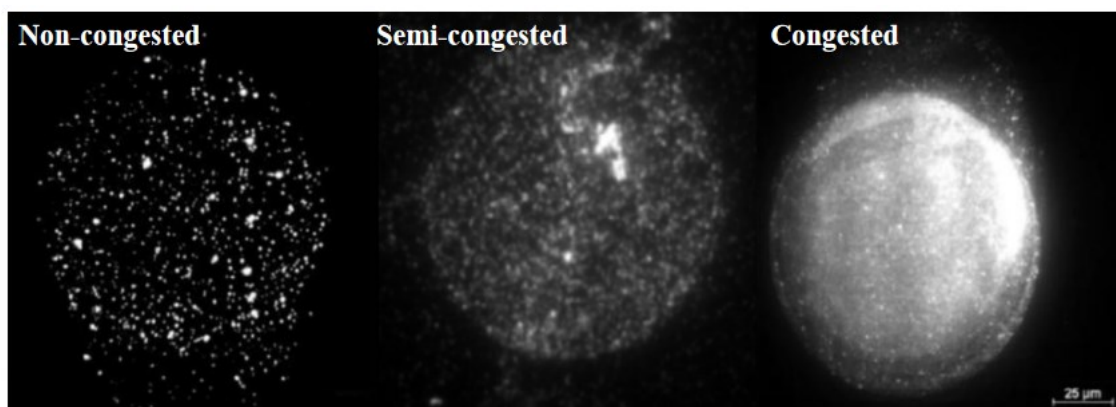
Figure 9 Comparison between epifluorescence (top) and TIRF (bottom) microscopy. The evanescent field formation at and above  $\theta_c$ , the fluorophores excitation in an aqueous environment occurs very close to a solid surface thereby decreasing the background. The image was retrieved from <sup>47</sup>

#### 1.4.4 Image processing

The data acquisition was followed by the image processing and single molecules counting with FIJI/ImageJ software. The macros for image handling, written by the former team member- Dr Alastair Magness, employ Localisation and ASMI algorithms for non-congested, semi-congested and congested data. The following section will describe in detail what type of data the MAC chip assay generates and how to process and analyse it using the above-mentioned codes.

#### 1.4.4.1 Single molecule counting and image analysis

The collected raw data is a stack of 512×512 pixel 16-bit multi-frame images. Prior to the further analysis, the images are categorised into three groups based on the fluorescence density on each frame. The images with densely populated fluorescence, where single fluorophores cannot be separated and identified, are classified as congested images (Figure 10). In contrast, non-congested images allow spatial resolution of fluorescent single molecules until the Rayleigh Criterion (Figure 10). The third group includes images representing somewhat a combination of congested and non-congested images and are called semi-congested images.



**Figure 10** The three types of images could be obtained from experiments using the MAC chip: (left) Non-congested, (center) Semi-congested, (right) Congested images. The depicted raw images of microspots were generated by assaying different concentration of recombinant protein p53 (at  $10^3$ ,  $10^4$  and  $10^8$  molecules/nL, respectively) on a MAC chip. The scale bar =25μm

The techniques to identify single molecule peaks and fit them with 2-dimensional Gaussian are widely used in fluorescent microscopy. These methods are adopted from Single Molecule Localisation Microscopy (SMLM) which is a class of super-resolution microscopy techniques. The most extensively exploited SMLM methods in fluorescence microscopy are PALM, STORM, STED, COLD and etc. In general, the techniques differ in used fluorophores types and the way their emission is modulated to allow temporal separation. Although the mentioned methods are powerful tools for sub-molecular resolution beyond the diffraction limit, these strategies are not feasible to apply for MAC chip assay due to its idiosyncrasies: 1. MAC chip has a wide dynamic range 2. during the experiment the fluorophores are not photobleached and, hence, cannot be temporally resolved 3. our experimental set-up is not

configured for using low temperatures to slow down photochemical reactions 4. our detection agent can be multiply labelled, displaying quite a broad intensity distribution.

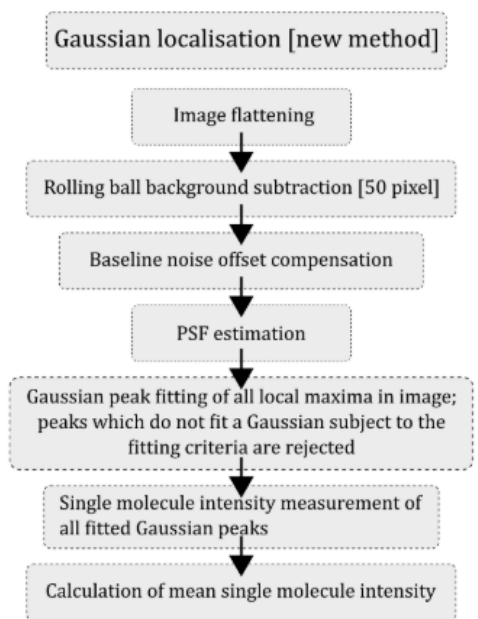
#### **1.4.4.2 Image processing workflow and algorithms**

The MAC chip data is processed and analysed with Fiji/ImageJ using four algorithms: the baseline noise offset calculation and single molecule counting for both congested and non-congested images. The algorithms for image processing are written in ImageJ macro language. In addition to processing the set of images with ImageJ built-in functions, the macros also apply two externally-compiled ImageJ Java plugins to perform Gaussian peak fitting with University of Sussex's GDSC Single Molecule Light Microscopy [SMLM] plugins and to display histograms of single molecules localised in the counting process with the Stowers Institute for Medical Research's plugin 'hist columns jru v1', written by Dr Jay Unruh. The choice of these plugins was determined by several reasons: 1. they run solely on ImageJ 2. the output data is easy to handle as it records the number of single molecule localisations per frame in a tabular format.

The methods to apply for further MAC data processing and analysis depend on the fluorescence density on the frame and hence, subcategorised into non-, semi- and congested images.

#### **1.4.4.3 Non-congested algorithm**

This section outlines the image processing and general work principle of each stage for non-congested images. The Figure 11 describes the main processes of the raw image analysis.



**Figure 11 Non-congested images processing and analysis algorithm involves three pre-processing steps (Image flattening, Rolling ball background compensation and Baseline noise offset compensation) which followed single molecule localization and its intensity measurement (PSF estimation, Gaussian peak fitting and parameters measurement). Taken from <sup>12</sup>**

The MAC raw data requires pre-processing steps before the analysis and therefore, the image handling starts with image flattening, background subtraction and baseline noise offset compensation.

The image frames with sparse fluorescence are flattened to compensate a non-homogeneous spots illumination due to a Gaussian laser intensity profile. This feature implies a weaker laser power at the periphery of the image resulting in apparent brightness deviation of excited fluorophores. The images are normalised for uneven laser intensity profile by dividing the raw image by an image of the laser profile. The laser profile images are obtained from imaging five spotless analysis chambers with blank samples during MAC chip experiment. These images should have low fluorescent signal and be measured from the same experimental run as the data for analysis. The algorithm recreates a close approximation of the laser profile by applying a median intensity projection through a stack of five frames, followed by a Gaussian blur ( $r=50$  pixel), to smooth out discontinuities and finally subtracting the camera bias from the profile (100 analogue-digital units for the Andor iXon 897).

The intensity variation in the image is still observed even after the flattening procedure implementation indicating the presence of additional sources of variation apart from a non-

uniform laser power. The extra fluorescence alteration is mainly caused by laser interaction with the walls of the PDMS structure or defocussed light from intrinsic autofluorescence in either the sample or antibody patch itself. The unwanted spots formed due to the named sources are further removed by a rolling ball background subtraction. The fluorescent objects of the intensity distribution larger than the rolling ball are eliminated from the image. The radius of the ball [50 pixels] was chosen so to effectively subtract the unwanted features whilst keeping true single molecules intact. As single molecule spatial frequency (only a few pixels) is narrower than the ball size, the rolling ball does not affect its relative intensity preserving the necessary information.

#### 1.4.4.3.1 Baseline Noise Offset compensation for non-congested data

The next step in the image pre-processing is a Baseline Noise Offset compensation (BNO). The previously described procedures generate a 32-bit float image. These frames have a considerable number of dark pixels which contain no intensity information of single molecules and their grey value is close to zero but not precisely zero. The presence of which results in single molecule over-counting for the processed image. Therefore, the measures have to be taken to compensate the offset introduced by dark pixels. The baseline noise level or BNO is calculated from the image peripheries of 5 blank analysis chambers and is equal to the average of a sample of non-single molecule pixels. The obtained value is then subtracted from every image compensating the offset.

$$BNO = \frac{1}{i} \sum_i P_i \quad \text{Equation 11}$$

where  $P_i \in \mathbb{D}$  is the brightness of the  $i$ th member of the set  $\mathbb{D}$  of dark pixels.

#### 1.4.4.3.2 PSF estimation

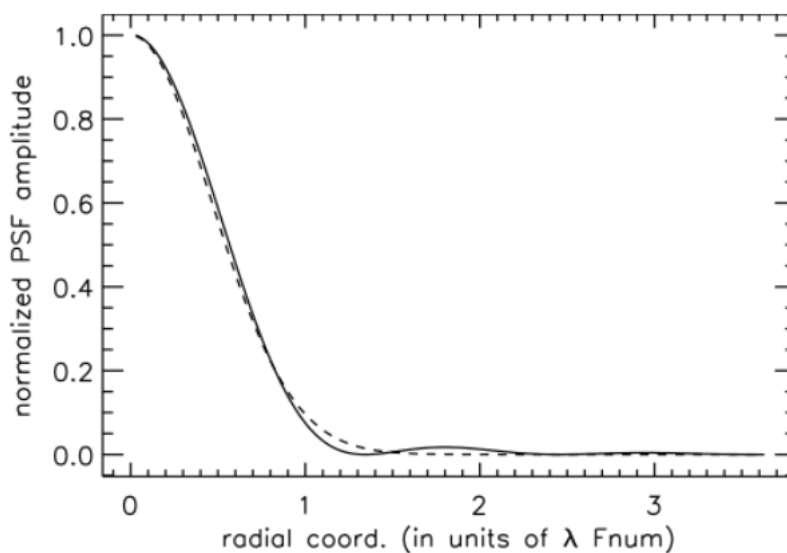
The images emerged from the previous procedures contain the brightness information of single molecules only. The next step is to estimate the point of spread function of the microscope for the single molecules. Essentially this process allows to define a reference point of a true single molecule prior to the single molecule identification and localisation on the data collected with EMCCD camera. In general, single molecules are defined as a diffraction-limited light points which characteristic intensity shape and distribution is governed by Airy

function. Thus, all fluorescent objects on raw images are rejected unless their signal shape of distribution corresponds to the pre-estimated reference.

The true single molecule has a 2D intensity distribution defined by a point of spread function. The Gaussian profile approximates the Airy pattern of the single molecule intensity, Figure 12:

$$I(q) \approx I_0 \exp\left(\frac{-q^2}{2\sigma^2}\right) \quad \text{Equation 12}$$

where  $q$  is a radial distance from central maximum and  $\sigma$  is the RMS width of Gaussian.



**Figure 12 Gaussian (dashed line) approximation of the Airy pattern (solid line). Image taken from Wikimedia Commons**

A 2D Gaussian fitting is performed using the PSF Estimator plugin of the GDSC SMLM toolset. The module estimates the best Gaussian parameters for each peak by randomly selecting  $N$  peaks ( $N=1000$  by default) in the image and fitting the intensity distribution of each peak to least-squares Gaussian function. The calculated average of the Gaussian parameters for all randomly selected spots are then used as starting points for initial true single molecule guess. The fitting iterates until the parameters of the function do not significantly change.

#### **1.4.4.3.3 Single molecule fitting and counting**

The peak candidates are identified implementing non-maximal suppression which follows by their local maxima fitting to 2D Gaussian in descending height order using GDSC

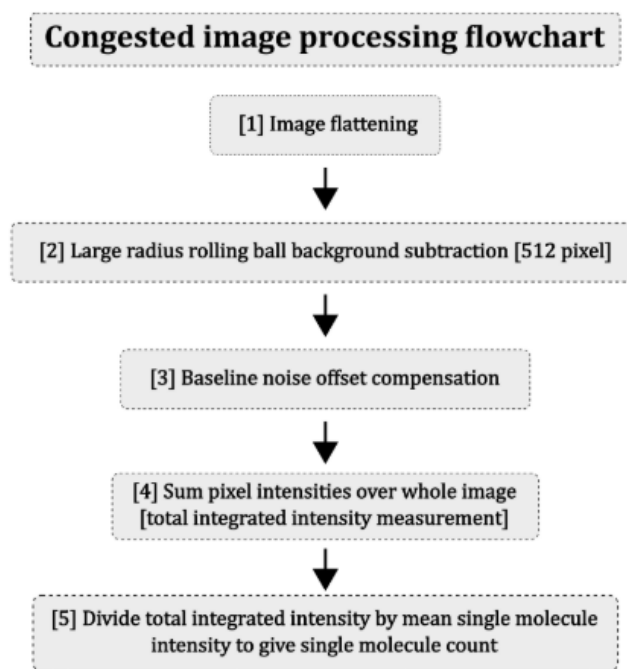
SMLM Peakfit algorithm. To start the molecules identification and fitting, the software users are asked to submit signal and width in the dialogue window. These two parameters control the degree of flexibility in the fit running the macro.

A 2D Gaussian is fitted to peak candidates using a region around the candidate of typically 2 to 5 times the estimated Gaussian standard deviation. This procedure checks the convergence of local intensity maxima to an ideal 2D Gaussian function approximating the point-spread-function of the microscope optics. Image regions which failed to attain convergence were ignored. The total number of single molecules in a given image is then the sum of all intensity maxima where Gaussian peak fitting is successfully performed.

The algorithm prints out the number of identified single molecule and average single molecule intensity per frame in the Fiji Log window.

#### **1.4.4.4 Analysis of congested images**

The analysis of sample containing a high target protein copy number usually results in images with high fluorescence signal, so called congested regime images. The Gaussian peak fitting algorithm is not feasible to apply for such images because of single molecule dense localisation. The Average Single Molecule Intensity analysis [ASMI] was developed specifically for congested images to quantify single molecule content.



**Figure 13 Congested images processing and analysis algorithm involves three pre-processing steps (image flattening, Rolling ball background subtraction and BNO compensation) which followed by estimating the single molecule count using the total intensity measurement and the mean single molecule intensity previously defined in the non-congested frames**

The congested images processing and analysis is depicted in Figure 13. The image flattening and background subtraction steps are performed identically as for non-congested images; the rolling ball subtraction is, nevertheless, implemented using a larger ball size (512 pixels). The baseline noise was found to differ from the one of non-congested images due to the selection of a larger rolling ball size for background subtraction. Although the BNO factor of non-congested regime cannot be used for congested images, the BNO for both is estimated from non-congested images.

After the BNO subtraction process the pixel intensities of the whole image is summed to estimate total integrated intensity which is then divided by mean single molecule intensity to calculate single molecule count. The mean single molecule intensity is obtained from running the set of non-congested images with localisation algorithm.

## 1.5 Conclusion

This chapter discussed the importance and necessity of single cell protein analysis. The single cell analysis allows to identify a subset of cells with distinct features within the isogenic



population that otherwise would be unnoticed using conventional bulk methods. It could be applied to understand molecular noise within and across cellular populations. The study of cellular heterogeneity can only be implemented on a single cell regime. Different technological advancements emerged to address cell-to-cell variation mapping proteins in single cells. The MAC chip is one of the platforms that was developed in our group to perform a single cell protein analysis.

Additionally, this chapter introduced the MAC chip technology as the platform to analyse protein copy number counting in single cells. Many studies successfully employing the microfluidic device to address different biological problems have been shown to be an effective tool for various biomarker evaluation in individual cells<sup>24,48-50</sup>. In addition to the engineering and construction of the device, there was discussed the theoretical aspects underpinning the MAC chip operating principles which explicitly explained the capability of the device in working at single-molecule resolution. Since the MAC chip analysis relies on multiple peripheral technologies, the most essential of them were introduced and described in this chapter. Also, the process of data acquisition, its processing and analysis introduced the distinct methods to extract quantitative information on the protein content from single cells depending on the type of obtained data.

# Chapter 2. Microfluidic Methods for Single Cell and Single Molecule Analysis of Circulating Tumour Cells in Blood

## 2.1 The aim of the study

Circulating tumour cells or CTCs are malignant tumour cells that can disseminate from the primary cancer site via entering and circulating in vasculatory system through which they subsequently infiltrate into a distant organ to form a secondary neoplasm<sup>51</sup>. This process is called metastasis and it frequently leads to fatal consequences<sup>52</sup>. Secondary tumour development accounts for approximately 90% of deaths and therefore it is vitally important to study CTCs<sup>51</sup>. The presence of CTCs is not ascribed to certain stages of cancer, rather they have been detected in the blood of patients with all different stages of disease progression<sup>52</sup>. Although the CTCs are in general associated with poor disease prognosis and CTCs levels in the circulating system have been shown to correlate with the clinical outcome, not all of them can metastasise, forming a secondary cancer<sup>53</sup>. Those, however, that successfully adapted and proliferated in a secondary organ, have often been found resistant to systemic anticancer therapies<sup>54</sup>. Additionally, some studies of cancer metastases revealed disease recurrence and decrease in survival rates of patients with persistent CTCs after undergoing surgery<sup>55</sup>. CTCs are believed to embrace the properties of whole tumour mass representing static and migratory cancer and thus, these cells may act as a useful multifunctional biomarker that can be utilised for disease diagnosis, prognosis and recurrence likelihood determination<sup>56</sup>. Also, CTCs obtained from a liquid biopsy which is less invasive and easier to extract than tissue biopsies of solid tumours<sup>52</sup>. CTC cells have also been found attractive for new therapy development and drug screening<sup>57-59</sup>.

Despite the potential that the analysis of CTCs might have, the cells are still poorly studied offering a relatively scarce information on the underlying mechanisms of cancer spread, human immune system circumvention and resistance to therapeutic agents. The lack of understanding stems partially from the low number of CTCs in the bloodstream<sup>55</sup>. The CTCs are rare in blood of individuals with metastatic cancer which ranges between one to few thousands per  $10^8$  haematologic cells<sup>60</sup>. Besides the extreme rarity, the analysis and CTCs

isolation is further complicated by extensive genetic variability, protein mutations, and abnormal expression of mRNAs and proteins <sup>61</sup>.

Many techniques have emerged to isolate and analyse CTCs, since Dr Thomas Ashworth first noticed CTCs in blood during postmortem examination of the patient and proposed the idea of the presence of cancer cells in the bloodstream as a fundamental prerequisite for metastasis development <sup>62</sup>. New technological advancements have allowed insight into some aspects of circulating tumour cell biology. For example, the widely employed CellSearch™ (Veridex, Janssen Diagnostics, USA) was approved by the FDA for CTCs isolation and enumeration in patients with breast, ovarian and prostate cancers <sup>52,55,56</sup>. However, there are concerns that CellSearch™ method is unable to recover dangerous subset of the stem—like CTCs. Partly, this problem stems from absence of universal definition of how to identify a CTC as opposed to a circulating epithelial cell or other cell type. Therefore, numerous novel techniques and approaches have been developed in recent years to study these cells. Regardless of the new technologies in the field of CTC, understanding of metastasis is still not comprehensive due to the many technical challenges and limitations. Rare cell analysis requires highly sensitive and specific methods for high purity yields <sup>60</sup>. Although the MAC-based chips are suitable for sensitive interrogation of CTCs, there is a need to develop a bridging technology for the cell isolation steps. This chapter describes an attempt to develop two separate but connected platforms for isolation and analysis of CTCs: 1) the in-house functionalised surface microtubing for cancer cell capture and 2) spinning top chip to conduct further CTCs enrichment and protein analysis in MAC chambers.

The analysis of single cells on the MAC platform has specific constraints. Firstly, the sample purity should be high enough to implement analysis of the target cell and avoid blood residuals and unwanted cells to affect the signal. Additionally, the high isolation recovery and specificity is important for rare cells like CTCs. Platforms such as CellSearch use fixed dead cells but the MAC assay is performed on viable cells. The isolation should be fast to prevent the target cells to enter apoptosis. Also, the sample should be not extremely dilute because the low cell concentration was found impractical to work with on a MAC platform.

The elaboration of isolating and concentrating methods is an important pre-step for the analysis of cancer cells at the single cell level. In this study we attempted to build a platform

to isolate rare cancer cells from liquid biopsies and study CTCs variability by employing a downstream protein analysis in the single cell regime.

## **2.2 Metastasis**

Cancer tends to spread throughout the whole body by invading secondary organs or tissues, gradually destabilising the organism and leading to death<sup>63</sup>. This process is known as metastasis. Most malignant neoplasms have a metastatic potential even in early stage of disease progression<sup>53</sup>. To metastasise, the adherent epithelial cells of primary solid tumour become motile, intravasate the circulating system and propagate throughout the organism<sup>51,64</sup>. There are several mechanisms for dissemination of cancer cells in the body which might occur through the epithelial to mesenchymal transition (EMT) or non-EMT pathways<sup>65</sup>. It has been determined that the considerable portion of disseminated single “seeds” is formed on the front tumour interface where the cells extrusion is stimulated by exerted pressure of rapidly expanding parental tumour<sup>53,66</sup>. Cells that gained the migratory features via a non-EMT cycle, maintain epithelial-like morphology, while EMT-conversion confers cells mesenchymal phenotype<sup>66,67</sup>.

### **2.2.1 Epithelial mesenchymal transition (EMT)**

Carcinomas account for the most cases among all cancer types. Carcinomas develop from mutated epithelial cells that possess abnormal proliferative properties. Some epithelial cancer cells are subjected to the epithelial-mesenchymal-transition or EMT prior to metastasis. The EMT process harnesses the pathogenic epithelial cells modifications whereby cells gain reversible phenotypic modifications and migratory features. To become motile, a cell loses polarity and ability for intracellular adhesion which in turn enhances migratory capacity and invasiveness<sup>65-67</sup>. The cancer cells with a stem-like profile were reported to have elevated resistance to apoptosis and drug therapy<sup>52</sup>. The TGF- $\beta$ , an EMT initiator, is released by platelets when they reach a site of lesion being recruited from blood vessels. Along with TGF- $\beta$ , the platelets release growth factors and cytokines that stimulate cancer to metastasise. Additionally, the EMT promoting transcription factors can modulate directly or non-directly E-cadherin repression. The loss of the E-cadherin adhesion molecule, causes upregulation of N-cadherins, fibronectin, and Snail markers in the cells with mesenchymal morphology<sup>67</sup>. Fischer et al. has established, using a mesenchymal-specific fluorescent marker, that only a small amount of invasive cells undergo EMT in lung metastasis but these cells are more aggressive, apoptosis tolerant and chemoresistant.<sup>65</sup>

## 2.2.2 The process of invasion by steps

The process of metastasis is depicted in Figure 14. In short, tumour cells, endowed with a migratory ability, enter the circulatory blood system via the lymphatic system or neovasculature. Those cells, which enter the fluid circulating system, are called circulating tumour cells or CTCs<sup>52</sup>. In 1920s, James Ewing proposed a theory which attributed the CTCs' circulating pattern to the mechanical factors of the vasculature anatomic structure. The cancer cells are carried by bloodstream to the organs' capillary beds where they are restricted by size<sup>63,68</sup>. The retained CTCs subsequently extravasate from the vessel and "seed" the tissue. The "seed and soil" theory had been first described by Stephen Paget to offer insight into the metastasis mechanisms. According to his hypothesis, the feasibility of secondary lesion formation for circulating tumour cells or "seeds" is determined by the secondary tissue or "soil" microenvironment<sup>68,69</sup>. The "seed" and "soil" compatibility proposal has been additionally supported with experimental observation of Cameron et al. where 87% of injected cancer cells were arrested in the liver but only a handful were able to proliferate generating a micrometastasis<sup>70</sup>. This phenomenon explicitly indicates the biological heterogeneity of cancer cells and highlights the importance of cancer analysis at a single cell level.

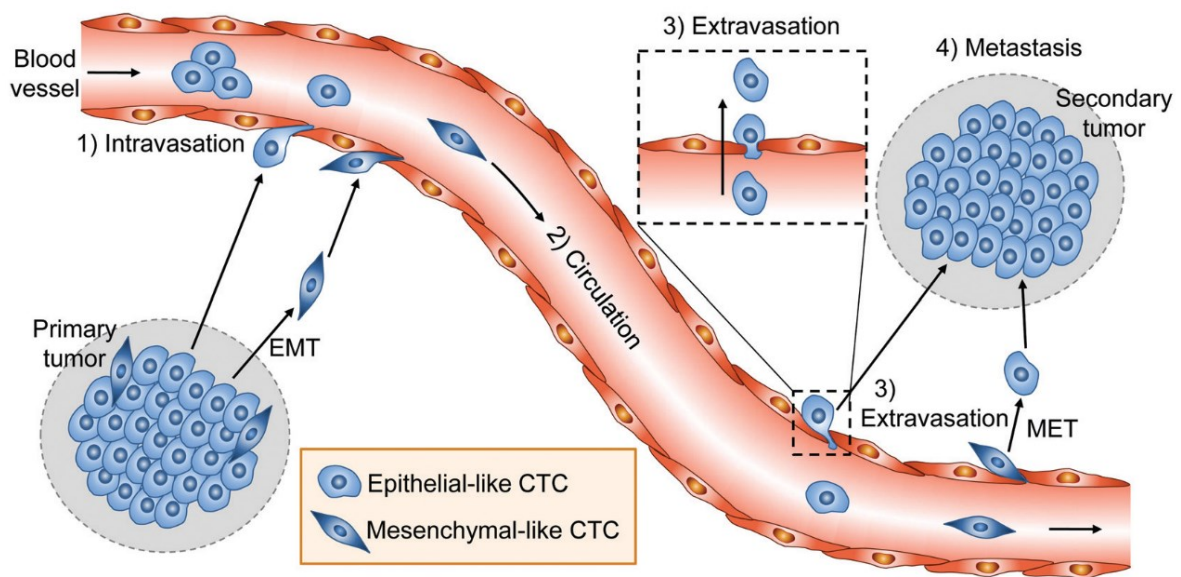


Figure 14 The mechanism of metastasis 1) epithelial phenotype retaining cancer cells and cells undergone the EMT process detach from the solid primary tumour and enter the blood circulating system 2) cancer cells circulate in the system 3) extravasate from the vasculatory system forming a secondary cancer 4) the mesenchymal-like cells transformed into epithelial cells through the EMT- reverse process and form a secondary cancer. The image adapted from<sup>71</sup>

However, CTCs can be used as prognostic and diagnostic indicators<sup>51</sup>. Generally, the presence of CTCs in patients' liquid biopsies is associated with unfavourable clinical outcome<sup>72</sup>. Thus, the quantification and analysis of CTCs in blood is an important objective (to predict the illness prognosis and evaluate the effectiveness of the treatment) but nevertheless, challenging to achieve due to an extremely small number of cells (1-100 cells/mL of whole blood) and cellular heterogeneity<sup>73</sup>. Additionally, the CTCs were characterised as highly heterogenic due to variety of modifications on genetic and protein levels<sup>74,75</sup>.

### **2.2.3 Existing methods for CTCs isolation and analysis**

Numerous endeavours were undertaken to capture and scrutinise CTCs to shed some light upon the mechanisms of cancer spread; however, little is still known about the behavior of CTCs. Thus, the CTCs isolation and enumeration from peripheral blood samples is a persistent conundrum that needs to be unraveled. To address this problem, scientists have reported hundreds of methods for efficient CTCs detection which is beyond the scope of this thesis to provide a review of all of them individually. However, the most common isolation strategies can be subdivided into four categories: label-free isolation, positive selection, negative selection strategy and combination of these strategies<sup>52</sup>.

#### **2.2.3.1 Label-free isolation**

The label-free approach exploits physical properties of CTCs to separate them from matrix. For instance, the isolation by distinct size and density is applied in gravity and density gradients, microfluidic technology and microfiltration. This process allows the isolated cells to undergo subsequent molecular analysis since the separation is implemented without exposure to chemicals. However, such methods may still inflict unwanted cellular damage and deformation. Although it is still a matter of debate, cancer cells are generally accepted to be larger than most but not all the haematological cells, but this feature may lead to false-positive results. Also, the mesenchymal CTCs, possessing a stem cell-like phenotype, were shown to be smaller in size. Thus, it is infeasible to capture mesenchymal CTC cells by restricting the isolation process to large cancer cells only. This strategy has been, nevertheless, employed in developments like Ficoll™, OncoQuick®, MetaCell®<sup>61,73,76</sup> which principle of isolation mechanism is described in the section below.

### 2.2.3.2 Positive selection strategy

The group of methods based on the positive selection strategy accounts in literature for the biggest proportion of all methods for CTC isolation. The methods usually utilise specific biomarkers that are expressed in the CTC cell or its surface to specifically identify and separate the target.

The most evidenced and widely exploited method that belongs to this group is a CellSearch™. The only FDA approved technique for tumour cells detection in whole blood, the CellSearch is a semi-automated fluorescent-antibodies-based system. The cells expressing epithelial-cell adhesion molecules are incubated with anti-EpCAM antibody coated ferrofluid nanoparticles and enriched applying high magnetic field to separate EpCAM+ cells from the solution. To distinguish leukocytes from cancer cells in the magnetically separated fraction, the fluorescently labelled antibodies specific for each cell type are added. The DAPI staining is additionally performed to assist in identification of nucleated cells. The detection and enumeration of CTCs is performed with the semiautomated fluorescence-based microscopy called CellSpotter system. The CellSpotter algorithm allows identification of CTCs which are defined as nucleated cells expressing cytokeratin and lacking CD45. This method has been applied in breast, ovarian and prostate metastatic cancers. The notable downside of CellSearch is the requirement for the fixation of cells which prevents further molecular analysis of the rare cells. Additionally, capturing only nucleated EpCAM+ cells, the immunomagnetic method disregards a mesenchymal subpopulation that is hypothesised to be more dangerous and prone to metastasise.

However, the positive selection strategy was also applied to microfluidic methods. The numerous and versatile designs of the microfluidic platforms were elaborated to capture and concentrate the rare cells. Microfluidic devices are of immense interest because of the ability to process extremely small volumes of samples with scarce number of cells. The two most reported microfluidic based isolation methods are the CTC chip and Herringbone chip. The devices have been proven efficient for CTC isolation from whole blood with high cellular viability. The CTC-chip is a PDMS structure, containing 78 000 anti-EpCAM-functionalised microposts<sup>77</sup>. The geometrical arrangement of the posts interrupts the streamline maximizing the interaction between the target cell and coated obstacle. The platform resulted in a high-efficiency capture which performance was demonstrated using bloods of patients with

colorectal, esophageal, lung, breast, and prostate cancer<sup>77</sup>. The alternative approach presented by the same group involved antibody-coated chevrons or herringbones patterns which geometry induce fluidic microvortices enhancing effective contacts between the cells and trapping surfaces. The evident advantage of these devices is the lack of blood pre-processing steps which commonly affect negatively the yield and viability of the cells<sup>48</sup>. However, the purity of the target cells could be considerably impaired by non-specifically captured leukocytes. Also, the process of the cell isolation using these chips is usually time-demanding due to the slow optimum flow rate. The literature additionally reported difficulties in releasing the captured CTCs from the chips for further analysis.

Another microfluidic-based method was reported to implement the rare cells isolation from liquid biopsy employing lumen-functionalised microtubes. This method is discussed in detail in the section below.

### **2.2.3.3 Negative selection strategy**

In contrast to positive selection methods, the negative ones target the biomarkers that are missing or not expressed in CTCs. The principle allows the elimination of unwanted cells like leukocytes from the solution and leaves the remaining cancer cells intact<sup>52</sup>. The CD45 depletion technique is widely employed for negative selection approaches<sup>52</sup>. Epithelial immunospot or EPISPOT is one of the representative systems of this strategy. The EPISPOT procedure involves CD45+ haematopoietic cells depletion from the blood sample following by culturing cells on a nitrocellulose membrane coated with CTC specific antibody<sup>78</sup>. The 48h-long-incubation is accompanied with the cancer cells' protein release or secretion. The immunospots capture secreted proteins which detection precedes by cells removal and introduction of fluorescently conjugated antibody. The protein fingerprints of the CTCs are subsequently evaluated under the microscope with further image analysis<sup>78</sup>. Although the results of this method corresponded to the metastasis status and poor survival in breast cancer<sup>57,79</sup>, the whole procedure is time-consuming and requires at least three days to obtain the results from a single sample<sup>52</sup>.



## 2.3 Methods and materials

### 2.3.1 Spinning top MAC chip fabrication

The employment of hydrodynamic single cell trapping on the microfluidic devices has been increasing over the years. In general, the method exploits mechanical barriers or obstructions to separate particles from the flow<sup>80</sup>. The hydrodynamic traps retain the target cells for the subsequent analysis or isolation. This concept has been utilized by<sup>81,82</sup>. Moreover, Guan et al has introduced structural modifications of the traps to maximise trapping efficiency for a particle of a defined diameter<sup>83</sup>. The Guan trap consists of an inlet channel, a trap aperture narrower than the dimensions of the target particle and two bypass channels, Figure 15a. The inlet flow has a lower resistance than it is in the bypass route Figure 15b. Hence, the cell in a laminar flow follows the center of the streamline that is largely directed into the trap if it is not occupied. The trapped cells occlude the main streamline diverting the flow to the alternate route and directing the following particle into the next trap.

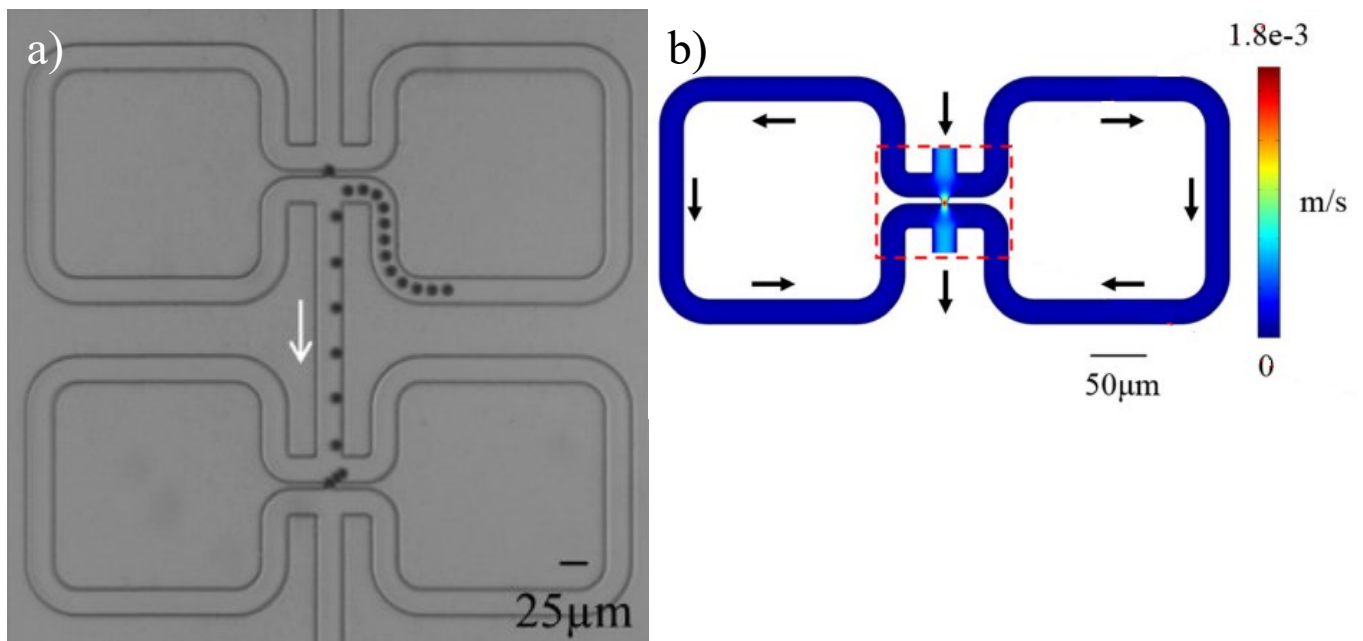


Figure 15 a) Trapping of synthetic beads by Guan traps with where the white arrow represents the flow direction. The scale bar= 25μm b) The dashed red rectangle points at the streamline velocity distribution in the unoccupied Guan trap and the black arrows show the flow direction. The scale bar= 50 μm. The images are taken from<sup>83</sup>

In their paper, Guan et al. demonstrated 100% trapping efficiency with no cell loss and excellent reproducibility<sup>83</sup>. The ability to isolate rare cells without loss is extremely attractive for CTCs extraction from clinical samples. Thus, the Guan traps were introduced into the spinning top chip design.

### 2.3.1.1 Spinning top chip design

The Spinning top microfluidic design was developed in the group with the idea to optically move the hydrodynamically trapped cells to the analysis chamber, Figure 16a. Therefore, along with the Guan traps, the device incorporates analysis MAC chambers that are positioned perpendicular to the inlet channel in a parallel array (Figure 16b). Such design enables an instantaneous screening of the biomarker expression in a target once it is trapped and transferred to the analysis chamber. The 5  $\mu\text{m}$  trap opening potentially allows the capture of particles with dimensions considerably exceeding the size of the structure's orifice. Additionally, to mitigate a high shear stress due to fluid flow rates, a strategy of inlet bifurcation was adopted which prevented cell deformation and lysis.

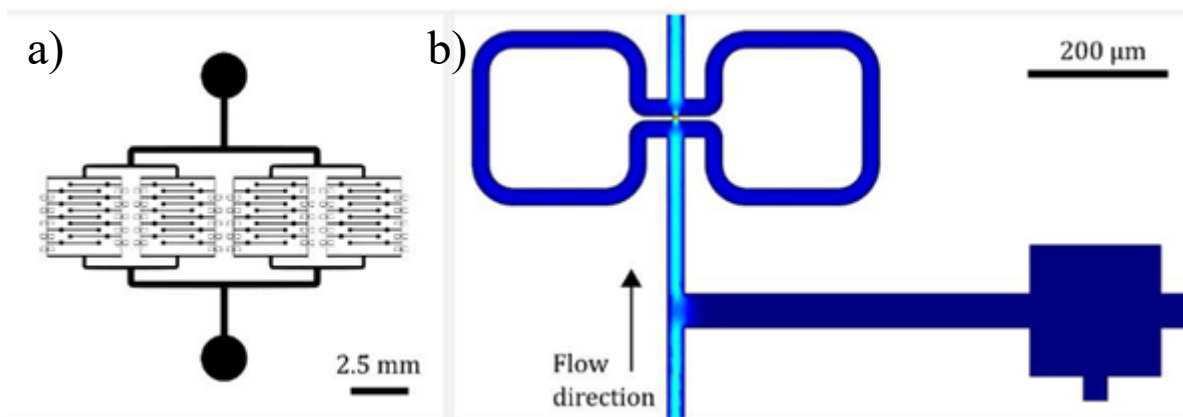


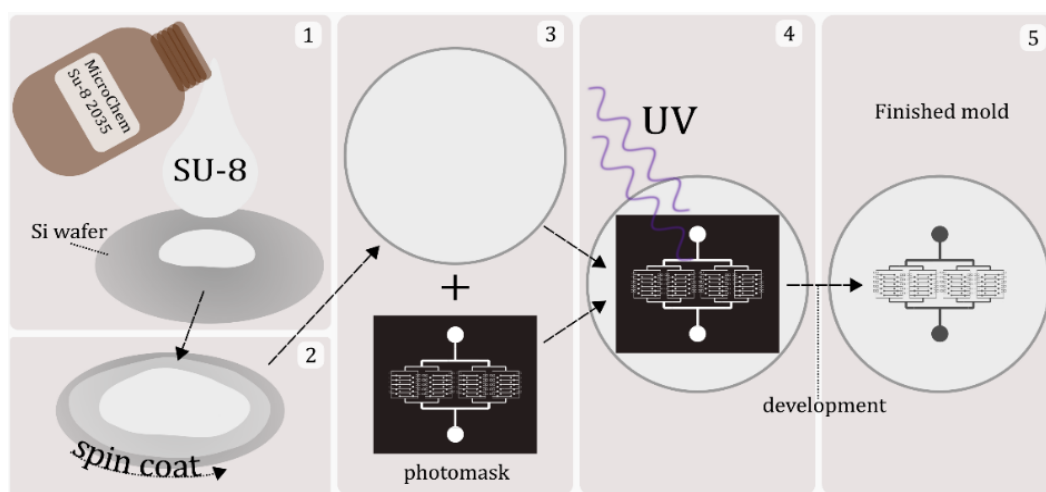
Figure 16 a) Spinning top chip design b) Guan trap and MAC chamber localization. Taken from<sup>12</sup>

### 2.3.1.2 Design fabrication

The CAD designs of the microfluidic platform were transferred to the chromium-glass photomask which transmits the UV light in the design region and blocks it everywhere else.

The chip manufacturing begins with a wafer production that is obtained with well-established photolithographic and soft lithographic methods (Figure 17). The wafer manufacturing was performed according to Microchem guidelines<sup>84</sup> which exploits the SU-8-based soft-lithography techniques. The epoxy negative photoresist, SU-8-2035 (MicroChem

Corp), was spun on a 100 mm Si wafer to form a 50  $\mu\text{m}$ -thick layer followed by a soft bake at 65°C for 1 min and 95°C for 6.5 min. The SU-8 coated wafer was then exposed to UV light through a high-resolution photomask (Mico Lithography Services Ltd, UK). The post-exposure bake was implemented at 65°C for 1 min and 95°C for 6 min to instigate thermally driven epoxy cross-linking. In the following step, the developing procedure was performed to remove the non-crosslinked SU-8 plunging the mould into propylene glycol monomethyl ether acetate for 6 min. The developed mould was then rinsed with IPA and silanised by vapour deposition of (tridecafluoro-1,1,2,2-tetrahydrooctyl)trichlorosilane (Sigma- Aldrich, UK) to achieve a hydrophobic surface promoting a better peel-off of the solidified gel afterwards.



**Figure 17 Microfluidic mould production diagram. 1) and 2) The Si-wafer is spin coated with a thin layer of negative photoresist SU-8. Th at the appropriate RPM for a set time. 3) The wafer is subsequently baked and aligned with the photomask with specific design. 4) in the following procedure the wafer with mask undergoes the UV exposure and post-exposure bake. The wafer is then submerged in a developer solution to remove the un-crosslinked SU-8. 5) The finished mould is silanised and ready for the following procedures. The image adapted from <sup>12</sup>**

The wafers were subsequently filled with a pre-mixed PDMS (Sylgard 184 Silicone Elastomer Kit, Dow Corning) at a ratio of 10:1 precursor to curing agent and degassed in a vacuum chamber. The gel is then cured at ambient temperature for 24+ hrs until hardened. The cured PDMS designs were cut and drilled to form inlet/outlet holes. To remove any contaminants from the gel surface, the chips were plunged into detergent solution (1% Alconox, Alconox Inc), sonicated for 1 hr, rinsed with water and dried with nitrogen.

### **2.3.1.3 Chip production**

To ensure the chip integrity during the experiments, the glass slide and PDMS design was treated in the plasma oven followed by an alignment of the components. As the prototype of the MAC-based spinning top chip at this stage of the research used no microarrayed biomaterial on the slide, the components of the platform were aligned by positioning PDMS design over the coverslip without the microscope exploitation. However, it was noticed that a single plasma treatment was unable to guarantee the chip's integrity during tests resulting in complete or partial delamination of the device particularly at relatively high flow velocities. This observation entailed the development of an alternative chip preparation method. The new strategy involved double plasma treatment of the components for 50 s with 2 min relaxation between the procedures. The PDMS was subsequently aligned with a cover slip and placed in oven at 55°C for 45 min with ~1kg weight on top. The 2cm-long tubing with fittings was connected to the inlet and outlet of the device.

### **2.3.2 Capture microtubes preparation**

The microtube device is a microscale flow setup which exploits polyurethane tubing with functionalised inner surface which mimics physiological cell trafficking and provide highly specific target cell capture<sup>25</sup>. The surface can be customised to specific cancer types by varying composition of the coating<sup>27</sup>. Hughes et al demonstrated the performance of the functionalised surface device with both, model blood samples supplemented with KG1a and buffy coats obtained from patients diagnosed with metastatic cancers<sup>25</sup>. The selectins and antibodies coated microtubes captured KG1a and primary CTCs from samples with roughly 50% recovery and purity up to 80%. The eluted cells were shown to maintain viability<sup>85</sup> which allowed to culture them performing subsequent analyses<sup>25</sup>. The similar strategy was employed to capture and kill HL60 cells with E-selectin and TRAIL (TNF Related Apoptosis Inducing Ligand) functionalised lumen<sup>27</sup>. Also, King et al implanted a vascular shunt prototype with a P-selectin coated lumen into the femoral artery of rats to capture CD34+ haematopoietic stem cells<sup>85</sup>.

The current research exploited method for microtubes lumen coating that was based on a protocol elaborated by Hughes<sup>86</sup> but with introduction of several modifications to adapt the system for our specific purposes and enhance the capture effectiveness of the device. The

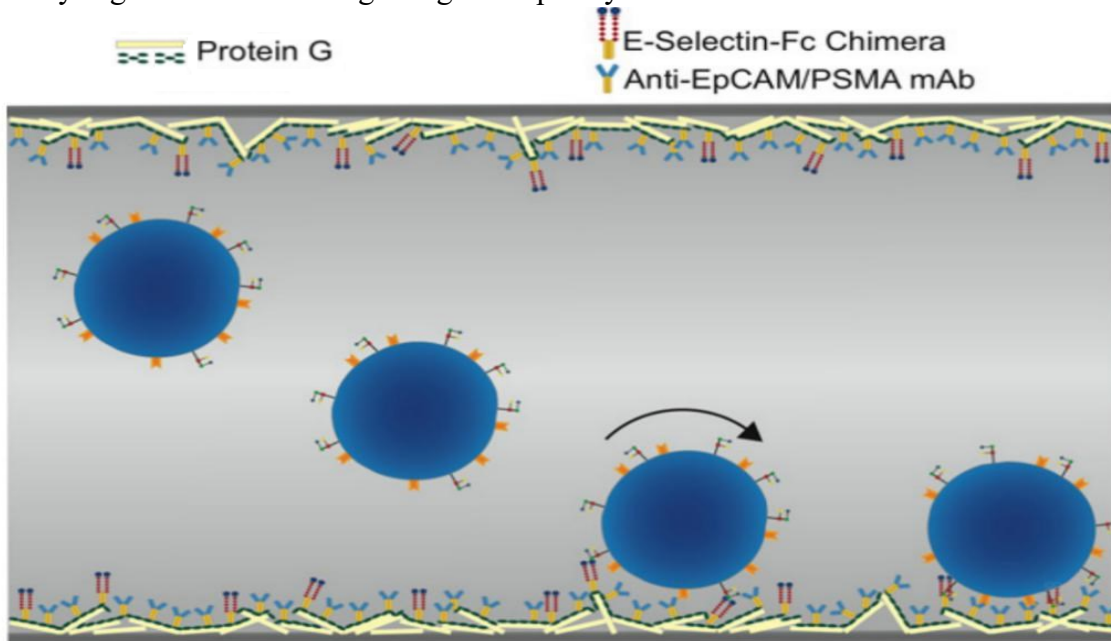
functionalised surface of the tubes is depicted on **Error! Reference source not found.** for which production procedure is described in detail in this section. Firstly, the 100 cm Micro-Renathane microtubing (300  $\mu\text{m}$  inner diameter, 35.3  $\mu\text{L}$  inner volume, Braintree Scientific) was washed with 70% ethanol and  $\text{dH}_2\text{O}$ . The tubes were subsequently treated with 0.02% poly-L-Lysine (Sigma-Aldrich, UK) solution for 5 min at ambient temperature. The solution was then replaced with water and left overnight. After 24 hours, PBS (Dulbecco's phosphate buffered saline, Invitrogen, UK) solution was drawn through the tubes and the surface was further incubated with 10  $\mu\text{g}/\text{mL}$  of Protein G (Sigma Life Sciences, UK) for 1.5hrs. Protein G is an immunoglobulin-binding protein which is commonly used as a bridging agent between surface and antibodies<sup>87</sup>. The tubes were further functionalised with a mixture of 25  $\mu\text{g}/\text{mL}$  of E-selectin and 50  $\mu\text{g}/\text{mL}$  of Human anti-EpCAM (R&D Systems, UK) for 2hrs. Since most of carcinomas exhibit upregulated EpCAM glycoprotein (epithelial cellular adhesion molecule)<sup>88</sup>, the surface coating with antibodies targeting epithelial marker was considered to provide a CTCs-specific separation from leukocytes<sup>25</sup>. Additionally, the E-selectin molecule inclusion to the modified lumen posed several advantages for the effective cancer cells retrieval. Firstly, it has been proposed that CTCs, akin to leukocytes, transiently bind to selectin molecules resulting in slow rolling on the lumen which potentiates the cancer cells interaction with the functionalised surface. Moreover, the EpCAM binding is slow and requires low flow rates; however, selectin-mediated cell adhesion allows more time for the IgG molecule to bind promoting cell isolation at faster flow velocities. The lumen functionalization finalised by blocking non-specific binding with 5% of milk protein (Blotting Grade Blocker Non-Fat Dry Milk, Bio-Rad, UK) solution for 1 hr and PBS washing. The coated microtubes were further halved and assembled into a meander on a glass slide.

### **2.3.2.1 White blood cells (WBC)-depletion tube production**

The early study setup included only a capturing tubing; however, the blood sample analysis necessitated to introduce a WBC-depletion or pre-capturing microfluidics to improve purity of the captured cells. The pre-capturing microtubing production was implemented following the afore-mentioned protocol but using another antibody to cover the lumen with. Thus, instead of an antibody targeting the epithelial molecule, a mixture of 25  $\mu\text{g}/\text{mL}$  E-selectin (R&D system, UK) and 50  $\mu\text{g}/\text{mL}$  anti-CD45 (Abcam, UK) antibody was used to coat the lumen of the pre-capturing device.

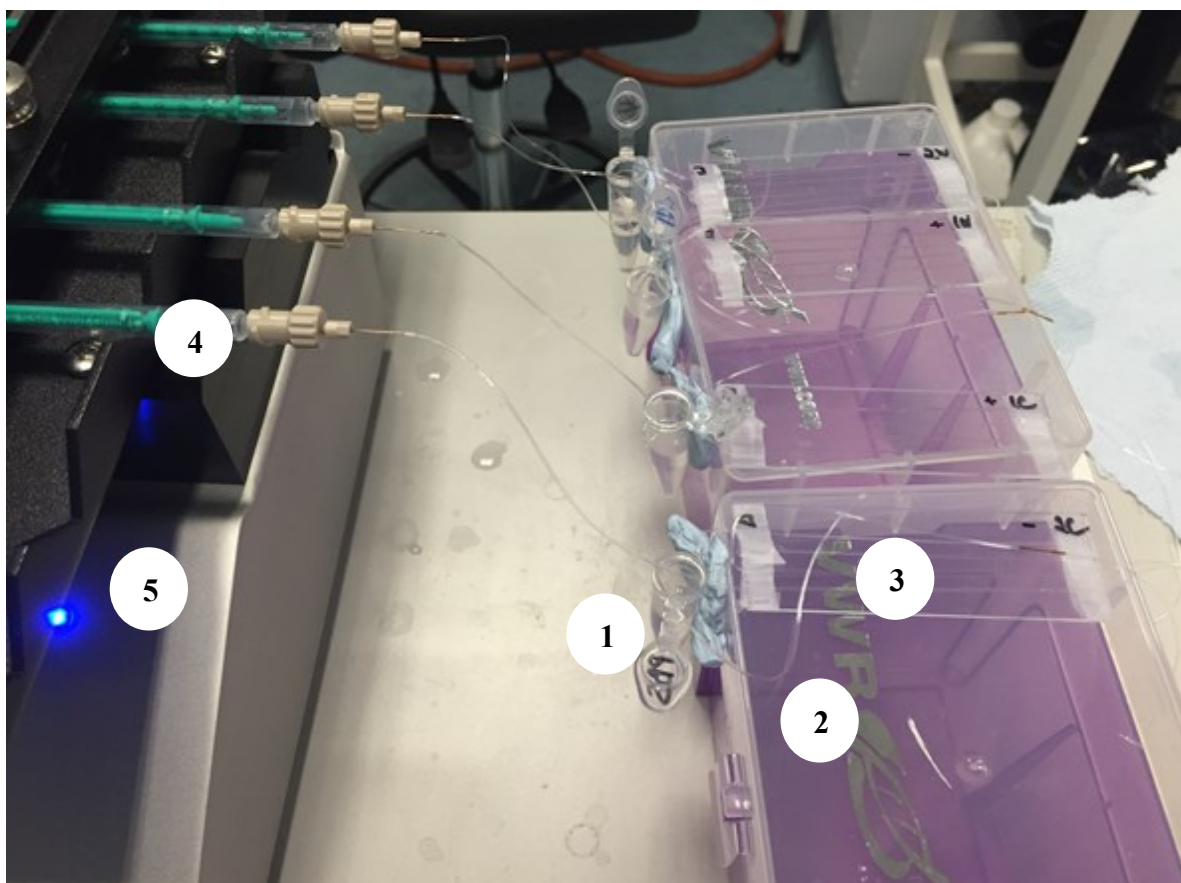
### 2.3.2.2 Microtubes set-up

Two compound assemblies were exploited for the current research: 1. For general protocol development using a model cell line and 2. For clinical sample analysis. The assembled system for the general protocol development was composed of a syringe pump (Cole-Palmer, UK), syringe, a single surface-functionalised microtubing (capturing tube) and a sample (Figure 19). The tube's inlet was submerged into the sample and the outlet connected to the syringe with PTFE fitting and glass capillary.



**Figure 18** The inner surface of the tube functionalised with a mixture of target biomarker and E-selectin showing cancer cells rolling on the lumen to promote antibody binding. The image adapted from <sup>26</sup>

For the blood samples analysis, the upgraded set-up was used instead to improve the purity of the recovered cells. Thus, a set of in tandem arranged surface-functionalised microtubing (pre-capturing and capturing tube) was incorporated into the assembly. The sample before the CTCs isolation procedure was perfused through the pre-capturing tubing which outlet was connected to the capturing tube via glass capillary to perform a subsequent target cells isolation (Figure 19).



**Figure 19** Microtubing set-up: 1. Sample, 2. WBC- depletion tubing (for blood samples analysis only), 3. Capturing tubing, 4. Syringe, 5. Pump

### 2.3.3 Samples preparation

#### 2.3.3.1 Polystyrene beads sample

15  $\mu\text{m}$  polystyrene bead (Sigma-Aldrich, UK) solution was prepared mixing 10  $\mu\text{L}$  of the beads stock in 990  $\mu\text{L}$  of 4% pBSA solution. The choice of the bead size was determined by the dimensions of the trap design and the size of the cancer cells which were considered to be  $>15\mu\text{m}$ .

#### 2.3.3.2 Model cell line samples

The experiments with MCF7 cells were conducted to establish a general protocol for the cancer cells analysis. The breast cancer cells were cultivated in Dulbecco's Modified Eagle's Medium (DMEM, Gibco, UK) with the addition of 10% Foetal Bovine Serum (FBS, PAA, UK DMEM) at  $37^{\circ}\text{C}$  and 4%  $\text{CO}_2$ . The 50-70% confluent cells were harvested and resuspended in 5% FBS solution to achieve concentration of  $5 \times 10^3$  cells/mL. Prior to the experiment, the cell solution was additionally adjusted to  $5 \times 10^2$  cells/mL in 5% FBS solution.

### **2.3.3.3 Spiked blood samples**

The blood samples were supplied by Imperial College London Charing Cross or Hammersmith Hospitals (Imperial College London, UK). 7.5 mL of peripheral blood from healthy volunteers was drawn into a BD Vacutainer tubes and delivered for analysis within 2 hours. The transported specimen was then gently mixed and spiked with 100 µl of MCF7 cellular solution at concentration of  $5 \times 10^3$  cells/mL to obtain a final concentration of 500 cells per 7.5 mL of blood.

#### **2.3.3.3.1 Blood sample processing**

The peripheral blood has a complex composition containing a variety of cells suspended in blood plasma including erythrocytes, leucocytes and thrombocytes. However, the current project was focused on the method development for CTCs isolation and analysis only. Therefore, the sample was required to be pre-processed to avoid unwanted cells to interfere the results. Once spiked, the blood samples were further transferred for the pre-isolation procedure. The comparison of two techniques was performed to determine the effectiveness of both and select the more suitable method. The Ficoll-Paque™ density gradient centrifugation and Red Blood Cells (RBC) lysis with subsequent centrifugation were tested and the results were collated on the basis of target cells quantity and purity.

The cells extraction from peripheral blood by the fore-mentioned methods required the sample to be <8hrs old and supplemented with anticoagulants. Thus, the samples were transferred and stored in a heparin tube until the handling procedure<sup>89</sup>. The blood processing and pre-isolation were conducted immediately after the blood spiking with MCF7 cells.

##### **2.3.3.3.1.1 Isolation of peripheral blood mononuclear cells using Ficoll-Paque™**

This method has been exploited in many studies<sup>90-92</sup>. For example, Tan et al. used this technique to isolate tumour infiltrating lymphocytes from a dissociated excised tumour tissues<sup>92</sup>. The method was determined to yield >80% viable MNC (mononuclear cells) with high purity containing only up to 5% of granulocytes and 10% of erythrocytes<sup>93</sup>. The separation principle is based on the diluted blood sample carefully layering over a Ficoll-Paque product as a result of centrifugation. The main component of Ficoll-Paque media is the Ficoll PM400 which is a branched synthetic sucrose polymer with a high molecular weight (Mr=400 000). Upon spinning, the cells of distinctive density form different layers which arrangement is



depicted in Figure 20. In short, the bottom layer is occupied by erythrocytes due to an interaction with Ficoll PM400 which efficiently aggregate the red blood cells promoting their sedimentation. The layer immediately beneath the Ficoll-Paque media contains granulocytes which density increase caused by a contact with hypertonic Ficoll-Paque media. Being not dense enough to penetrate through the synthetic polymer coat, the majority of MNCs migrate to the interface between plasma and Ficoll-Paque layer <sup>93</sup>. In the following procedures, the MNC layer is usually harvested, washed and resuspended in an appropriate buffer for the further analysis <sup>89</sup>.

In this research, the isolation of the mononuclear cells (MNC) from human peripheral blood by density gradient centrifugation was implemented according to Miltenyi Biotec GmbH protocol <sup>89</sup>.

The initial step of the protocol involves pipetting 16 mL of Ficoll-Paque™ ( $\rho=1.077$  g/mL, GE Healthcare Life Sciences, UK) into a Leucosep® tube (Greiner Bio-one GmbH) with a subsequent spinning at  $1000\times g$  for 30s to relocate the sucrose polymer to the bottom of the tube beneath the porous barrier. The spiked blood was halved (3.75 mL) and was subsequently diluted with a 2 mM EDTA buffer (EDTA dissolved in Dulbecco's PBS, pH=7.2). To obtain a better purity of the target cells, the sample dilution factor was set to 3x. The diluted sample was shortly transferred into the Leucosep® tube and filled till the tube's capacity with the 2mM EDTA buffer. In the following step, the sample was centrifuged at  $1000\times g$  for 10min which facilitated its stratification. The layer, where the MCF7s along with other MNC cells migrated during the spinning, is called buffy coat <sup>89</sup>. Since the buffy coat localised under the plasma layer, it was first needed to discard the layer impeding the isolation of the target cells. The buffy coat was carefully aspirated and transferred into the new tube to wash the harvested cells removing platelets, any contaminating Ficoll-Paque media and plasma <sup>93</sup>. The washing procedure was repeated 3x involving sample dilution with the buffer and a subsequent centrifugation at  $300\times g$  for 10 min <sup>89</sup>. Finally, the supernatant was discarded, the pellets reincorporated and resuspended in 500  $\mu$ L of 5% FBS solution.

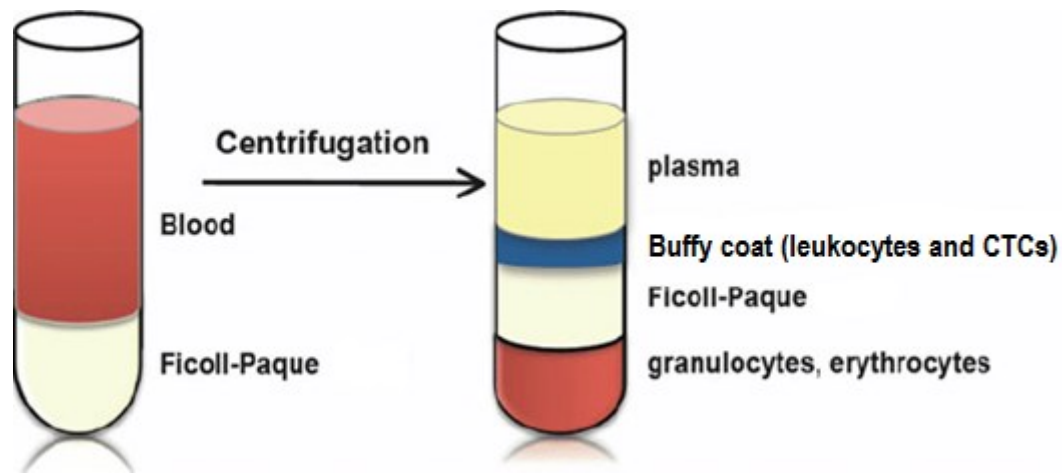


Figure 20 Layers formation with Ficoll-Paque™ density gradient centrifugation <sup>94</sup>

#### 2.3.3.3.1.2 Red Blood Cells (RBC) lysis

The high concentration of erythrocytes in whole blood interferes with the study of leucocytes phenotype and function. It is, therefore, necessary to remove and lyse the RBC cells prior the further white blood cells analysis. The Red Blood Cells (RBC) lysis is a widely used hemolysing media that ruptures erythrocytes without affecting leukocytes, normal tissues and tumour cells <sup>95</sup>.

The mechanism of action for this method is governed by osmoregulation of the cell. When an erythrocyte is placed in a hemolytic media, it swells exceeding a critical volume threshold eventually leading to cellular membrane rupture and lysis. The ammonia chloride and sodium bicarbonate are the principal reagents in the RBC lysis buffer that are frequently used as hemolysing and hemolysis mediating agents, respectively. Ammonia permeates through the membrane triggering the exchange of intracellular  $\text{OH}^-$  and extracellular  $\text{Cl}^-$  and resulting in  $\text{NH}_4\text{Cl}$  flux into the cell. Additionally, the  $\text{OH}^-$  diffusion is largely mediated through a  $\text{CO}_2/\text{HCO}_3^-$  exchange accelerating the erythrocyte's hemolysis at the presence of  $\text{NH}_4\text{Cl}$  <sup>96</sup>.

The RBC lysis protocol applied in this research is further described in detail in this section. The working 1× lysis buffer was prepared from a 10× stock solution which was composed of 1.5 M  $\text{NH}_4\text{Cl}$ , 0.1M  $\text{NaHCO}_3$  and 10mM EDTA solution. The half of spiked blood sample was transferred to the new tube and diluted to 50 mL with a cold 1× lysing solution. The tube was inverted for 10 min at room temperature until the liquid was clear red

which indicated the lysis completion. The sample was subsequently spun at 4°C for 10 min at 250×g and the formed pellet was washed with cold PBS solution at the same centrifugation conditions. The washing procedure facilitated the lysis-derived contaminants reduction. Finally, the pellets were incorporated, resuspended in 500 µL of 5% FBS solution and transferred immediately for the cancer cells isolation procedure.

### 2.3.4 The CTCs isolation experimental overview

The whole experimental workflow can be generally subdivided into sample processing, CTCs (or target cells) isolation, captured cells counting, elution, cells enrichment on the spinning chip and protein expression analysis in the target cells in MAC chambers.

#### 2.3.4.1 CTCs capturing and purification

Shortly before the experiment, the PBS solution was drawn through the microtubing system. To retrieve cancer cells from either MCF7 solution or processed spiked blood, the samples were loaded into the microtubing via programmable syringe pump. Different flow programs were investigated to determine the one with the highest recovery rate. In the post-program procedure, the capturing tubes alone (the pre-capturing tube was disconnected if used) were washed with 300 µL PBS at 1 mL/hr to remove unbound and loosely bound cells. The tubing sample was subsequently transferred for the concurrent cells discrimination and counting procedure where the tubes lumen undergone visual inspection under brightfield illumination (Nikon TE2000-U, Nikon Instruments, Japan). In the following step, the cell recovery was calculated as a ratio of captured cells to sum of captured and passed cells, Equation 13.

$$Recovery = \frac{n_{captured}}{n_{captured} + n_{passed}} \quad \text{Equation 13}$$

The elution procedure was further undertaken to harvest the captured cells. In the preliminary study different elution strategies were tested to establish a protocol for target cells collection. Initially, the retained cells were eluted into the 96-well plate where the liberated cells were counted. The protocol yielding the highest cell number was subsequently selected for the further analysis. Once the protocol was established, the cells were eluted directly into the spinning top chip where they were attempted to be hydrodynamically trapped and optically transferred for the analysis in the MAC chambers.

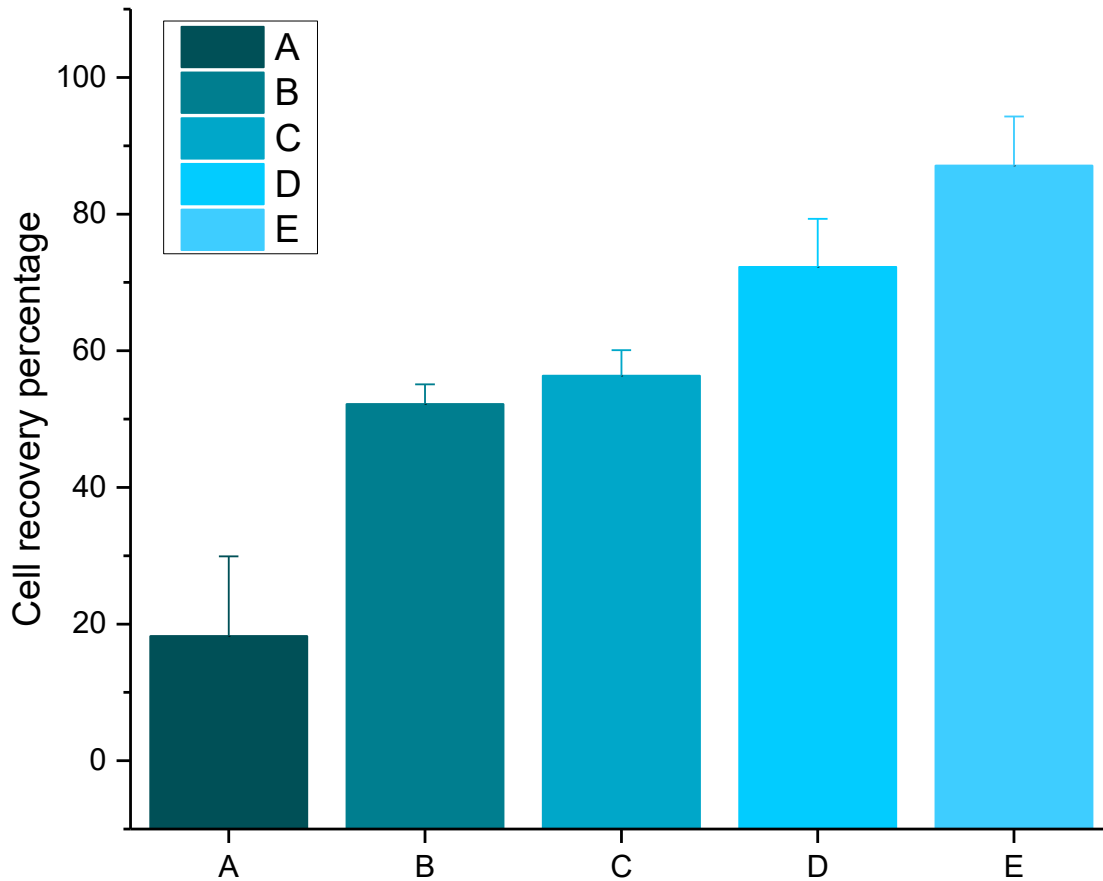
## **2.4 Results and discussion**

### **2.4.1 Method development for MCF7 cell capture from cellular solution**

The development procedures to determine optimal operating conditions were carried out with MCF7 cell solution. Table 1 shows 5 various flow programs that were tested to observe the flow effect on the tubes capturing performance. It was noted that there is a relationship between cell recovery and operating flow algorithm. The obtained results were obtained from at least 2 repeats.

The microscale fluid method described in Hughes et al. study<sup>86</sup> was initially chosen for the flow program because it was reported to yield >50% cell recovery (Table 1 program A). However, our data show that the employment of this method resulted in relatively low cell recovery which was found to be roughly 20%. The observed discrepancy might be explained by the fact that the Hughes group applied the device with differently modified surface to trap KG1a haematopoietic cancer cells. Thus, it was speculated that the binding between leukemia cancer cell and the anti-CD45 functionalised lumen occurs at the rate higher than the interaction between MCF7 and anti-EpCAM coated surface. This observation suggested that the program A is not suitable for the microfluidic device and required further optimization of working conditions.

Additionally, it was noted that the introduction of interval flow program (programs B-E) alternating flow and pause periods resulted in a considerable cell recovery growth (Figure 21). Although, programs B-E exploit a similar flow strategy, it was found that the program E outperformed other methods operating approximately at 80% cell recovery. The potential reason for the enhanced capturing of the tubes with program E is the lower time ratio of flow and pause intervals. Since the E program demonstrated the highest cell capturing, it was selected for further analysis.



**Figure 21** Average percentage of MCF7 cell recovery with functionalised microtubes by programs A-E which operating conditions are shown in Table 1

**Table 1** Tested flow programs for the MCF7 cells trapping

A*	1 mL/hr
B	60s flow (2mL/hr), 60s stop. Repeat 14x
C	60s flow (2mL/hr), 90s stop. Repeat 14x
D	50s flow (2mL/hr), 50s stop, 10s flow, 50s stop. Repeat 14x
E	30s flow (2mL/hr), 50s stop, 30s flow, 50s stop. Repeat 14x

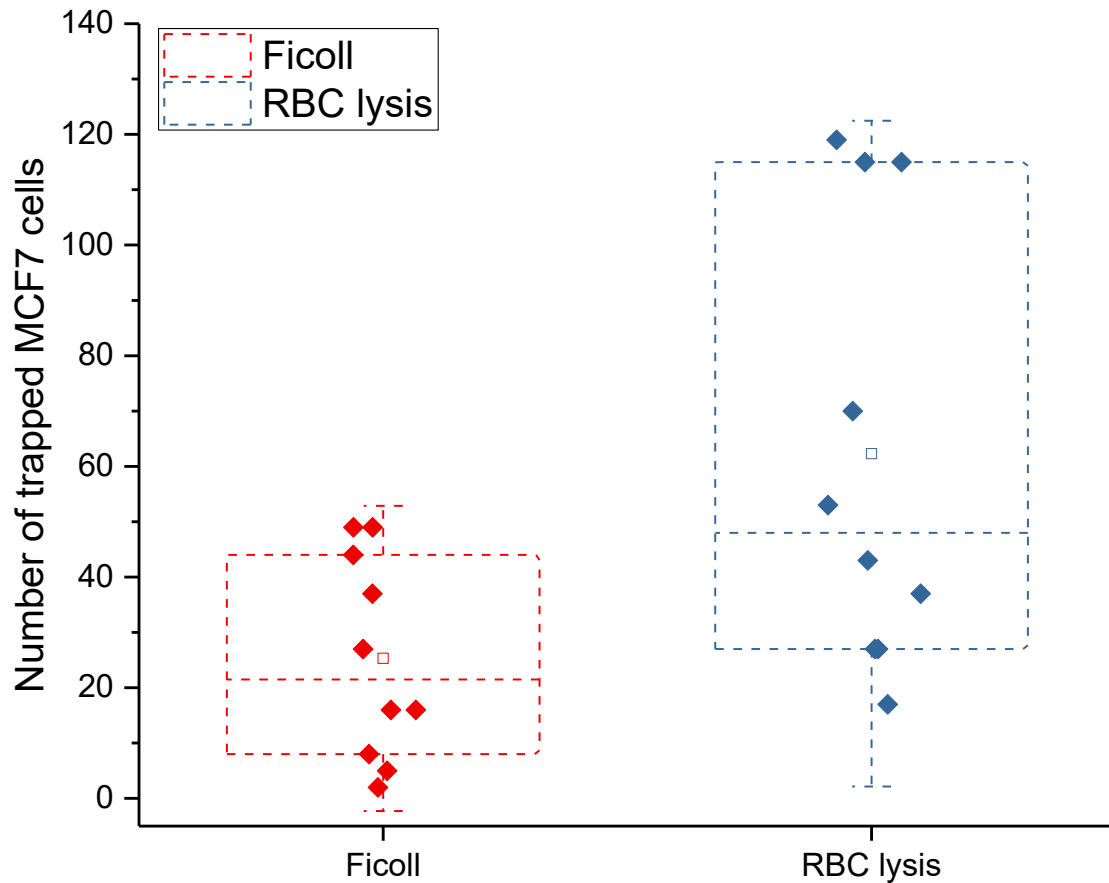
\* The method used in Hughes study to capture CTCs from blood samples of cancer patients

## 2.4.2 Isolation of MCF7 cancer cells from model blood samples

The buffy coats of the spiked blood samples were obtained using Ficoll-Paque™ density gradient centrifugation (Ficoll) and Red Blood Cells lysis (RBC lysis). The comparison

of two concentrating techniques was implemented to determine the more suitable method for further target cells isolation with microtubes. The obtained results using Ficoll and RBC lysis were collated on the basis of target cells quantity and purity. Overall, 10 experiments with model blood samples were performed for each blood concentrating technique.

The Figure 22 clearly shows that there is a high variability in captured cell number using either of the blood enrichment methods. The inconsistent retrieved cell number is presumably due to supernatant aspiration during either washing procedures and crude buffy coat isolation or uneven coating of tube the lumen. Additionally, it was observed that the target cells enriched using Ficoll resulted in a lower number of captured cells comparing to RBC lysis approach. The microtubes captured between 2-49 cells from processed samples with Ficoll technique and 17-119 cells with RBC lysis. Considering the 3.75mL blood sample contained 250 breast cancer cells, the methods enabled to extract roughly 1-20% and 7-48% of spiked MCF7s for Ficoll and RBC lysis, respectively. The source of pronounced scarcity of recovered cells for Ficoll might be a migration of cancer cells from buffy coat to the adjacent layers during the centrifugation process. The MCF7 vary in size and density what can supposedly cause them to be suspended in the neighbouring layers and hence be lost during aspiration. It could also be a higher number of washing steps involved in Ficoll protocol that negatively affect the retrieved cellular count presumably due to the repeated aspiration and spinning.



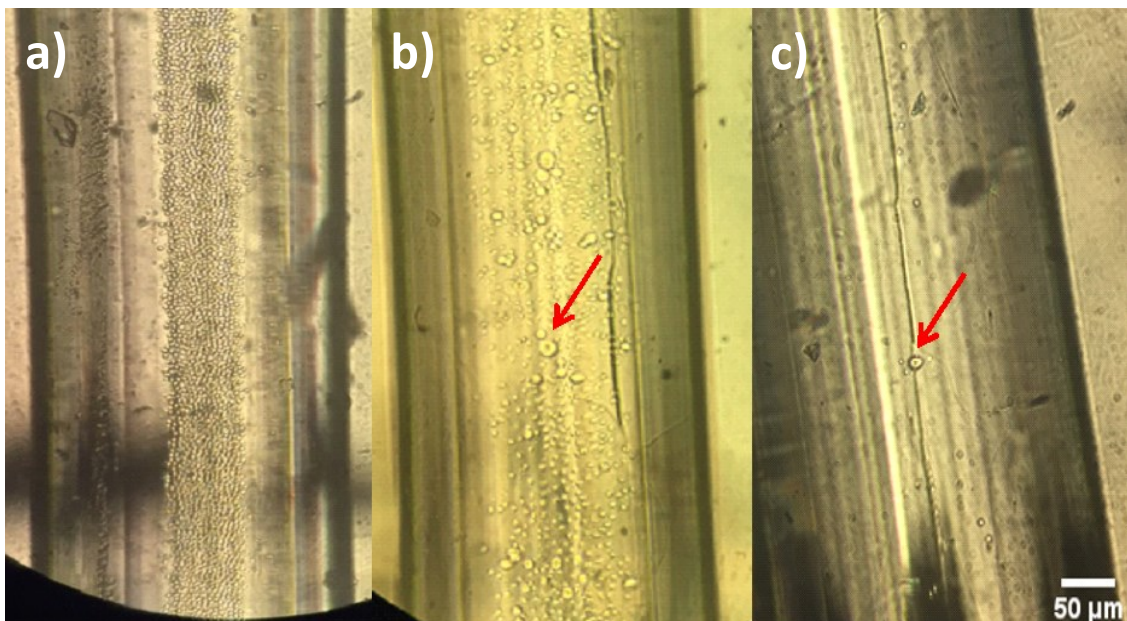
**Figure 22** Captured cells number from spiked blood samples processed by RBC lysis and Ficoll. The square represents mean, the dashed lines represent median of 10 experiments and whiskers are standard error

The buffy coats, despite the applied enrichment techniques, were still composed of a significant number of unwanted cells like platelets and leukocytes. The purity of extracted cancer cells from buffy coats was, nevertheless, evidently different for Ficoll and RBC lysis. The Ficoll yielded a visibly lower unwanted to target cell ratio than RBC lysis. The results were assumed to be distinguishable because of different washing strategies. It is apparent that inclusion of additional washing steps led to a high sample purity but also loss of a considerable portion of target cells. In contrast to RBC lysis, the Ficoll technique required a specific reagent and involved more processing steps and therefore it was considered to be more expensive and time-consuming. The RBC lysis was found to be more favourable method because it yielded a higher cancer cells recovery; however, it produced a low purity of the enriched target cells.

#### 2.4.2.1 WBC-depletion tube introduction

In the preliminary study, the buffy coat experiments revealed a shortcoming of the setup used for the validation with MCF7 solution. The assembly composed of a single E-

selectin/anti-EpCAM coated tube produced a relatively low purity of isolated cancer cells from blood samples which enumeration was extremely complicated, Figure 23a. The existing system necessitated an upgrade and hence, the pre-capturing microtube was introduced. Although the pre-capturing tube with anti-CD45 functionalised surface reduced dramatically the number of contaminating cells on the capturing tubes (Figure 23b), the purity was still not sufficient for the sample to be eluted into the spinning top chip for the further analysis. The strategy to modify the pre-capturing lumen combining E-selectin and anti-CD45 was, therefore, employed. The complementary E-selectin coating facilitated retaining of the most unwanted cells on the pre-capturing tube lumen yielding a high purity of the isolated carcinoma cells, Figure 23 c. The pre-capturing tube mimics the physiological arrest of white blood cells that is typically involved during inflammatory response. E-selectin is a glycoprotein expressed on endothelial cells which assist in leukocytes attachment during inflammation <sup>97</sup>. The adhesive E-selectin molecule promotes leukocytes' slow rolling on the endothelium inducing stronger integrin binding <sup>97,98</sup>.



**Figure 23** Captured cell purity from spiked blood sample by capturing microtubing a) without pre-capturing tube, b) with anti-CD45 coated WBC-depletion tube, c) with additionally E-selectin functionalised pre-capturing tube. Red arrows show captured cancer cells

#### 2.4.2.2 Elution

To conduct further sample concentration and analysis of the target cells on the chip, the elution of the captured cells had to be undertaken. Different elution protocols were investigated



to establish the one that would satisfy most of the requirements. The ideal elution method was expected to a) recover 100% of captured cells b) yield a volume of up to 100  $\mu\text{L}$  to avoid excessive dilution of the sample c) remain viability of target cells throughout the whole process (for instance, preventing the MCF7s exposure to a high shear stress or strong proteases solutions) and d) maintain the spinning top chip integrity by employing low flow pressures.

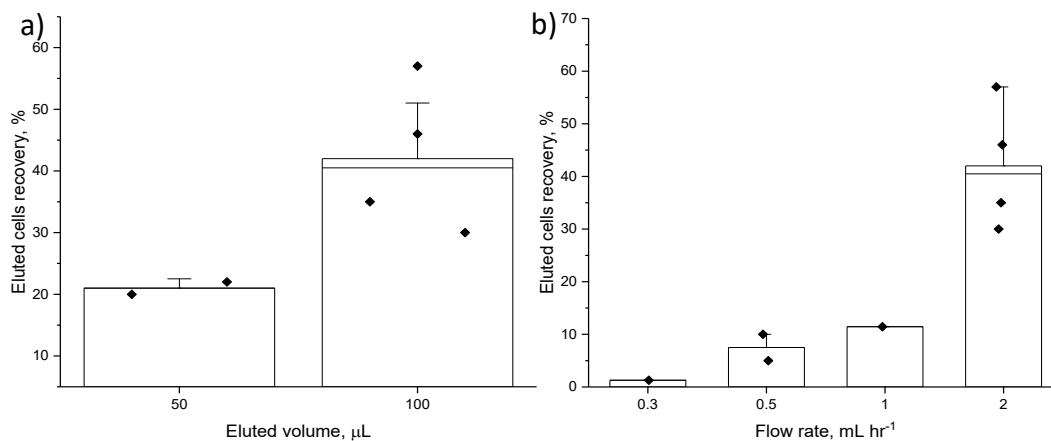
For this set of experiments the elution procedures were tested on either MCF7 cellular solutions or spiked blood samples. The target cells capturing from buffy coat or cellular solution samples was performed with a set of microtubing containing or not the WBC-depleting microtubing, respectively. The MCF7s isolation for both samples was implemented using the flow program E.

The studies of CTCs capturing with surface functionalised microtubing employed different strategies to elute the adherent cells from the lumen. For example, Hughes et al has exploited Accutase for 10 min incubation with a subsequent wash at a high flow rate to harvest the captured cells<sup>25,86</sup>. Unexpectedly, this method was unable to produce a satisfying outcome in our case resulting in cells shearing and undesirable eluate volume increase due to a subsequent PBS perfusion. This observation might be attributed to difference in the utilised capturing flow programs that has been applied in the referred studies. It was speculated that the E flow program facilitated a stronger cells adhesion to the functionalised lumen and therefore, the tested elution method was observed to be not suitable to collect the captured cells.

The absence of an operating elution protocol brought us to explore of air embolism technique. This technique has been previously applied in some studies to retrieve viable cells from the functionalised tubes<sup>27,29,85</sup>. For example, Narasipura et al. eluted target cells employing a combination of 2.5  $\text{dyn}/\text{cm}^2$  high shear stress and air embolism, whereas King et al. harvested the isolated cells with 5mM EDTA and air embolism at 10  $\text{dyn}/\text{cm}^2$ <sup>27,29</sup>. As it was previously observed, the high shear stress ruptured the captured MCF7s in our experiments and therefore, the exploited methods in the referred studies clearly required adjustments before being applied.

The combination of different eluting solutions with air embolism were tested to determine the effect on the captured cells recovery. The air embolism with 5% FBS buffer was found to be ineffective because the major proportion of cells remained trapped failing to vacate the microtube. The positive result was observed applying Accutase solution which promoted

cells detachment and ejection from the tubing. The Accutase solution is composed of proteolytic and collagenolytic enzymes which facilitate detachment and dissociation of cells. Being routinely exploited in standard tissue culture procedures, Accutase has shown an increased cell viability in comparison with trypsin/EDTA <sup>99</sup>. However, the examination of the eluate generated by this method revealed the solution to contain cellular aggregates and clusters. The cellular clusters can potentially occlude traps and channels of the spinning top chip complicating the single cell analysis. The similar result was obtained testing air embolism with trypsin/EDTA; however, this method was dismissed because trypsin requires incubation at 37°C and quenching <sup>99</sup>. Considering the obtained results, the elution protocol further development was pursued with the focus on the Accutase/air embolism application. The effect of volume and flow rate was further tested on the eluted cells recovery.



**Figure 24 a) Eluted cells recovery with different perfused volume at flow rate of 2 mL/hr b) Eluted cells recovery with different flow rate**

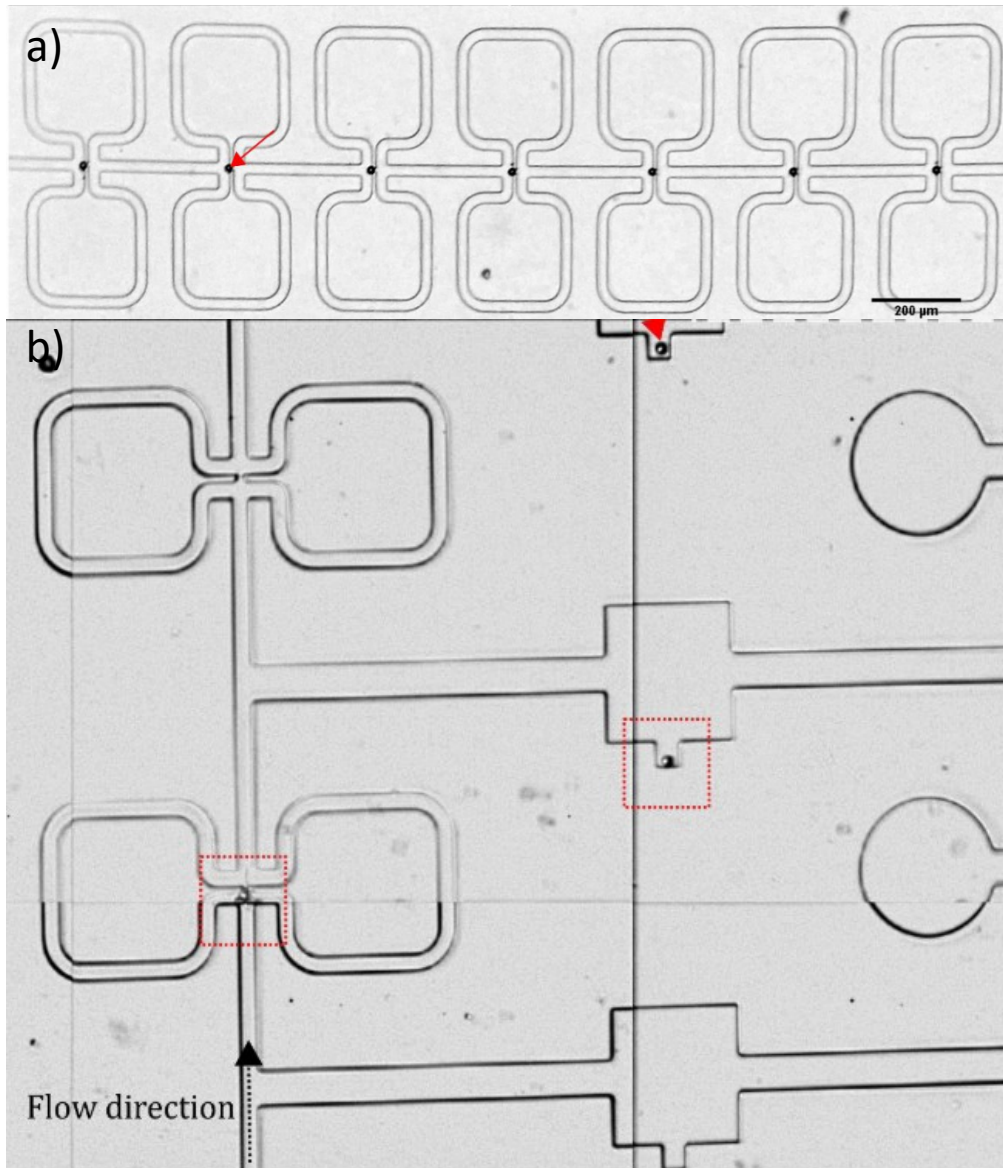
Figure 24a demonstrates the effect of perfused solution volume on the cell recovery. As it can be noted the bigger volume withdrawal led to a higher cells recovery for the elution procedures at flow rate of 2 mL/hr. It was speculated that enhancement in cell recovery might be associated with the time required for the bigger volume perfusion which promotes cells to stay in mobile state longer (than for smaller volume) preventing interaction with the functionalised lumen.

Since the application of high shear stress was employed in several studies, the effect of flow rate on the elution process was assessed combining air embolism with withdrawal of 100  $\mu\text{L}$  of Accutase. It was observed that the higher cellular number was recovered with the elution at higher flow rates, Figure 24b. The cells detached from their primary binding sites can

potentially be bound a second time whilst travelling in the tube. The anti-EpCAM binding is, however, slow and requires time to occur even with the static cells. Thus, the possible explanation for the observed flow rate effect is that at higher flow velocities the eluting cells are restricted to contact the functionalised surface residing in a continuous mobile state. Additionally, the viability of the eluted cells was confirmed with trypan blue and showed MCF7s to successfully survive the flow rate without being ruptured or lysed. Although the 100% recovery was not achieved with neither of the tested protocols, a combination of 100  $\mu$ L of Accutase perfusion with air embolism at flow rate 2 mL/hr produced the highest cellular yield resulting in roughly 50% recovery of the captured cells.

### **2.4.3 Validation of spinning top chip methodology with polystyrene beads**

Before the analysis of blood and MCF7 samples, the spinning chip device was first tested with polystyrene beads to validate its performance. To avoid particles adhesion to the chip's surface, the microfluidic device was pre-blocked with 4% BSA solution. The sample solution was introduced to the platform with a pump-driven flow. In the preliminary study, the chip sealing was achieved via single plasma treatment of the components. However, it was established that the platform failed to withstand even a low flow rate which caused the chip to dissociate in nearly 90% cases. The protocol clearly required modifications to ensure the microfluidics integrity during the experimental runs. To enhance the bond between glass and PDMS superstructure, the plasma treatment was repeated twice with relaxation step between the procedures. The new strategy provided the chip integrity at flow velocities as high as 100  $\mu$ L/min in 70% cases. The beads trapping was, nevertheless, implemented at 30  $\mu$ L/min to improve the likelihood of the device successful performance. The Figure 25a and b demonstrate the Guan traps trapping efficiency maintaining the platform's integrity. The group was also able to accomplish optical transfer of the hydrodynamically trapped 15  $\mu$ m beads to the MAC compartments. This progress allowed for the current study to move towards isolation and concentration of human cells.



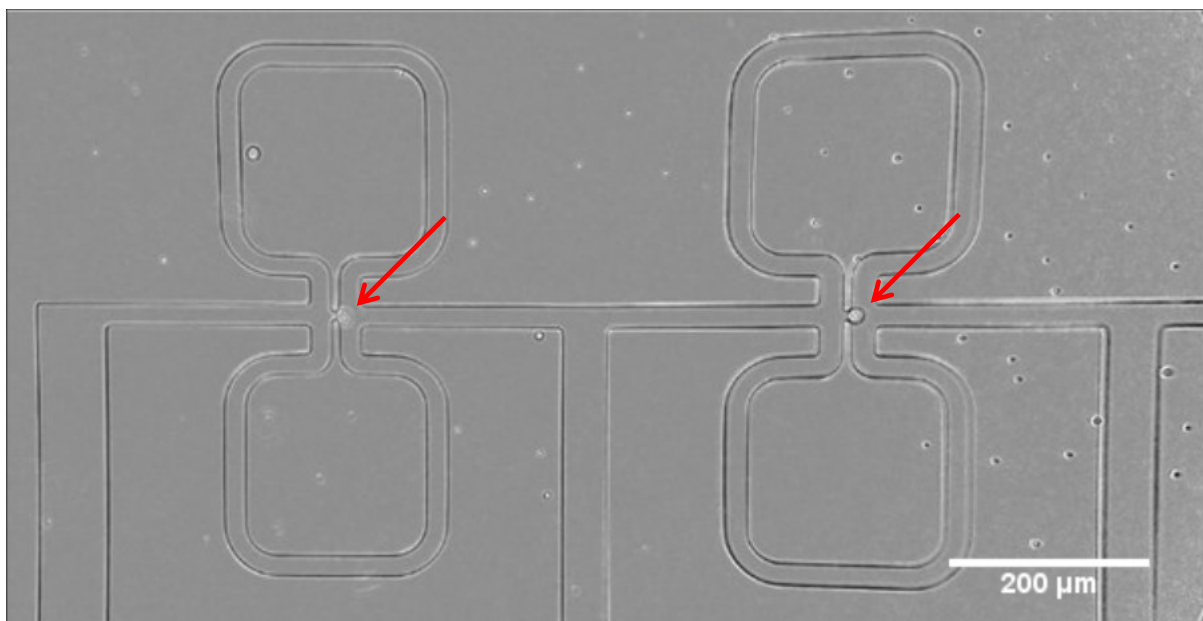
**Figure 25** a) The polystyrene beads trapped by the Guan trap. Red arrow points at the trapped bead. b) The optical transfer of the hydrodynamically trapped beads into the MAC analysis chambers. The rectangles highlight the position of the hydrodynamically trapped beads before optical trapping and transfer to the analytical chamber and after

#### **2.4.3.1 MCF7 cells enrichment on the spinning top chip**

MCF7 as well as CTCs are larger than most of white blood cells which allowed the hydrodynamic traps to discriminate target cells restricting their passage through the trap's aperture due to the size.

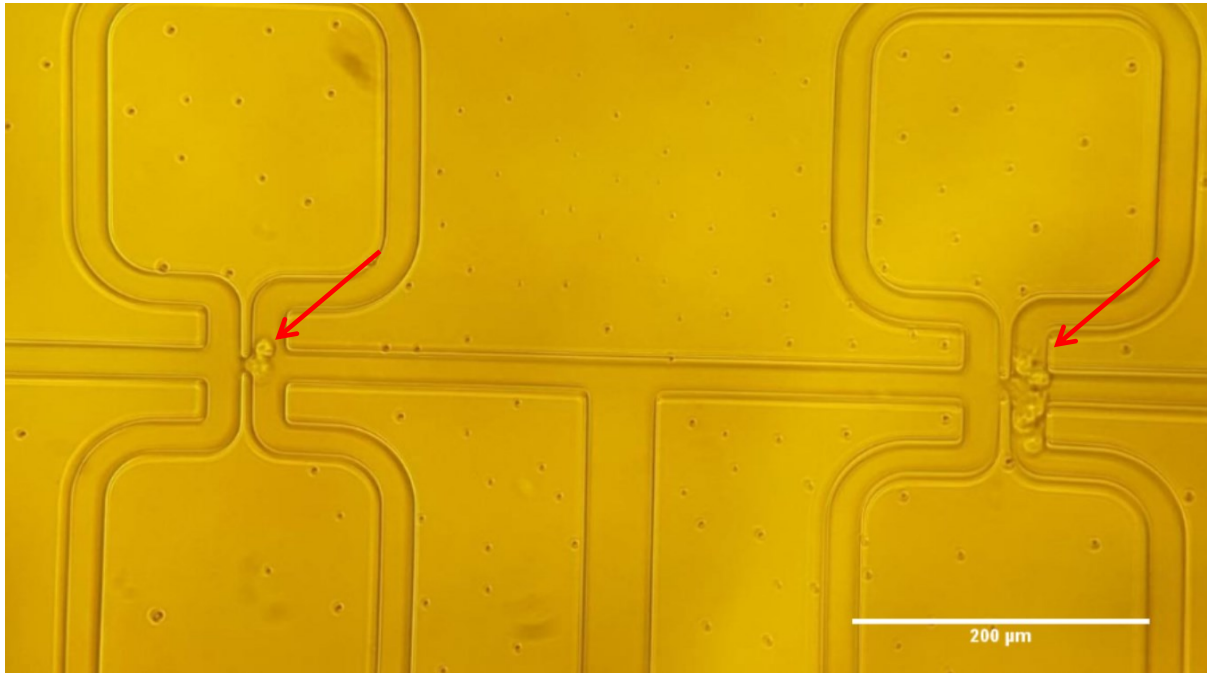
The first tests conducted with MCF7 cancer cells revealed that the chosen operating conditions required optimisation. Despite the bifurcated flow inlet of the device, the flow rate

for polystyrene beads experiments was found to be too high for the trapping of cancer cells. At 30  $\mu\text{L}/\text{min}$  the MCF7s were observed to deform and squeeze through the trapping orifice and therefore, the procedure was subsequently implemented at a lower flow velocity. The cells were found to be stably immobilised in the traps throughout the duration of experiment at 10  $\mu\text{L}/\text{min}$ , (Figure 26). Although the slower flow rate prolonged the experimental run, the complete sample processing on the chip could be attained within 10 minutes assuming the sample volume after elution does not exceed 100  $\mu\text{L}$ .



**Figure 26** The spinning top MAC-based chip validation with the MCF7 cellular solution. The flow rate reduction at which cells were fed into the chip resulted in the successful trapping of individual MCF7 cells. The arrows indicate hydrodynamically trapped individual cells. The scale bar = 200 $\mu\text{m}$

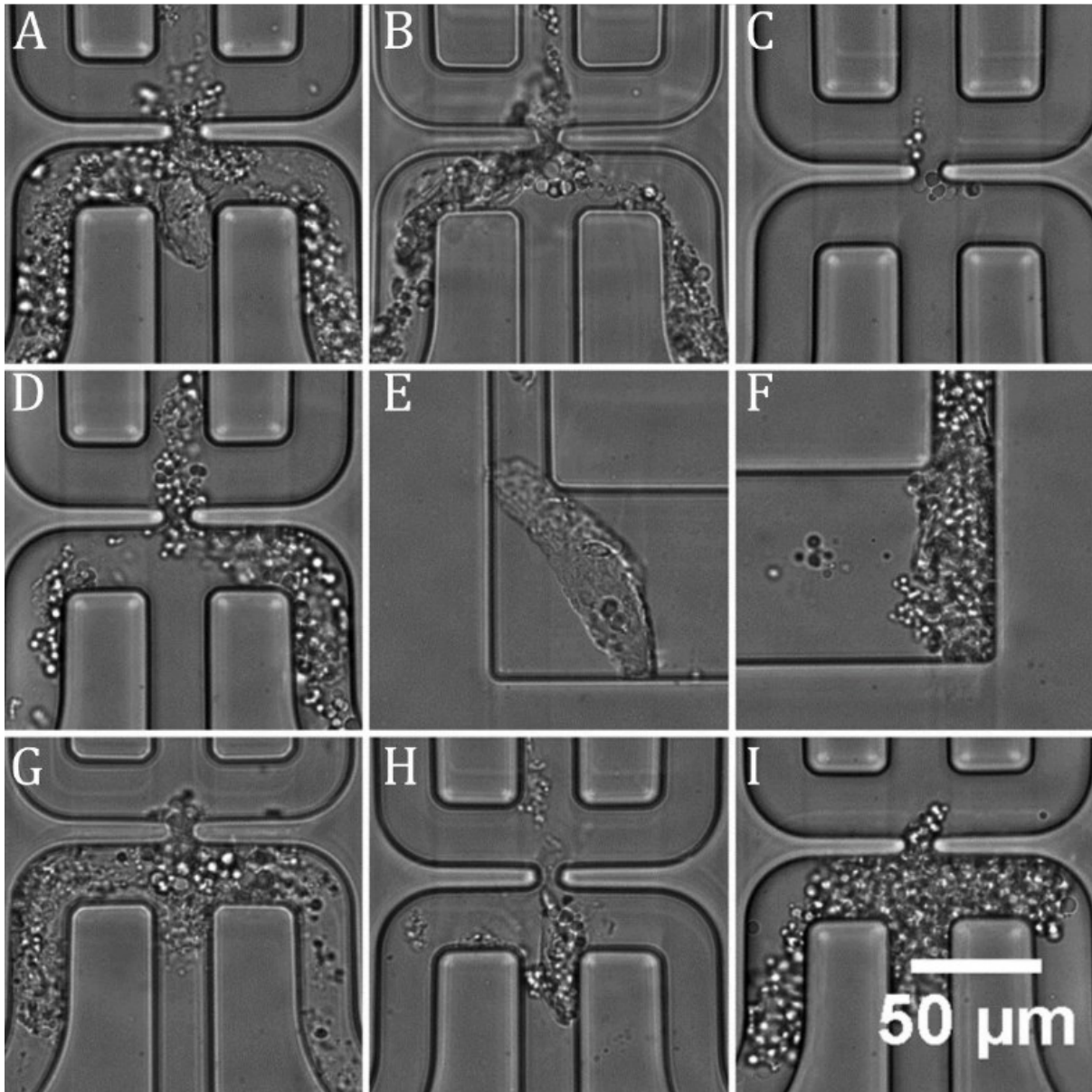
Additionally, it was observed in some occasions that multiple cells occupied a single trap; however, it is unknown whether a gradual accumulation of multiple single cells in a trap preceded clogging or the cell cluster formed before entering the device (Figure 27). The cellular aggregation jeopardised the platform's efficiency and therefore, needed to be avoided. To reduce cluster formation, the MCF7 confluency was kept below 70% and the working solution was supplemented with chelating agents such as EDTA.



**Figure 27** The spinning top MAC-based chip validation with MCF7 cellular solution. Clogging of some Guan traps of the tested platform was observed by the MCF7 cell clusters. The arrows show the trapped MCF7 aggregates. The scale bar= 200μm.

#### **2.4.4 Incorporation of microtubes and spinning chip to isolate MCF7 from model blood samples**

Prior to elution, the capturing CTC-microtube was directly connected to the spinning top chip to reduce the loss of the targeted cells. This is an important step especially when applying this technique to more precious samples such as CTCs. The isolated cells from buffy coat were eluted combining Accutase with air embolism technique at 10 μL/min. The experiment was performed without introduction of an additional WBC-depletion step. As it can be seen on Figure 28, the chip failed to retrieve MCF7 cells due to clogging of traps and channels, presumably by residual blood components and cellular clumps.



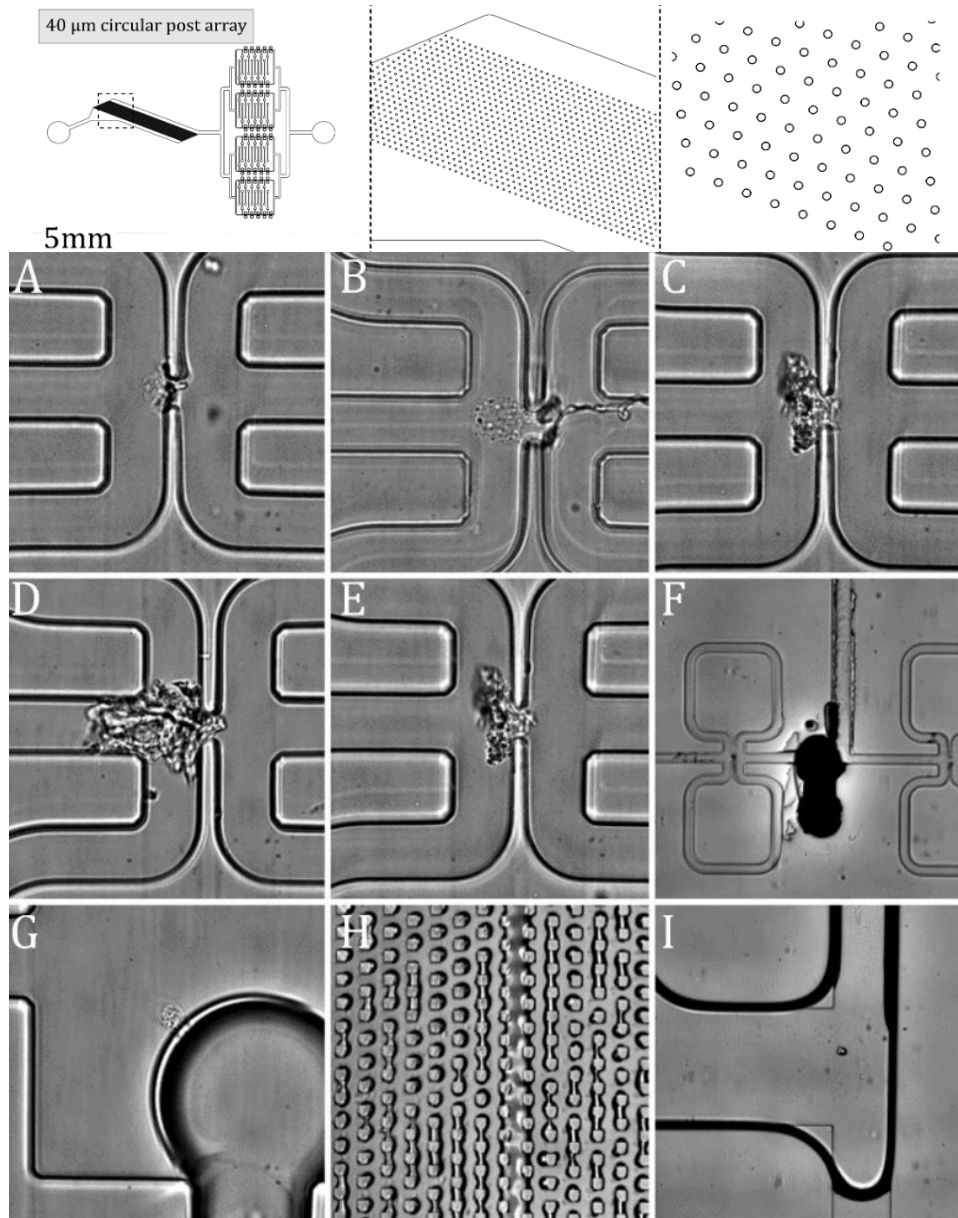
**Figure 28** The images of clogged Guan traps and channels (A-I) upon the retrieved cells elution obtained from buffy coat. The experiment was performed without WBC-depletion tube.

#### 2.4.4.1 Spinning top with debris filter

Due to persistent chip clogging problem, the group introduced microfluidic size-exclusion filter situating it before the trapping region, Figure 29. The filter was designed to retain large debris preventing it from obstruction of trapping area. The filter is composed of hydrodynamically not-optimised microposts that would presumably filter the cellular agglomerates and blood residuals.

The cancer cells were attempted again to be enriched from the model blood sample via buffy coat perfusion through the set of microtubes to facilitate WBC-depletion and target cells capture with the following on-chip enrichment and analysis. The cells elution from capturing tube was performed at 10  $\mu\text{L}/\text{min}$  combining Accutase and air embolism. Although the introduction of pre-capturing tubing and the upstream filter notably reduced traps occlusion, some unwanted residuals penetrated through and clogged the traps (Figure 29 A-E). Moreover, the experiment was forcibly stopped because after few minutes of continuous flow the device delaminated, Figure 29 F-I. The unsuccessful performance of the device was assigned to the filter which negatively affected integrity of the chip by increasing the contactless surface area of the design.





**Figure 29** Top: the design of the modified spinning top chip with the filter upstream the trapping area  
 Bottom: A-E occluded Guan traps with the blood residuals and cellular aggregates, F-I delamination of the chip due to the filter introduction. The experiment was implemented with WBC-depletion procedure. The images are adapted from <sup>12</sup>

## 2.5 Conclusion

This chapter discusses the endeavours to develop a set of platforms for CTCs analysis on the MAC-based platform. A potentially useful composite device combined microtubing for specific target cells isolation and MAC-based spinning top chip for hydrodynamic cells

enrichment and single cell protein analysis. The development of the compound setup was divided into two discrete steps: elaboration of the microtube and spinning chip platforms.

The first part of the research was focused on the employment of microtubes for cancer cells recovery which operating concept is based on the mimicking of cell trafficking in the biological systems. The performance of lumen modified tubes were first observed with MCF7 cellular solution. Upon the investigation of different operating flow programs, the program E was found to produce the highest cell recovery which presumably conferred the most favourable dynamics for the slow nature of the EpCAM bonding.

The tubing was subsequently tested with buffy coats obtained from the model blood samples using Ficoll and RBC lysis techniques. The samples immediately revealed the marginal purity of the captured target cells which clearly indicated the need for a purification step introduction prior to the capturing. The WBC-depletion tube was, therefore, connected in tandem with the capturing device. The following modification of the pre-capturing tube's surface with a mixture of anti-CD45 antibody and E-selectin protein improved purity of the retrieved MCF7s from the model blood samples. The cancer cells recovery rate in spiked blood samples was, however, noticed to be markedly lower than expected supposedly due to the repeated cycles of centrifugation and aspiration for Ficoll and RBC lysis. The spinning with a subsequent aspiration reduced prominently the number of cancer cells in the processed sample which is a concern for the rare cells like CTCs. Although both Ficoll and RBC lysis were found to produce suboptimal results, the RBC lysis protocol was selected for further experiments because it yielded a notably higher number of recovered target cells than Ficoll.

Additionally, different strategies to liberate the adherent cells from the capturing lumen were explored. It was established that the combination of Accutase with air embolism was the most suitable technique to elute the cancer cells. A similar concept of using air embolism to detach viable cells from the surface has been previously reported and exploited in several studies. The optimisation of the elution procedure parameters showed the positive correlation between higher eluate volume and eluted cell recovery. Also, the elution flow rate was observed to affect the procedure outcome. Whilst too rapid flow velocity exposed cells to intolerable sheer stress leading to cellular lysis, the inadequately slow elution negatively affected the cellular recovery. Thus, the optimal flow rate was determined to be 2 mL/hr.

Before the microtubes incorporation with the spinning top platform to optically transfer the trapped cells for the concurrent MAC-based protein analysis, the chip was first tested and validated with synthetic beads and MCF7 cancer cells. After resolving the chip's integrity problem that occurred during the experimental runs, the microfluidic platform was demonstrated to be effectively used for the beads hydrodynamic trapping and optical transportation to the MAC chamber. The operating conditions were, nonetheless, found unsuitable for the MCF7s due to their propensity to deform and squeeze through Guan's traps at the chosen flow velocity. The flow rate was, therefore, reduced to 10  $\mu\text{L}/\text{min}$  to facilitate the target cells retaining in the traps.

The coupling of microtubes with the spinning chip was implemented to validate the setup with the spiked blood samples. The cancer cells extraction was carried on microtubing device which was subsequently connected to the chip to elute the captured cells directly into the chip. The eluate was noticed to clog the channels and traps of the microfluidic platform by blood residuals. This result led to an introduction of the WBC-depletion tube and the on-chip filter upstream the trapping area. Although the system's upgrades reduced the biological-clumps-derived obstruction of channels and traps, the filter upstream the trapping area of the chip weakened the structure integrity disabling the platform to withstand the flow and causing it to burst apart.

Although the MAC-based chip is an effective platform for the rare cells analysis, the isolation and delivering cells like CTCs to the chip remained unresolved which hindered successful performance of the developed composite device addressed in this chapter. It is, nevertheless, believed that the described attempts of CTCs isolation with ensuing single cell protein analysis will be considered for the future studies of cancer metastasis. The potential route to address this biological problem is further described in 6.2.2.

# Chapter 3. A microfluidic capture affinity assay development for FOXO3 protein

## 3.1 Why is it important to study FOXO3?

The abundant expression of FOXO1 and FOXO3 transcription factors in nearly all tissues suggests that these proteins are important in the regulation of many vital processes although through as yet unidentified mechanisms. Current research is mainly focused on gaining insight into the functions of FOXO3 proteins at a single cell level which will presumably reveal the missing information in understanding the biology of lung cancer, asthma, COPD and other respiratory diseases. It has been speculated that FOXO3 plays an essential role in COPD and other respiratory diseases development which became a major motivation for the FOXO3 assay establishment in this research. In order to track protein expression in single cells the methodologies are required with high dynamic range and the sensitivity to detect protein molecules. The MAC chip has already been successfully employed to evaluate the p53 protein expression in single cells of human cancer cell lines and disaggregated xenograft<sup>24</sup>; however, there is a need to investigate the single cell response for the biomarker levels relevant to other specific diseases. This chapter details the FOXO3 immunoassay development process and its adaptation to the MAC chip platform to conduct a single cell protein analysis.

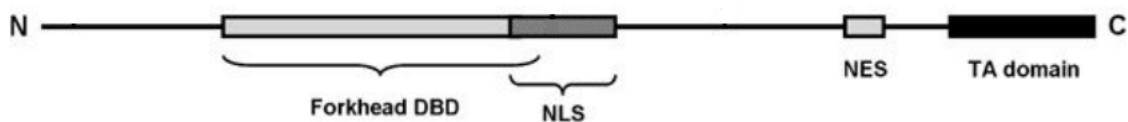
### 3.1.1 FOXO transcription factors

The forkhead box family (FOX) proteins are evolutionarily conserved transcription factors that are involved in regulation of many biological processes<sup>100,101</sup>. The three-dimensional structures of FOX proteins show they have a conserved winged-helix DNA binding domain (DBD) which is called the forkhead domain (FKH). The FKH domain is composed of ~100 amino acid residues constituting three  $\alpha$ -helices, three  $\beta$ -sheets and two wing-like loops that flank the third  $\beta$ -sheet<sup>102</sup>. The amino acid sequence motif of the DBD is almost invariant for different family members. The FOX family is classified into 19 clades based on the structural similarity in the FKH domain -from FOXA to FOXS<sup>102</sup>.

The “O” sub-family of FOX proteins contains four members- FOXO1, FOXO3, FOXO4 and FOXO6 which are all mammalian homologues of the *Caenorhbditis elegans*

longevity and dauer arrest gene DAF-16<sup>103,104</sup>. FOXO transcription factors activate or inhibit genes responsible for processes such as proliferation, metabolism, inflammation, ageing, stress resistance, apoptosis, reproduction and differentiation.

FOXOs show extensive sequence homology for four regulatory motifs of the forkhead domain, a COOH-terminal transactivation domain (TA domain), a nuclear localisation (NLS) domain located in the COOH-terminal basic region of DBD and a nuclear export domain (NES) located downstream of the DBD (Figure 30). Despite high sequence homology, the mouse FOXO knockout experiments have revealed that each FOXO gene exhibits a unique regulatory function in different biological processes<sup>105</sup>.



**Figure 30 Schematic representation of FOXO proteins which contain four regulatory motifs: a forkhead DNA binding domain (DBD), a nuclear localisation domain (NLS), a nuclear export domain (NES) and a transactivation domain (TA)<sup>106</sup>**

Each FOXO isoform displays distinct DNA-recognition motifs and regulatory mechanisms. However, all FOXO proteins bind to the insulin response element (IRE) with the consensus sequence of 5'-T(G/A)TTTTG-3' and the Daf-16 family binding element (DBE) with consensus sequence of 5'-T(G/A)TTTAC-3'. FOXOs have regions of natively unstructured elements and therefore, the binding of C-terminal transactivation domain is implemented through an induced-fit model which requires multiple modifications to provide a high-affinity DNA binding conformation<sup>107</sup>.

FOXO1 and FOXO3 are larger proteins that are composed of 655 and 673 aa, respectively, whereas FOXO4 and FOXO6 are 505 and 492 aa long. FOXO1 and FOXO3 are ubiquitous and have been detected in nearly all tissues. FOXO4 is predominantly expressed in colon, ovary, testis, muscle and kidney tissues. FOXO6 has been reported to be highly expressed in brain and female specific tissues.

### 3.1.1.1 Properties of FOXO3

FOXO3 is a transcription factor encoded by the FOXO3 gene. The protein has been found to play an essential role in tumour suppression, glucose homeostasis, immune cell regulation, (cancer) stem cell maintenance, inflammation, lifespan and human longevity<sup>108</sup>.

The structural analyses show that promoter recognition helix H3, wing1 and the C-terminal regions are actively involved in DNA binding. The NLS domain, which is localised in C-terminus of FOXO3-DBD, has a coil structure inserted into the major groove of DNA, Figure 30. The DNA promoter recognition is implemented via a series of van der Waals interactions and hydrogen bonding between methyl groups of thymine bases and the conserved residues of Arg 211, Ser215 and His 212<sup>101</sup>. The DNA binding sequence for the FOXO3 has been reported to be 5'-GTAAACA-3'. Similarly to FOXO1, Tsai et al. has shown that homodimer can form between two FOXO3-DBD molecules<sup>101</sup>.

FOXO3 has been also found to bind distantly from the promoter region of genes. Enhancers presumably contribute to the FOXO3-DNA binding. The enhancer activity helps to determine the outcome of FOXO3 binding activity. In addition, the combination of enhancer sequence and chromatin context affects the transcription factor outcome. It has been speculated that clustered binding sites promote the FOXO3 binding affinity.

FOXO proteins are regulated by a wide range of external stimuli, such as insulin, insulin-like growth factor (IGF-1), other growth factors, neurotrophins, nutrients, cytokines and oxidative stress stimuli<sup>100</sup>. FOXO transcriptional activity is tightly controlled by multiple mechanisms which include posttranslational modifications including phosphorylation, acetylation, ubiquitination and possibly others. The modifications can promote nuclear import or export, change the DNA binding affinity, and alter the pattern of transcriptional activity for specific target.

Since the regulation of FOXO3 controls the vital bioprocesses in human cells, the disruption in transcription activity provokes a cascade of biological events leading to cell's faulty operation and development of pathologies. However, due to intrinsic and extrinsic variation, not all cells response to the stimuli identically. Therefore, the ability to characterise the FOXO3 level in the single cell regime would assist in understanding the disease underlying

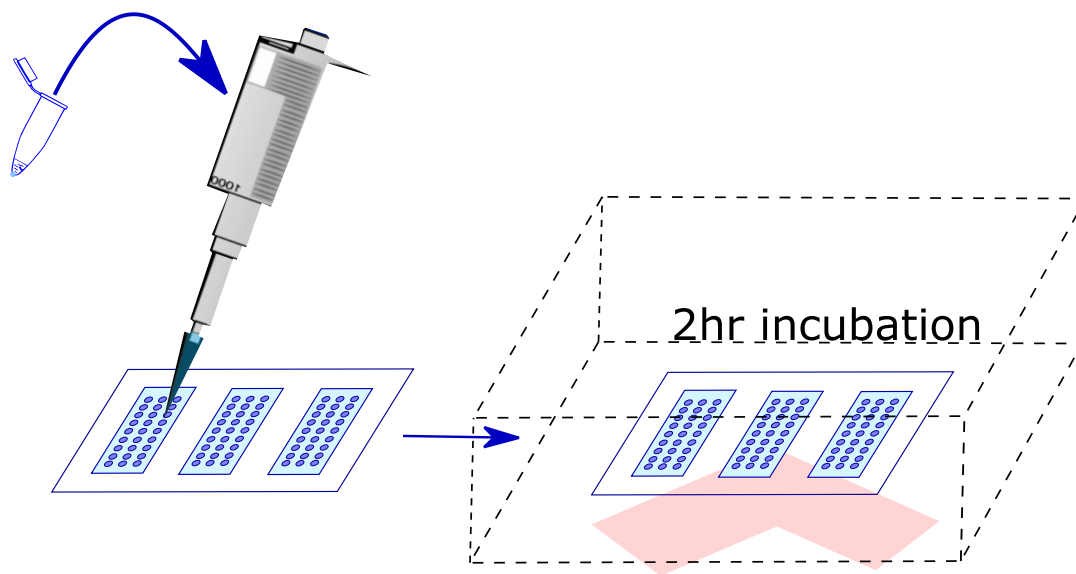
physiological processes and novel therapy discovery. In the following sections, the development of an analytical tool for FOXO3 protein evaluation in single cells is described.

## 3.2 Methods and Materials

Various microfluidic platforms were used in this research to pursue different objectives. The devices employed can be subdivided into two categories: Open chip and MAC chip. Additionally, the single cell analysis was implemented using two MAC chip designs that contain either 4.5nL or 1.2nL analysis chambers. In the following section, the in-house preparation of these microfluidic tools is described.

### 3.2.1 Experimental overviews

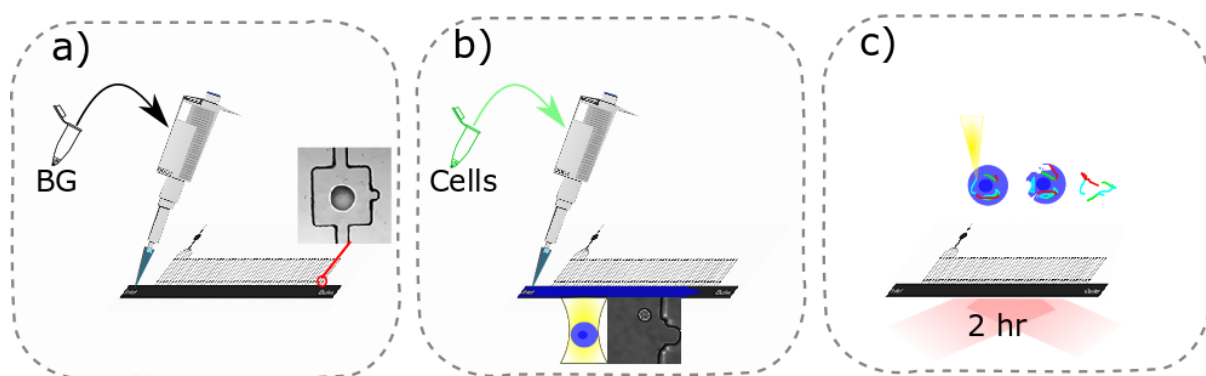
The Open chip was predominantly deployed as a preliminary step during assay development to observe the performance of different reagents and to screen, in parallel, antibody pairs for determining suitable candidates for a FOXO3 analysis in single cells. Additionally, this platform allows rapid adjustment and optimisation of operational conditions to reach the best performance of a matched agent pairs.



**Figure 31** Open chip experimental workflow starts with XY-coordinates recording of the printed spots', the three analysis wells of the platform are subsequently filled with 100 $\mu$ L of sample of interest. In the following step, the recorded coordinates are imaged under TIRF illumination during 2hrs incubation every 30-60 min at room temperature.

The analyses performed on the Open chip platform are relatively straightforward and comprise four steps, Figure 31. Firstly, the XY coordinates of the microarrayed spots of different capturing agents were recorded on the programmable microscope stage (Nikon, Japan) with the NIS Elements software (Nikon, Japan) and imaged under a brightfield illumination. In the next step, the wells of the microfluidic platform were filled with 100  $\mu$ L of previously prepared samples (described below). Once samples were transferred into the chip, the filled device was immediately sealed in the case to prevent the solution evaporating. The signal readout from the pre-recorded coordinates of the spots was performed under TIRF during 2 hours of incubation every 30-60 minutes. The collected data, a set of 16-bit raw images with a resolution of 512x512 pixels, were further analysed with FIJI software to determine the single molecule count per image (data analysis was described in detail above). The reagents resulting in the highest signal were subsequently chosen for the MAC chip device to execute a second round of antibody screening.

Unlike the Open chip, the MAC chip enables evaluation of the assay performance in a single cell regime. Since the MAC chip device is intended for the final application and is distinctive from the Open chip, the experimental pipeline differs notably too. The schematic of sample analysis with the MAC chip device is illustrated on the Figure 32.



**Figure 32 a) MAC chip experiments start with printed spots' XY-coordinates recording and the platform filling with the background solution (black). b) The cellular solution (green) is then perfused through the main channel of the design where the cells of interest are optically trapped and corralled into the cubicle of analysis chamber. c) Prior to the laser-induced cellular lysis, the coordinates of the spots are imaged under TIRF. In the post-lysis procedure, the signal is TIRF imaged during 2hrs of incubation time**

Experiments were performed optically and based around a standard inverted microscope Nikon TI-E (Nikon, Japan) using a 60 $\times$ , NA=1.49 oil immersion objective. The precise XY



coordinates of the printed microspots in each MAC chip chamber were recorded on the programmable microscope stage (Nikon, Japan) and imaged under bright field. Roughly 50  $\mu\text{L}$  of background solution (described below) was pipetted on the chip's inlet and outlet to subsequently fill the platform in the vacuum. The device filling with background solution before cell handling and analysis facilitates optical trapping and reduces background signal from non-specific interactions due to BSA surface coating/blocking, Figure 32 a. Once filled with the background solution, the device was returned to the microscope stage and connected to a programmable syringe pump (Labsmith, USA) via glass capillary. The solution containing the cells was subsequently flowed down the main channel at 5  $\mu\text{L}/\text{min}$ . The cells were then transferred from main channel into the cubicles of the analysis chambers by optical tweezer manipulation and imaged under the brightfield. The optical traps were generated by a continuous wave Ytterbium fibre laser (YLM-5; IPG Photonics, UK) with a spectral output of 1070 nm and operational power of 0.5-0.7 W. The beam was focused through the Nikon 60x objective (Nikon, Japan) enabling dielectric particles like cells to be held close to the focal point of the light. The trapped cells were individually transferred into the analysis chambers via translating the motorised stage. The imaging of the pre-recorded antibody spot coordinates with TIRFM followed the cellular trapping to estimate the background signal of the immunospots before the lysis step. The corralled single cells were optically lysed using a 6 ns laser pulse from a Q-sw Nd:YAG laser (Surelite SL I-10, Continuum, USA) at  $\lambda=1064$  nm and 14  $\mu\text{J}$  energy. The applied pulse produces a cavitation bubble 10  $\mu\text{m}$  above the cell which expansion leads to the mechanical shearing of cellular membrane and consequently, releasing the encapsulated nuclear and cytoplasmic contents into the analysis chamber<sup>31</sup>. This lysis method preserves native protein states and protein-protein complexes<sup>109</sup>. To reach a thermodynamic equilibrium between assay and the analyte, the microfluidic device was incubated for 2 hrs. During the incubation, the microspots were imaged under TIRF illumination every 30-60 min. The assay readout was performed by TIRF with an electron-multiplied CCD camera (IXON DU-897E, Andor Technologies, Ireland). The fluorescent molecules were excited by a solid state cw laser (MBL-473-200, Laser 2000, UK) at  $\lambda=473$  or 651 nm. The design PDMS superstructures were retrieved at the end of the experiment and sonicated overnight in the detergent solution. Finally, the collected data was analysed using FIJI software to assess the single molecule count for various samples.

### **3.2.2 Chip preparation**

The MAC chip and Open chip manufacturing was carried out in-house and their production involves a multi-step process. The chips represent an assembly of two components sealed together: a cured PDMS superstructure and pre-functionalised, microarrayed cover slide. The manufacturing of both is laid out in detail in the following protocol.

#### **3.2.2.1 Design fabrication**

The MAC chip designs exploited in this research in AutoCAD software (Autodesk Inc.) by Dr Alastair Magness. The mold fabrication is described in detail in 2.3.1 section.

The obtained molds were subsequently filled with a pre-mixed PDMS (Sylgard 184 Silicone Elastomer Kit, Dow Corning) at a ratio of 10:1 precursor to curing agent. The filled wafers were degassed and cured at ambient temperature for 24+ hrs until hardened. It is feasible to accelerate the curing process at elevated temperatures; however, the heat-driven material expansion causes the MAC chip chambers to have no longer a 500 $\mu$ m spacing. Therefore, the preference was given to the slow curing at room temperature. Once cured, the PDMS designs were cut and drilled to form inlet/outlet holes.

The Open chip device has a 3-well format which is obtained by cutting out three 1x0.5cm rectangular openings from the plain, cured PDMS by scalpel. To remove the contaminants from the gel surface, the chips are plunged into detergent solution (1% Alconox, Alconox Inc), sonicated for 1 hr, rinsed with water and dried with nitrogen.

#### **3.2.2.2 Slide preparation**

##### **3.2.2.2.1 Coverslip functionalisation and passivation**

Protein analysis at a single-molecule resolution requires slides with a high-quality surface passivation<sup>110</sup>. The surface passivation suppresses high background fluorescence from non-specifically interacting debris and avoids glass impurities-induced malfunction and denaturation of immobilised proteins<sup>110</sup>. Protein adsorption into bovine serum albumin (BSA) blocked surfaces has been found to yield a relatively noisy background for a single molecule protein study and therefore, there was a need in a less adhesive surface passivation technique<sup>110,111</sup>. The introduction of surface PEGylation (or polyethylene glycol surface coating)

decreases protein adsorption to an undetectable level and has universally become the method of choice for single molecule fluorescence analysis <sup>110</sup>.

Previous work carried out in the group compared the performance of three different functionalised surfaces in terms of the signal-to-noise ratio and the suitability for the antibody and antigen pairing <sup>49</sup>. The tested surfaces are commercially available Schott Nexterion Type H, PolyAn 3D functionalised slides and an in-house custom made 'PEG-Neutravidin<sup>®</sup>' slide. The substrate generated with an in-house custom protocol has been determined to have an optimal surface for all our research purposes.

A multi-step treatment was employed to produce 'PEG-Neutravidin<sup>®</sup>' coverslips with functionalised and passivated surfaces. The process can be subdivided into 4 sequential procedures: cleaning/hydroxylating/etching, APTES coating, surface passivation and Neutravidin<sup>®</sup> coating.

The purpose of the first step is to remove background fluorescent molecules and introduce hydroxyl (-OH) groups to the surface. To obtain clean and -OH modified coverslips, the slides were firstly rinsed 3 times with deionised water and 1M KOH solution, and subsequently sonicated in the hydroxide solution for 20 min. In the next step, the KOH solution disposal was followed by triple rinsing the slides with acetone and sonication in the solvent for another 15 min. Since it is critical to achieve a highly hydrophilic surface prior to the amino-silanisation reaction <sup>110</sup>, it was additionally etched with 1M KOH for another 20 min and rinsed with deionised water afterwards.

The surface functionalisation step generates the amine groups on the surface that further can be conjugated with PEG molecules. The amino-salinization of the slides was obtained by sonicating them in methanol for 20 min and subsequently incubating in 1% (3-Aminopropyl)triethoxysilane (APTES, Sigma-Aldrich, UK) solution. During the 20 -min -long incubation, the slides were sonicated once for a minute to ensure an even distribution of amines on the surface. The functionalised slides were subsequently rinsed with methanol, water, dried with nitrogen and stored until the next step at 4°C in a parafilm-sealed container.

The preparation of the PEGylation solution for the surface passivation involved mixing of 5-15mg of biotin-PEG-SVA with 50mg of mPEG-SVA (M<sub>w</sub> 5000, Laysan Bio, USA) in 400µL of 1 mM NaHCO<sub>3</sub> buffer. The surface passivation initiated with delivering 80 µL of

mPEG/biotin-PEG-SVA mixture onto the functionalised coverslip surface and pairing (sandwich-aligning) it immediately with another functionalised slide over the solution. The sandwich assemblies were subsequently incubated in the dark for 2hrs to provide PEG molecules attachment to the surface. The slides, upon the incubation process, were rinsed with water, dried and stored until next procedure.

Finally, the passivated cover slips were NeutrAvidin® coated to bridge the biotinylated surface with biotinylated proteins or DNA. This step was required for biotin modified capturing agents only. Due to its high binding affinity to biotin, NeutrAvidin®, an avidin derived protein, is extensively exploited to provide agents' immobilisation and fixation on substrates <sup>112</sup>. According to the current protocol, the 80µL of the NeutrAvidin® at 0.1 mg mL<sup>-1</sup> in Dubelcco's phosphate buffered saline (PAA Laboratories GmbH, USA) solution was dispensed on the PEGylated coverslip which followed by pairing with another slide and incubation for an hour in the dark and humid environment. After the treatment, the slides were washed with water, dried with nitrogen and stored at 4°C until the next step.

### 3.2.2.2.2 Slide printing

FOXO3 assay development involved testing the performance of different reagent pairs to identify those with the highest signal-to-noise ratio. The microarrayed capturing agents exploited for the FOXO3 assay development are listed in Table 2.

**Table 2 The list of the tested capturing agents to establish the FOXO3 assay**

Assigned Name	Commercial name	Additional information on content
CA1	DNA, Sigma Aldrich	Lyophilised
CA2	NOVUS	PBS, no preservative
CA3	D12, Santa Cruz	Each vial contains 200 µg IgG <sub>1</sub> kappa light chain in 1.0 ml of PBS with < 0.1% sodium azide and 0.1% gelatin
CA4	AbCAM	PBS 49%, Sodium azide 0.01%, Glycerol 50%, BSA 0.05%
CA5	D19A7, Cell Signalling	10 mM sodium HEPES (pH 7.5), 150 mM NaCl, 100 µg/ml BSA, 50% glycerol and less than 0.02% sodium azide
CA6	Monoclonal, ProteinTech	PBS with 0.02% sodium azide and 50% glycerol pH 7.3
CA7	Polyclonal, ProteinTech	PBS, no preservative
CA8	mab6165, RnD	Lyophilized from a 0.2 µm filtered solution in PBS with Trehalose, resuspended in PBS

#### 3.2.2.2.2.1 Primary antibodies biotinylation

The selected antibodies were biotinylated to improve the capture antibody immobilisation on the NeutrAvidin coated slide. In addition to having a high affinity towards avidin-like proteins, when biotin is covalently attached to proteins there is a low probability of harming their functional properties<sup>113</sup>. The protein biotin conjugation was executed with Biotin (Type B) Fast Conjugation Kit (ab201796, Abcam, UK) following the Abcam protocol.

#### 3.2.2.2.2.2 Microarray production

In this research, the microarrays were fabricated using a contact pin printing because this method has a low requirement for printing sample volume and a good control of the transferred sample amount.

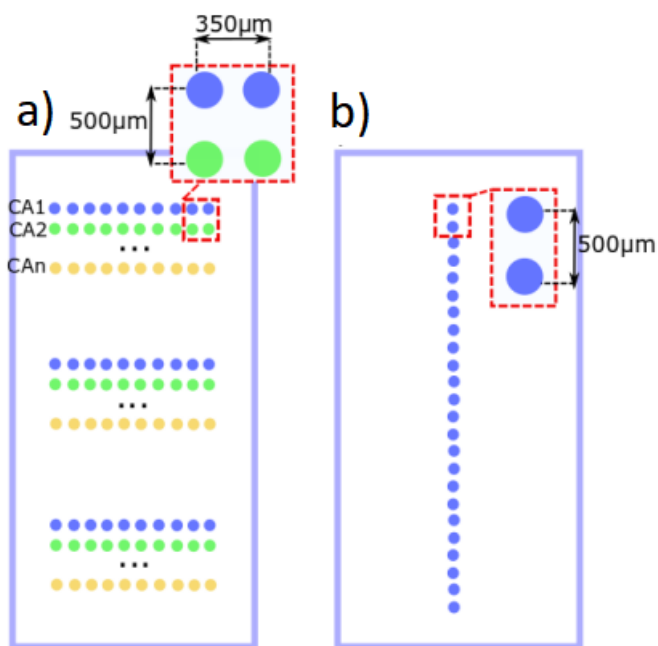
Prior to the printing, 10  $\mu$ L of pre-mixed samples with a printing buffer were transferred into the 384-microwell plate. The effect of 1x ArrayIt (ArrayIt Corporation, USA) and 3x SSC (saline sodium citrate)/1.5 M betaine printing buffers on immunosorbents generation and performance was tested. The printed capturing agent concentration varied between 0.1-1 mg/mL depending on the capture affinity, composition and additives of the sample. The biomaterials were deposited on the slides using OmniGrid Micro microarrayer (Digilab, UK) and 946MP2 pin (ArrayIt Corporation, USA).

As it is stated in the manufacturer's technical description<sup>42</sup>, the selected pin yields spots with up to 62.5  $\mu$ m diameter which was found to fit into the CCD camera field of view; however, the actual printed patch dimensions were observed to depend on the loaded sample composition and printing conditions. The relative humidity for the printing was usually set to 40-55% to avoid sample rapid evaporation and obtain a spot with desired dimensions.

The microarrays were addressed on the functionalised planar substrates in 2 different fashions to perform analyses for different purposes. The Figure 33 shows the microarrays designs for the Open and MAC chips. Before printing either of microarrays, the program executes a pre-print procedure dispensing a series of 30 spots for each capturing agent to adjust the spot blotting and obtain a better quality of the array.

The Open chip microarray is composed of ten-spot-strings printed for each capturing agent 3 times. The Open chip algorithm limits printing of up to eight different capturing agents

per slide due to the dimensions of the substrate slide. To prevent cross-contamination of distinct microarrayed samples for the Open chip, the intermediate washing step was performed between different samples loading. In turn, the MAC chip microarray represents a string of 50 spots with a spot-to-spot distance of 500  $\mu\text{m}$ . Once the coverslips were microarrayed, they were stored in a sealed container at 4°C before use.

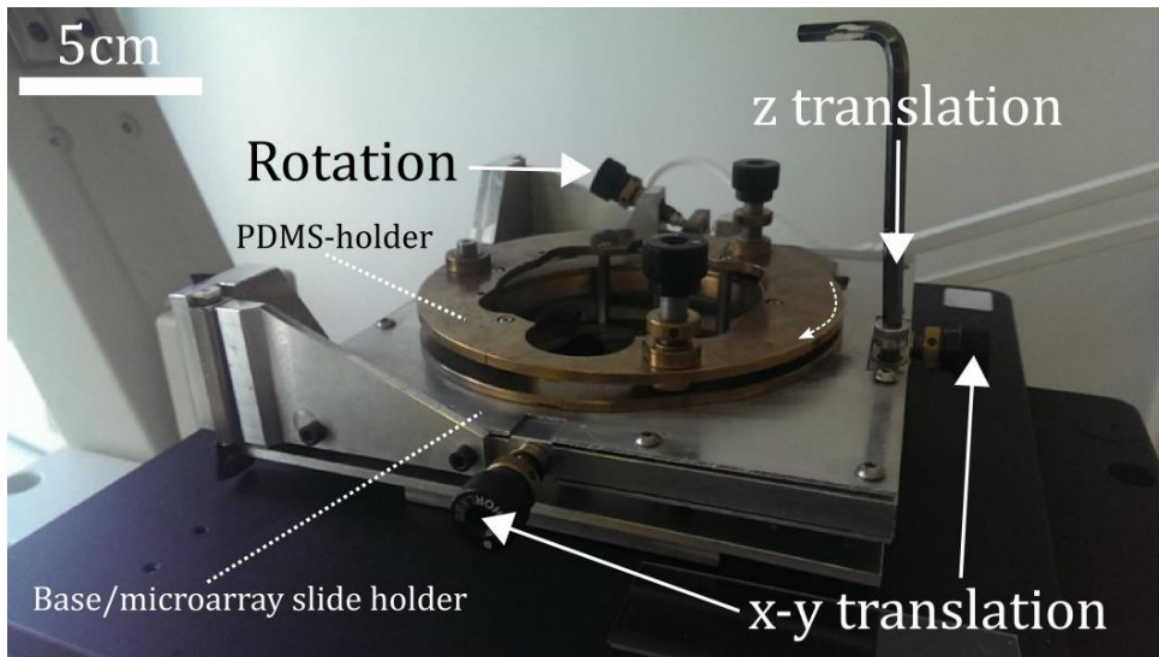


**Figure 33** The microarray design of different capturing agents (CA1, CA2 , ..., CAn) for a) Open chip b) MAC chip

### 3.2.2.3 Aligning and storing

The two components, PDMS design and microarrayed passivated slide, were subsequently aligned to manufacture the ready-to-use MAC or Open chips. The alignment procedure was performed under the inverted microscope (Nikon, Japan) using a custom-built alignment rig (Figure 34). During this process the position of the analysis chambers were adjusted to ensure the microarrayed spots were placed in the centre. The PDMS piece was translated in x,y,z dimensions and rotated in x-y plane by manipulating tuning screws of the alignment rig. Prior to the alignment, the PDMS underwent a plasma treatment to obtain a more robust bond between the glass slide and the polymer providing the device with strengthen integrity and minimising the chance for its delamination during the experiment. It is possible

to reuse the PDMS structure after the experiment by separating it from the substrate and cleaning it as described before.



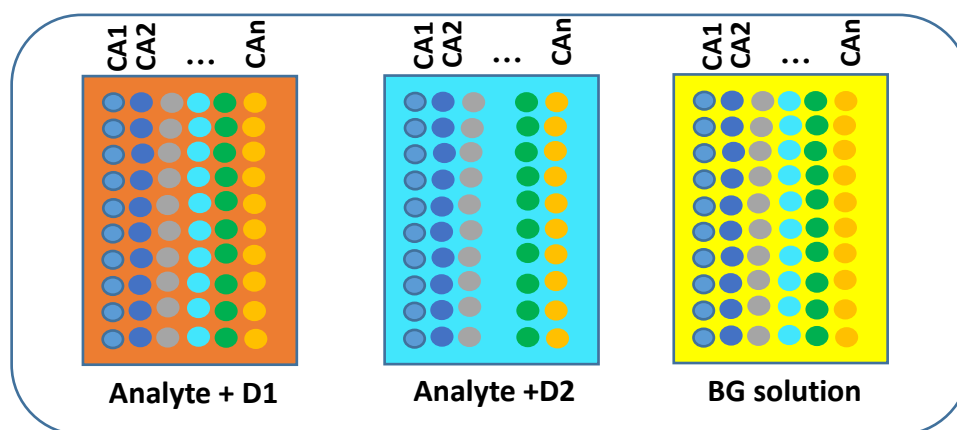
**Figure 34** The custom-built alignment rig to assemble microarrayed glass slides and PDMS design for MAC chip fabrication. The adjustment screws allow to control and tune the position of the PDMS piece before it contacts the planar substrate

### 3.2.3 Devices filling and cell handling

#### 3.2.3.1 Samples analysed with the Open chip

The Open chip was used to analyse the performance of different sensing and detecting reagents with recombinant protein solutions at  $10^2$ - $10^7$  molecules/nL or a whole cellular lysate.

The 3-well format of this platform allowed simultaneous measuring of signal from three different samples. Although the samples loaded into the wells varied depending on the purpose, Figure 35 exemplifies one of the experiments performed for the study.



**Figure 35 Example of the Open chip utilization: first two wells loaded with the samples containing analyte + detecting agents (D1 or D2) whereas the third well was used to measure the non-specific binding with a background (BG) solution.**

The control or background solution was prepared diluting the fluorescently tagged antibody, either D1 (Anti-Foxo3 antibody EPR1949Y, Alexa Fluor 647) or D2 (FKHRL1 Antibody D-12, Alexa Fluor 488, Santa Cruz), to  $10^6$  molecules/nL in a sterile 4% pBSA solution. To obtain the sterile 4% pBSA solution, 0.2g of BSA were dissolved in 5mL of Phosphate Buffered Saline (PBS, Dubelcco's Corning) followed by the subsequent solution purification using 0.45  $\mu$ m pore size filter.

The solutions of recombinant protein at  $10^2$ - $10^7$  molecules/nL were prepared from 0.26 mg/mL FOXO3 recombinant protein (MRC PPU Reagents and Services, University of Dundee) by serial dilution in a background solution.

The cellular lysates were generated using Sandwich ELISA lysis buffer (1X) (PathScan®, 7018S, Cell Signalling Technology, UK) from 70% confluent H1975 cells (adenocarcinoma, non-small cell lung cancer) cultured at normal conditions (described below). The cellular extracts were obtained following the manufacturer's protocol. The active lysing component in the current lysis buffer is 1% Triton which ruptures (solubilises) cellular membranes while preserving the retrieved protein in its native structure and conformation.



### **3.2.3.2 Samples analysed with the MAC chip**

#### **3.2.3.2.1 Background and standards solutions**

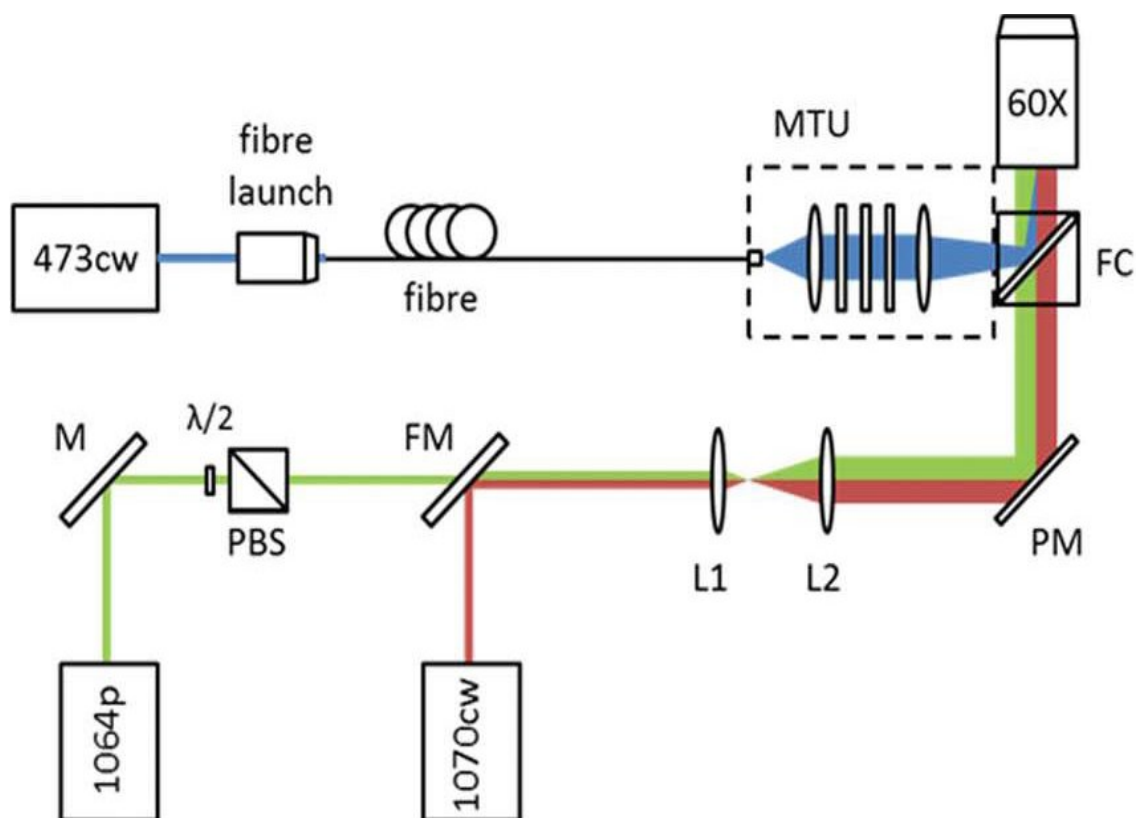
The background and recombinant protein at  $10^2$ - $10^7$  molecules/nL were produced with secondary antibody D1 at  $10^6$  or  $10^7$  molecules/nL. The sample preparation is identical to those used for the Open chip analysis.

#### **3.2.3.2.2 Cell culturing and handling for analysis**

The experiments were carried out using a human lung cancer cell line (H1975), breast adenocarcinoma (MCF7) and B cell lymphoma (Toledo). The H1975 and Toledo cells were cultured at 37°C and 5% CO<sub>2</sub> in RPMI-1640 Medium (RPMI, Gibco, UK) with the addition of 10% Foetal Bovine Serum (FBS, PAA, UK) whereas the MCF7 were grown in 10% FBS supplemented DMEM (Dulbecco's Modified Eagle's Medium, Gibco, UK) at the same culturing conditions. Prior to the analysis, the cells were incubated in 6 mL of medium for ~48 hours to reach about 70% confluency. Shortly before the experiment the cells were detached from the culture flask using 0.5 mL of Accutase (PAA, UK) and diluted up to 5 mL with media. 1mL of cell suspension was immediately transferred into Eppendorf and centrifuged at 300rcf for 5min. The cellular pellet was resuspended in 50µL of secondary antibody solution at  $10^6$  or  $10^7$  molecules/nL. The solution was subsequently loaded into the main channel of the microfluidic platform to perform the experiment and collect the data.

#### **3.2.3.3 Readout and data acquisition**

The assay readout was performed by total internal reflection microscopy (TIRFM) with an electron-multiplied CCD camera (IXON DU-897E, Andor Technologies, Ireland). The fluorescent molecules were excited by a solid state cw laser (MBL-473-200, Laser 2000, UK) at [ $\lambda$ =473 or 651nm]. The optical set-up is displayed in Figure 36.



**Figure 36** The experimental set-up configuration shows the coupling of the optical peripherals to the TIRF microscope to manipulate and perform readout of a sample. Taken from <sup>114</sup>

The fluorescence of single molecules at the capture spot was imaged before lysis, for background signal quantification, and during 2 hours post-lysis, to directly measure protein content in single cells. Images were either taken in time series, to observe the signal increase over a certain period of time, or in single time-points upon the system reached equilibrium. The collected raw data represented a sequence of single molecule fluorescence images that were taken from the printed antibody spots. The data acquisition was followed by the image processing and single molecules counting with the FIJI/ImageJ software.

### 3.3 Results and Discussions

The search for a matched reagents pair with selectivity and sensitivity high enough to measure FOXO3 protein in single cells was initially conducted using the Open chip platform. In the preliminary study the performance of 5 capturing agents (Listed in Table 2 CA1-CA5) and 2 detection antibodies (D1, D2) was tested using recombinant protein or cellular lysate. The detection antibody concentration was kept at  $10^6$  molecules/nL and microarrays of

different capturing agent were printed with SSC/betaine buffer at rh=40-55%. The assays readouts were performed for recombinant protein at  $10^2$ ,  $10^3$  and  $10^7$  molecules/nL. The best matched pairs were selected based on the microspot morphology, background signal and the single molecule counts obtained after the background (blank sample signal) subtraction. The Open chip data was generated from at least two separate experimental runs.


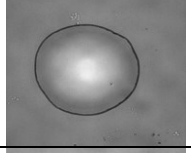
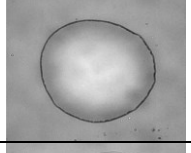
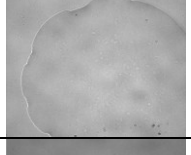
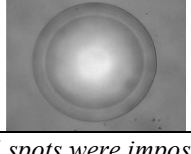
### **3.3.1 Capturing agents' spots morphology analysis**

The capturing agents' spots were first examined under brightfield illumination to characterise the printed microarray spot morphology. The spot shape, size and form (hydrogel, crystallised form and etc.) serves as a preliminary indicator for the agent's performance and also reveals the suitability of chosen printing conditions. The ideal capturing agents' spots were expected to have a circular shape, fit the field of view of EMCCD camera (512×512 px) and have an even distribution with no defects or discontinuities.

The Table 3 shows an average area and circularity of at least 15 spots for each tested capturing agent. All immunospots except for CA4 were found to fit the setup field of view limits indicating the suitability of the chosen printing materials, methods and conditions. The spots generated with CA4 had a stretched morphology and size larger than the camera's field of view which inevitably led to a loss of information upon single molecule counting. To obtain a microarray with smaller spot dimensions for CA4, the printing humidity was further reduced to 40%; however, this endeavour to diminish the spot size was found to be not sufficiently efficient (data not shown). The reason for the CA4 to produce microarrays of specific morphology might find its explanation in the antibody composition (Table 3).

It was observed that spots of highest circularity were obtained with CA1 and CA5 resulting in  $0.85 \pm 0.05$  for both. The CA2 and CA3 yielded spots with approximately the same area but noticeably different circularity.

**Table 3** The physical parameters of the microarrayed spots for different capturing agents

Capturing agent	Image of the spots	Measurements	
		Area $\pm$ SD	Circularity $\pm$ SD
CA1		$3.5 \times 10^3 \pm 0.3 \times 10^3$	$0.85 \pm 0.05$
CA2		$5.1 \times 10^3 \pm 1.1 \times 10^3$	$0.80 \pm 0.08$
CA3		$5.6 \times 10^3 \pm 0.4 \times 10^3$	$0.68 \pm 0.15$
CA4		NA*	NA*
CA5		$6.4 \times 10^3 \pm 1.5 \times 10^3$	$0.85 \pm 0.05$

\* NA the measurements of CA4 spots were impossible to acquire due to the area exceeding the field of view

### 3.3.2 Background analysis

The assay background measurement is a crucial indicator of its sensitivity, signal-to-noise and LOD determination. Low signal-to-noise ratio is frequently a limiting factor for microarray sensitivity in a single molecule regime. It is likely for the true single molecule signal to be lost in the high noise of non-specific binding and therefore, the ideal assay has to have a low background level.

The signal from blank samples was compared between the tested assay systems on the Open chip platform, Table 4. The TIRF readout of the background solution under 647nm illumination showed in general a lower signal than the one obtained under 488nm, meaning that there is less non-specific interaction with D1 than with D2 for the tested capturing agents. Most of the tested immunosorbents with D1 yielded a signal of <100 binding events; the background fluorescence of the CA4 with D1, however, showed the highest non-specific signal comparing with other candidates. The main source of the background signal for the Open chip

set of experiments was considered to originate from either a non-specific interaction between the detection and sensing agents or autofluorescence of the immobilised capture agents.

**Table 4 The mean background signal with standard deviation for 10 spots of each tested capturing agent (CA1-CA5) with detection agents (D1 and D2) in Open chip experiments**

Capturing agent	Average background signal, binding events number	
	D1	D2
CA1	10±8	82±74
CA2	72±15	752±74
CA3	67±9	79±10
CA4	251±46	74±64
CA5	36±12	42±29

### 3.3.3 Assays performance comparison using FOXO3 recombinant protein

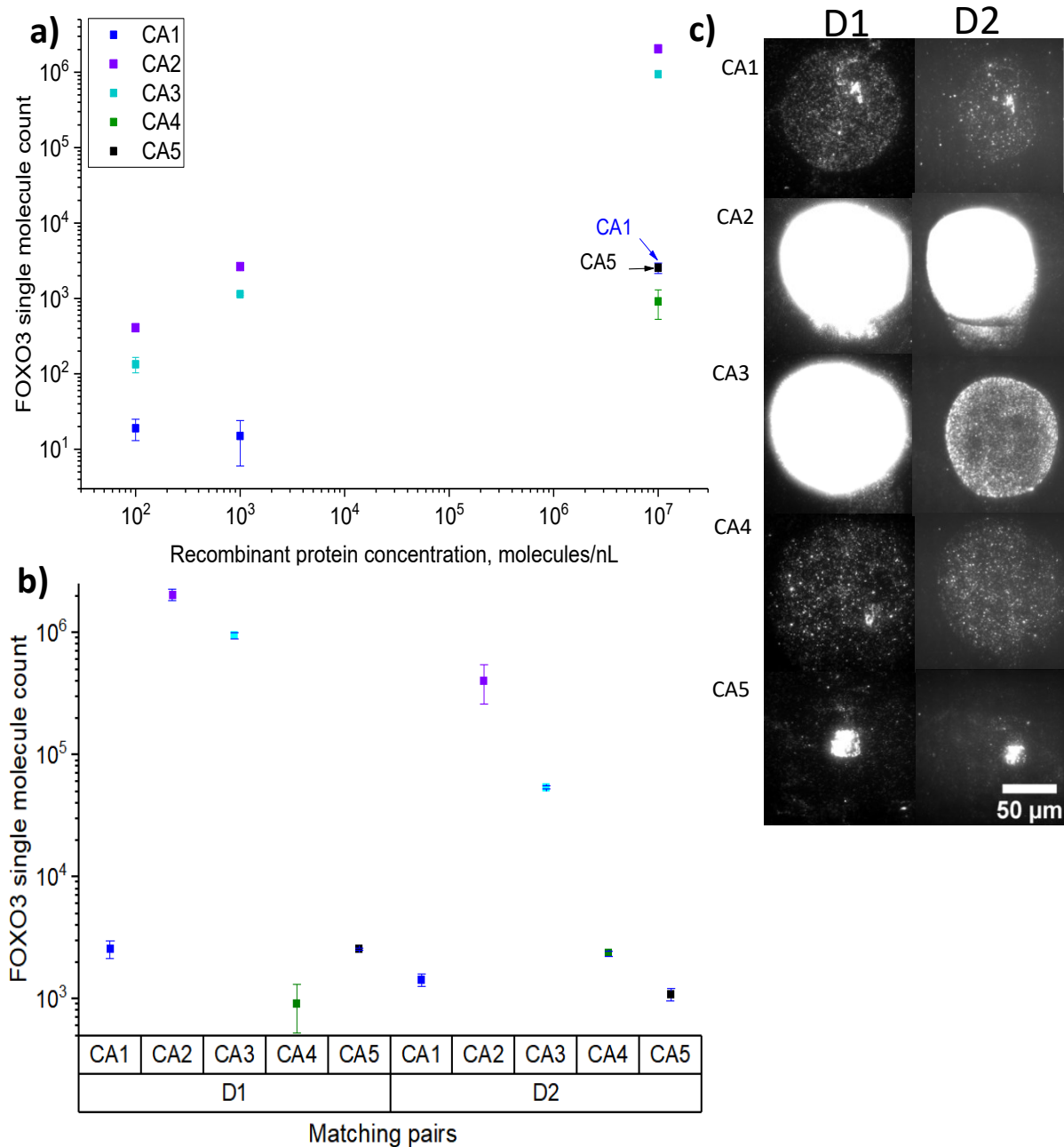
The screening of different capturing agents CA1-CA5 with detection antibodies D1-D2 was implemented to identify the best matched sandwich pair of agents for “pulled-down” FOXO3 protein evaluation. The performance of 10 different pairs was compared on the basis of single molecule signal above background at FOXO3 recombinant protein concentration of  $10^2$ ,  $10^3$ ,  $10^7$  molecules per nL.

The data (Figure 37 a) reveals that CA2 and CA3 outperformed all the other capturing candidates in yielding the highest single molecule signal above background at recombinant protein concentration of  $10^7$  molecules/nL with the D1 detection antibody; resulting in mean single molecule count of  $2 \times 10^6 \pm 2 \times 10^5$  and  $9 \times 10^5 \pm 5 \times 10^4$ , respectively. The binding signal of CA1, CA4 and CA5 with D1 was found to be lower by 3 orders of magnitude than the fore-mentioned antibodies (at recombinant protein concentration of  $10^7$  molecules/nL). Despite having a good spot morphology and low background signal, the CA5 demonstrated relatively poor antigen pull-down efficiency even at high analyte concentration yielding readings of only  $\sim 2.5 \times 10^3$  single molecules. The best performing agents, CA1-CA3, were further selected to assess their sensitivity in an Open chip assembly by decreasing the recombinant protein

concentration to  $10^3$  and  $10^2$  molecules/nL. As it was expected, the CA2 and CA3, resulting in prominently higher single molecule count, demonstrated higher sensitivity and affinity to the analyte than CA1.

The performance of CA1-CA5 capturing agents with D2 detection antibody was observed to result generally in a lower single molecule count than D1, Figure 37 b.

The Figure 37 c exhibits the raw data of CA1-CA5 capturing agents upon 2 hrs of incubation with the analyte at  $10^7$  molecules/nL. The images of immunosorbents demonstrate the bound antigen distribution within the microspots which can be directly correlated with active binding sites allocation within the spot. Since the best performing antibodies CA2 and CA3, showed an even distribution of fluorescence within the spot, the performance of microarray was therefore implied to be heavily conditioned by the homogeneity of the primary agent allocation within the immunospot. The data suggests that visibly uneven distribution of the active binding sites within the CA5 resulted in a lower FOXO3 protein recovery because the bound antigen accumulation was mostly observed in the spot center showing low fluorescence on the spot edges. The peculiar CA5 spreading pattern within the micropatch could be a resultant of either antibody composition or a not optimised printing buffer.



**Figure 37** a) Mean single molecule counts of recovered FOXO3 recombinant protein by CA1-CA5 capturing agents with D1 detection antibody b) The comparison of FOXO3 mean single molecule count between different capturing/detection agents pairs, whiskers correspond to standard deviation of the signal between different spots c) The active sites distribution within microspots with D1 and D2 at recombinant concentration  $10^7$  molecules/nL

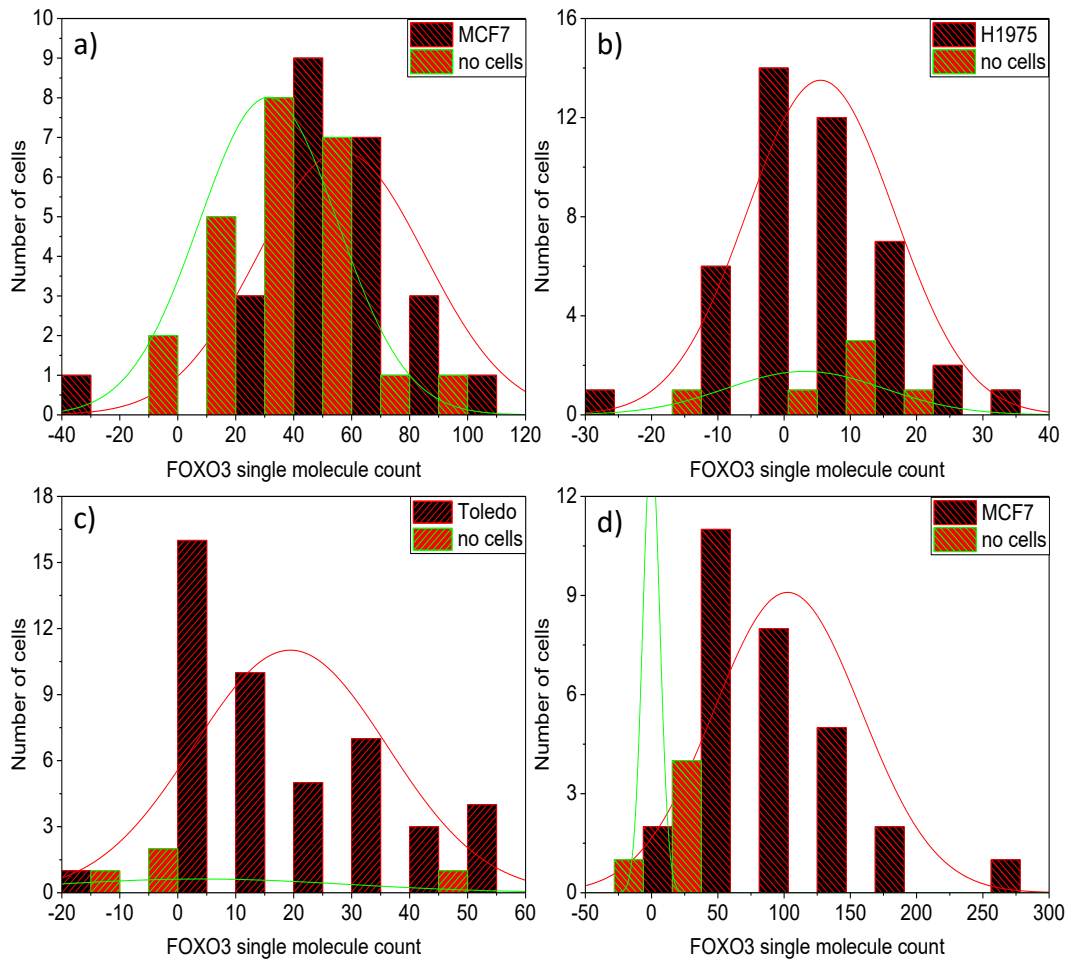
### 3.3.4 Single cell analysis using MAC chip

The best performing antibody pairs (CA2/D1 and CA3/D1), having selected based on the results of the Open chip experiments, were further tested on the MAC chip to determine

the FOXO3 expression in single cells of different cell lines. Two separate repeat MAC chip experiments with CA2/D1 were conducted with MCF7, H1975 and Toledo cell lines under normal culture conditions. The CA3/D1 MAC chip assay was implemented on MCF7 cell line only. Also, multiple chambers were left empty to observe if photobleaching has an effect on loss of single molecule content as it is usually a problem for time-lapse fluorescence microscopy.

The Figure 38 shows a poor performance for both pairs of antibodies. The insignificant difference in signal was observed between chambers with and without cells. Surprisingly, the CA2, resulting in high single molecule count for the Open chip experiments, showed a negligible or no signal increase post cellular lysis (Figure 38 a, b and c). In contrast, a small fluorescence increase was registered for the CA3 (Figure 38 d) despite its evidently lower sensitivity observed in the set Open chip experiments with the recombinant protein. However, due to the insignificant binding signal, the selected antibody pairs, CA2/D1 and CA3/D1, were found not promising as a potential system for FOXO3 expression evaluation in single cells.





**Figure 38 a) FOXO3 single molecule count for MCF7 single cells by CA2/D1 system b) FOXO3 single molecule count for H1975 single cells by CA2/D1 system c) FOXO3 single molecule count for Toledo single cells by CA2/D1 system d) FOXO3 single molecule count for MCF7 single cells by CA3/D1 system**

### 3.3.5 Open chip experiments with cellular lysate

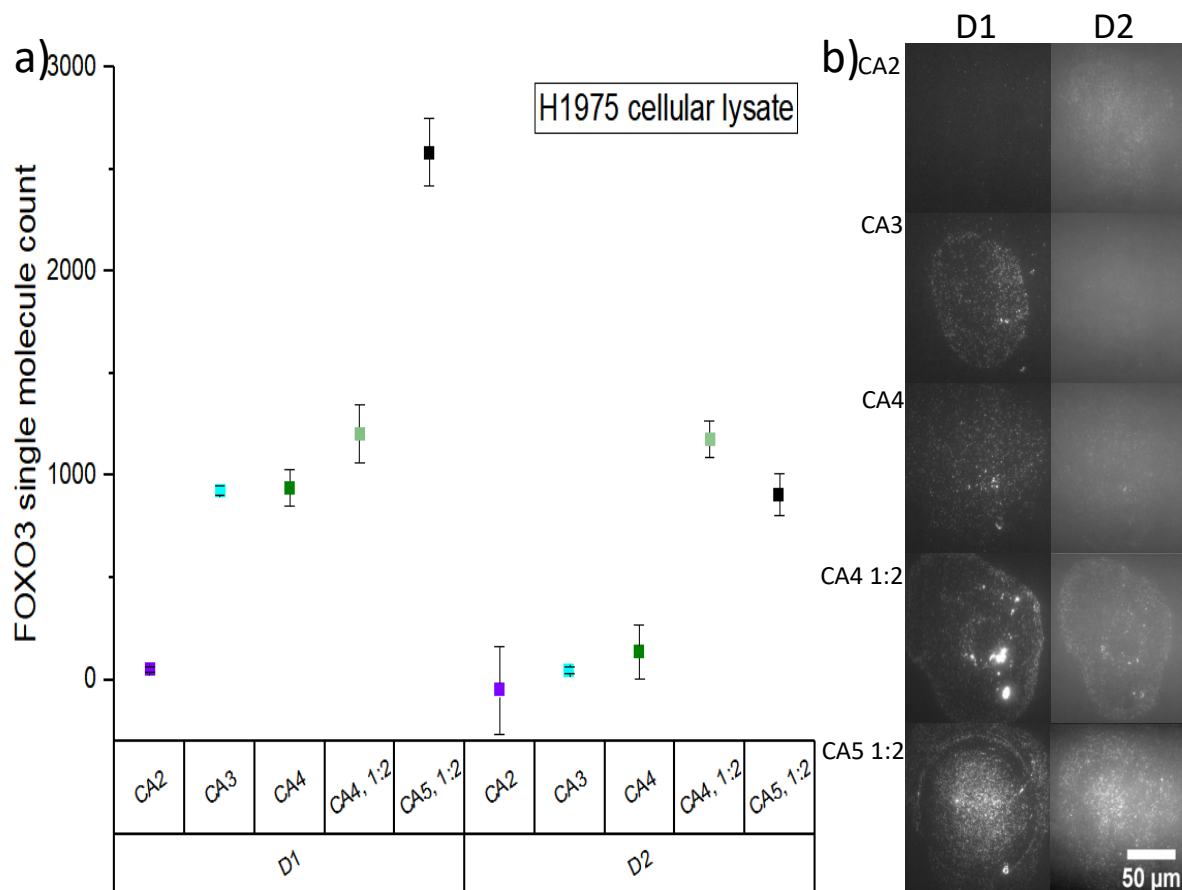
The single cell analyses using MAC chip produced unforeseen results suggesting insufficient sensitivity of the tested assays in the single molecule regime despite the successful performance demonstrated at a low standard concentration with the Open chip. Also, the MAC chip data unexpectedly demonstrated a higher signal for CA3 comparing to CA2 what contradicts the results generated with recombinant protein on the Open chip platform. This experimental outcome required re-testing of the agents again using the Open chip platform but with the cellular lysate instead.

The Open Chip experiments were conducted with H1975 cellular lysate to screen the performance of CA2-CA5 in combination with D1-D2, Figure 39a. All the tested primary antibodies resulted again in the single molecule count to be prominently higher using D1 than D2 which might be explained by a lower affinity of the latter towards the FOXO3 transcription factor. Thus, the D1 antibody was selected for further experiments.

Interestingly, regardless the high sensitivity the CA2 demonstrated in the recombinant protein experiments, it failed to bind the FOXO3 transcription factor in cellular extracts as efficiently. Such a marked distinction in single molecule count between different analyte samples could be explained by the conformational discrepancy between the proteins of different origin. Hence, it is believed that FOXO3 of human origin (like H1975 cell line) has a different native structure than the FOXO3 recombinant protein generated in *E. coli* bacteria. The antibody dysfunction in a cellular lysate environment was presumably due to a steric hindrance resulting in unfavourable conformation for ligand-receptor interactions precluding the epitope recognition and sensing by the CA2. Since the objective of this project was to measure the protein level in human cells, the CA2 was dismissed as a potential candidate for single cell analysis.

The CA3 was observed to yield a considerable signal above the background; however, the MAC chip experimental runs using CA3/D1 assay showed a low number of single molecules inferring that the antibody was not sensitive enough for the single cell application. The prominent single molecule count in bulk lysates for CA3 was, nevertheless, observed because the extract was produced from a bulk solution containing thousands of cells which upon the lysis release the protein into media giving the concentration sufficient to overcome the assay's limit of detection.

The signal obtained from CA4/D1 assay was noticed to be comparable with CA3/D1, however, the background fluorescence was observed to be roughly 15x higher and the spots were of stretched morphology not fitting the field of view (Figure 39b). Thus, the obtained results imposed to neglect the CA4 as a potential agent for the single cell analysis.



**Figure 39** a) Testing of capturing antibodies performance with detection antibodies D1 and D2 for FOXO3 protein pull down from H1975 cell lysate b) TIRF images of different capturing agents spots with D1 and D2 after cellular lysate addition

### 3.3.6 Finding the reason for the failure to develop the FOXO3 assay

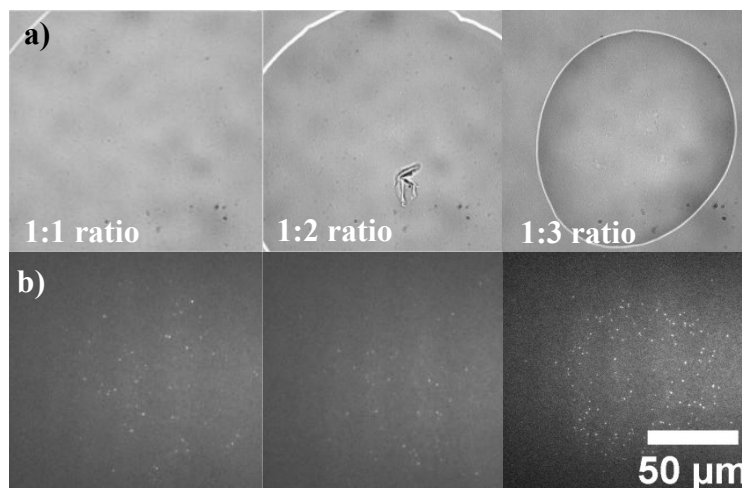
A meagre choice of commercially available reagents for FOXO3 protein analysis and unsuccessful endeavour to establish a well-operating assay system necessitated to scrutinise the substrate chemistry, printing buffer and antibody composition.

#### 3.3.6.1 Microarrayed agents' composition influence

As it is seen from Table 2, both CA4 and CA5 stock solutions contain 50% of glycerol. This excipient is frequently added to biomaterials as a cryo- or lyo-preservative to extend the product shelf life. The literature provides rather contradictory conclusions about the effect of glycerol on a microarray fabrication. While some sources display a positive influence of glycerol on the print due to its hygroscopic properties<sup>115-117</sup>, others report evidence of signal decrease<sup>39</sup>. To check this excipient influence on the microarray quality for our system, the

glycerol containing antibodies, namely CA4 and CA5, were diluted with printing buffer in a ratio of 1:1-1:3 to obtain final concentration of the hygroscopic additive in the print to be 25-12.5%. The diluted capturing agents were tested with D1 and D2 for H975 cellular lysate analysis.

The Figure 39a illustrates an upward trend for single molecule count as the CA4 antibody is further diluted. The CA4/D1 combination yielded the signal increase by approximately 30% as the capturing antibody/printing buffer ratio was reduced from 1:1 to 1:2 resulting in average of  $940 \pm 88$  and  $1204 \pm 140$  molecules, respectively. The capture dilution produced even more pronounced signal boost with D2 yielding mean signal of  $135 \pm 133$  molecules for 1:1 ratio and  $1179 \pm 88$  molecules for 1:2 ratio. Additionally, the CA4 dilution led to the spot size shrinking and nearly 2-fold background decrease (data not shown). The Figure 40 demonstrates the glycerol effect on the spot morphology and IgG molecules distribution within the microspot. As can be observed, the CA4 spots at 1:1 and 1:2 ratios exhibit a stretched or smeared morphology with dimensions larger than the camera's field of view. The extended area of the microspots at higher glycerol concentrations was presumed to occur due to the excipient effect on the balance between cohesive and adhesive forces affecting the surface tension of the droplets' interface and leading to a higher wettability and lower contact angle<sup>118</sup>. Also, the data assumes that glycerol affects the behaviour of the capturing agents' adsorption by surface tension depression which, in turn, hinders the favourable molecular orientation for analyte binding. Additionally, the experimental results from Fainerman et al have suggested the dependence of surfactant molecules orientation on the interfacial pressure<sup>118</sup>.



**Figure 40 a) The CA4 microspot morphology at different antibody/printing buffer ratios (glycerol content 25%, 16.5% and 12.5%, respectively) b) The TIRF images of the spots taken after 10 min of the cellular lysate addition**

Since glycerol constitutes the CA4 biggest fraction, it was thus hypothesised that the antibody dilution and consequently glycerol content reduction in the print facilitates a smaller spots production with an improved morphology and a uniform deposition of biomaterial. It was also speculated that the spot size affects signal-to-noise ratio yielding a higher background signal for larger spots due to the bigger area exposure to the source of potential non-specific interactions. Moreover, the spots stretched beyond the instrument's field of view resulted in bound single molecule under-counting and misleading signal generation due to infeasibility to acquire and further analyse the missing information.

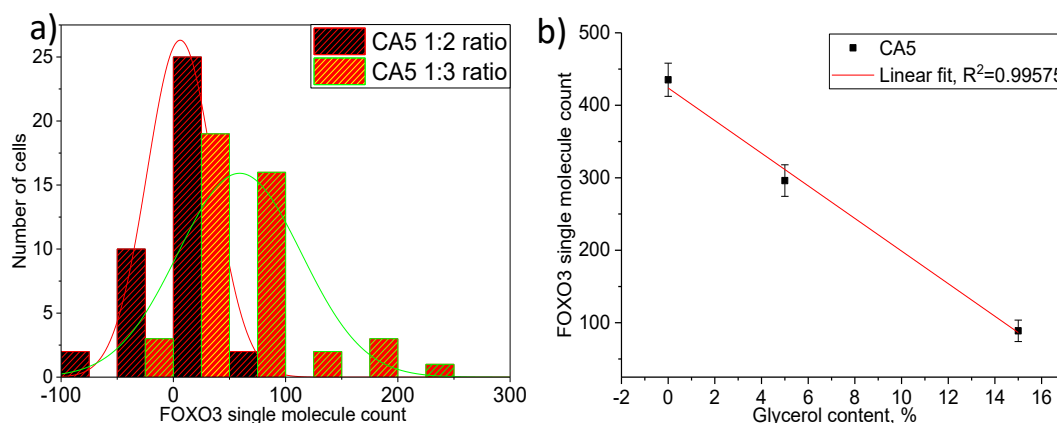
Surprisingly, the CA5 dilution resulted in a considerably more intense signal for the analysed cellular lysate which accounted for  $2584 \pm 166$  and  $905 \pm 102$  molecules for D1 and D2, respectively. The dilution effect of CA5 is clearly visible in Figure 37 c and Figure 39 b. It was observed that active sites distribution within the CA5 spot was no longer confined in the spot's centre but rather allocated somewhat evenly throughout the whole area.

### **3.3.6.2 Effect of capturing agents' dilution in MAC chip platform**

The interesting finding in the experiments with antibody dilution suggested a negative impact of glycerol on the microarrayed antibody performance. To provide evidence for this assumption, a series of MAC chip experiments were carried with CA5.

The CA5/D1 performance was assessed analysing H1975 single cells on the MAC chip at antibody/buffer ratio of 1:2 and 1:3. As expected, the single molecule count was observed to grow as the antibody fraction in the printing solution decreased, Figure 41a. The positive shift in the mean single molecule count was noted for CA5/buffer at dilution of 1:3 in comparison with 1:2 ratio.

To eliminate crowding effect or other additives as a possible reason for the analyte binding signal improve, the customised glycerol free CA5 was obtained from the manufacturer. The effect of the additive on the microimmunoassay for single cell analysis was subsequently investigated comparing the single molecule count between CA5 with different glycerol concentrations in the print: CA5 no glycerol, CA5+5% glycerol and CA5+15% glycerol. What can be clearly seen in the Figure 41b is that the glycerol content increase led to a linear fit of the analyte binding signal which was found to be consistent with the previous observations. It can be concluded that in our microfluidic platform glycerol prevented IgG molecules adsorption to the substrate surface presumably due to surface tension decrease.



**Figure 41 a) H1975 single cell analysis on the MAC chip platform using different CA5 dilutions with D1 antibody b) Mean binding signal of CA5 with no, 5% and 15% of glycerol for H1975 single cell analysis on the MAC chip platform, the whiskers represent a standard error between different chambers**

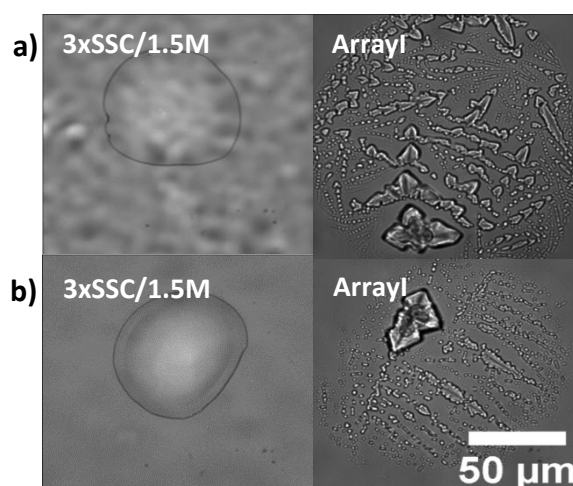
### 3.3.6.3 Printing buffers comparison

The microarray print buffers are directly related to the printed agents' performance determining the likelihood of reliable data obtaining and analysis. However, due to unknown formulation of most commercially available buffers the impact of some additives is yet to be

determined. Also, many vendors optimised the buffers for a limited and particular number of surface chemistries <sup>39</sup>.

Two printing buffers were tested with CA5 and CA8 antibodies (Table 2) to optimise the system and inspect its impact on the analyte binding signal from single cells. The previous trials carried in our group demonstrated two printing buffers, ArrayIt and 3×SSC/1.5M betaine, to be the most suitable candidates for our microfluidic platform <sup>119</sup>. ArrayIt is a commercial buffering system containing a proprietary mixture of ionic and polymeric materials, solvents, viscosity enhancers, and buffering components that stabilises and protects protein samples during the printing procedure. The ArrayIt produces crystallised microspots promoting protein coupling to the substrate and better immobilisation for the functional protein<sup>119</sup>. On the other hand, 3xSSC/1.5M betaine solution is an in-house prepared buffer which facilitates effective reduction of uncontrolled evaporation by forming a microarray of hydrogel spots<sup>120</sup>. The solution evaporation cessation or retardation is a critical factor in the spotting process because it is frequently a cause for an antibody bioactivity impairment and structural damage. The uncontrollable evaporation elicits a rapid solute concentration, ionic strength and pH shifts which might finally deteriorate the antibody performance<sup>115</sup>. Additionally, it was reported for the evaporation to be a primary reason of inter- and intraspot variations <sup>115</sup>.

The tested buffers were compared in terms of spot morphology, inter- and intra-spot variation, background and analyte binding signals. The Figure 42 displays the spots' morphology and size for both ArrayIt and 3xSSC/1.5M betaine.



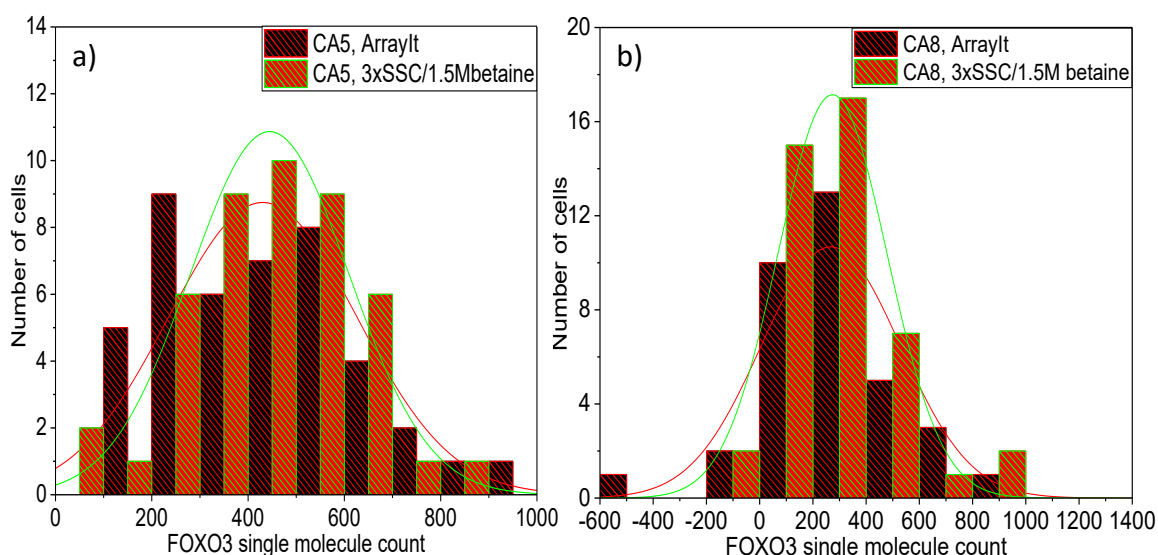
**Figure 42** The spot morphology comparison for ArrayIt and 3×SSC/1.5M betaine print buffers for a) CA5 and b) CA8

The crystallised microspots were found to be almost 1.6-fold bigger than the drops obtained with 3xSSC/1.5M betaine. As it was mentioned earlier the extended antibody-coated surface led to undesirable increase in non-specific binding and as a consequence, ArrayIt background was observed to yield roughly two-fold greater signal than it was for hydrogel spots (Table 5). To improve signal-to-noise ratio, the coated area decrease could be suggested; however, it might also lead to the binding signal fall. Alternatively, the immunospot surface diminishment with corresponding decrease of instrument's field of view might result in signal-to-noise ratio rise<sup>36</sup>.

**Table 5** The mean of background and analyte binding signal for CA5 and CA8 using ArrayIt and 3xSSC/1.5M betaine buffers

	Background signal		FOXO3 single molecule count above background	
	ArrayIt	3xSSC/1.5M betaine	ArrayIt	3xSSC/1.5M betaine
<b>CA5</b>	311±80.9	208±68.8	430±196.1	445±165.2
<b>CA8</b>	579±183.2	338±55.2	267±257.9	285±205.1

The dimensions of ArrayIt spots resulted in inter- and intra-spot variation of 7.7% and 8.5% whereas hydrogel spots produced 6.2% and 5.9%, respectively. Thus, the microspots printed with ArrayIt were found to vary more between the spots of the same batch as well as between batches.



**Figure 43** The comparison of FOXO3 expression in H1975 cells using a) CA5 and b) CA8 microarrays produced with two print buffers, ArrayIt and 3xSSC/1.5M betaine



The Figure 43 indicates the effect of both print buffers on the performance of the CA5 and CA8 with D1 in H1975 single cells. It can be surmised that the tested print buffers, regardless of the divergence in their composition, affect similarly the efficiency of the primary antibodies manifesting no prominent difference in mean binding signal of FOXO3 protein. Despite the results featured insignificant difference in the protein single molecule counts between the microarrays produced with ArrayIt and 3×SSC/1.5M betaine, we opted for an in-house printing solution because it enabled a fabrication of smaller spots and therefore, produced a lower background signal and facilitated an easier spots alignment with PDMS design.

#### **3.3.6.4 Effect of detection antibody concentration**

Each 1.25nL (190×190µm) analysis chamber in the MAC chip device accommodates  $1-2 \times 10^6$  molecules of detection antibody at a concentration of  $10^6$  molecules/nL. However, for the samples with an overexpressed protein of interest this amount of fluorescent antibody might be insufficient. To counteract this problem, the number of available antibody molecules to bind the analyte must be elevated. Since the detection agent's concentration increase leads to a considerable antibody proportion to remain in excess, the level of non-specific binding is also expected to grow.

The effect of D1 concentration rise was monitored with CA5 capture for the H1975 single cell analysis. Two separate experimental runs were carried for each D1 concentration -  $10^6$  and  $10^7$  molecules/nL. The data shows that the mean single molecule count at a greater detection antibody concentration yields a twofold signal increase in comparison with the more dilute D1 sample (Figure 44); notwithstanding, the background was revealed to stay almost identical for both D1 concentrations. This observation was interpreted as the evidently higher affinity of D1 to the FOXO3 and hence, it is more favourable for the antibody to interact specifically with the antigen than non-specifically. It was hypothesised that the elevation of detection agent concentration produced more antibody/antigen duplexes which in turn led to a higher single molecule readout due to a greater labelled fraction on the antibody spot (in the form of trimolecular complexes).

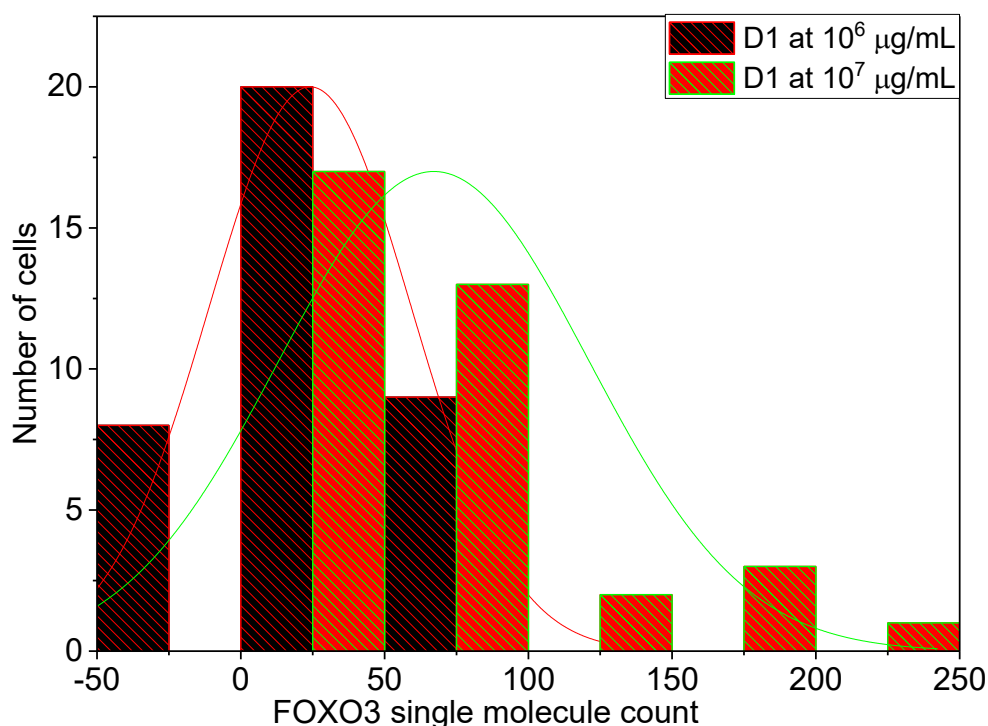


Figure 44 FOXO3 expression in H1975 single cells with CA5 1:3 ratio at D1 concentrations of  $10^6$  and  $10^7$  molecules/nL

### 3.3.6.5 The effect of immobilised antibody biotinylation on the assay performance

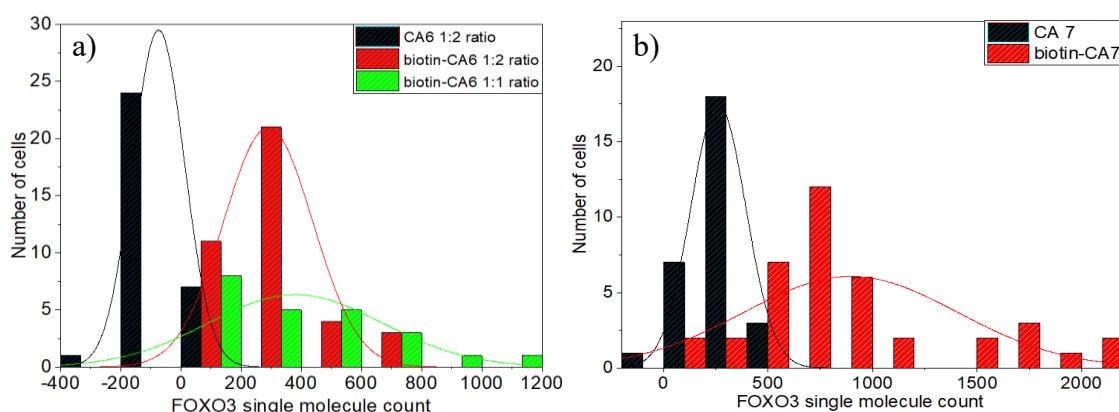
As it was shown before in the experiments with glycerol-containing antibodies, capturing agents' fixation on the functionalised substrates is a crucial element that determines the likelihood of the miniaturised assay to perform efficiently. To further refine immobilisation of the active sites within the microspot, the protein biotinylation effect was investigated. Biotin-labelling of proteins is an extensively exploited technique for immobilisation on the avidin functionalised surfaces because of the biotin's strong non-covalent interaction with avidin-like derivatives.

Although the CA5 and CA8 reliably detected FOXO3 in H1975 cells, the CA6 and CA7 were additionally tested as a more sensitive alternatives to the fore-mentioned antibodies.

Hence, the CA6 and CA7 (Table 2) were in-house biotinylated following the supplier's protocol and their performance was compared with unmodified equivalents on the MAC chip with H1975 single cells using D1 at  $10^7$  molecules/nL. It should be noted that CA6 contains 50% of glycerol (Table 2) and therefore, the effect of glycerol dilution along with biotinylation

was tested. The single molecule signal was compared between biotinylated CA6/buffer diluted at 1:1-1:2 ratios and unmodified CA6/buffer at 1:2 ratio.

The single molecule count indicates an apparent signal difference between the tagged antibodies and their not-modified counterparts for CA6 and CA7, Figure 45. Both biotinylated antibodies resulted in nearly 5 times signal augmentation for mean FOXO3 single molecule count. Intriguingly, despite its high glycerol content, the biotin-CA6/buffer at 1:1 ratio yielded signal higher than the same antibody at 1:2 printing ratio, Figure 45a. The signal of CA6/buffer at 1:1 dilution accounted for about a 30% increment in comparison to modified CA6/buffer at 1:2 ratio. Such an outcome might be explained by a higher antibody concentration in the print and consequently more active sites immobilised on the surface to bind the analyte. Additionally, this observation assumes that the immunosorbent immobilisation is attainable even for the glycerol containing agents which undoubtedly simplifies the search for a suitable candidate to establish a miniaturised immunoassay. Although the CA6 biotinylation procedure improved the assay sensitivity, the microspot shape, which can be characterised as not homogeneous and stretched, remained unaffected due to the high glycerol content. Also, it is noteworthy that the CA7 demonstrated a better performance than CA6 presumably because of its higher affinity/sensitivity. As the biotinylated CA7 yielded the highest FOXO3 signal in single cells, it was selected for further experiments.



**Figure 45 Biotinylation effect on the a) CA6 and b) CA7 performance for H1975 single cell analysis on MAC chip**

### 3.3.7 Calibration curve with CA7/D1 assay

The calibration curve was established using the best performing CA7/D1 antibody system in 190×190 chambers with 2.5µg/mL (or 10<sup>7</sup> molecules/nL) of detection antibody using

FOXO3 recombinant protein, Figure 46. Ekins defined sensitivity as the precision of zero dose measurement what is essentially equivalent to lower limit of detection. The sensitivity depends on the error (imprecision) in the measurement of the response variable<sup>36</sup>. The assay limit of detection was calculated according to Armbruster<sup>121</sup> and found to be 433 molecules bound to the spot. The number of protein molecules present in the analysis chamber can be determined by extrapolation from the single molecule signal giving 14839 molecules.

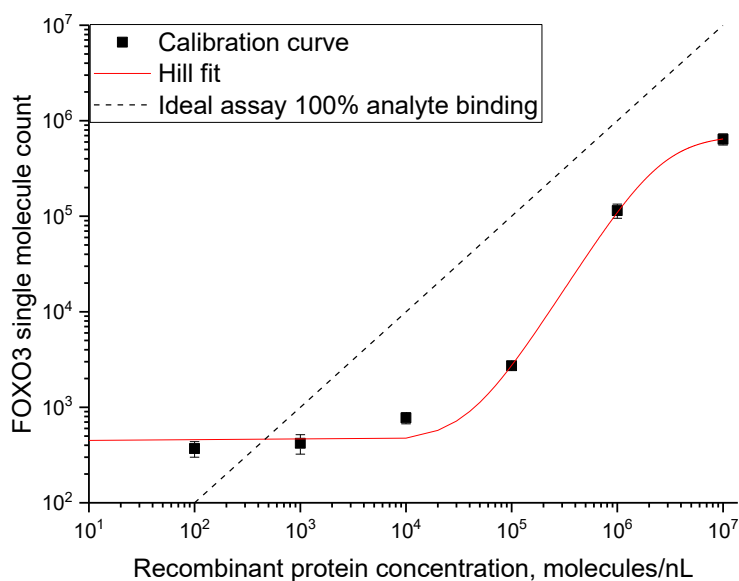


Figure 46 FOXO3 protein calibration curve for CA7/D1 assay

### 3.4 Conclusion

The current chapter described FOXO3 assay development for the MAC chip platform to quantify FOXO3 protein expression in the single cell regime. As a preliminary step of assay elaboration, the screening of several candidates was executed using an Open chip device and FOXO3 recombinant protein. The best matching pairs, CA2/D1 and CA3/D1, were subsequently tested in the MAC chip for the biomarker detection in single cells of different cell lines. However, the attempts to retrieve FOXO3 from single cell lysates with these antibody pairs were unsuccessful probably due to the insufficient sensitivity and affinity of the primary antibodies. The outcome of these experiments added consideration of whether the recombinant protein accurately represents its wild-type analogue.

The unrealised FOXO3 assay establishment necessitated to scrutinise the immunosorbents' stock buffer composition which revealed the very undesirable effect of glycerol on the microarray performance. It was hypothesised that glycerol precluded capturing agents' fixation on the substrate's surface leading to a major fraction of the available binding sites to be washed away during the MAC chip filling procedure. The reduction of the additive concentration or its complete removal resulted in a single molecule count elevation for both glycerol-containing antibodies, CA4 and CA5. Moreover, glycerol content decrease in CA4 facilitated production of smaller spots with improved morphology. This observation is supposedly due to increase of surface tension in the microarrayed droplet.

Furthermore, immobilisation of capture agents was enhanced through a biotinylation process. The biotin-labelled antibodies yielded signal higher than their unmodified counterparts. Also, biotinylation of antibody CA6 resulted in considerable increase of single molecule count regardless the immunosorbent's high glycerol content.

The experiments to evaluate an effect of two print buffers on the microarray performance showed no significant difference in the mean single molecule count. The preference was, nevertheless, given to a hydrogel forming 3×SSC/1.5M betaine print buffer because it yielded spots of a smaller area which, in turn, diminished background signal and facilitated an easier spots alignment with PDMS design.

The concentration of developing antibody was shown to have a significant influence on the single molecule count generating a higher signal for the system with the increased detection agent concentration.

The best performing MAC chip single cell assay was observed to be glycerol free, biotinylated CA7/D1 which reliably detected FOXO3 expression in the H1975 cell line.

# Chapter 4. The MAC assay validation and FOXO3 protein quantification in single cells

## 4.1 Aim of the study

This study demonstrates the importance of human cell analysis on the individual basis. The single cell regime analysis enables investigation of inter- and intracellular heterogeneity which could revealing cellular subpopulations potentiate the novel drug discovery.

This chapter also details the previously tested MAC chip FOXO3 assay validation in different cell lines. The drug perturbation experiments were implemented to compare the treatment effect on the FOXO1 and FOXO3 isoforms expression in human model cell lines.

Some epidemiological studies pursue objectives that require analysis of chemically derived lysates like for example evaluation of total protein of interest content. Therefore, the MAC chip FOXO3 assay was also employed to explore the effect of chemical lysis on the protein extraction from single cells. The successful coupling of chemical lysis with the platform can potentially broaden the spectra of the MAC chip applications diversity allowing too evaluate FOXO3 expression in different states. It is believed that the ability to alternate between the lysis modes enables evaluation of different protein parameters that assist in understanding the protein regulation within the individual cell. Current research is mainly focused on gaining insight into the functions of FOXO3 proteins at a single cell level, which will hopefully reveal the missing information in understanding the biology of lung cancer, asthma and COPD.

## 4.2 FOXOs regulation

FOXO proteins are regulated by a wide range of external stimuli, such as insulin, insulin-like growth factor (IGF-1), other growth factors, neurotrophins, nutrients, cytokines and oxidative stress stimuli<sup>100</sup>. FOXO transcriptional activity is tightly controlled by multiple mechanisms which include posttranslational modifications including phosphorylation, acetylation, ubiquitination and possibly others. The modifications can promote nuclear import or export, change the DNA binding affinity, and alter the pattern of transcriptional activity for specific target.

### 4.2.1 Phosphorylation

Phosphorylation of FOXO transcription factors modulate levels of the proteins in the nucleus by their shuttling, activation and inhibition.

FOXO proteins undergo a negative regulation through the PI3K pathway in response to insulin, insulin-like growth factors, growth factors and neurotrophic factors. Insulin mediates the activity of insulin receptor tyrosine kinase (IR) which, in turn, recruits and further phosphorylates receptor substrates such as IRS family proteins. Tyrosine phosphorylated IRS is then linked to signaling partners like PI3K. The latter initiates an intercellular signal transduction through a cascade of phosphorylation events. The PI3K's primary role is to escalate the levels of phosphatidylinositol (4, 5)-bisphosphate (PIP<sub>2</sub>) and subsequently phosphorylate it to form phosphatidylinositol (3, 4, 5)-trisphosphate (PIP<sub>3</sub>). These lipids further recruit Akt to the plasma membrane and activate it via phosphorylation. The active Akt translocates to the nucleus and triggers downstream signalling. Akt inhibits FOXOs by phosphorylating at three conserved residues<sup>107,122</sup>. Once the first site is modified, the phosphorylation rate of the following amino acids is executed at a higher rate most likely as a result of a the protein conformation change induced by the initial phosphorylation step<sup>100</sup>. Wang et al. has reported that the alteration in FOXO binding ability to DNA is mainly conditioned by Akt phosphorylation of the second site (Ser256 for FOXO1 and Ser253 for FOXO3) which introduces a negative charge in the positively charged DBD<sup>123</sup> resulting in steric and electrostatic repulsion. In contrast, Brent et al. has shown that Akt-mediated phosphorylation of FOXOs has no effect on DNA binding activity and affinity<sup>124</sup>. The phosphorylation of the proteins increases association with the 14-3-3 family of proteins which results in formation of a FOXO/14-3-3 complex. The protein complex is then subjected to cytoplasmic localisation, thus blocking its transcriptional activity.<sup>107,122</sup> SGK and PDK1 act in a similar fashion, phosphorylating FOXOs which are then subjected to the nuclear export through a mediation of binding to protein partners and changing the physico-chemical properties of the FKH domain<sup>100,125</sup>. The phosphorylation of FOXOs by growth factor-activated protein kinases such as casein kinase 1 leads to interaction with export machinery and Ran and Exportin/Crm1, which mechanism involves extracellular signal-regulated kinase, IκB kinase beta, and cyclin-dependent kinase 2.

The protein kinases responsible for FOXOs activation via phosphorylation, are JNK, p38, AMPK, cyclin-dependent kinase 1, and macrophage stimulating 1. AMPK is activated by a high AMP to ATP ratio in response to nutrient deprivation, which in turn instigates a further kinase-induced phosphorylation of several substrates, including FOXOs. In the absence of growth factors, the AMPK-mediated activation of FOXOs occurs despite their subcellular localisation. It was speculated that AMPK activation of FOXO3 transcriptional activity might differ from FOXO1. In contrast, the JNK-mediated FOXO activation is conducted through an insulin pathway inhibition by negatively affecting IRS activity, resulting in FOXO/14-3-3 complex disintegration<sup>107</sup>.

#### **4.2.2 Acetylation**

Acetylation of FOXO proteins has been reported to govern both activation and inhibition of transcriptional activity. The acetylation-mediated inhibition of the proteins results in DNA binding affinity decrease and protein modification. Additionally, these changes result in the FOXO substrate becoming more favourable for further Akt-induced phosphorylation, leading to a negative regulation of the transcription factor. The FOXOs are typically acetylated on several Lys residues. Although the acetylation mechanism remains to be elucidated, immunoprecipitation analysis has shown that CREB binding protein (CBP) and its paralogue p300 acetylate lysine residues of FOXOs attenuating DNA binding activity<sup>126</sup>. Consistent with this finding, it was established that FOXO3 interacts with the DNA phosphate groups via lysines in the FKH domain<sup>101</sup>. In contrast, Perrot and Rechler showed that p300 activates partially the FOXO1 transcriptional potency via acetylation<sup>127</sup>. Also, Perrot et al. has reported that p300 acetylation promotes FOXO-induced transactivation in the absence of insulin<sup>127</sup>.

Similar to acetylation, it is a matter of debate whether deacetylation of FOXO proteins activates or suppresses the transcriptional activity. Daitoku et al. have demonstrated that sirtuin family enzymes (SIRT 1, SIRT2, SIRT3) potentiate FOXO transactivation function through its deacetylase activity<sup>128</sup>. In contrast, Motta et al. have reported the SIR2 ortholog, SIRT1, has a repressive effect on the ability of FOXO1, FOXO3 and FOXO4 to activate transcription<sup>129</sup>.

#### **4.2.3 Ubiquitylation**

Ubiquitylation plays an important role in both the activation and degradation of the FOXO protein. In response to insulin and serum growth factors, the protein is ubiquitinated and



degraded via the ubiquitination-proteasome pathway. The covalent attachment of a ubiquitin molecule to the proteins is implemented after the target protein is recognised through previously phosphorylated side chains. The ubiquitin-proteasome system sequentially recruits three enzymes for further modification of substrates: ubiquitin-activating enzyme (E1), ubiquitin-conjugating enzyme (UBC, E2) and ubiquitin ligase (E3). MDM2 and KP2, priming and branching E3 ubiquitin ligases respectively, regulate FOXO by mono- or polyubiquitylation. The monoubiquitylated FOXO is activated and transferred from the cytoplasm to the nucleus where it can be subsequently polyubiquitylated by MDM2 or SKP2 and subjected to degradation. Ubiquitylation and acetylation are competitive processes because both PTMs have been observed to occur on Lys residues.

In contrast to ubiquitylation, deubiquitylation removes ubiquitin molecules from the side chains. The ubiquitin moiety elimination is carried out through a deubiquitylating enzyme called herpesvirus-associated ubiquitin-specific protease (HAUSP/USP7)<sup>130,131</sup>. It has been determined that both monoubiquitylation and deubiquitylation are induced by oxidative stress<sup>131</sup>. The study of kinetics for the aforementioned processes revealed that the monoubiquitylation occurs faster than the counteracting process after hydrogen peroxide treatment. Monoubiquitylation has been found to increase within 5 min compared to USP7 binding at approximately 15 min<sup>131</sup>. The deubiquitylation process delay is thought to be due to oxidative stress having no effect on the USP7 activity, affecting only monoubiquitylation which in turn initiates deubiquitylation. The deubiquitylation process has been defined as a FOXO inhibiting process because deubiquitylation of monoubiquitylated protein leads to cytoplasmic translocation<sup>131</sup>.

## **4.3 Methods and Materials**

### **4.3.1 Cell culturing and handling**

The H1975 and Toledo cell lines were cultured as previously described (3.2.3.2.2 section). The MDA-MB-231 is a metastatic breast cancer cell line that was incubated in DMEM media supplemented with 10% FBS. The culture was incubated at 37°C with 5% CO<sub>2</sub>. The 70% confluent cells were detached from the flask and centrifuged at 300×g for 5 min. The pellet was subsequently resuspended in FOXO1 or FOXO3 detection antibody solution (described before).

### 4.3.2 FOXO modulation with ZSTK474

Class I PI3K kinases play an important role in different processes directly or indirectly regulating the function of downstream proteins. Disruption of PI3K activities has been implicated in different diseases like inflammation and cancer<sup>132</sup>. The drug has been tested in vivo against a human cancer xenograft exhibiting a potent antitumor activity<sup>132</sup>. Orally administered ZSTK474 strongly inhibited proliferation of tumour cells by arresting the cell cycle at G1 phase. ZSTK474 (2-(2-difluoromethylbenzimidazol-1-yl)-4,6-dimorpholino-1,3,5-triazine) is a s-triazine derivative that specifically inhibits PI3K activity<sup>133</sup>. It has been suggested that ZSTK474 competes with the ATP for the ATP-binding pocket of PI3K, inhibiting phosphorylation of downstream signaling molecules like Akt. The Akt activity is in turn directly associated with FOXOs level and function<sup>132,133</sup>.

The ZSTK474 was obtained from Cell Signaling, UK. The drug was dissolved in DMSO (Sigma Aldrich Corp, UK) to a stock concentration of 10 mM, aliquoted and stored at -20°C. In the current study, the effect of PI3K inhibitor was tested on the H1975 and Toledo cell lines. The cells, cultured at normal conditions as previously described, were treated with the ZSTK474 supplemented media at a concentration of 10µM. The cells were incubated with the agent for 2 or 15 hr. For the control, the cells were treated with 0.1% DMSO for 2 or 15 hr. Following the incubation, the cells were immediately collected and transferred for the MAC chip analysis to observe the treatment effect on the transcription factors FOXO1 and FOXO3.

### 4.3.3 HOECHST staining

Depending on the FOXO activation state, the transcription factor might be retained either in nucleus or cytoplasm of a cell. To verify the protein release from both subcellular compartments, the cell nucleus was stained with HOECHST (ThermoFischer, UK), which enabled monitoring of the optical lysis efficiency on cell nuclei.

The staining procedure was implemented as described by manufacturer. The H1975 cultured at normal conditions were incubated with 1µg/mL HOECHST for 10 min at ambient temperature followed by PBS washes. The cells were then harvested and analysed for FOXO3 expression on a MAC chip platform.

### 4.3.4 Chemical lysis

The chemical lysis of H1975 was implemented on-chip following the optical trapping process. The RIPA Lysis Buffer, 10X (20-188, Millipore UK) was purchased to perform lysis. The methods and protocols to undertake chemical lysis are further described in 4.4.3 section.

### 4.3.5 Analysis platforms

The FOXO1 and FOXO3 analyses were performed using MAC platforms with a 4.5nL (300× 300 μm) and 1.25nL (190×190μm) analysis chamber volume, respectively. The single cell experiments were performed as described in Chapter 3.

Two assays were employed to analyse the total and active FOXO1 levels. The capture and detection agents used for FOXO3 and FOXO1 quantification are denoted in Table 6.

**Table 6 The exploited reagents for the FOXO1 and FOXO3 assays**

<b>Assay</b>	<b>Capturing agent</b>	<b>Detection agent</b>
Active FOXO1	CA12 (Eurogentech, UK)	D3 (Anti-FOXO1 antibody, EP927Y, Alexa Fluor® 647, AbCAM, UK)
Total FOXO1	CA13 (anti-FOXO1 antibody, S266B, MRC PPU, University of Dundee, UK)	D3 (Anti-FOXO1 antibody, EP927Y, Alexa Fluor® 647, AbCAM, UK)
FOXO3	CA5	D1
FOXO3	CA7	D1
FOXO3	CA8	D1

## 4.4 Results

### 4.4.1 Different cell lines analysis with the CA7/D1

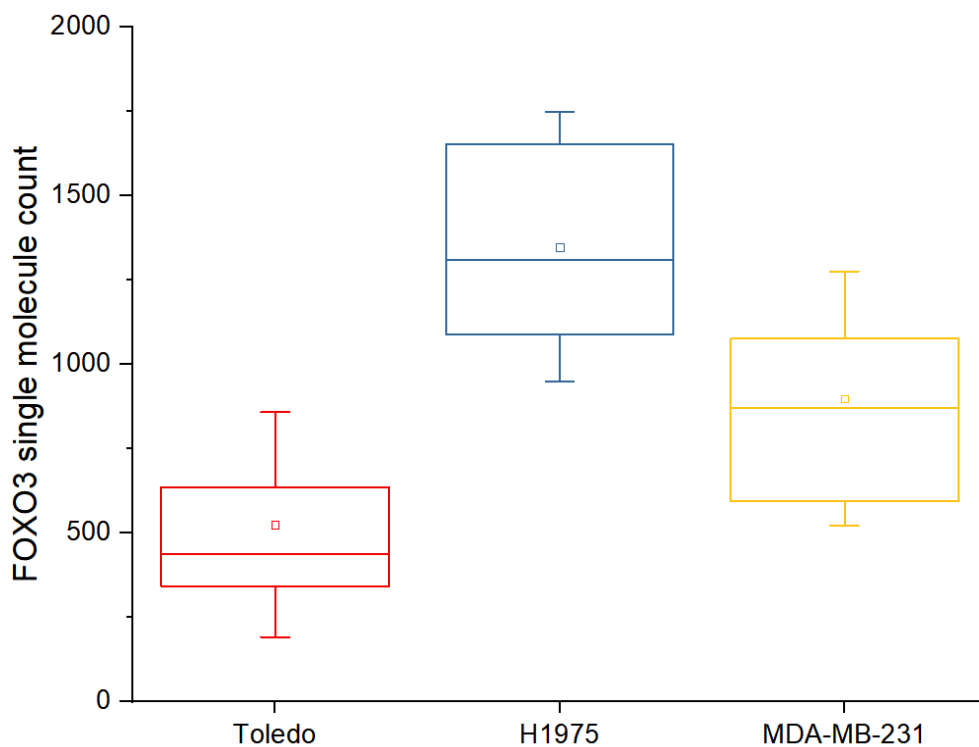
The established CA7/D1 assay was employed to measure the FOXO3 level in different cell lines using the MAC chip platform. The presented results were obtained from H1975, Toledo and MDA-MB-231 cell lines from at least two repeats.

The H1975, Toledo, MDA-MB-231 cell lines, sourced from different tissues, were found to express distinct levels of FOXO3 (Figure 47). The difference of biomarker level in the tested human cell lines represent a heterogeneous distribution of FOXO3 protein in different tissues

of the human body. It was noticed that among the analysed cell lines, the H1975 lung cancer cells express the highest FOXO3 protein quantity resulting in around  $1400 \pm 350$  single molecules. The breast cancer and B-lymphoma cell lines, MDA-MB-231 and Toledo, were found to contain less protein than H1975 by roughly 23% and 61%, respectively.

Additionally, the Figure 47 demonstrates the difference in FOXO3 protein expression between as well as within cell types. The protein content variation between single cells of the same population indicates asynchrony in bioprocesses and cellular heterogeneity despite the fact that the cells were cultured and processed at identical conditions. The observed deviation in protein copy number might be due to the nonparallel manner in which cells enter the cell cycle phases, dissimilar response to pathogen or environment, or transiting multiple dynamic paths simultaneously (cell undergoes cell cycle transition while additionally adapting to the environmental change and adjusting its response to the pathogen presence).

The exhibited data suggests that the MAC chip could be effectively utilized to study intrinsic and extrinsic cellular noise in different human tissues.



**Figure 47 The FOXO3 expression measured from single cells of different cell lines. The square represents mean and, line-median, box 25 and 75 percentile, whiskers  $1 \times$  standard deviation**

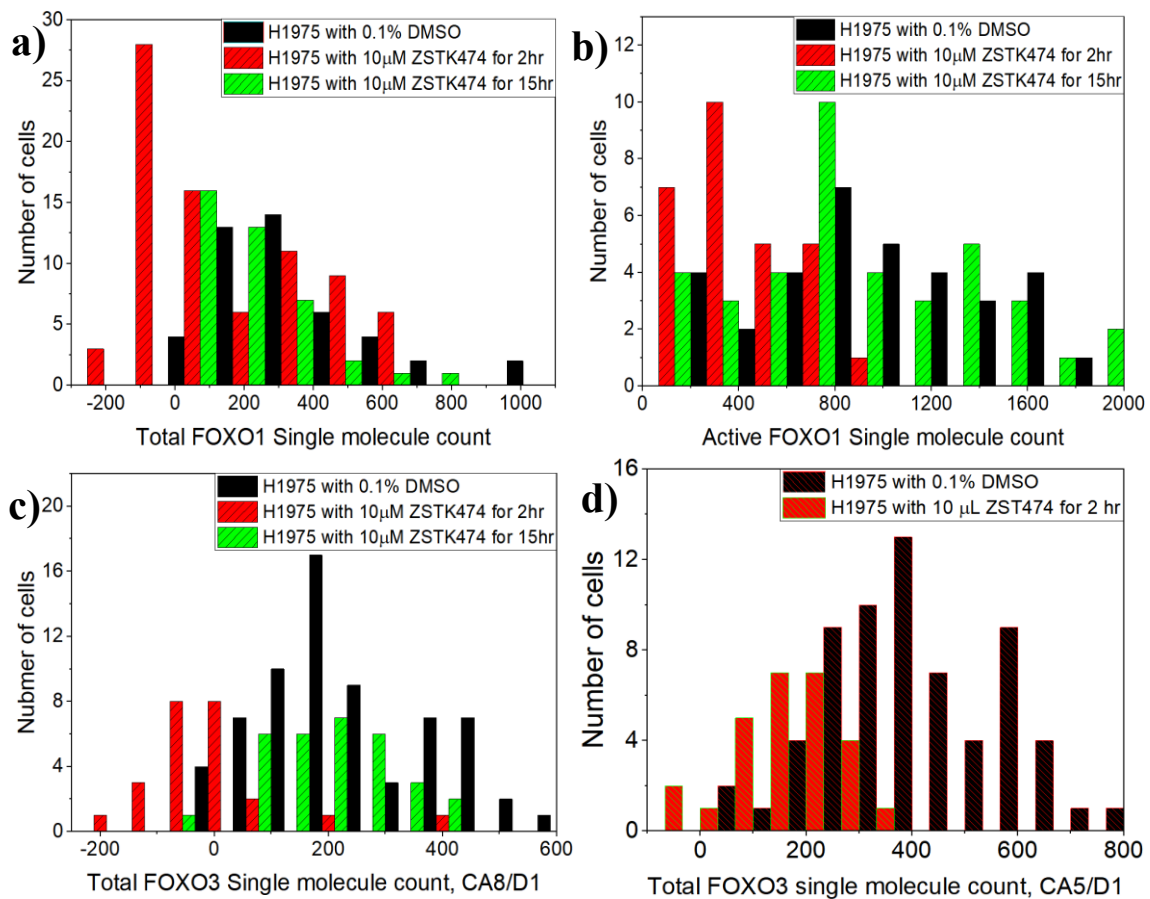
#### 4.4.2 Drug perturbation experiments with H1975

The drug perturbation experiments were performed to investigate the response of H1975 in terms of FOXO1 and FOXO3 proteins expression. Both biomarkers are considered to play an important role in COPD and lung cancer development. Although FOXO1 and FOXO3 control different functions and bioprocesses, the proteins have a similar regulatory pathway.

To date, there has been no literature elucidating the ZSTK474 drug effect on the FOXO1 and FOXO3 level in the non-small cell lung carcinoma (NSCLC) cells, H1975 at a single cell level. To gain an insight into the proteins function in these cells, the total/active FOXO1 and FOXO3 level was measured upon ZSTK474 treatment and compared with the control. ZSTK474 is a pan-isoform PI3K inhibitor that was expected to modulate the FOXO1 and FOXO3 transcription factors levels through the PI3K/Akt pathway. The cellular response was analysed after 2 and 15 hrs of treatment with either 10 $\mu$ M ZSTK474 or 0.1% DMSO. The active and total FOXO1 expression was quantified on the MAC chip platform using CA12/D3 and CA13/D3 assays, respectively. The FOXO3, in turn, was analysed in H1975 with CA5/D1 and CA8/D1 matched pairs in H1975 cells.

The activation of PI3K is known to indirectly repress the FOXO proteins and therefore, the drug was anticipated to increase the FOXOs level in the cells. However, the opposite trend was observed in the ZSTK474 treated cells. The PI3K inhibition was found to reduce the FOXO1(both total and active) and FOXO3 content in H1975 cells. Figure 48a-c demonstrates a sharp signal decrease for all of the proteins relative to the control after 2 hours of treatment, with signal restoration being observed after 15 hours of treatment. The negative shift in the signal following 2 hours of drug incubation is particularly prominent for the FOXO3 protein, with which the mean binding signal observed to be below the CA8/D1 assay detection limit, Figure 48 c. To test whether the obtained trend was associated with a possible fault of the assay itself, the experiment was repeated for 2 hrs drugging using CA5/D1 system. Figure 48d depicts the results obtained with CA5/D1 assay in which the same trend was noted for the FOXO3 transcription factor level. The results do not agree with the findings of other studies. Link et al. showed that U2-OS cells exhibit an increase in the FOXO3 levels and a drop in p-FOXO3 levels upon a PI3K inhibition by ETP-7382 drug<sup>134</sup>. Additionally, it was reported that PI-103, a multi-targeted PI3K inhibitor, activated the FOXO3 protein in the neuroblastoma cell lines SY5Y and SKNBE(2c)<sup>135</sup>. However, Stamatkin et al. revealed that non-small lung carcinoma

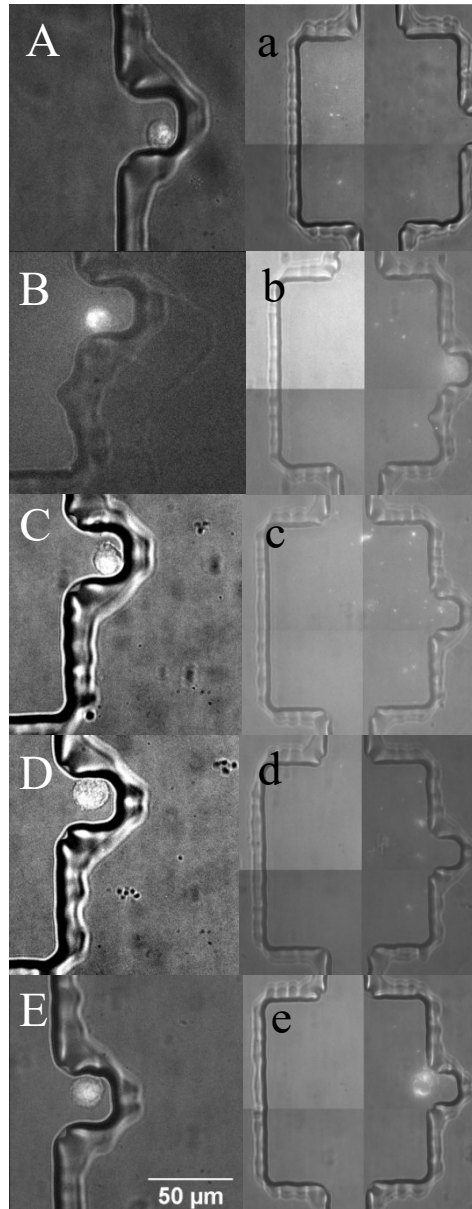
cell lines (inc. H1975 cell line) are not sensitive to the isoform selective PI3K inhibitors, suggesting alternative pathways or isoforms mutual compensation as a possible explanation for the observed Akt activation. Also, his group has demonstrated that ZSTK474-induced inhibition of PI3K pathway instigates only a transient cell cycle arrest in H1975 but not cell apoptosis. Thus, it was speculated that the possible reason for the observed result is the unique H1975 intracellular response to the drug perturbation. Additionally, the current method exploited an optics-based lysis to shear cellular membranes and hence, the alternative hypothesis for the abnormal results with the drugged H1975 was proposed to be inability of the lysis laser to break the cellular nuclei, leaving its content unreleased and encapsulated within this subcellular compartment.



**Figure 48** The H1975 response to the 2 and 15 hrs-long drug treatment was measured at a single cell level on the basis of a) total and b) active FOXO1 expression. Additionally, the FOXO3 expression upon drug incubation was compared with control (0.1% DMSO) using c) CA8/D1 and d) CA5/D1 assays

#### 4.4.2.1 Optical lysis efficiency testing

As previously mentioned, ZSTK474, fosters indirect FOXO3 transcription factor activation. The FOXO3 protein can be distributed in either nucleus or cytoplasm of a cell. Once in the active form, the protein is normally translocated from the cytoplasm to the nucleus. Thus, it was hypothesised that the negative shift in FOXO3 in the drugged cells might be due incomplete nuclear lysis when using optical methods, leading to a fraction of the FOXO3 protein remaining trapped in the nucleus. To monitor the efficiency of optical lysis on the nucleus, the H1975 cells were stained with HOECHST. Figure 49 demonstrates pre- and post-lysis images of the cells clearly indicating their complete lysis as no intact nucleus was detected after an optical cell breakdown. Although complete lysis was achieved in 100% of cases, the medium sized nucleus remnants were observed to be scattered around the chamber. This residual nuclear debris might contain a fraction of the bound protein of interest. This experiment implies that the optical lysis is unlikely to be the cause for the observed protein concentration reduction in the drugged H1975 with the PI3K inhibitor. Thus, the drug induced FOXO3 decrease was thought to be related to the unique response of the tested cell line to the drug.



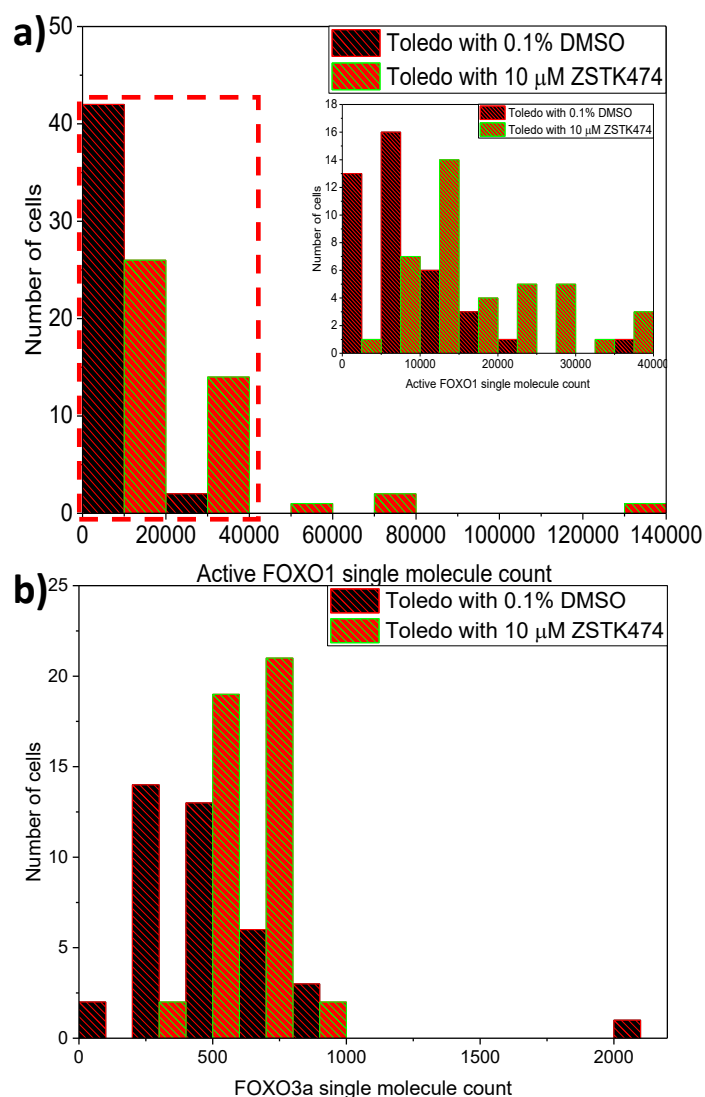
**Figure 49** A-E the HOECHST stained H1975 cell pre-lysis imaged under epifluorescence a-e The Post-lysis image of the corresponding cell. The optical lysis performs a complete cellular lysis without remaining nuclei intact in 100% cases

#### **4.4.2.2 The response uniqueness hypothesis testing**

To test whether the drug perturbation results were associated with the unique H1975 drug response, the Toledo cell line was selected to investigate the ZSTK474 effect on the FOXO1 and FOXO3 transcription factor levels. The active FOXO1 signal following 2-hour-treatment with either the control or drug were compared using the CA12/D3 assay. Additionally, the FOXO3 isoform level was measured with CA7/D1 system in drugged and control Toledo cells.



As it is seen on Figure 50a, the active FOXO1 copy number is higher in Toledo cells treated with the PI3K-inhibitor for 2 hrs. On average, a 3-fold difference was observed in active FOXO1 expression between two cell populations. Moreover, the experiments to estimate the FOXO3 expression in drugged cells revealed a similar trend when comparing ZSTK474 effect against the control group, Figure 50b. The FOXO3 content was found to be roughly 35% less in control cells in contrast to the ones incubated with the inhibitor. Similar results were also reported in literature with other cell lines. Additionally, our research group has tested the ZSTK474 effect on the active FOXO1 expression in cardiac fibroblast cells, where the PI3K pathway inhibition led to the biomarker level increase. Thus, the collected data suggests that the observed anomaly in H1975 response to ZSTK474 is an unusual response associated with this particular cell line that may be caused by the mutations or abnormality in underlying biochemical processes.



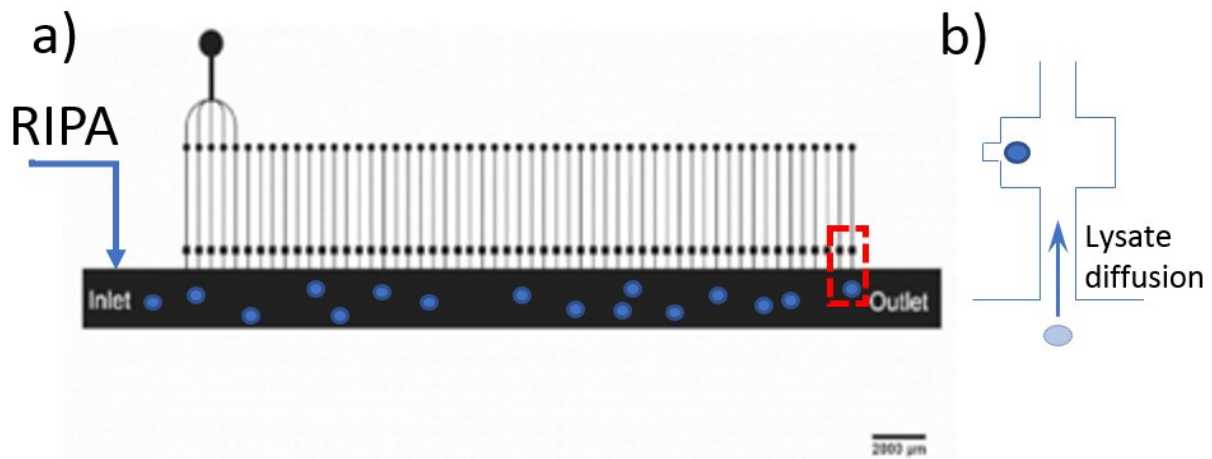
**Figure 50** a) Active FOXO1 and b) FOXO3 content measured in Toledo single cells upon 2 hrs of treatment with 10  $\mu$ M ZSTK474 and 0.1% DMSO. Both biomarkers level, FOXO1 and FOXO3, increased in cells drugged with the PI3K inhibitor in relation to the control

### 4.4.3 Chemical lysis methods testing

The experiments with HOECHST staining revealed that the optical lysis was sufficiently effective in releasing the cellular content encapsulated within the membrane as well as the nucleus. The complete lysis was achieved in 100% of cases and the cellular residuals were dispersed around the chamber. It is a possibility that this cellular debris could contain a fraction of clustered or bound protein of interest impeding the analyte's epitope to be effectively sensed and detected by the assay system. The effect of chemical lysis was therefore explored in order to observe whether it affects the FOXO3 single molecule count in single cells.

The RIPA lysis buffer was chosen to conduct the chemical lysis of the trapped single cells because it is a widely exploited solution that is capable of rapidly and effectively solubilising proteins from adherent and suspension mammalian cells<sup>136</sup>. The lysis buffer ensures the protein retrieval from cytoplasm, nucleus and membrane<sup>137</sup>. The immunoprecipitation studies showed that RIPA is compatible with antibodies because it does not cause protein degradation, impairment of immunoreactivity and biological activity<sup>136</sup>. Due to this property, RIPA buffer is extensively employed in immunoprecipitation and molecular pull-down assays including protein assays, immunoassays and protein purification<sup>137</sup>. Additionally, the lysis buffer has been reported to reduce non-specific binding which is facilitated by the mixture of salts and detergents it contains<sup>136</sup>. Low background noise enables the measurement of analyte signal at a low concentration. However, the buffer was found to be an unsuitable candidate for the protein-protein interaction study because it breaks protein complexes, failing to preserve a bond between analyte and its co-binding partner<sup>137</sup>.

To investigate whether the lysis method has an effect on the FOXO3 single molecule count, the signal obtained via optical or chemical lysis of individually trapped H1975 cells was compared. Although the MAC platform was empirically proven to hold a suitable design for effective laser-induced lysis, the on-chip chemical lysis process required elaboration of a protocol to adapt it to the features of the microfluidic device. Since the MAC chip is not equipped with an extra channel to supply lysis buffer directly to the analysis chambers, the only option to deliver the RIPA was through the main channel of the structure. However, due to the sample loading into the chip, the main channel contained thousands of cells (Figure 51).



**Figure 51 a)** The MAC chip prior the lysis contains a considerable number of cells in the main channel. The chemical lysis buffer introduction (shown with the blue arrow) can only be implemented through the main channel which inevitably leads to the unwanted cells lysis. The dashed rectangle shows part of the chip zoomed in b) where the cellular lysate diffusion from the main channel into the analysis chambers interferes the single cell interrogation. The arrow represents the direction of unwanted lysate diffusion

Hence, the direct lysis buffer perfusion through this channel would cause unwanted cell lysis which content can diffuse into the analysis chambers. This would in turn prevent single cell protein analysis. To avoid this, the on-chip chemical lysis of the single cells could only be performed following cell removal from the main channel. Different strategies to implement chemical lysis on the MAC chip platform were therefore tested to select the optimal one (

Table 7). The criteria for the ideal method were the following:

1. The applied method would efficiently lyse the trapped cells
2. Protein pulldown post-lysis should only be from the lysed cells in the chamber and not from any unwanted protein diffusion from the main channel
3. Applicable to different cell lines
4. The method would be easy to implement and not be time-consuming

**Table 7 The protocols for chemical lysis methods**

	<b>Washing procedures and chemical lysis</b>
<b>Method 1</b>	<ol style="list-style-type: none"> <li>1. Main channel wash with background solution at 5 <math>\mu\text{L}/\text{min}</math></li> <li>2. Air embolism</li> <li>3. Main channel wash with background solution at 10 <math>\mu\text{L}/\text{min}</math></li> <li>4. Air embolism</li> <li>5. 10<math>\mu\text{L}</math> of RIPA lysis buffer perfusion at 10 <math>\mu\text{L}/\text{min}</math></li> <li>6. 10 min incubation with RIPA</li> <li>7. Main channel wash with background solution at 10 <math>\mu\text{L}/\text{min}</math></li> </ol>
<b>Method 2</b>	<ol style="list-style-type: none"> <li>1. Main channel wash with background solution at 5 <math>\mu\text{L}/\text{min}</math></li> <li>2. Air embolism</li> <li>3. Accutase introduction to the main channel and 5 min incubation</li> <li>4. Air embolism</li> <li>5. Main channel wash with background solution at 5 <math>\mu\text{L}/\text{min}</math></li> <li>6. 20<math>\mu\text{L}</math> of RIPA lysis buffer perfusion at 10 <math>\mu\text{L}/\text{min}</math></li> <li>7. 3 min incubation with RIPA</li> <li>8. Main channel wash with the background solution at 10 <math>\mu\text{L}/\text{min}</math></li> </ol>
<b>Method 3</b>	<ol style="list-style-type: none"> <li>1. Main channel wash with background solution at 5 <math>\mu\text{L}/\text{min}</math></li> <li>2. Air embolism</li> <li>3. 20<math>\mu\text{L}</math> of RIPA lysis buffer perfusion at 30 <math>\mu\text{L}/\text{min}</math></li> <li>4. Main channel wash with the background solution at 10 <math>\mu\text{L}/\text{min}</math></li> <li>5. 3 min incubation with RIPA</li> <li>6. Main channel wash with the background solution at 10 <math>\mu\text{L}/\text{min}</math></li> </ol>

The protocol for each listed method could be basically subdivided into three procedures: 1. main channel wash 2. Single cell lysis with RIPA 3. replenishment of the detection antibody. The washing procedure was aimed predominantly at reducing the number of cells in the main channel before the lysis buffer introduction. The initial attempts to establish a chemical lysis protocol were accompanied by a failure to significantly diminish the unwanted cells left in the main. This is because the H1975 are adherent cells that tend to stick to the surface of the chip

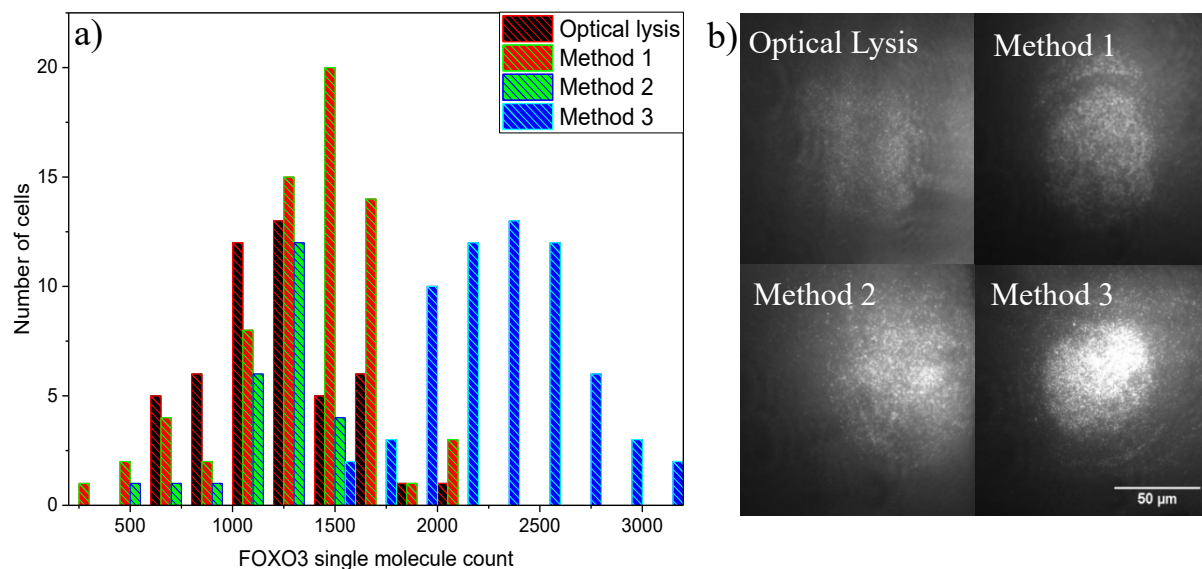
after a relatively short time of trapping (30-45 min) despite the BSA coating. The cellular count in the sample was therefore decreased in order to aid cell removal and thus minimize any FOXO3 signal being attributed to protein diffusion from the main channel. These preliminary amendments served as a ground for the development of the methods described in

Table 7. Figure 52a demonstrates the FOXO3 protein recovery from single H1975 cells by using different lysis methods. A significant signal increase was noted for all the chemical lysis methods tested when compared with an optical approach.

Although Method 1 produced a higher FOXO3 signal than optical lysis, the method had its downside. To decrease the number of cells in the main channel, an air embolism/background solution perfusion was performed. However, this approach was found to be inefficient in cell removal from the main channel. This is likely due to cell line adhesiveness to the glass surface. Additionally, the repeated introduction of an air pocket into the chip caused air bubbles to get into the chambers pushing the fluid from the main channel to the chambers and dislocating the trapped cells from the trapped positions. However, it was observed that continual perfusion of RIPA buffer through the channel successfully removed the stuck cells from the channel to the outlet. Once the channel was free of cells, the RIPA was incubated for 10 min to allow the solution to diffuse into the chambers and lyse the single cells. The incubation time selected was found to be too long as the cells were already observed to start lysing after 3 min of incubation. From Figure 53b it is clear that there is no considerable difference between some chambers with and without cells. Unexpectedly, the signal for some empty chambers was nearly as high as it is for single cells which implied the bulk lysate diffusion from the main channel during the procedure. Thus, additional steps were necessary before incubating with RIPA lysis buffer.

Similar to Method 1, Method 2 employed an air embolism strategy which was additionally combined with Accutase to improve the washing procedure outcome. Despite the extensive application of the Accutase solution in cell culturing to detach cells, this approach unfortunately resulted in a considerable number of cells to remain in the channel. However, applying a continual flow of RIPA buffer through the main channel did lead to eventual removal of the excess cells from the chip, which is consistent with the previous observation. Reducing the lysis time to 3 min was again observed to be sufficient to perform a complete lysis of the trapped cells. Additionally, the method diverged by introducing a background solution before the RIPA buffer, which facilitated cell removal from the chip. The signal from chambers devoid of cells was detected to be much lower than for single cells and it fluctuated roughly within the same diapason as for the optical lysis, Figure 53a and c.





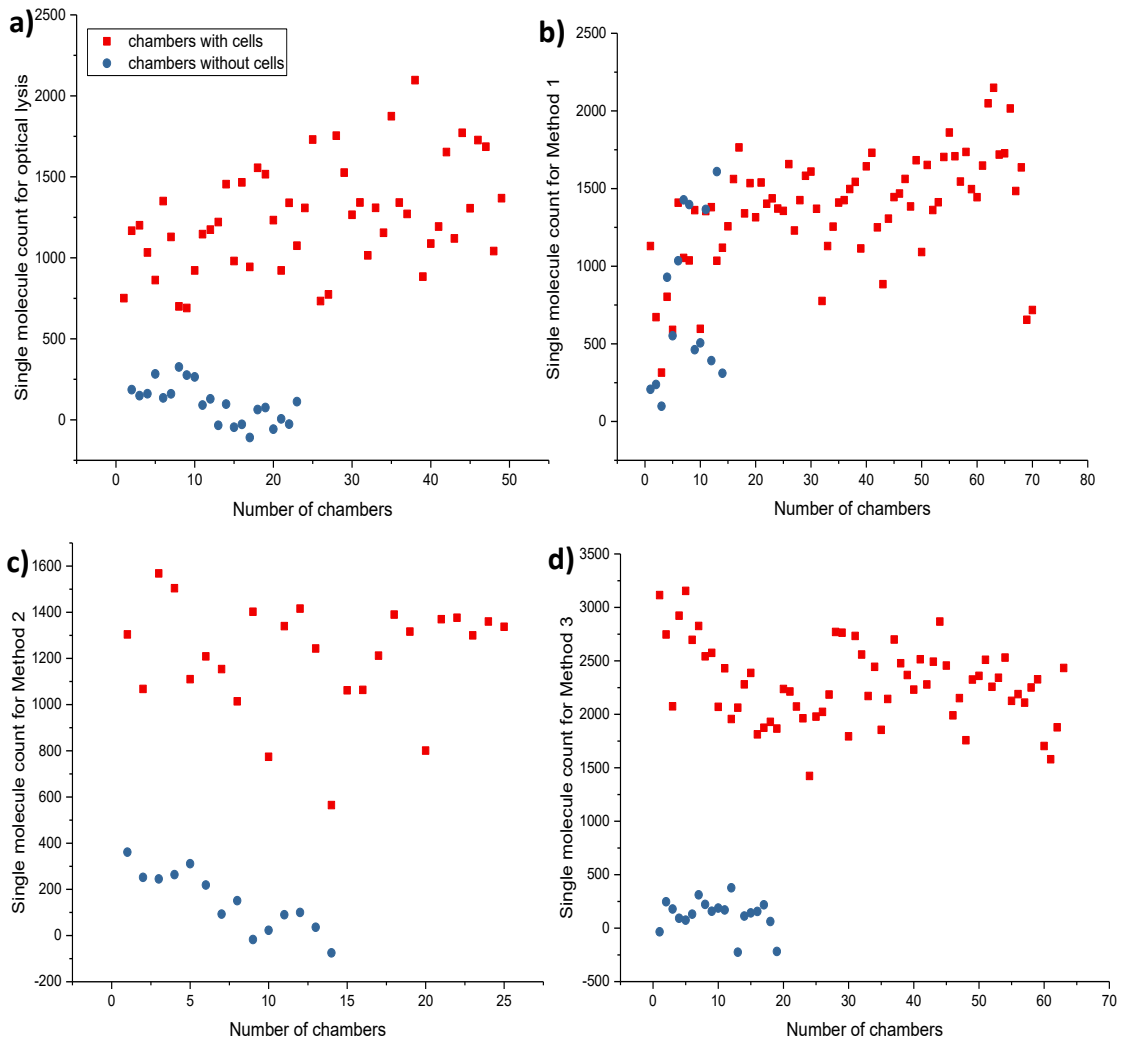
**Figure 52 a)** The FOXO3 signal comparison from H1975 single cells lysed optically or chemically (Method 1-3) **b)** raw data images collected after thermodynamic equilibrium establishment representing the FOXO3 retrieval capacity from H1975 by different methods

Method 3 was aimed at eliminating some of the drawbacks encountered during the implementation of Method 1 and Method 2 such as the introduction of air into the chambers. Although the air was eventually dislodged from the main channel through the introduction of lysis buffer or background solution, the bubbles downstream of the analysis chambers remained trapped. It is thought that this phenomenon occurred due to the characteristic design of the MAC chip that was intended to prevent or prolong diffusion of biomaterial into the analysis chambers. Due to the structure of the microfluidic device, the flow of solution from the main channel into the analysis chambers is slow if no external stimuli are applied. Thus, once the void had formed, gradual filling was observed to occur throughout the entire imaging and incubation duration. This process caused the lysates from the analysis chambers to be drawn towards the void, leading to a drop in the analyte concentration and reduction in the detected FOXO3 number. In Method 3, the attempted cells removal via repeated cycle of air embolism was abandoned in favour of an additional washing step involving RIPA buffer. The buffer was withdrawn at a higher flow rate in order to aid rapid removal of cellular components to the chip's outlet. The lysis buffer was immediately replaced by a background solution which prevented diffusion of the main channel's lysate into the chambers and helped to further remove and dilute any residuals left there. The signal was revealed to differ roughly 5 times between empty and chambers with single cells (Figure 53d) showing that the method can be

robustly applied for the single cell analysis on the MAC chip. Also, the method resulted in the highest FOXO3 copy number yield compared to other chemical lysis protocols which might be explained by the absence of air trapped within the capillaries and analysis chambers that would otherwise cause a drop in the protein concentration following cell lysis.

A positive shift in the FOXO3 single molecule count was detected upon using chemical lysis instead of optical lysis. Although it remains unclear what exactly underpins this observation, the FOXO3 interaction with co-partners was speculated to cause a dramatic decrease in the biomarker recovery using optical lysis. Unlike chemical lysis, the optical cellular breakdown preserves protein complexes with co-binding partners which presumably hinder analyte's epitopes and detection by the assay. In contrast, RIPA lysis buffer facilitated protein complex dissociation, liberating the FOXO3 from its co-binding partner and consequently allowing more protein to be pulled down. It was, therefore, hypothesized that chemical lysis reveals the total FOXO3 copy number content in a single cell whilst the FOXO3 single molecule count obtained with optical lysis represents its unbound level in a single cell.

Additionally, the empty chambers displayed a signal of unknown source, which was calculated to be above the background signal. This is believed to originate from either non-specific interaction, a small proportion of the protein diffusing from the main channel or a counting algorithm error. In response to this, the average signal of empty chambers was used to correct the detected single molecule count for the biomarker in single cells.



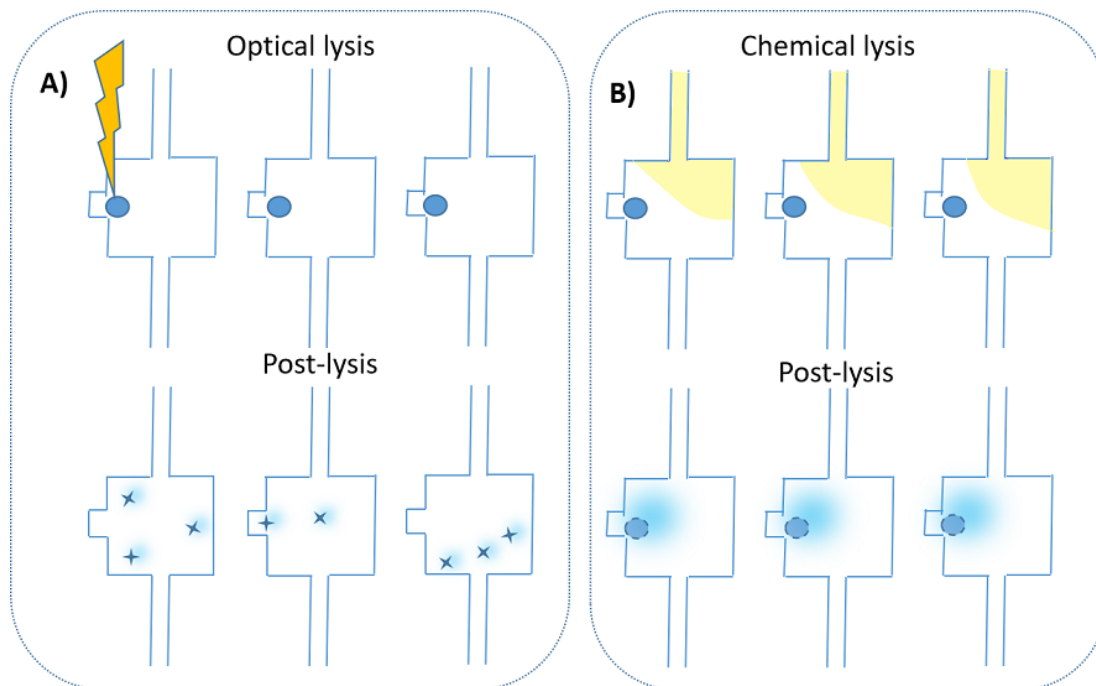
**Figure 53** The signal comparison between empty and chambers with single H1975 cells for different lysis methods: a) Optical lysis, b) Chemical lysis Method 1 c) Chemical lysis Method 2 d) Chemical lysis Method 3

#### 4.4.3.1 Incubation time determination for chemical lysis

Additionally, the FOXO3 binding kinetics was investigated by imaging the signal throughout the incubation time from optically or chemically- derived lysates. The chemical lysis was implemented using Method 3. The TIRF readout was performed at three time points during the incubation process: right after lysis (0 min), 60 min post-lysis and 120 min after lysis. The time-lapse data from optically and chemically lysed H1975 was collected and analysed to estimate whether the system achieved equilibrium upon the 2-hr-incubation, with the binding kinetics of FOXO3 extracted by using different lysis methods being compared. As indicated earlier, FOXO3 pulldown via chemical lysis resulted in a single molecule count that was markedly higher than via optical lysis even at very early incubation time points. Thus,

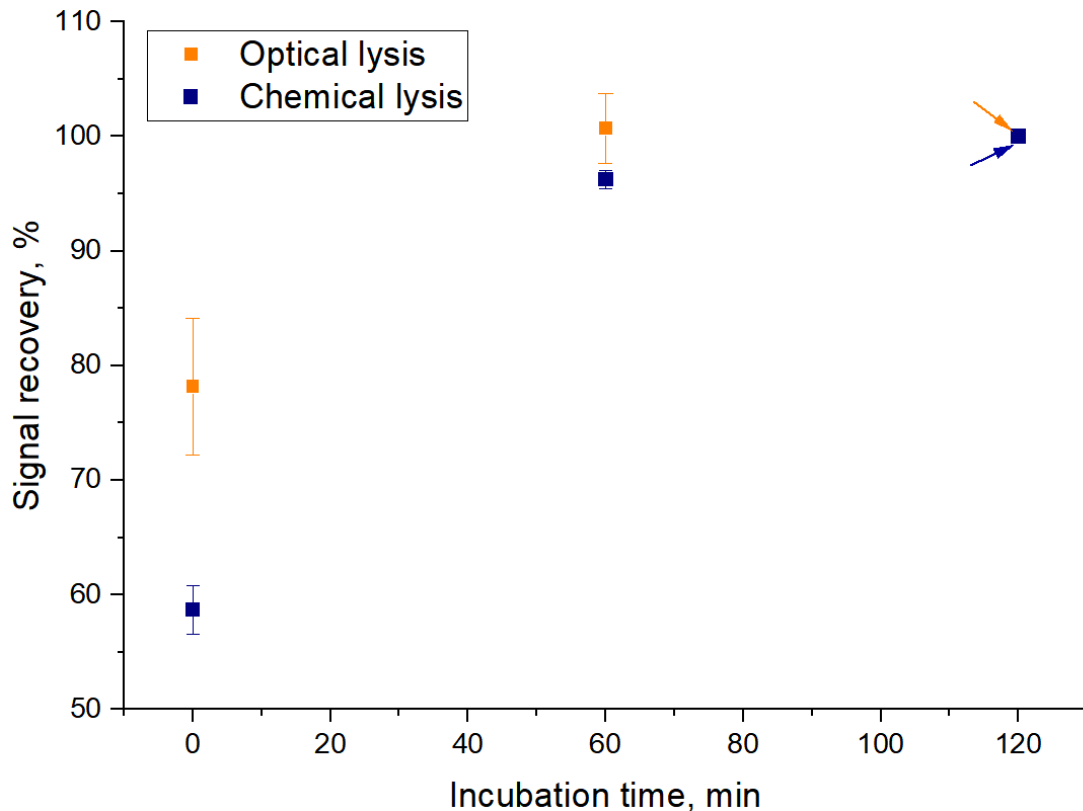
direct comparison of single molecule counts between the lysis methods at each timepoint would not accurately represent the binding kinetics. Instead, the signal obtained after 2 h of incubation was nominally set to 100% to calculate the percentage of the signal at earlier incubation time points. Figure 55 demonstrates the dynamics of a normalized average FOXO3 protein signal during incubation for optical and chemical lysis methods.

As expected, the FOXO3 signal obtained from both lysis methods followed the Michaelis-Menten model. It was, however, noted that the FOXO3 signal percentage immediately after lysis (at 0 min) was evidently higher for optical cellular breakdown. This observation might be due to the laser pulse used which leads to the propagation of a cavitation bubble promoting lysates mixing and scattering throughout the analysis chamber (Figure 54 A). This is likely to decrease the diffusion time. In contrast, chemical lysis operates by disrupting the cellular membrane structures, releasing protein content into the chamber in a more controlled fashion than optical lysis therefore increasing the time of protein diffusion towards the immobilised antibody (Figure 54 B). Also, the signal percentage variation between cells at the initial incubation stages was found to be evidently higher for optical lysis than for chemical lysis. The variation phenomenon could possibly be explained by a relative synchronism of exploited lysis methods. The chemical lysis was performed concurrently for all trapped single cells within 3 min whereas optical lysis was implemented asynchronously, lysing the cells one-by-one and thus causing a time lag between the first lysed cell and the last one. The additional contributor to the signal variation was believed to be random scattering of cell debris throughout the analysis chamber. It was noticed that in some chambers the single cell residuals were more dispersed within the volume than in others, which could potentially be a source of variation as well (Figure 54 A).



**Figure 54 Schematic of the two different lysis approaches: A) Optical and B) Chemical lysis. The diagram represents asynchronism of the optical lysis for the trapped cells. Upon laser lysis, the cellular remnants of different size are randomly scattered around the chamber. The chemical lysis occurs in a more synchronised way breaking down simultaneously all the trapped cells**

From Figure 55, it is clear that nearly 100% of the signal was attained for both methods after just an hour of incubation, with the signal reaching a plateau two hours' post-lysis. Since the signal was detected to be mostly stable after 1+ hr, the 2 hrs incubation period was found to be sufficient to reach a thermodynamic equilibrium between the antibodies and antigen. Also, the dramatic decrease in signal variation between single cells for both lysis methods was observed as the incubation progressed which could also serve to indicate the proximity of the thermodynamic equilibrium achievement.



**Figure 55** Average signal increase from single cell lysates during the incubation time of two hours for optically and chemically lysed cells. Whiskers are standard errors

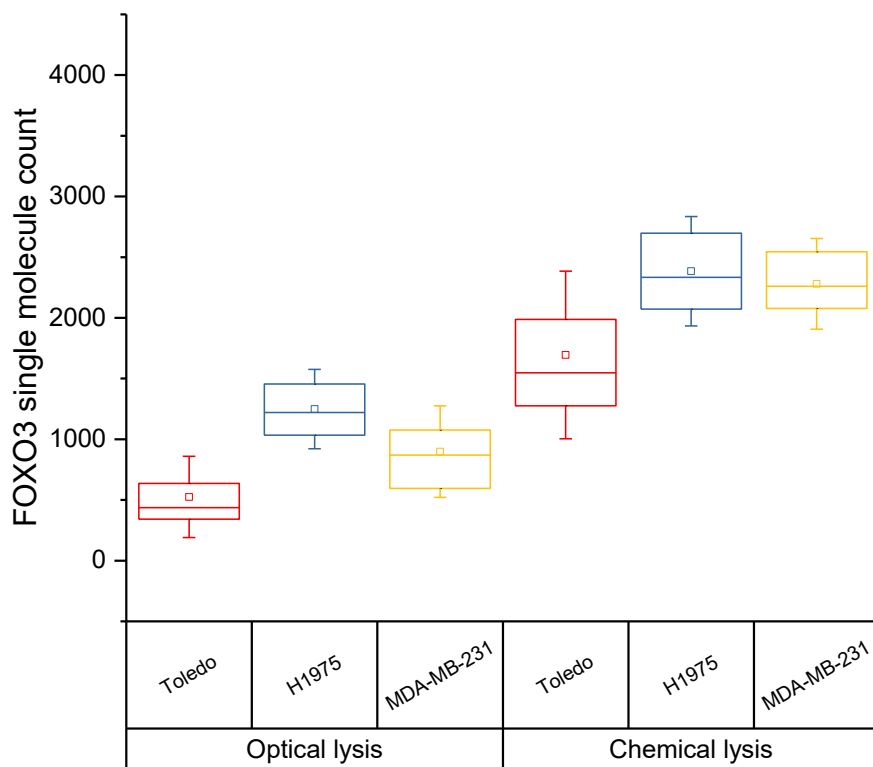
#### **4.4.3.2 Optically and chemically derived single cell lysates analysis for FOXO3 expression**

The FOXO3 content in previously analysed model cell lines (Toledo, MDA-MB-231, H1975) was also extracted via chemical lysis to investigate the effect of lysis method on the biomarker level in different cell lines. Since Method 3 was identified as the most robust and reliable protocol, it was subsequently employed to determine the FOXO3 levels from the aforementioned cell lines. The results obtained from two individual experiments were further compared with the FOXO3 copy number detected after optical lysis.

The Figure 56 demonstrates the FOXO3 single molecule count in the tested cell lines applying optical and chemical lysis. The FOXO3 single molecule count was observed to be considerably higher in samples obtained with chemical lysis. The increase in extracted biomarker number for chemical lysis in relation to optical breakdown was found to be in range of 1.9 -3.2 times depending on the cell type. The observed cell type effect on the ratio of free and total protein level might indicate a different role of FOXO3 transcription factor in

regulation of biological processes in different tissues of human organism. Assuming the total and unbound FOXO3 levels could be measured using chemical and optical lysis respectively, the evidence suggests that a significant fraction of the protein in all the analysed cells is in a bound form. The amount of protein in the bound form could, therefore, be interpolated knowing total and free protein levels. Thus, the average copy number of the bound FOXO3 protein was calculated to be roughly  $1170 \pm 767$ ,  $1136 \pm 516$ ,  $1381 \pm 531$  in Toledo, H1975 and MDA-MB-231, respectively.

The obtained results demonstrated that depending on the purpose of the study, the MAC chip can be effectively exploited to directly measure either total or unbound FOXO3 protein abundance in single cells. This method enables biomarker measurement in different forms without the need for expensive reagents that specifically target only a part of known protein interaction partners.



**Figure 56** The FOXO3 protein signal in different cell lines obtained with optical or chemical lysis. The whiskers are  $1 \times$  standard deviation, squares are the means, boxes represent 25 and 75 percentiles

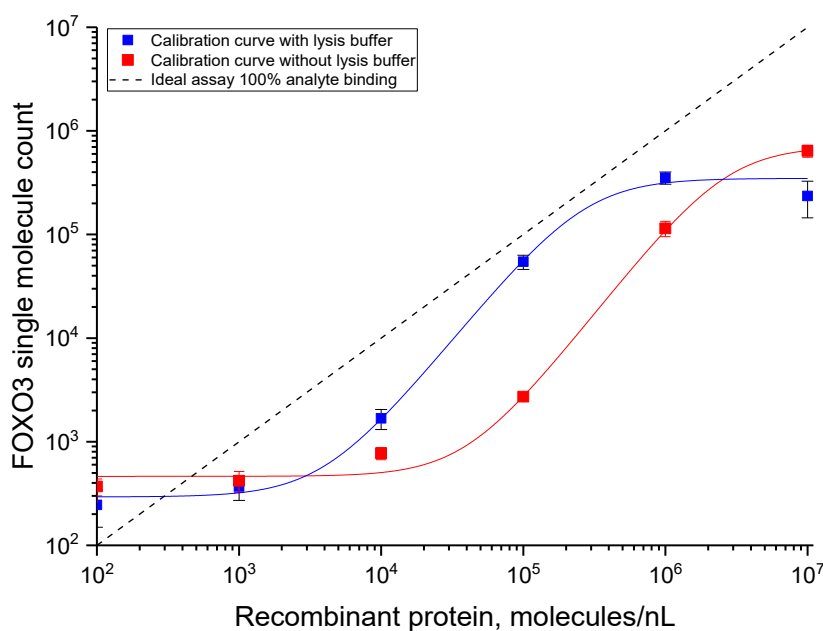
#### 4.4.4 Calibration curve with chemical lysis buffer addition

Due to the prominent effect of the chemical lysis buffer on FOXO3 protein extraction from single cells, a set of experiments using CA7/D1 assay were carried out with recombinant FOXO3 protein solution supplemented with the lysis buffer, Figure 57.

. The standard solutions at the protein concentrations of 0-10<sup>7</sup> molecules/nL were mixed with 1×RIPA and loaded into the MAC chips to investigate the effect of buffer addition on the calibration curve. The standard curves obtained with and without lysis solution were compared on the basis of FOXO3 signal abundance. Intriguingly, the assay's sensitivity was found to be enhanced when 1×RIPA was included into the standards' solutions. The observation might be explained by the protein aggregates dissociation. Protein aggregation in aqueous solution is a widely reported problem that occurs due to the unstable protein forming multimeric assemblies. It was hypothesised that the lysis buffer stimulates the dissociation of protein aggregates, preventing obstruction of the epitope and as a result leading to a higher assay sensitivity.

The assays limit of detection for the new calibration curve was calculated according to Armbruster et al<sup>121</sup>, which was found to be 249 molecules bound to the spot. The number of protein molecules present in the analysis chamber can be determined by extrapolation from the single molecule signal, giving 1185 molecules of FOXO3.





**Figure 57 Comparison of two FOXO3 calibration curves obtained with and without 1×RIPA lysis buffer addition.**

## 4.5 Conclusion

The FOXO3 MAC chip assay was employed to measure the biomarker level in different cell lines. The obtained results showed the protein expression to differ both within and between cell populations. This data suggest that MAC chip is a suitable tool for study of inter- and intra-cellular heterogeneity because it enables detection of analytes in single cells.

Additionally, the study delivered the results produced from the drug perturbation experiments. Initially, the ZSTK474, a PI3K inhibitor, effect was analysed on the active and total FOXO1, and FOXO3 proteins in H1975. Surprisingly, the biomarker level was observed to decrease after the cells incubation with the drug. The unexpected outcome of the analysis could be due to the chosen cell lines unique response to the drug or incomplete cellular lysis.

It has been reported that the activated FOXOs are translocated from cellular cytoplasm to nucleus. Therefore, if the lysis procedure leaves the nucleus intact then a considerable fraction of proteins remains trapped in the nucleus. This would thwart the assays ability to sense and detect the encapsulated analyte. To rule out optical lysis as an interfering factor, the H1975 cells were stained with HOECHST, enabling observation of the nucleus integrity both pre- and

post-lysis. However, the HOECHST staining revealed that the cell undergoes a complete breakdown including nucleus with optical lysis.

Since the hypothesis of incomplete lysis was dismissed as a potential cause for the FOXOs drop in drugged H1975, alternative cell lines were used in order to test whether the same response would be seen. Therefore, the Toledo cell line was employed to repeat the drug perturbation experiments. As expected, the data demonstrated the active FOXO1 and FOXO3 levels increase after the 2 hr treatment period with ZSTK474. The response of H1975 to the drug was therefore considered to be a unique attribute of this cell line. Also, the literature has shown that NSLC cells are immune to the PI3K inhibitors by possible activation of alternative pathways of FOXOs regulation.

It was noticed that the optically lysed cells generate biological debris being scattered around the chamber. This debris was speculated to retain the protein trapped in the biological matrix in the bound form. It is believed that the epitopes of bound FOXO3 might presumably be hindered from the detection system. As a result of system being unable to sense and recognise the obstructed epitopes, the detection of FOXO3 single molecules is limited to only identifying those that are liberated from complexes. However, a lysis method which can induce decomposition of protein-protein complexes enables the total FOXO3 biomarker level to be evaluated. Therefore, the RIPA lysis buffers effect on the FOXO3 retrieval was investigated as an alternative strategy to optical lysis. To adapt chemical lysis to the microfluidic device, its structural idiosyncrasies should be considered. Thus, different chemical lysis protocols were tested to select the most suitable one yielding the highest S/N ratio.

Once determined, the developed method was subsequently employed to extract the protein from different cell lines. A comparison of FOXO3 signal from single cells was conducted between optical and chemical lysis. Intriguingly, the single molecule count was observed to be higher for chemically ruptured cells than for optical lysis. The difference might be attributed to the fact that RIPA buffer promotes protein complexes dissociation, which results in the release of the epitope from the biomarker's co-binding partner. The obtained data suggests that the MAC chip can be successfully used to measure free or total FOXO3 protein in single cells by using optical or chemical lysis, respectively. It is important to mention that the quantitative information on the biomarker levels in different states could be obtained without purchasing expensive reagents.

The experiments with recombinant protein showed that the addition of RIPA buffer to the standard solution improved the assay's sensitivity. The comparison of the FOXO3 signal with or without RIPA demonstrated a difference, which might be due to the unstable nature of the recombinant protein in aqueous environments. Having a propensity to form aggregates, the FOXO3 transcription factor is believed to be dissociated from clusters in the presence of 1x RIPA, leading to the higher signal detection of the analyte.

# Chapter 5. Measuring of FOXOs expression in clinical samples

## 5.1 The aim of the study

COPD and number of other chronic respiratory diseases are associated with acute inflammation and imbalanced immune response which leads to lung tissue damage and progressive reduction of pulmonary function. Because they are affected by various environmental stimuli, lung cells, including epithelial and immune cells, undergo pernicious changes<sup>138</sup>. The accumulation of corrupted cells combined with a dysregulated immune system leads to accelerated ageing or senescence of the whole organism<sup>139</sup>. The FOXO proteins are presumably involved in bioprocesses that play a vital role in COPD development<sup>140,141</sup> and therefore, they are believed to reveal the missing information on disease pathogenesis and treatment. The immunohistochemical staining of peripheral lung tissues has demonstrated that FOXO proteins are underexpressed in epithelial and immune cells of COPD patients<sup>140,141</sup>. To date, the FOXOs expression evaluation has only been implemented on whole lysates extracted from the lung tissue, lavages or sputum cells providing only an averaged estimate of the protein content in bulk samples. The research outlined here presents for the first time the data of FOXO1 and FOXO3 content in single cells from clinically relevant samples that were analysed on a MAC chip device.

The current study looked into the expression of two senescence biosensors, FOXO1 and FOXO3, in epithelial and CD3+ T cells from sputum samples of both healthy and COPD+ individuals. Additionally, nasal samples from the healthy control group were analysed for FOXO3 protein only via combining nasosorption and MAC chip tools. A major hurdle in clinical epidemiological studies is to gather appropriate biospecimens in sufficient amount for analysis. The non-invasive NASAM tool has previously been applied in analysis of inflammatory mediators in nasal secretions to study respiratory diseases such as asthma, RSV, bronchiolitis. Several cytokines have shown correspondence in levels between nose and bronchi following the stimuli exposure. Nasal epithelial cells have been, furthermore, validated as a surrogate for bronchial epithelial cells to measure physiological response to stimuli<sup>138,142,143</sup>. Also, there is a hypothesis that senescence from COPD can spread to other organs<sup>30</sup>. Therefore, it is hoped that nasal samples will be able to distinguish between healthy and COPD volunteers using markers already validated in sputum.

To sum up, this study pursued the following objectives:

- Is there a difference in FOXOs expression in cells from the lower respiratory tract (sputum) between the healthy and COPD+ individuals?
- To determine the cellular profile distribution in the sputum of the healthy and ill donors
- To develop a protocol for nasosorption-MAC chip analysis of biomarkers expression in single cells from nasal mucosal lining fluid
- To establish the healthy baseline level for FOXO3 protein levels in epithelial and CD3+ T cells
- To compare FOXOs expression in single cells between the upper (nasal) and lower (sputum) respiratory tract

## **5.2 Overview of Chronic Obstructive Pulmonary Disease**

According to the British Lung Foundation, Chronic Obstructive Pulmonary Disease or COPD is the second most common disease of the lungs in the UK,<sup>144</sup> predominantly affecting persons older than 45 years. It has also been predicted to be the third leading cause of death worldwide in 2020 after heart disease and stroke<sup>145</sup>. COPD is a complex and heterogeneous disease that caused 5.3% of the total number of UK deaths in 2012<sup>144</sup>.

The WHO in collaboration with the US National Institutes of Health launched a Global Initiative for Chronic Obstructive Lung Disease (GOLD) to develop a ‘Global Strategy for the Diagnosis, Management and Prevention of COPD’<sup>146</sup>. GOLD has defined COPD as “a common, preventable and treatable disease that is characterized by persistent respiratory symptoms and airflow limitation that is due to airway and/or alveolar abnormalities usually caused by significant exposure to noxious particles or gases”<sup>145</sup>.

### **5.2.1 Causes of COPD**

Although the disease is yet of unknown aetiology, the causative or risk factors can be classified into host factors and environmental exposures.

### 5.2.1.1 Host factors

This group of risks include genetic factors, gender, atopy and airway hyperresponsiveness and nutrition and lung growth.

It has been reported that complex genetic-environment factors may be involved in susceptibility to COPD. One of the best documented genetic risk factors is, however, an  $\alpha$ -1 antitrypsin (AAT) deficiency<sup>146,147</sup>. Tanner *et al.* claimed that emphysema is associated with both null mutations (no protein produced) and with mutations producing defective or non-exported  $\alpha$ -1 antitrypsin<sup>147</sup>.

Although some reviews state that COPD affects women and men equally, other studies, have shown the COPD cases to be more prevalent in females in comparison with men<sup>146</sup>. The statement is, however, controversial and requires more extensive research<sup>146</sup>.

Atopy is a hereditary predisposition to produce high-affinity immunoglobulin E (IgE) antibodies as a response to allergen exposure<sup>148,149</sup>. Although there is insufficient knowledge on understanding the impact of atopy in the pathogenesis and development of COPD, it has been suggested that atopy is likely to be one of the risk factors for development of the disease<sup>148</sup>. The study showed that around 18% of COPD patients has an atopic phenotype. This feature is frequently associated with asthma and therefore, the “Dutch hypothesis” proposed the idea of asthma and COPD to be the illnesses of the same basic process<sup>146,150</sup>. However, this hypothesis was later confronted by GOLD highlighting the difference between pathology and pharmacology of these diseases<sup>146</sup>. In addition to atopy, bronchial hyperresponsiveness has also been found to be associated with COPD<sup>149,151</sup>. Up to two-thirds of COPD subjects exhibited bronchial hyperresponsiveness which is linked to airway inflammation and increased sensitivity to a wide variety of airway narrowing stimuli<sup>151</sup>. The attempts to discriminate COPD phenotypes brought hyperresponsiveness to a thorough scrutiny which revealed this symptom to be present in subjects of most COPD subgroups<sup>151</sup>. Although the genomic linkage of bronchial hyperresponsiveness is less clear, both conditions (atopy and hyperresponsiveness) are suggested to stem from the genetic predisposition<sup>146,149</sup>.

Insufficient intake of antioxidant vitamins (A, C and E) and magnesium has been found to be associated with increased risk of COPD. The low dietary intake of the important micronutrients plays a significant role in lung development especially in early life<sup>146,152</sup>.

### **5.2.1.2 Environmental factors**

Smoking is considered to be the most common determinant of COPD globally. The direct correlation between smoking cessation and the rate of lung function decline has been established. It has been documented in many studies that smoking termination decelerates COPD progression over time, as well as exacerbations and smoking-related comorbidities (lung cancer and cardio-vascular disease), which results in mortality decrease in patients with COPD<sup>146,153</sup>.

Inhalation of air pollutants from the burning of biomass fuels, both indoors and outdoors, may be an important risk factor for COPD. Occupational exposure to noxious substances may also trigger the COPD development and progression<sup>30,146,154</sup>.

COPD phenotypes are related to different causes and can differ in patterns of inflammation, but it was found that indoor air pollution and smoking display analogous pathology progression over the course of the disease, suggesting that the response of respiratory tract is associated with the same basic process<sup>155</sup>.

Respiratory-tract infection during childhood lead to unhealthy lungs which might become a risk factor for COPD development in later life<sup>150</sup>.

## **5.2.2 Pathology, pathogenesis, pathophysiology of COPD**

COPD is associated with a chronic inflammatory response which leads to a progressive airflow limitation caused by irreversible structural changes in the lungs. These changes include peribronchiolar fibrosis, chronic bronchitis, emphysema- enlargement and destruction of alveolar walls, and mucus hypersecretion. The changes are believed to be a result of inflammation which predominantly affects peripheral airways, lung parenchyma and even large airways.

Along with the structural pathology of the airways, the pathogenesis of the malady includes chronic inflammation, accelerated organism ageing and increased oxidative stress.

### **5.2.2.1 Pathogenesis**

#### **5.2.2.1.1 Chronic inflammation**

Although the biological mechanisms of COPD are yet to be fully understood, it has been observed that inflammation increases with progression of the illness. At the initial stages of the

disease, the number of innate immune cells grows up which follows by a later activation of adaptive immunity<sup>30</sup>. Upon exposure to the irritant, the respiratory tract activates Toll-like receptors which recruit proteins for subsequent downstream signaling in the innate immune system. These events lead to an elevation in the number of neutrophils and macrophages, activation of structural cells- epithelial cells, endothelial cells and fibroblasts, and mucus secretion in the lungs<sup>139</sup>. T and B lymphocytes number also escalate as the disease advances<sup>30</sup>. Macrophages release inflammatory mediators, including cytokines, chemokines and proteases, to maintain inflammation and uptake of circulating cells into the lungs. Epithelial cells express TGF- $\beta$  which causes local fibrosis<sup>30</sup>. Also, it has been found that concentrations of hepatocyte growth factors are reduced in COPD patients, what presumably promotes emphysema development<sup>146</sup>.

#### **5.2.2.1.2 Oxidative stress**

The free radical theory of ageing is based on the idea that oxygen breakdown in cellular mitochondria, before it is reduced to water, is accompanied by the sequential generation of short-lived intermediates with high reactivity. According to the theory, these reactive radicals inflict significant damage to biological tissues, thus accelerating ageing<sup>156</sup>. The high levels of oxidative stress biomarkers in the expired breath condensate, sputum and blood of COPD patients show evidence of the entire organism being exposed to increased oxidative stress from irritant particles and inflammation caused by innate immunity. Reactive oxygen species (ROS) induce the expression of NF- $\kappa$ B and p38 MAPK and inhibit antiproteases like  $\alpha$ 1-antitrypsin which lead to inflammatory response gain and elastolysis<sup>30</sup>. The TGF- $\beta$  expression is also attributed to ROS activity leading to lung fibrosis<sup>30</sup>. It is believed that excessive ROS induces accelerated ageing favouring chronic inflammation.

#### **5.2.2.1.3 Accelerated ageing**

Since the overwhelming number of diagnosed COPD cases are detected in elderly individuals, the main pathological features of ill patients are believed to derive from accelerated ageing owing to dysfunction of anti-ageing mechanisms (for example those that involve sirtuins) and failure of anti-oxidants to terminate the oxidation which lead to cellular senescence and telomere shortening<sup>30</sup>. Accumulating evidence suggests that the level of SIRT1 is reduced in lung cells of individuals with COPD which regulates FOXO transcription factor via deacetylation<sup>139,157</sup>. Senescent cells, also called “inflammaging”, remain metabolically



active releasing damaging biochemical and inflammatory mediators and inflicting changes to surrounding tissues which inevitably lead to a negative impact on the whole organism <sup>139</sup>.

#### **5.2.2.1.4 Protease-antiprotease imbalance**

The oxidative stress in the lungs of COPD patients results in a catabolic-anabolic enzymes imbalance, inactivating endogenous antiproteases and triggering an acute pulmonary response involving proteases. This imbalance of counteracting compounds results in lung parenchymal destruction.

The inflammatory and epithelial cells release a variety of proteases, including neutrophil elastase, proteinase 3, matrix metalloproteinases (MMPs), and cathepsins. It has been suggested that these proteases interact with each other by mutual activation or “support”, simultaneously deactivating their endogenous inhibitors. These proteases catabolise connective tissues cleaving components of the extracellular matrix, elastin fibers and collagen. The disintegrated fragments from elastin or collagen-derived peptides have been shown to be a chemotactic factor for some immune cells. It is believed that protease-mediated destruction of elastin is a prominent feature of emphysema <sup>158</sup>.

#### **5.2.2.2 Pathophysiology of COPD**

There are mainly two pathological processes behind progressive airflow obstructions in patients with COPD: remodeling and narrowing of the small airways, and destruction of the lung parenchyma with consequent loss of the alveolar attachments of these airways as a result of emphysema<sup>155</sup>.

COPD is a complex systemic disease which encompasses a variety of abnormalities. The pathological features of COPD include obstructive bronchiolitis, emphysema and, in many cases, mucus hypersecretion (chronic bronchitis). Frequently, patients show coexistence or combination of these conditions with one disease predominant manifestation than the other <sup>153</sup>.

##### **5.2.2.2.1 Chronic bronchitis**

The COPD patients with chronic bronchitis are sometimes called “blue bloaters” because of the cyanosis that develops during disease progression. Chronic bronchitis is characterised by perpetual inflammation in the lining of bronchial tubes. In response to the irritants exposure, goblet cells are evoked to overproduce mucus resulting in secretions to build up in airways occluding normal gas exchange <sup>159</sup>. The process is further compounded by a gradual decline in

mucus elimination system. The poor secretions clearing is conditioned by impaired ciliary function, distal airway obstruction, respiratory muscle weakness and reduced peak expiratory flow. Mucous metaplasia causes increased mucus hypersecretion and airway surface tension alteration leading to expiratory collapse. The examination of lung peripheral airways biopsies of subjects with chronic bronchitis revealed an increased number of goblet cells. The progression of COPD and its outcome has been found to be correlated with chronic mucous metaplasia and goblet cells hyperplasia<sup>159</sup>.

Disturbed pulmonary gas exchange hinders O<sub>2</sub> transfer through alveoli efficiently resulting in hypoxia and V/Q mismatch which in turn develops hypoximia and hypercapnia<sup>145,146</sup>. Due to low concentration of O<sub>2</sub> in blood, the organism is forced to produce more red blood cells concomitantly invoking hemoglobin concentration increase. Additionally, abnormally elevated CO<sub>2</sub> levels in blood causes respiratory acidosis. The more advanced COPD stages are accompanied by cyanosis derived from polycythemia and respiratory acidosis<sup>146</sup>.

#### **5.2.2.2.2 Obstructive bronchiolitis**

The progression of COPD is aggravated by obstructive bronchiolitis induced by epithelial layer thickening obstructing airway lumen<sup>159</sup>. The inflamed lumen obliteration and concurrent fibrosis is incorporated with the small airways abnormal remodeling. It is, nevertheless, debatable whether the prevailing reason of occlusion is bronchiolitis and fibrosis or loss of lung elasticity even at the absence of emphysema. It is probable that both factors contribute to airway obstruction<sup>146</sup>.

#### **5.2.2.2.3 Emphysema**

Emphysema is a long-term, progressive obstructive lung disease which is characterised by small airways destruction and as a result, an impaired gas exchange. The emphysematous symptoms include shortness of breath, cough and in advanced cases “barrel chest”.

The inflammatory response of subjects with emphysema leads to elastic fiber break down and loss of alveoli integrity which in turn, prevents from normal air circulation causing air-trapping and lungs volume expanding. The exposure to irritants stimulates macrophages to secrete proteases and cytokines. The cytokines attract neutrophils from circulation to the area and provoke the white blood cells to produce elastases which, upon release, attack elastic tissue around the alveoli. This process leads to a loss of elastic recoil and decline in ventilation.

Additionally, the discharged proteases by macrophages cause a destruction of alveoli walls and capillaries resulting in deficit in V/Q ratio. Such drastic modification in lung elasticity and structure invokes a considerable gas proportion to be trapped in the alveoli even after expiration. This phenomenon is known as “air-trapping” which promotes expiratory volume increase and over-inflating of alveoli. This hyperinflation of the lungs limits airflow and results in clinical outcomes of lower functional capacity, dyspnoea and limited exercise performance <sup>160</sup>.

### **5.2.3 Diagnosis**

COPD diagnosis is frequently complicated by the individual’s misleading judgments about the symptoms which are erroneously assumed to be the natural cause of smoking habit, ageing or job exposure <sup>30</sup>. The respiratory symptoms of the disease include cough, expectoration of sputum, and shortness of breath or frequently occurring respiratory tract infections. The advanced stage of the disease is accompanied with high respiratory rate, the presence of rhonchi (rattling sounds), coarse crackles and wheezes and, in the most advanced cases, cyanosis (blue skin discolouration, a sign of hypoxaemia). The spirometry test is often used as a diagnostic tool for the COPD whereby the FEV1/FVC ratio is recorded determining the Forced Expiratory Volume in the first second to Forced Vital Capacity of air exhaled in one full breath <sup>161</sup>. Patients are often evaluated by a chest X-ray or a chest CT (high resolution computed tomography) to exclude other diagnoses and estimate the degree of structural changes<sup>30</sup>.

### **5.2.4 Treatment**

To date, there is no effective treatment to completely stop the disease progression although smoking cessation markedly reduces the rate of the COPD development <sup>30</sup>. The existing treatments; antibiotics, bronchodilators and corticosteroids, are used to treat co-morbidities, breathlessness and asthma. It is believed that the development of a new therapy based on the inhibition of excessive ROS might have a potential for curing COPD; however, more research is needed to find biomarkers for the disease’s response to the treatment<sup>30</sup>.

### **5.2.5 Markers**

There is a need to identify biomarkers that characterise disease “activity” and predict responsiveness to the treatment<sup>30</sup>. The attempts to find biomarkers in sputum, exhaled air condensate bronchoalveolar lavage or serum have not been successful. However, the level of several biomarkers is measured to predict hospitalization and mortality<sup>30,157</sup>. C-reactive protein

(CRP) and several cytokines are used to only vaguely characterize occurring inflammation and possible infections<sup>30,145</sup>.

It is hypothesised that senescence markers like sirtuins and FOXO might reveal the missing information about COPD mechanisms, accelerated ageing and defects of endogenous antiageing system<sup>139,157</sup>. It has been previously shown that FOXO1 and FOXO3 proteins were underexpressed in peripheral lung epithelium of COPD patients<sup>141</sup>. The similar trend for the senescence markers has been observed during the analysis of macrophages, neutrophils and T-cells from sputum of ill individuals<sup>140,162</sup>.

### **5.3 Methods for sampling**

The biggest hurdle in epidemiological studies is to obtain clinical samples for biomarker content analysis.

Evaluation of biomarker abundance from different anatomical compartments may clarify inflammatory and immunological processes which are not yet understood in different airways segments of individuals with COPD<sup>163</sup>. To address this problem, the samples such as blood, sputum, exhaled gas condensate, mucous lining fluid and lung biopsy have undergone scrutiny to identify the biomarkers assisting in disease endotype classification, disease severity determination, susceptibility to exacerbations, co-morbidities and disease progression.

Venepuncture is a blood sampling method that is typically performed by clinicians or trained staff. The method is invasive and the blood samples do not provide a direct relation of the inflammation processes occurring in the airways<sup>161,164</sup>. However, the difference in some blood markers levels of healthy and COPD individuals was found to directly represent lung inflammation in ill subjects<sup>161,164</sup>.

#### **5.3.1 Lower respiratory tract sampling**

Lower respiratory tract sampling techniques including bronchoalveolar lavage, lung aspirates and lung biopsy are highly invasive<sup>165,166</sup> and can cause inflammation exacerbation<sup>166</sup>. The procedures are costly, time-consuming and require technical personnel, equipment and anaesthesia<sup>166</sup>. Due to washing procedures, samples obtained from bronchoalveolar lavage are dilute<sup>22</sup>.

The exhaled breath condensate is collected via cooling the expired air at 4°C. The method is non-invasive and therefore, attractive for epidemiological studies. Regardless of its potential as a screening or diagnostic tool, this method showed difficulties to obtain reproducible measurements of biomarkers which is presumably compounded by extremely low concentration of the agents (in some instances below the limit of detection) and saliva- and nasal-air-derived contamination of the collected sample <sup>161</sup>.

### **5.3.1.1 Sputum analysis**

Sputum collection is one of the standard sampling techniques of lower respiratory tract that is harnessed to explore heterogeneous cellular profiles and determine inflammation biomarkers <sup>161,164,166</sup>. Since sputum production is initiated directly on the inflammation site, the major advantage of this specimen analysis is the feasibility to accurately track the inflammation process of the stricken tissue <sup>166</sup>. The sampling, either induced or spontaneous, is regarded to be safe and based on stimulation of expectoration production and its further collection. Whilst most COPD individuals generate sputum naturally or spontaneously, some of the subjects are required to resort to induced methods of sample collection. It is typical of research practices to hire healthy donors to establish a healthy baseline and/or compare it against ill individuals. Naturally, healthy control group cannot produce sputum in sufficient amounts for analyses and therefore, an induced sampling must be employed. The induced sputum collection distinguishes two basic protocols that promote phlegm expectoration: 1) inhalation of nebulised hypertonic saline solution or 2) chest/abdomen massage technique <sup>166</sup>. Despite its advantages, sputum induction is not favourable method for children because they tend to swallow the generated sputum rather than cough it out. Additionally, it requires full patient cooperation which is impossible to achieve in some instances (e.g. comatose individuals, infants). Additionally, the sample is contaminated with saliva <sup>167</sup>, contains a high number of cellular debris and dead cells and requires liquefaction <sup>165</sup>.

### **5.3.2 Upper respiratory tract sampling**

Nasal secretion is a heterogeneous fluid of a complex composition which physical properties, cellular profile and biological activity varies between and within individuals <sup>168</sup>. Nasal mucus derives from four major sources: goblet cells, submucous glands, transepithelial ion, water transport and plasma transudation <sup>168</sup>.

The nasal mucosa, occupying the upper respiratory tract, is easily accessible, and it has long been recognized to have a strong histological and immunological relationship with bronchial mucus lining fluid (MLF) <sup>169</sup>. Upon the exposure to noxious stimuli, several inflammation biomarkers extracted from nasal samples showed correspondence to the equivalent mediators in bronchi mucous lining <sup>170</sup>. Moreover, the genetic studies of nasal and bronchial epithelial cells have demonstrated the activation of similar genes in subjects affected by various airways irritants <sup>138,142</sup>. This evidence suggests that nasal samples are easy extractable surrogates that can characterise inflammatory processes occurring in distant and often hardly reachable lower respiratory tract. Despite the apparent correlation of biomarkers in response to irritants, the mucosal immunological processes vary significantly at different sites within the body and therefore, immune system compartmentalisation necessitates a thorough scrutiny. Additionally, it is believed that mucosal immune response to stimuli exposure could provide targets for new treatments against the disease <sup>163</sup>.

#### **5.3.2.1 Nasal sampling**

Examination of nasal mucosa can advance the understanding of underlying immune mechanisms during inflammation by evaluating specific antibody, inflammatory mediator and cytokine levels <sup>168</sup>. For instance, Jochems *et al.* used nasal curettes to analyse composition and activation state of immune cells with flow cytometry <sup>163</sup>. In clinical practices, the exploited sampling of nasal secretion can be mainly divided into spontaneous collection, washes, aspirates and absorption techniques.

#### **5.3.2.2 Spontaneous sampling**

Spontaneous sampling is an uncontrollable method of mucus collection that frequently results in varying sample quantities <sup>168</sup> and therefore, difficulty to obtain reproducible results. The technique was, nevertheless, employed to measure lactoferrin and eosinophilic cationic protein in blown secretions to enable discrimination of sinusitis from natural colds <sup>171</sup>. Furthermore, this sampling method is limited to only individuals with spontaneously secreted fluid which excludes healthy subjects from nasal sample analyses <sup>168</sup>.

#### **5.3.2.3 Nasal lavage**

Nasal lavage is one of the commonly applied nasal sampling techniques which is implemented by instilling the sterile saline solution with pipette or syringe in nares. The procedure is relatively poorly tolerated by individuals because it is frequently accompanied by

saline buffer swallowing and choking. Washing of nasal cavity could generate unpredictably dilute samples containing a target analyte at concentration below the assay's limit of detection. The method yields slightly improved results using ultrasonic nebulisation of saline water for 5 min following by blowing a nostril <sup>168</sup>. However, the samples obtained with nebulisation are more viscous due to higher mucin content and hence, are more difficult to handle. Regardless of its drawbacks, the technique is still ubiquitously exploited. Thus, Lü *et al.* measured immunoglobulins, inflammatory mediators and allergen specific antibodies from nasal samples collected by lavages. Also, Hansel *et al.* applied this technique to subsequently detect rhinovirus infection by PCR from nasal lavage samples.

#### **5.3.2.4 Nasopharyngeal aspiration**

Nasopharyngeal aspiration (NPA) is another standard method to obtain samples for upper airways mucus analysis <sup>172</sup>. The samples are collected by advancing the catheter into the nasopharynx and applying suction to the catheter with an intervening mucus trap. The suction step is usually preceded by instilling a small volume (about 1 mL) of saline solution into a nostril to simplify aspiration of viscous sample <sup>173</sup>. However, this procedure have a reproducibility problem due to unknown and variable dilution of mucosal secretions<sup>172</sup>. The NPA technique is, nevertheless, recognised as a gold standard for collecting specimens to identify respiratory viruses. The method demonstrated 97% sensitivity for detecting RSV positivity in patients with acute bronchiolitis <sup>174</sup>. The NPA is notwithstanding invasive and is generally a not well tolerated method requiring individual's cooperation. Several studies reported upper airways trauma and nasal bleeding during the sampling procedure. Also, the NPA requires specifically trained staff or nurses to perform nasal aspiration <sup>173</sup>.

#### **5.3.2.5 Nasal absorption**

Nasal absorption or so-called "precision mucosal sampling" gained its name due to the ability to perform sample collection directly from respiratory mucosa providing a sample free of saliva-derived contamination <sup>167</sup>. Nasal absorption (NA) or nasosorption sampling is implemented by a collector with absorptive properties such as synthetic electrophoresis wick, cotton or filter paper nasal swabs, and sinus packs. The absorption technique was used in numerous studies to sample mucosal lining fluid (MLF) to evaluate levels of chemokines, cytokines, pollen, LPS and rhinovirus.

For the first time, the method was described in Alam *et al* in 1992 where nasal fluid collection was performed with filter paper consisting of natural cellulose<sup>175</sup>. The collected sample was consequently analysed to measure histamines and cytokines concentrations after controlled nasal allergen challenges and with natural allergen exposure. Although the method provided undiluted nasal fluid, some immunological mediators were found trapped in the porous absorptive material<sup>165</sup>. The increasing evidence also suggests that coarse material like cotton and cellulose may irritate nasal epithelial lining and contaminate the sample with blood<sup>168</sup>. Thus, there was a necessity to test and investigate properties of different absorptive materials that would help to overcome these problems.

Ideally, the nasosorption device should possess the following attributes: 1) generate reproducible results and have high detectability; 2) not traumatise or irritate the epithelial lining; 3) minimise air flow blockage during sampling; 4) release the collected proteins or biomarkers from absorptive matrix; 5) require little or no patient's cooperation; 6) provide sufficient amount of non-diluted samples for analysis; 7) offer an easy handling and processing of the samples<sup>168</sup>. Both, natural<sup>174</sup> and synthetic<sup>168</sup> sponges were exploited and characterised for mucus lining fluid sampling. Lü *et al.* has evaluated performances of various polyurethane foams based on fluid and protein recovery<sup>168</sup>. It has been concluded that polyurethane foams at 110 and 60 PPI had met the fore-mentioned requirements and consequently were recognised as a suitable tool for MLF sampling on a daily practice<sup>168</sup>. In addition, Chawes *et al.* employed a synthetic, fibrous, hydroxylated polyester medium to assess the levels of nasal mediators in epithelial lining fluid from healthy and children with symptomatic allergic rhinitis<sup>169</sup>. As it was observed, despite the feasibility to perform ELF absorption with different materials, the most favourable sampler comprises synthetic absorptive matrix.

Synthetic absorptive matrix (SAM) typically contains an absorptive polymer fibers or foam with enhanced hydrophilicity and reduced biomolecular binding<sup>169</sup>. This tool has been extensively used to develop new protocols for investigation of immunological responses in biological fluids of individuals with respiratory diseases. Owing to its highly absorbent surface and minimal retention of eluting protein from the absorptive matrix, the SAM has become a widely exploited material for nasal absorption (NA) to perform biomarker analyses on nasal secretions<sup>165</sup>.



This device is exceptionally gentle and facilitates MLF obtainment even from inflamed noses at frequent intervals over extended periods of time. Due to its tremendous potential in clinical studies, this method drew attention of scientific community which compared nasosorption with other respiratory tract sampling techniques. Thus, the absorptive matrices have been found superior for inflammatory mediators recovery in comparison with nasopharyngeal aspirate<sup>174,176</sup> and nasal lavages<sup>168,172,177</sup>. The SAM nasosorption (NASAM) method has been repeatedly recognised as a well-tolerated and non-invasive method for nasal sample collection requiring no patient's cooperation. This feature was found to be particularly useful in analysis of sourcing nasal secretions from children and comatose patients<sup>168</sup>.

Thus, the inflammatory mediators' detection with absorptive matrices could impact on our understanding of immunological signatures of the respiratory diseases as well as susceptibility and resistance to immunotherapy. It also opens new perspectives for diagnostic tools<sup>168</sup>.

## **5.4 Method and Materials**

### **5.4.1 Working solution preparation for FOXO1 and FOXO3 assays**

The working solution was prepared by mixing detection and surface marker (anti- Human CD3, Alexa Fluor®532 UCHT1, ThermoFisher, UK) antibodies in a phenol red free RPMI-1640 media. The detection antibody concentrations for FOXO1 and FOXO3 analysis were  $10^6$  and  $10^7$  molecules/nL, respectively. The final concentration of anti-CD3 antibody in the working solution was obtained by diluting its stock 20x.

### **5.4.2 Samples and processing**

#### **5.4.2.1 Sputum sample collection, storing and handling**

The sputum samples collection was undertaken via induced sampling from healthy and spontaneous sampling from individuals with COPD in the NHLI (Imperial College London) in collaboration with Peter Barnes' group. The induced sampling procedure was initiated with inhalation of 200 µg of salbutamol delivered by pressurised metered dose inhaler. To induce sputum generation, the subjects underwent a subsequent hypertonic saline challenge which involved inspiration of nebulised 3.5% saline solution with an atomiser (De Vilbiss 99, Heston, UK). The subjects were invited to expectorate phlegm into a sterile container throughout the entire hypertonic saline challenge duration. The sampling terminated upon 1 mL of sputum specimen obtainment.

In the previous study, our group investigated different protocols of the sputum samples storage and freezing following the sputum collection. The storage conditions were optimised to yield the highest viability of the resuscitated cells in a solution after thawing. The optimal method produced roughly 60% cellular viability and it involved sputum cells treatment with dithiothreitol (DTT) followed by the sample dilution in freezing media (2 mL of Hanks balanced salt solution (HBSS) supplemented with 10% DMSO). Immediately after processing, healthy and COPD sputum samples were stored at -150°C until further analysis.

Prior to the MAC chip analysis, the frozen sputum sample was pre-processed which involved a rapid sample thawing in a water bath at 37°C with a subsequent centrifugation at 300×g for 5 min and concomitant supernatant replacement with a working solution (the preparation is described above). The prepared sample was stored on ice for a short time before loading it into the analysis platform.

#### **5.4.2.2 Nasal sampling**

##### **5.4.2.2.1 Participants recruitment**

Healthy, non-smoking volunteers aged 18+ were sourced from members (staff/students) of Imperial College London in South Kensington and White City campuses. Participants were recruited through word of mouth (

Appendix A: Volunteer recruitment). The potential donors were approached by informing them of the study and its purpose and were asked if they would like to volunteer.

#### **5.4.2.2.2 Study Approval**

This clinical study received Research Ethics Committee approval (ICREC reference: 18IC4779) and written informed consent was obtained from all participants prior to inclusion in the study. The used consent form is in (Appendix B: Consent forms). The volunteers were handed a participant information sheet (Appendix C: Participant information sheet) to familiarise with the study design, participants inclusion criteria and the sampling technique.

#### **5.4.2.2.3 Inclusion and Exclusion Criteria**

The subjects were eligible for inclusion if they were healthy, non-smoking and aged 18+. Smokers, those with symptoms of asthma, hay fever or allergic rhinitis, cold, flu or other infection/respiratory diseases were excluded from this study. Also, for the purposes of the current research, volunteers with no known history of any significant respiratory diseases were sampled <sup>167</sup>.

Pregnant or breastfeeding women and any subject who had contact with infants or the elderly at home or at work were excluded <sup>167</sup>.

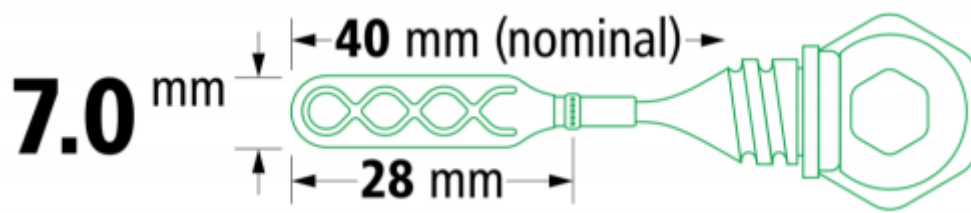
#### **5.4.2.2.4 Study Design**

Each recruited volunteer underwent a nasal sampling procedure up to maximally 5 times. The nasosorption was performed from either of nares and on different days to investigate intrapersonal variation of the signal for a specific biomarker. The collected samples were stored anonymously and were only identifiable by a sample number with no other personal information. The code assigned to the nasal samples was used by the researchers to identify key information about the sample, including the date of collection, gender of the donor and a unique sample identification code. The code had the following format: date of collection (DD/MM/YYYY) – gender (F/M) – sample number (01, 02, ..., n).

#### **5.4.2.2.5 Nasosorption**

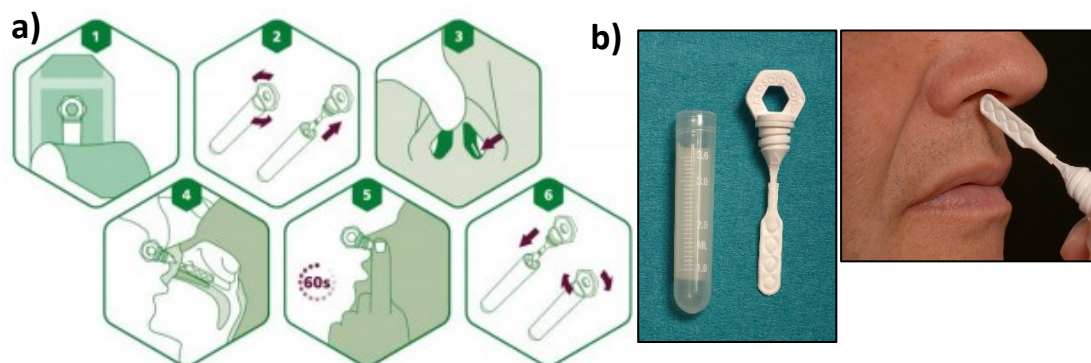
The nasal sampling was performed with a Nasosorption™ FX·I swab (Mucosal Diagnostics, Hunt Developments Ltd., Midhurst, UK) composed of hydrophilic synthetic absorptive matrix (SAM). The applied nasal absorption device (Figure 58) is manufactured as

a CE-marked medical device from medical grade materials using clean rooms and are free of dust and allergens<sup>165,167</sup>.



**Figure 58 Schematic of Nasosorption™ FX·i, working length 40mm, swab size 7 x 28mm long. The device is a non-sterile device consisting of polyester absorptive matrix strip attached to an applicator handle. The image adapted from<sup>178</sup>**

The sampling was performed by the author according to the method described elsewhere<sup>165,178</sup>. To summarise, the nasal cavity of a donor was examined before the sampling initiation using light and speculum. The nasal ELF was obtained by carefully inserting the Nasosorption™ FX·i into the nostril and gently locating the absorbent strip flat against the surface of the interior turbinate<sup>44</sup>. The swab was incubated in the nasal cavity for 60s before it



was retrieved from the nostril and placed back into the tube<sup>44</sup>. The Figure 59 demonstrates step-by-step manipulations of the sampling procedure. The nasal fluid samples were processed immediately after collection.

**Figure 59 a) The diagram of the sample collection procedure which includes unpacking the swab, inspecting the nasal cavity, inserting gently the nasosorption tool into the nose, incubate it for 60 s and return the sample into the tube<sup>44</sup>. b) the Nasosorption™ FX·i device<sup>31</sup>.**

#### 5.4.2.2.6 Nasal samples processing

In the preliminary study, the MLF collection and processing was undertaken at NHLI (St Mary's Hospital, Imperial College London) in collaboration with Trevor Hansel group. The nasal samples were processed shortly after absorption under aseptic conditions. In details, the

SAM swab was detached from the sampler device and subsequently transferred into the tube containing 300  $\mu$ L of RPMI. The tube was gently vortexed to promote the absorbed biomaterial elution into the media. The SAM was further secured on the tube's wall so, to prevent the contact between the swab and solution. The vial was, afterwards, spun down at 2000  $\times$ g for 5 min and the pellet was resuspended in fresh RPMI media. The processed sample was transferred on ice for further analysis to the South Kensington campus. Upon arrival, the sample was spun down again at 300 $\times$ g for 5 min followed by cellular pellet resuspension in 50  $\mu$ L of pre-made working solution. The collected samples were handled immediately after the withdrawal and left on ice till the analysis procedure. The analysis of the samples was performed within 6hrs of withdrawal.

However, the fore-mentioned sample pre-processing method required amendments because the nasal eluate was very dilute in cells presumably after two cycles of centrifugation. The mechanical stress caused by centrifugation of cellular suspension is a well-studied phenomenon that negatively affects cell viability and yield <sup>179</sup>. Also, despite the low minimal cell number requirement to perform a MAC chip experiment, the workflow is less challenging when more concentrated cellular solutions are used. Thus, different sample handling methods were explored to extract more cells from the absorptive matrix.

### **5.4.3 Analysis platform**

The clinical samples analysis was carried out using MAC chip platforms with 4.5nL (300 $\times$  300  $\mu$ m) and 1.25nL (190 $\times$ 190 $\mu$ m) analysis chambers for FOXO1 and FOXO3 copy number evaluation, respectively. The single cell experiments were essentially performed as described in Chapter 3, with the addition of an intermediate step involving on-chip cell sorting.

The FOXO1 assay was performed using CA13/D3 assay (described in Chapter 4 Table 6). The FOXO3 protein was assessed in the clinical samples with both CA8/D1 and CA7/D1 systems (Chapter 3 Table 2).

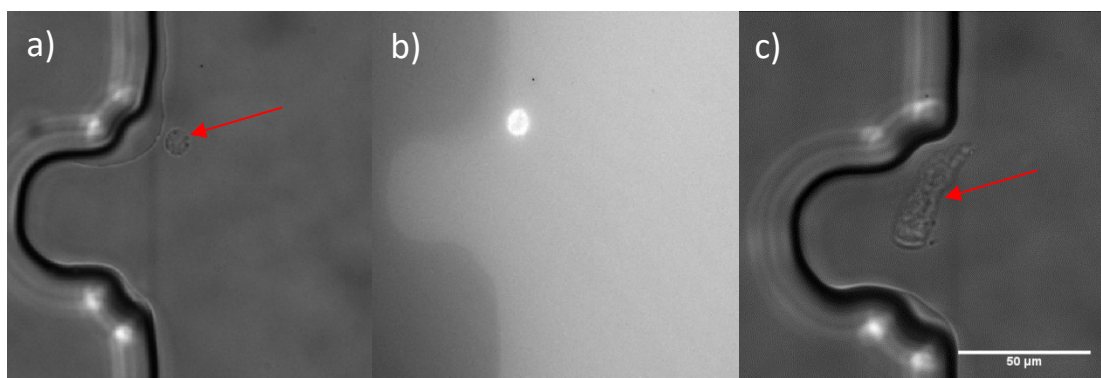
### **5.4.4 On-chip cell sorting**

The clinical material can be heterogeneous containing high amount of debris and unwanted cells. This research was, however, focused on analysis of senescent biomarkers in epithelial and CD3<sup>+</sup> T-cells only. The selection of target cells from the biological matrix was implemented using a custom-built, manually operated optical trap to transfer the relevant cells

into the analysis chambers. The identification and sorting of the target cells during the experiment was based on visual inspection of cell morphology for epithelial cells and fluorescent anti-CD3 labeling for T-cells. It is worth mentioning that no cell viability marker was used to monitor live cells and the selection of target cells was implemented via visual inspection. It has been previously shown that viability dyes and labels may affect native cell behaviour confounding results <sup>180</sup> and therefore, the live cells were just visually examined before trapping and analysis.

Although the EpCAM surface marker labeling is a widely exploited method to unambiguously distinguish epithelial cells, these cells can also be easily recognised by a unique stretched shape (Figure 60c). The epithelial cells were selected for analysis because they were repeatedly reported to have an active role in inflammatory processes in the COPD disease development <sup>30,159</sup>.

Due to a complex content of clinical samples and a lack of apparent morphological attributes of T cells, the surface marker labeling technique was instead chosen to identify the specific lymphocytes. The CD3 antigen is found on the membranes of no other cell type than T cells. This high specificity makes CD3 a useful marker for T cells identification which is extensively used in immunohistochemical studies. As COPD is associated with a chronic inflammation, the rate of inflammatory response was shown to increase with neutrophils, macrophages and lymphocytes number elevation in the lungs along the disease progression <sup>30</sup>. The T cells number growth in the lungs occurs later in the course of the disease progression indicating COPD severity, staging and prognosis.



**Figure 60** The corralled cells into the analysis chambers from the sputum samples a) T-cell bright-field image (red arrow indicates the trapped T-cell) b) the anti-CD3 labeled T-cell image under the epifluorescence c) epithelial cell (red arrow points at the trapped epithelial cell). The scale bar=50μm

#### 5.4.4.1 Cells counting

It is important to characterise cellular number and profile in the specimen because it can potentially provide complementary information in understanding of the COPD development and progression. It was observed that COPD is accompanied by the abnormal cellular number increment in the respiratory tract.

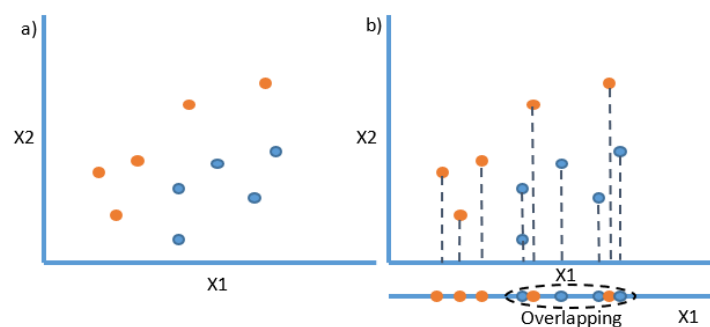
Thus, the single cells counting for both, sputum and nasal samples, was implemented on the MAC chip. Since the cells mostly localised on the same Z-plane of the main channel, images of the channel's segments were taken to retrospectively estimate the number of cells in the sample. The set of 112 frames was taken in three different sections of the main channel (near the inlet, in the middle and next to the outlet) under brightfield and 555nm Epi-fluorescent illumination. The epithelial and CD3+ T-cells were then manually counted from three sections and the mean value was obtained.

#### 5.4.5 Statistical analysis

To statistically describe the collected data on FOXO3 expression in target cells of donors, the independent samples t-test was chosen. The two-tailed t-test was used to compare the means of two groups using SciPy.stats package in Python 3.6. Selection of a 2-sample t-test was predefined by the type of data, its distribution, number of groups and the aim of statistical question.

##### 5.4.5.1 Linear discriminant analysis

Linear Discriminant Analysis or LDA is a technique that finds a linear transformation of data reducing dimensionality to represent the data. LDA is commonly used in pattern classification, groups differences modelling, separating two or more classes and projecting features of higher dimension space into a lower dimension space.



**Figure 61** a) The signal distribution of two populations for features X1 and X2 b) Data set classification with one feature only

For instance, two different classes, possessing multiple unique attributes, often result in incomplete separation if only a single feature is considered leading to a partial overlapping Figure 61. Thus, to achieve efficient classes resolution, more features need to be involved to regard useful information from other attributes. However, the increase of feature number augments the dimensionality of the data which is either hard or impossible to represent graphically on a 2D planes (like paper or computer screen). The LDA method is designed to overcome this limitation by finding a projection plane or line to classify the observations.

Although the LDA classifier can resolve a multiclass dataset, it was originally formulated for a 2-class problem by Ronald Fischer in 1936. He proposed an alternative way to separate the data-cases which roots in finding a linear projection  $y = ax$  for data that maximizes the variance between classes relative to the variance for data from the same class <sup>181</sup>. The linear projection computation conducted for input vector  $x$  and projection vector  $a$  which parameters are obtained using between- and within-class scatter matrices:

$$S_b = (\mu_1 - \mu_2)(\mu_1 - \mu_2)^T \quad \text{Equation 14}$$

$$S_w = \sum_{i,c_i=1} (x_i - \mu_1)(x_i - \mu_1)^T + \sum_{i,c_i=2} (x_i - \mu_2)(x_i - \mu_2)^T \quad \text{Equation 15}$$

where  $S_b$  is between-class matrix,  $S_w$  - within-class matrix,  $\mu_1$  and  $\mu_2$  - means for two classes,  $x_i$  - feature value for a sample.

$a$  is subsequently found by solving:

$$J(a) = \frac{a^T S_b a}{a^T S_w a} \quad \text{Equation 16}$$

Which leads to a solution:

$$a = S_w^{-1}(\mu_2 - \mu_1) \quad \text{Equation 17}$$

The LDA classification was performed using Python 3.6. The eigenvalue and eigenvector were obtained to build the linear projection using a predefined *LinearDiscriminantAnalysis* class in the *scikit-learn* library.



## 5.5 Results and Discussion

### 5.5.1 Sputum cells analysis

The sputum obtained from the healthy and COPD individuals was tested on the MAC chip device to compare the cellular profile and the senescence biomarker levels between the samples. The FOXO1 expression was measured in 15 healthy epithelial cells, 56 healthy T cells and 68 T cells from the ill subject. Due to a healthy sputum shortage and impossibility to gather more biospecimen, two FOXO3 assays were applied to evaluate the protein content in T cells alone from the COPD+ patient only. Overall, 88 CD3+ T cells underwent FOXO3 analysis. All the results were produced from at least two experimental repeats.

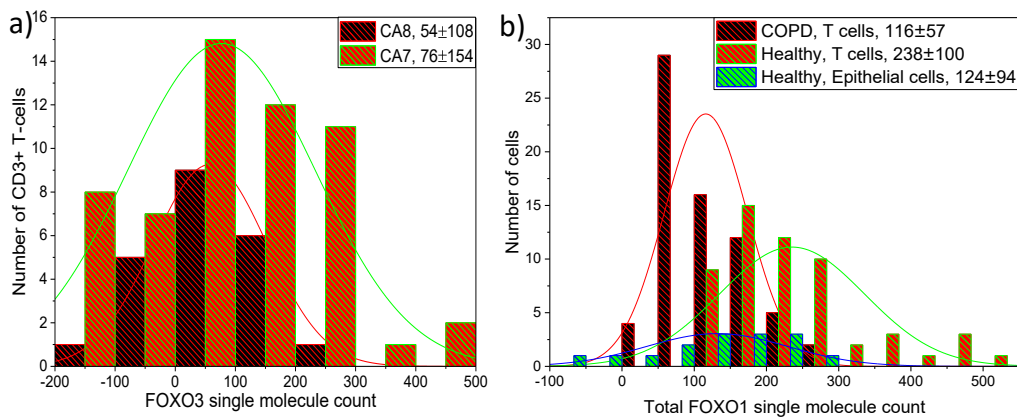
The on-chip cellular count revealed a difference in cellular profile distribution between healthy and COPD samples. A considerably lower ratio of epithelial to CD3+ T cells was observed in the COPD+ individual comparing to the healthy control. The healthy donor possessed roughly an equal number of epithelial and T cells in the fluid. Additionally, the number of epithelial cells in the healthy volunteer was estimated to be roughly 20-30 times greater than in the COPD specimen (data is not shown). Unlike COPD+ patient, the healthy individual was not able to produce sputum spontaneously and therefore, the sampling was implemented via induced method. However, the noted discrepancy in cell ratio is unlikely to be caused by difference in sampling strategies that were applied to harvest the samples from healthy and ill subjects. The studies have previously estimated the difference in cellular yield and profile to be negligible comparing spontaneous and induced sputum<sup>182,183</sup>. Also, the induced method has been observed to produce higher viability of the cells<sup>182,183</sup>. The dissimilar cell ratio across samples was therefore speculated to indicate abnormal inflammation processes that occur in the lungs of the ill donor. This result is consistent with other studies which analysed the cellular distribution in BAL (bronchoalveolar lavage) and lung tissue samples from healthy and ill patients showing the leucocytes quantity increase along with the disease progression and inflammation aggravation<sup>30,184</sup>.

Given the number of epithelial cells in the COPD sample was extremely low, the analysis of FOXOs expression in these cells was a challenge to implement and hence, compare with a healthy group.

Initially, the FOXO3 expression was estimated in CD3+ T cells of COPD sputum using CA8/D1 assay. The Figure 62a shows that the protein level in a considerable proportion (~27%) of the target cells was lower than the LOD of the applied assay. This result implies that FOXO3 analysis in the cells of interest can only be implemented on the MAC chip device with an assay having higher sensitivity. The sensitivity, in turn, can be enhanced by using more active binding sites immobilised on the chip's surface and a capture agent with higher affinity towards the analyte. Thus, the biotinylated-CA7/D1 system was exploited instead to measure the FOXO3 in CD3+ T cells from the samples of the ill volunteer. Interestingly, it was also observed that roughly a third of the tested T cells expressed FOXO3 beneath the assay's sensitivity. Considering both FOXO3 assays failed to detect the senescence marker in about 30% of the cells, it was speculated that low protein expression in these cells might be caused by a cascade of biochemical processes underlying the COPD illness. Although this assumption is supported by several studies <sup>140,162</sup>, there is a need to test a healthy control group first to compare the FOXO3 expression in ill subjects against a healthy baseline. However, this initiative was left out of the scope of this study due to a hurdle to obtain a clinical sample from a healthy donor.

Figure 62b displays the FOXO1 distribution in the epithelial and CD3+ T cells from control and COPD samples. The protocol to analyse total FOXO1 content in epithelial and CD3+ T cells from sputum samples was established by the member of our group- Dr John Simpson. Although it was impossible to collate data on the FOXO1 expression in the epithelial cells between two groups, there is an obvious difference in the transcription factor level in T cells between healthy and COPD+ individuals. The mean binding signal of the senescence marker was observed to be approximately two-fold bigger in T cells from healthy sample in comparison to COPD+ sputum. Thus, the data provides an evidence of FOXO1 assay potential to be efficiently exploited as a diagnostic and prognostic tool for the COPD disease.

Additionally, the heterogeneous expression of the FOXO1 and FOXO3 proteins was noted within as well as between different cell types. The observed cell-to-cell variation might be a key to understanding of the COPD development. This data suggests that MAC chip is a useful tool to single cell proteomics which could possibly advance early stage diagnostics of the disease and elaboration of targeted therapy <sup>24,185</sup>.



**Figure 62 a) FOXO3 expression in T cells of COPD donors b) Total FOXO1 expression in the epithelial and CD3+ T cells from healthy and COPD sputum.**

### 5.5.1.1 Statistical analysis

The data evidently suggests a distinctive FOXO1 protein expression in cells of COPD+ and healthy individuals. To quantify how statistically significant is the disparity of the senescence biomarker level in T cells of healthy and ill volunteers, the two-tailed Student's t-test was applied. It was only possible to statistically describe data generated for FOXO1 protein in CD3+ T cells because there were no or little epithelial cells to analyse in sputum samples of the ill individual. Also, the lack of clinical samples provision precluded FOXO3 protein measurement in epithelial and CD3+ T cells of healthy volunteers disabling the statistical comparison of the transcription factor between the samples of the COPD+ and control groups.

Independent Samples t-test was applied to compare the means of two groups using SciPy.stats package in Python 3.6. The normal distribution of FOXO1 protein in T-cells was observed within two groups (healthy and COPD+ cells). The alpha threshold was fixed at 0.05.

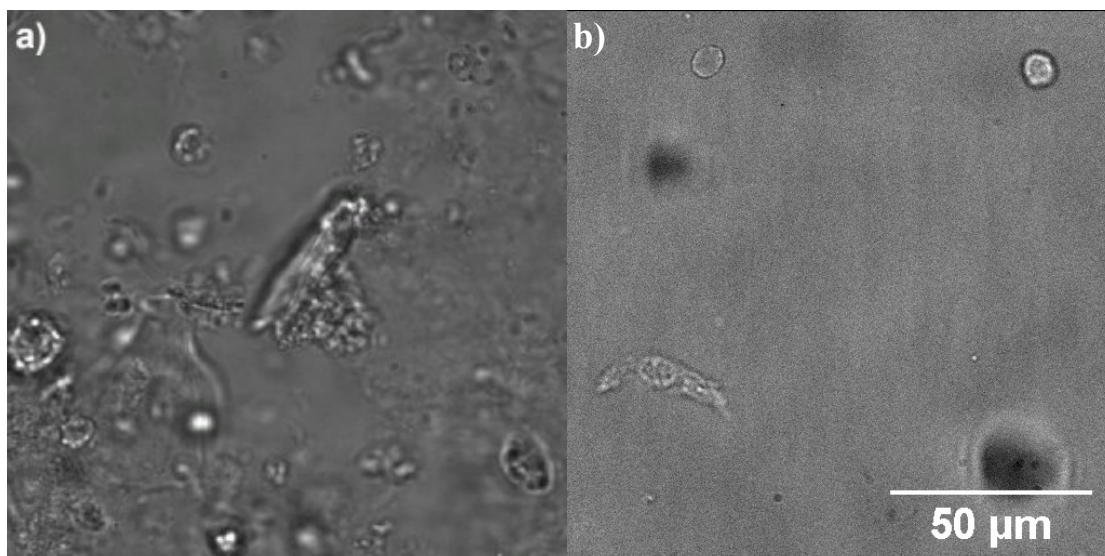
The means of FOXO1 level in T cells between two populations were analysed resulting in t-score and p-value of 8.28 and  $1.76 \times 10^{-13}$ , respectively. The statistics confirms that there is a significant difference in FOXO1 expression between CD3+ T cells from COPD+ and healthy

individuals. This result suggests FOXO1 assay to have a potential to distinguish to some extent a COPD+ individual based on the protein expression.

### **5.5.2 Nasal Samples analysis**

All the sampled individuals characterised nasosorption as a well-tolerated technique for a sample collection. According to the participants, the sampling caused only minor inconvenience like lachrymation and nose tickling. The device inflicted no pain or trauma to the inferior turbinate which inferred NASAM to be a non-invasive tool and hence, valuable for clinical studies. This observation was found to be in consistence with literature <sup>166,186,187</sup>.

Additionally, unlike sputum collection, where dissimilar protocols had to be applied to obtain samples from healthy and ill donors, the nasosorption exploited the same method for all subjects eliminating variation derived from protocol deviation. As opposed to nasosorption, the sputum sample, containing a high mucin level, was more difficult to handle due to its viscosity. Also, the inspection of the MAC device's main channel revealed that the nasal fluid contained minimal biological debris and unwanted biomaterial than the sputum samples (Figure 63). The biological matrix of the main channel can potentially diffuse into the analysis chambers contaminating the single cell signal, decreasing the signal-to-noise level and giving a false signal on the antibody spot. However, despite the obvious reduction in unwanted biological gunk, the nasosorption sample yielded a much lower target cell number than sputum which caused inconveniences associated with handling of dilute samples (hard to find cells in the main channel of the platform, the analysis takes longer time, the adherent cells are difficult to trap) .



**Figure 63** The 512×512 px frame of the main channel after loading a) sputum b) eluted nasal samples into the MAC chip device

### 5.5.2.1 Optimisation of the nasal sample protocol

Different methods for cellular elution and handling were tested to elaborate a protocol with the highest cellular yield. To compare the output cellular number between the employed methods, the two individuals were sampled on consecutive days followed by sample processing described in Table 8. The results were produced from one experiment per method only.

**Table 8** The methods investigated for the nasal MLF sample processing characterised by the mean cellular count in the main channel

Method number	Protocol	Mean cellular count±SD, cells/2mm <sup>2</sup>			
		Epithelial cells		CD3+ T-cells	
		Ind. 1 <sup>a</sup>	Ind. 2 <sup>b</sup>	Ind. 1 <sup>a</sup>	Ind. 2 <sup>b</sup>
<b>Method 1</b>	<ul style="list-style-type: none"> <li>SAM soaked in 300 μL of RPMI,</li> <li>spun down at 2000 ×g for 5 min,</li> <li>pellet resuspended in RPMI,</li> <li>centrifuged 300 ×g for 5 min,</li> <li>resuspended in a working solution</li> </ul>	1±1	1±1	2±1	5±4
<b>Method 2</b>	<ul style="list-style-type: none"> <li>SAM washed with 150 μL of Accutase incubated for 5 min at 37°C,</li> <li>SAM washed with 150 μL of RPMI</li> <li>spun down at 700 ×g for 5 min,</li> <li>pellet resuspended in a working solution</li> </ul>	19±6	4±1	21±12	21±8
<b>Method 3</b>	<ul style="list-style-type: none"> <li>SAM washed with 150 μL of Accutase incubated for 5 min at 37°C,</li> </ul>	4±1	NA <sup>c</sup>	10±7	NA <sup>c</sup>

	<ul style="list-style-type: none"> <li>• SAM washed with 150 <math>\mu</math>L of RPMI</li> <li>• spun down at 300 <math>\times</math>g for 5 min,</li> <li>• pellet resuspended in a working solution</li> </ul>				
--	---	--	--	--	--

<sup>a</sup> Individual 1

<sup>b</sup> Individual 2

<sup>c</sup> Not available due to individual's withdrawal from the study

Table 8 clearly shows a correlation between the mean cellular number and a chosen protocol. The intra-individual variation was considered as a least likely reason for the difference in cellular yield of post-processed samples because a similar trend in cell count was observed in MLF of both individuals.

It is evident that Method 1 resulted in the lowest cellular yield for both cell types compared with the other handling protocols. The possible explanation for this is the involvement of two centrifugation cycles in the handling process which presumably damage the cells leading to a decrease in cell quantity. Additionally, the first spinning was performed at a very high g-force (2000 $\times$ g) causing a mechanical stress to cells and affecting negatively cell viability<sup>179</sup>.

The samples eluted with Method 2 yielded the highest cell number presumably due to performing a single spinning procedure only at a relatively low speed. Epithelial cells are adhesive and tend to attach to surfaces impeding their retrieval from the absorptive matrix. To counteract the epithelial cells' adhesiveness, an Accutase treatment step was included in the protocol. Consequently, the introduction of 5 min Accutase incubation resulted in higher epithelial cells retrieval.

Method 3 applies a similar strategy as Method 2 except the pellet formation was performed at 300 $\times$ g instead. However, it was impossible to test this protocol on the sample from Individual 2 and therefore, more evidence must be adduced to extrapolate a conclusion on this protocol efficiency.

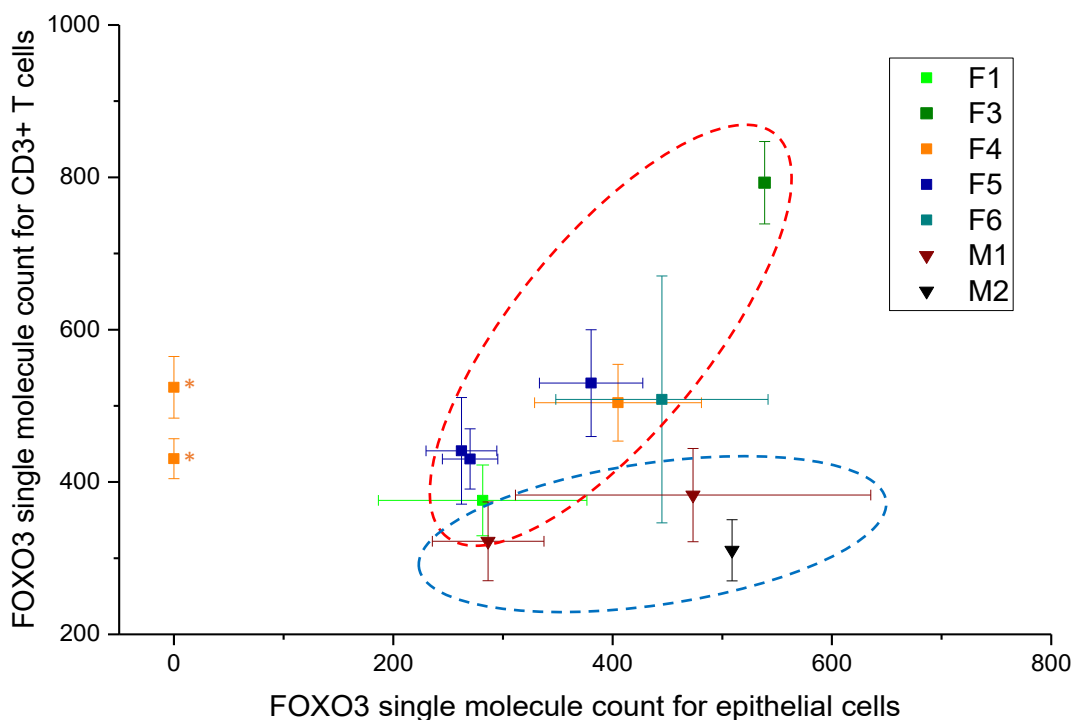
### 5.5.2.2 Evaluation of FOXO3 level in epithelial and CD3+ T-cells

The samples were collected from 7 individuals and several of them were sampled multiple times which enabled the observation of intra- and inter-individual variation of the biomarker. Method 2 was selected for sample processing because it showed a pronounced increase in cellular content in comparison with other tested methods. In this study, the epithelial and CD3+ T cells sorting, and trapping were performed on-chip to further evaluate the FOXO3 expression at a single cell level. The biomarker in clinical samples was measured with biotinylated-

CA7/D1 system. Herein, for the first time we present a data on FOXO3 expression measured in single cells from clinically relevant samples collected via non-invasive nasosorption method.

Figure 64 demonstrates the healthy baseline for FOXO3 expression in nasal epithelial and CD3+ T cells. There is an observed inter- and intraindividual variability in the protein level for both cell types. It was noticed that the protein level in epithelial cells varied between 200-600 molecules per cell whereas most of the T cells expressed the protein in the range of 300-600 molecules per cell. The variability phenomenon was previously described by Riechelmann *et al.* who compared different sampling methods to evaluate inflammatory markers levels from nasal MLF <sup>177</sup>. Additionally, the data might suggest the difference in the protein level between healthy men and women. Although this hypothesis requires more datapoints to be validated, its statistical testing is described in the section below.

The results suggest that MAC chip FOXO3 assay is a perspective method for the biomarker level quantification in nasal ELF samples. Although one of the aims of this study was to investigate whether the nasal epithelial and CD3+ T cells are suitable surrogates for the FOXO3 protein level monitoring in the cells of lower respiratory tract (bronchi), this ambition was not achieved due to the lack of healthy sputum samples. The obtained results are, however, believed to contribute in future attempts to explore and understand development of respiratory diseases like lung cancer and COPD.



**Figure 64** The healthy baseline for FOXO3 expression in epithelial and CD3+ T cells sourced from nasal MLF of 7 donors. F- are the nasal samples obtained from females, M- are the samples obtained from males. Each data point represents the mean FOXO3 single molecule count per sample with standard error. \* No epithelial cells were found in the main channel. There might be a difference in FOXO3 levels between men and women: the red dashed area covers the FOXO3 expression in females whereas blue dashed area represents the range for the protein level in males.

### 5.5.2.3 Statistical analysis

It has been previously reported about a significant gender effect in the healthy baseline of nasal inflammatory biomarkers which showed men to express them at higher levels than women<sup>188</sup>. The gender derived difference in FOXO3 levels in epithelial and T cells was, therefore, also investigated in this research. The data delivered in Table 9 shows an average FOXO3 protein expression in target cells per sample which was used to statistically explore the difference and significance of two populations employing a Student's t-test.

**Table 9** Single molecule mean value of FOXO3 in Epithelial and CD3+ T-cells per sample

Sample nr	Epithelial cells	SE for epithelial cells	T cells	SE for T cells	ID nr	Gender
S1	380	47.2	530	70.0	F5	F
S2	270	25.3	430	39.5	F5	F
S3	262	32.3	441	70.0	F5	F
S4	539	NA <sup>b</sup>	793	54.2	F3	F



S5	445	96.8	508	162.0	F6	F
S6	473	162.0	383	61.2	M1	M
S7	286	50.9	322	51.7	M1	M
S8	509	NA <sup>b</sup>	310	40.1	M2	M
S9	282	95.1	376	46.5	F1	F
S10	NA <sup>a</sup>	NA	430.7	26.2	F4	F
S11	NA <sup>a</sup>	NA	524.3	40.5	F4	F
S12	405	76.1	504	50.3	F4	F

<sup>a</sup> No epithelial cell was found in the main channel to trap for FOXO3 analysis

<sup>b</sup> Low number of cells were analysed to calculate SE

Independent samples t-test was chosen to compare the means of two groups using SciPy.stats package in Python 3.6. Selection of a 2-sample t-test was predefined by the type of data, its distribution, number of groups and the aim of statistical question. The FOXO3 content in epithelial and T-cells were considered to be normally distributed within two groups (female and male).

To test whether the means of FOXO3 level in epithelial cells between genders are statistically removed, the t-score and p-value were calculated resulting in 0.72 and 0.49, respectively. The low t-score indicates no or negligible difference of FOXO3 expression in epithelial cells between men and women. Prior to the test run, the alpha level was selected and set to 0.05. It is noteworthy, that the p-value is much larger than the chosen threshold (0.05) which means that the result is insignificant. Given the test's t-statistics, the null hypothesis failed to be rejected and therefore, it could be concluded that the difference across the two populations for FOXO3 in epithelial cells is not statistically significant.

The gender effect on the FOXO3 content in CD3+ T cells was also statistically tested which produced t-and p-values equal to 2.28 and 0.045, respectively. Interestingly, the t-score reveals the groups to be roughly twice as different from each other as they are within each other. Additionally, the low p-value implies that the result is significant, and the data did not occur by chance. Thus, the alternate hypothesis was supported suggesting the difference in the means of both genders.

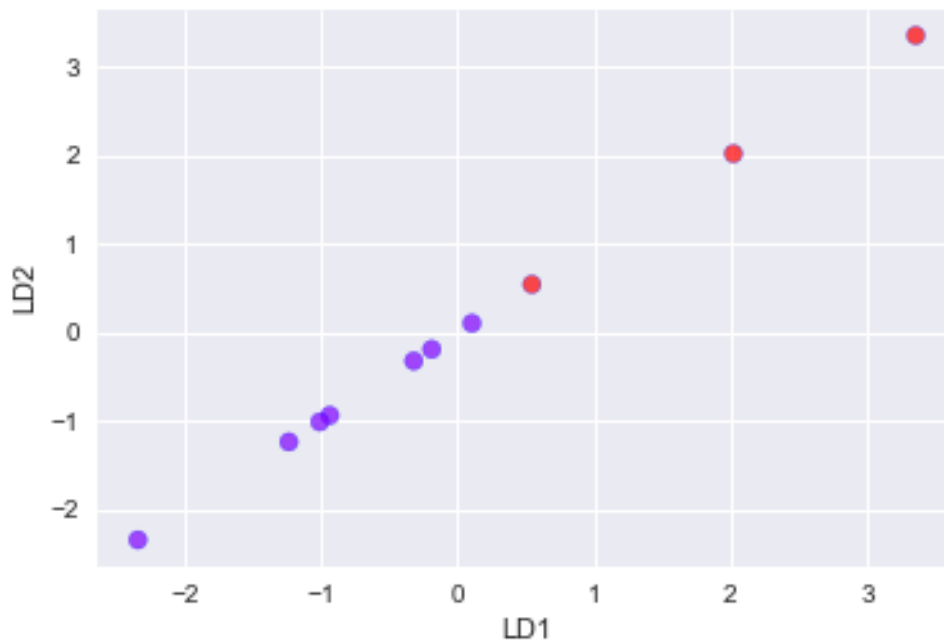
The statistical analysis showed that there is a significant difference of FOXO3 expression in CD3+ T cells between men and women; however, the comparison of the protein abundance in epithelial cell showed no or negligible difference between genders. This might be explained by the fact that the mean value for FOXO3 was obtained implementing analysis on different

types epithelial cells (like goblet, squamous or ciliated epithelial cells) whereas the analysis of lymphocytes was limited to CD3+ T cells only.

Although the different tendencies for FOXO3 distribution in epithelial and T-cells across males and females are notable from the collected data, the bigger sample size is required to validate it.

#### **5.5.2.4 FOXO3 expression classification by gender**

In this study, the analysis of FOXO3 expression in nasal cells of interest was conducted to establish a healthy protein baseline. Intriguingly, the data suggests a gender-derived discrepancy in the protein level. This observation, however, led to a question of how to identify whether the individual's FOXO3 expression falls in the healthy range or beyond it. Assuming the individual with an average FOXO3 expression of 400 molecules in epithelial cells and 300 molecules in T cells, it becomes harder to determine whether there are pathological processes in the persons' respiratory tract or not. Such protein level could be inferred to be within a healthy range if the person is a man but somewhat beneath the norm if this is a woman. The transcription factor expression below the healthy baseline may indicate anomaly in the underlying biochemical processes and abnormal inflammatory response. Hence, there is a need to classify the data by gender to determine a healthy range for FOXO3 abundance. The LDA was used as a tool to find a linear projection for the two populations resolution. The eigenvector and its corresponding eigenvalue for the projection were calculated to be [0.69042293, -0.72340596] and 2.09, respectively. The found projection resulted in a good separation between groups as it is seen on Figure 65.



**Figure 65** The FOXO3 expression in healthy epithelial and T-cells resolved by gender using LDA. ●-females and ●-males

The current model is capable to predict classes based on the FOXO3 level with 90% accuracy. This classifier could be further expanded to predict the health status for both genders based on the FOXO3 protein expression in epithelial and CD3+ T cells. Additionally, the model can be re-trained to classify the data considering more than 2 variables. For example, more accurate assumption on whether the donor is ill or healthy might be obtained considering FOXO1 along with FOXO3 expression in the epithelial and CD3+ T-cells.

## 5.6 Conclusion

The current chapter presents the data on clinical samples analysis obtained from lower and upper respiratory tract. The cells of interest were on-chip sorted and trapped for the subsequent analysis. The content of senescence biomarkers, FOXO1 and FOXO3, was measured at a single cell level in epithelial and CD3+ T cells from both sputum and nasal fluid.

The sputum of healthy and COPD+ individuals was examined for the cellular profile distribution on the MAC device. The difference in epithelial to T cell ratio was observed between two samples. The healthy sputum contained more epithelial cells than the sample collected from the ill donor. The cause for this observation was not attributed to difference in

sampling methods to obtain the specimens from healthy and COPD+ volunteers. Instead, the noted increase of T cells in ill patients might presumably be related to the nature of the COPD disease which is associated with chronic inflammation and dysregulated immune system.

The FOXO1 expression in CD3+ T cells was assessed in sputum of healthy and ill individuals whereas epithelial cells were analysed from healthy sample only because they were underrepresented in the COPD+ sputum. Interestingly, the FOXO1 level in T cells from two sample groups was found to be dissimilar resulting in a lower protein expression in samples from donor diagnosed with COPD. The statistical analysis showed that FOXO1 protein expression in T cells is significantly distinguishable between healthy and COPD+ groups. This result suggests that MAC chip FOXO1 assay has a potential for the disease diagnosis and prognosis and treatment efficiency tracking.

The lack of healthy sputum samples precluded evaluation of the FOXO3 protein in the target cells leading to infeasibility to compare the biomarker expression between healthy and ill volunteers. The FOXO3 was, nevertheless, measured in CD3+ T cells of COPD+ sputum using two different assays, CA8/D1 and biotinylated- CA7/D1. Unexpectedly, both assays showed a very low transcription factor content in the cells failing to detect biomarker in a considerable proportion of the analysed CD3+ T cells. Although the analysis of healthy control group samples is required to identify the reason for this observation, the decrease of FOXO3 level in COPD+ samples could presumably be caused by the abnormal biochemical processes underlying the illness.

The MAC chip FOXO3 assay was applied for the first time to measure the protein level in single cells of nasal ELF. The nasal fluid analysis protocol was developed in this study which preceded by investigation of different methods to elaborate the one (Method 2) with the highest cellular yield. Unlike sputum samples, the nasosorption fluid was more convenient to handle because of the considerably lower viscosity and a lower abundance of the unwanted biomaterial. The healthy FOXO3 baseline was established in epithelial and CD3+ T cells. It was noted, however, that there is a gender effect in the expression of FOXO3 in the target cells. This assumption was statistically tested which was confirmed for FOXO3 expression in CD3+ T cells and rejected in epithelial cells. Additionally, the Linear Discriminant Analysis supported the difference in the FOXO3 level between males and females by finding a data projection for a fine resolution of two populations. Regardless of the small sample size and a need to involve

more participants in the research, the MAC chip FOXO3 assay demonstrated the ability to assess the protein level in single cells of clinically relevant samples.

Also, the missing data on FOXO3 expression in healthy sputum hindered the comparison of the protein levels between upper and lower respiratory tracts. Thus, it left unconfirmed whether the FOXO3 content in the nasal cells correlates with ones in sputum. However, the effort to assess the biomarker level at individual basis in samples obtained by non-invasive means is believed to be worthwhile and meaningful in studying the COPD and other chronic respiratory diseases.

# Chapter 6. Conclusion and future work

## 6.1 Conclusion

Early studies of isogenic cellular populations discovered unexpected variability in protein abundance between cells. The observation was ascribed to biochemical noise (for example, gene expression fluctuation, and variations in the amounts or states of other cellular components) which serves to induce different cellular states and consequently different functional outcomes<sup>5,8</sup>. Numerous examples were provided to demonstrate correlation between protein level noise and population-level co-operation, co-ordination, and survival<sup>5</sup>. These regulatory mechanisms can only be explored in a single-cell regime. This thesis describes the development of methods to analyse protein expression in single cell from clinical samples. Microfluidic-based platforms were used to investigate to isolate, purify, concentrate and analyse single cells.

The inherent proteome heterogeneity between cells may induce a graded endogenous response across a population leading to a survival advantage. This phenomenon is frequently encountered in oncology when a small cancer sub-population is observed to survive and remain proliferative capacity during treatment and initiating disease recurrence and metastasis. The metastasising cells, due to their poor susceptibility to the existing therapy regime, are the most dangerous cancer cell subset that accounts for most cases of death. Before forming a secondary neoplasm, these cells circulate in the vasculatory or lymphatic system which defines them as Circulating Tumour Cells or CTCs. The biology of CTCs is of significant interest in understanding the underlying mechanisms of cancer progression; however, CTC analysis and isolation poses challenges which we attempted to address in this thesis research. Here, we demonstrate the potential of the compound platform that we built to interrogate CTCs protein expression at single cell level. The composite assembly consisted of E-selectin/anti-EpCAM coated microtubes, to isolate and purify the cancer cells, and MAC-based spinning top chip to implement the subsequent analysis of the hydrodynamically trapped cells in the MAC chambers. Despite the successful performance of the devices with the validation samples, the setup faced severe difficulties in delivering cancer cells for single cell protein analysis from the model blood samples. It is, nevertheless, believed that MAC -based tool with further work will be suitable to measure protein abundance and cellular heterogeneity in rare cells like CTCs.

As the CTCs investigations reached a dead end, the research pivoted to establishment of a new MAC chip assay. The selection of the FOXO3 transcription factor to evaluate its abundance in single cells was driven by the protein involvement in regulation of bioprocesses like cell fate decision, glucose homeostasis, immune cell regulation, oxidative stress and human longevity. Disruption in control of the downstream mechanisms of the various processes might lead to the development of diseases like lung cancer and COPD. COPD is a complex and poorly understood illness that is characterised by chronic inflammation, irreversible airway structure remodelling, accelerated ageing and pulmonary function dysregulation. To date, there is no treatment to completely terminate the disease or biomarkers to trace the progression and the effectiveness of the therapy. However, epidemiological reports have found FOXO1 and FOXO3 senescence markers to be downregulated in lung tissues of patients diagnosed with COPD. These speculations around the FOXO3 involvement in development of the illness were a major motivation for the establishment of MAC chip FOXO3 assay. In the course of the assay development the effect of the glycerol and biotinylation on the active binding sites immobilization and performance was discovered. The established system allowed us to investigate the FOXO3 expression heterogeneity between and within human cell populations. The assay was further applied to measure the FOXO3 level in single epithelial and CD3+ T-cells from the sputum of COPD+ individuals. Unfortunately, our NHLI collaborators were not able to provide us with more sputum samples from healthy subjects and hence, the FOXO3 biomarker expression in control group remained unknown. Consequently, it was not feasible to compare the protein abundance in epithelial and CD3+ T-cells from healthy and ill sputum samples. However, FOXO1 expression measurements were implemented in single cells obtained from sputum of both COPD+ and healthy donors. Differences in FOXO1 level were observed in CD3+ T-cells between the tested groups. It was found that the protein was underexpressed in the ill subject in comparison to the healthy sample. This result suggests that we established a successful protocol which distinguishes, to a certain extent, an individual with COPD based on the FOXO1 expression.

Additionally, the method was successfully elaborated to evaluate FOXO3 copy number in single cells of mucousal lining fluid (MLF). The samples sourced from healthy volunteers were non-invasively collected with the nasosorption tool (NASAM). The NASAM device is of high interest for epidemiological studies due to certain advantages. The NASAM is exceptionally gentle and non-invasive tool that enables sampling with no or negligible cooperation required

from the individual patients. The swab absorbs a heterogeneous matrix of nasal fluid providing undiluted samples with no saliva-derived contamination. However, there was a need to elaborate the protocol in order to release cells from the synthetic matrix and load them into the MAC chip for subsequent protein analysis. At the time of study, no previous research had been conducted to estimate FOXO3 protein content in viable single cells from nasal MLF and therefore, we were motivated to fill the gap by establishing the healthy baseline for the biomarker level in single epithelial and CD3+ T-cells. The obtained results imply that the newly established platform could be effectively used for the protein analysis in single epithelial and CD3+ T-cells from nasal samples.

## **6.2 Future work**

### **6.2.1 Strategies for MAC chip analysis improvement**

Although the presented data was obtained by analysing one protein at a time, the MAC chip device allows measurement of multiple analytes simultaneously. The number of targets measured at the same time is, however, limited by the available TIRF channels. Our setup is equipped with four excitation wavelengths and the 4.5nL MAC chip design can maximally accommodate up to four microspots. Thus, the currently utilised system potentially enables a parallel screening of up to 16 different proteins on the individual cell basis. However, the structural modifications of the MAC chambers can possibly increase this number to  $N_{\text{spots}} \times N_{\lambda}$  where  $N_{\text{spots}}$  and  $N_{\lambda}$  are the numbers of spots and excitation wavelengths, respectively. The MAC chip multiplexing experiments have been previously conducted in the group to concurrently assess p53 and its phosphorylated counterpart in cells from disaggregated tumour xenografts<sup>24</sup>. Additionally, the employment of quadruplexed MAC chip carried out a parallel evaluation of c-Jun, two phospho-c-Juns, and AP-1 in different model cell lines. The ability to concurrently measure proteins and their PTM modified equivalents would move the single cell proteomics field from abundance-based models to more dynamic representative assays<sup>189</sup>. For example, the simultaneous monitoring of upstream proteins like PI3K and Akt along with FOXO3 would help in better understanding of the mechanism of FOXO3 regulation and the factors disturbing this biochemical pathway. Therefore, a future direction should be the development of a robust multiplexed assay with the specific signal significantly higher than the present background noise.

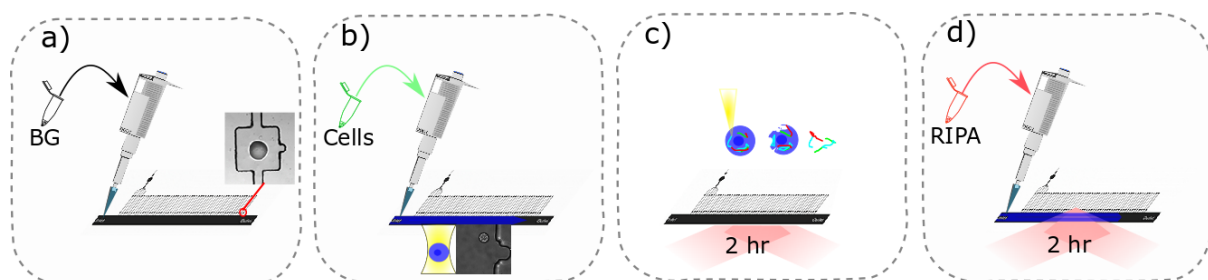


High sensitivity and high affinity assays are required for a parallel monitoring of multiple analytes on the MAC chip. As it was demonstrated in Chapter 3, the development of immunoassays is complicated by the search for well-performing antibody pairs which is time consuming and costly. Additionally, the ideal system for multiplex assays must have low cross-reactivity and high stability. The group has explored double-stranded DNA (dsDNA) as a substitute to immobilised antibodies to measure active DNA-binding form of FOXO1 protein. The dsDNA-antibody assay proved to be a more favourable system than FOXO1 antibody-antibody assay showing a stable performance even after several months of microarray dispensing. This assay has been successfully applied to evaluate active FOXO1 expression in single cells of clinical samples like lung resection and sputum. Other alternatives to antibody and dsDNA application and exploitation of are aptamers and affimers. Aptamers are short single-stranded sequences of oligonucleotides that bind proteins with high sensitivity and affinity<sup>190,191</sup>. The production of aptamers is easy, cheap, fast and animal free in contrast to antibody production<sup>4</sup>. The molecules can be conjugated with linkers or fluorescent tags. Affimers, in turn, are small binding proteins whose dissociation constants are similar or higher than those of antibodies<sup>4</sup>. Due to their small size, the immobilized aptamers or affimers spots have more active binding sites resulting in higher signal. Unlike antibodies, these binding molecules are stable, non-toxic and not immunogenic agents that makes them ideal candidates for therapeutic, in vitro and in vivo biomedical studies<sup>192</sup>. The non-antibody capture agents have been employed in laboratory research, clinical diagnostics and therapy of cancer and cardiovascular and viral diseases<sup>4</sup>. For example, Gold et al. showed in the clinical study of chronic kidney disease (CKD) the utility of an aptamer-based assay to identify two well-known CKD biomarkers and additionally screen 58 potential candidates for CKD biomarkers<sup>193</sup>.

In Chapter 4, the experiments were performed to investigate the effect of chemical lysis on FOXO3 level. Interestingly, the chemical lysis resulted in the protein signal increase in all the tested cell lines relative to the optical cell breakdown. This observation was attributed to the ability of the chemical lysis buffer to dissociate the protein complexes which otherwise retain the FOXO3 bound to the binding partners and disable the biomarker detection. As the RIPA buffer releases FOXO3 from its complexes, there is higher concentration of the analyte in the solution available for the assay system to sense and detect. The data collected with optical and chemical lyses presumably revealed the abundance of the FOXO3 in different states- free and total, respectively. Having shown the feasibility of implementing chemical lysis on the

MAC chip, the obvious future prospect should be coupling both breakdown methods in one experiment to facilitate the simultaneous measurement of free and total FOXO3 expression at a single cell level. The starting point for such experimental design (Figure 66) would be to perform the single cell protein analysis as described in Chapter 3 followed by using Method 2 (outlined in detail in Chapter 4) to deliver chemical lysis buffer into the analysis chambers and subsequently incubate the system for 2 hrs. The apparent advantages of this experiment are:

- The simultaneous data obtaining on free and total FOXO3 content per single cell. This information collection can potentially help to monitor the dynamics of the protein regulation identifying harmful interruptions in the process.
- This method enables a rough estimation of the protein fraction bound to its co-interacting partners. The direct measurement of the bound FOXO3 fraction presents a challenge that partially stems from an incomplete knowledge of the protein co-binding partners along with their binding sites. Even if the full list of the binding proteins was established the acquisition of expensive reagents specific to the partners would be required. Additionally, measuring simultaneously the full library of FOXO3 bound complexes is most likely to be beyond the scope of the MAC chip multiplexing capacity. Therefore, the simplest way to find the bound FOXO3 fraction is to retrospectively calculate the difference between the measured free and total protein levels.
- Combining two experiment in one. The fusion of two tests in a single analysis would require in total less time and reagents than one would spend performing separate experiments for optical and chemical lysis, Figure 66.



**Figure 66** MAC chip workflow to quantify free and bound FOXO3 protein in single cells: a) XY-coordinates of printed spots are recorded and the platform is filled with the background solution. b) the cellular solution is loaded into the main channel and the cells of interest are optically trapped into the MAC analysis chambers. c) the coordinates of spots are imaged under TIRF to measure the background signal. The cells are optically lysed and the signal is then imaged

under TIRF for 2 hr every 30-60 min. d) The RIPA buffer is introduced into the MAC chambers as described in Chapter 4 and the signal is imaged under TIRF for another 2 hr every 30-60 min.

### 6.2.2 Alternative ways for CTCs interrogation

The attempts to develop a composite setup to isolate and analyse CTCs from blood of individuals with metastatic cancer were not successful. However, several novel approaches have emerged and been developed to capture and analyse CTCs during this current study.

The inertial focusing-enhanced microfluidic CTC capture platform, termed CTC-iChip was reported to capture rare circulating cancer cells with 90% efficiency and 98% purity. The platform has been demonstrated to sort CTCs from magnetically labelled cells in whole blood<sup>194</sup>. The iChip integrates sequential pre-processing steps in a single device replacing bulk RBC lysis and centrifugation, hydrodynamic sheath flow in flow cytometry, and magnetic-activated cell sorting (MACS). The microfluidic on-chip functions involved in CTCs extractions are: i) sorting out the white blood cells and CTC from blood matrix using deterministic lateral displacement ii) inertial focussing of the separated target cell fraction into a single line iii) deflection of magnetically tagged cells into a reservoir. The CTC-iChip has been tested in patients with prostate cancer to retrieve the EpCAM+ CTCs for further RNA-based analysis. Also, the device was employed to isolate EpCAM- CTCs from bloods of patients with metastatic breast and melanoma cancers<sup>194</sup>.

Another microfluidic device which combines aqueous phase partitioning with inertial focusing (APPI chip) has been demonstrated to efficiently separate red blood cells (RBCs) from nucleated cells (WBC and CTCs) with >99% efficiency and 94% efficiency. This is a high throughput method whose isolation principle is based on inertial focusing effects and differences in surface energy. The sample and dextran (DEX) solutions were simultaneously introduced into a microfluidic channel so that a thin stream of sample occupied the center of the channel with a DEX stream flanking on both sides. The partition of the sample occurred due to the RBC migration into the DEX phase with the nucleated cells remaining confined to the center stream. This microfluidic device can substitute for the RBC lysis method as well as commonly used techniques to fractionate whole blood by the density gradient centrifugation resulting in significantly lower target cells loss and higher purity<sup>195</sup>.

There are two potential ways in the future to combine the scientific advancements presented by the fore-mentioned groups with our work to enable protein analysis in live CTCs.

The first option is to modify the structures of iChip or APPI devices by introducing the region with Guan traps and MAC chambers to concentrate CTCs and subsequently interrogate them for protein content at a single cell level, provided the chip integrity problems are resolved. The ability to perform isolation, trapping and analysis of CTCs within a single platform would allow a high throughput analysis with a decreased loss of rare cancer cells. Alternatively, it will be possible to perform the analysis of the CTCs using a multi-step sample processing using three individual microfluidic platforms: 1) CTCs separation via iChip or APPI device 2) CTCs hydrodynamic trapping and concentrating on spinning top chip 3) protein analysis using the MAC chip.

### **6.2.3 Directions for further COPD research**

Although the sputum sample analysis was implemented to measure FOXO1 transcription factor in single epithelial and CD3+ T-cells, the abundance of FOXO3 protein was impossible to measure due to clinical samples deficiency. Nevertheless, it is important that future research investigates FOXO3 expression in sputum of both COPD+ and healthy individuals because this protein is believed to be an informative biomarker for COPD development and progression. Also, follow-up studies are necessary to validate the proof of concept analysis extending the number of donors. The clinical picture of COPD includes extensive diversity of symptoms and hence, it is expected to observe discernible FOXOs expression between different ill patients whose biomarkers levels might presumably be correlated with various symptoms. FOXOs analysis in samples of larger patient groups will help to validate the diagnostic and prognostic capacity of the established MAC assays.

The generation of sputum in lungs of ill subjects occurs in proximity to the lesion site. Thus, the sputum expectorated by a COPD+ patient represent anomalies of bioprocesses in the lower airway tract. The inhalation of noxious substances is proposed to be one of the causative factors promoting development of the respiratory diseases. The frontline to the toxic stimuli exposure is, however, an upper airway respiratory tract (e.g. nasal cavity, pharynx, larynx). Therefore, the FOXO1 and FOXO3 analysis in nasal samples of ill and healthy groups might shed some light on the mechanism of COPD development at early stages. The data collected in the present research demonstrates the successful performance of our newly established method to quantify FOXO3 protein in nasal cells from healthy volunteers (Chapter 5). We hope to further expand the study to measure FOXOs in nasal samples of both ill and healthy donors. Also, it is crucial to determine if the inflammation processes in upper respiratory tract can

reflect those occurring in lower respiratory tract. This is a vital question for future research how to identify whether nasal cells could be validated as a surrogate for the bronchial cell analysis. This could be attained by comparing FOXOs expression between nasal and sputum samples sourced from COPD+ and control groups.

Intriguingly, the analysis of nasal samples suggested a gender effect on FOXO3 content. Although more samples are needed to be analysed to validate this observation, the presented data showed a statistically significant difference in signal of CD3+ T cells between two populations of samples for males and females. A gender effect has been previously reported in literature where the baseline level of nasal mucosal IL-8 has been found to be higher in men than in women<sup>188</sup>. These observations suggest that a FOXO3 level considered to be healthy for men might actually indicate pathological processes for women. Therefore, the data generated from the nasal samples analysis was used to train the LDA model to classify the input data into gender categories. Future studies should be devoted to extending the classification model capacity which would then predict the health status of a person based on the FOXO3 abundance in epithelial and CD3+ T cells. This objective will be possible to achieve, only if there is enough data collected from nasal samples of ill and healthy females and males. Also, since the group has elaborated other assays to quantify different proteins in single cells, it is probable that the multiplexed assays could be used to produce multidimensional data sets including signal abundances for several proteins which might be effectively used by LDA model to more accurately relate the datapoints to specific categories as well as to determine the biomarkers' potential to indicate the severity or presence of the disease.

### **6.3 Summary**

Our current research addresses the importance of single cell proteomics and demonstrates analytical capacity of the MAC-based technology as a tool to study human cells on an individual basis. Although the attempts to develop a multi-step platform to capture and analyse CTCs from blood samples were not successful, the results obtained propose a route for future experimental studies.

A novel MAC assay was established to quantify the FOXO3 senescence biomarker expression in model cell lines, and clinical or clinically relevant samples. The methods that we developed to extract target cells from clinical samples, measure protein level with MAC chip

and analyse the collected data is an important contribution in the field of single cell proteomics, cancer and COPD studies. The study investigated the effect of different lysis methods on FOXO3 retrieval on chip which in future will provide information on the protein content in different states; unbound and total. The MAC chip was also successfully employed to measure FOXO1 or FOXO3 in samples from upper and lower respiratory tracts. We believe that the work in this thesis provides a step forward to understanding of the COPD pathogenesis and novel treatment elaboration.

# References

1. Robert Hooke. *Micrographia*. (The British Library, 1665).
2. Liu, Y. Darwin's Pangenesis: A Theory of Everything? in *Advances in Genetics* 1–30 (Elsevier Inc., 2018). doi:10.1016/bs.adgen.2018.05.001
3. Regev, A., Teichmann, S. A. & Lander, E. S. The Human Cell Atlas. *Elife* **6**, (2017).
4. Antonia Sánchez-Romero, M. & Casadesús, J. Contribution of phenotypic heterogeneity to adaptive antibiotic resistance. *PNAS* **111**, 355–360 (2014).
5. Levy, E. & Slavov, N. Single cell protein analysis for systems biology. *Essays Biochem.* **62**, 595–605 (2018).
6. Wei, W. *et al.* Microchip platforms for multiplex single-cell functional proteomics with applications to immunology and cancer research. *Genome Med.* **5**, (2013).
7. Komin, N. & Skupin, A. How to address cellular heterogeneity by distribution biology. *Current Opinion in Systems Biology* **3**, 154–160 (2017).
8. Elowitz, M. B., Levine, A. J., Siggia, E. D. & Swain, P. S. Stochastic Gene Expression in a Single Cell. *Science (80-. )*. **297**, 1183–1186 (2002).
9. Godet, I. & M. Gilkes, D. BRCA1 and BRCA2 mutations and treatment strategies for breast cancer. *Integr. Cancer Sci. Ther.* **4**, (2017).
10. Dagogo-Jack, I. & Shaw, A. T. Tumour heterogeneity and resistance to cancer therapies. *Nat. Rev. Clin. Oncol.* **15**, 81–94 (2018).
11. Chen, W. *et al.* Single Cell Omics: From Assay Design to Biomedical Application. *Biotechnol. J.* **15**, 1–10 (2020).
12. Magness, A. J. Diagnosing cancer one cell at a time with single molecule spectroscopy. (Imperial College London, 2017).
13. Lim, S. Bin, Lim, C. T. & Lim, W. T. Single-cell analysis of circulating tumor cells: Why heterogeneity matters. *Cancers (Basel)*. **11**, 1–22 (2019).
14. Shapiro, E., Biezuner, T. & Linnarsson, S. Next-generation sequencing Single-cell sequencing-based technologies will revolutionize whole-organism science. *Nat. Rev. Genet.* **14**, 618–630 (2013).
15. Ye, X. *et al.* Integrated proteomics sample preparation and fractionation: Method development and applications \*. (2019). doi:10.1016/j.trac.2019.115667
16. Willison, K. R. & Klug, D. R. Quantitative single cell and single molecule proteomics for clinical studies. *Current Opinion in Biotechnology* **24**, 745–751 (2013).
17. Rifai, N., Gillette, M. A. & Carr, S. A. Protein biomarker discovery and validation: the long and uncertain path to clinical utility. *Nat. Biotechnol. Vol.* **24**, (2006).
18. Chen, P., Chen, D., Li, S., Ou, X. & Liu, B.-F. Microfluidics towards single cell resolution protein analysis. *Trends Anal. Chem.* **117**, 2–12 (2019).
19. Amos Tanay & Aviv Regev. Scaling single-cell genomics from phenomenology to

- mechanism. *Nature* **541**, (2017).
20. Li, L., Yan, S., Lin, B., Shi, Q. & Lu, Y. Single-Cell Proteomics for Cancer Immunotherapy. in *Advances in Cancer Research* **139**, 185–207 (Academic Press Inc., 2018).
  21. Kumar, A. *et al.* Single Cell Isolation and Analysis. *Front. Cell Dev. Biol.* **4**, 1–12 (2016).
  22. Yang, L., George, J. & Wang, J. Deep Profiling of Cellular Heterogeneity by Emerging Single-Cell Proteomic Technologies. *Proteomics* 1900226 (2019). doi:10.1002/pmic.201900226
  23. Burgin, E. *et al.* Absolute quantification of protein copy number using a single-molecule-sensitive microarray. *Analyst* **139**, 3235–44 (2014).
  24. Magness, A. J. *et al.* Multiplexed single cell protein expression analysis in solid tumours using a miniaturised microfluidic assay. *Converg. Sci. Phys. Oncol* **3**, 1–11 (2017).
  25. Hughes, A. D. *et al.* Microtube device for selectin-mediated capture of viable circulating tumor cells from blood. *Clin. Chem.* **58**, 846–853 (2012).
  26. Hughes, A. D., Mattison, J., Powderly, J. D., Greene, B. T. & King, M. R. Rapid Isolation of Viable Circulating Tumor Cells from Patient Blood Samples. *J. Vis. Exp.* **64**, 4–7 (2012).
  27. King, M. R., Western, L. T., Rana, K. & Liesveld, J. L. Biomolecular Surfaces for the Capture and Reprogramming of Circulating Tumor Cells. *J. Bionic Eng.* **6**, 311–317 (2009).
  28. Hughes, A. D. & King, M. R. Use of Naturally Occurring Halloysite Nanotubes for Enhanced Capture of Flowing Cells. *Langmuir* **26**, 12155–12164 (2010).
  29. Narasipura, S. D., Wojciechowski, J. C., Charles, N., Liesveld, J. L. & King, M. R. P-selectin-coated microtube for enrichment of CD34+ hematopoietic stem and progenitor cells from human bone marrow. *Clin. Chem.* **54**, 77–85 (2008).
  30. Barnes, P. J. *et al.* Chronic obstructive pulmonary disease. *Nat. Publ. Gr.* **1**, 1–21 (2015).
  31. Salehi-Reyhani, A. *et al.* A first step towards practical single cell proteomics: a microfluidic antibody capture chip with TIRF detection. *Lab. Chip.* **11**, 1256–1261 (2011).
  32. Willison, K. R. & Klug, D. R. Quantitative single cell and single molecule proteomics for clinical studies. *Curr. Opin. Biotechnol.* **24**, 745–751 (2013).
  33. Bruus, H. Basic concepts in microfluidic. in *Theoretical Microfluidics* **28**, 391–397 (2008).
  34. Dynamic Biosensors. *Binding Theory*.
  35. Ekins, R. P. Ligand assays: from electrophoresis to miniaturized microarrays. *Clin. Chem.* **44**, 2015–2030 (1998).



36. Ekins, R. P. & Chu, F. W. Multianalyte Microspot Immunoassay—Microanalytical ‘Compact Disk’ of the Future. *CLIN. CHEM* **37**, 1955–1967 (1991).
37. Ekins, R., Chu, F. & Biggart, E. Development of microspot multi-analyte ratiometric immunoassay using dual fluorescent-labelled antibodies. *Anal. Chimica Acta* **227**, 73–96 (1989).
38. Atkins, P. & Paula, J. de. *Atkins’ Physical Chemistry. Oxford* **94**, (2010).
39. Bergeron, S., Laforte, V., Lo, P.-S., Li, H. & Juncker, D. Evaluating mixtures of 14 hygroscopic additives to improve antibody microarray performance. *Anal Bioanal Chem* **407**, 8451–8462 (2015).
40. Barbulovic-Nad, I. *et al.* Critical Reviews in Biotechnology Bio-Microarray Fabrication Techniques—A Review Bio-Microarray Fabrication Techniques—A Review. *Crit. Rev. Biotechnol.* **264**, (2006).
41. Ihalainen, P., Määttänen, A. & Sandler, N. Printing technologies for biomolecule and cell-based applications. *Int. J. Pharm.* **494**, 585–592 (2015).
42. Welcome. Available at: <http://www.arrayit.com/>. (Accessed: 10th October 2019)
43. Welch, N. G., Scoble, J. A., Muir, B. W. & Pigram, P. J. Orientation and characterization of immobilized antibodies for improved immunoassays. *Cit. Biointerphases* **12**, 2–301 (2017).
44. Tahirbegi, B. *et al.* Probing Synaptic Amyloid-Beta Aggregation Promoted by Copper Release. *Biophys. J.* **114**, 430a (2018).
45. Axelrod, D. Total internal reflection microscopy in cell biology. *Methods Enzymol.* **361**, 1–33 (2003).
46. Axelrod, D. *Cell-Substrate Contacts Illuminated by Total Internal Reflection Fluorescence. The Journal of cell biology* **89**, (1981).
47. Capsid Constructors. Available at: <https://capsidconstructors.github.io/lab-book/imaging/tirf.html>. (Accessed: 10th January 2020)
48. Stott, S. L. *et al.* Isolation of circulating tumor cells using a microvortex-generating herringbone-chip. *PNAS* **107**, 18392–7 (2010).
49. Salehi-Reyhani, A., Burgin, E., Ces, O., Willison, K. R. & Klug, D. R. Addressable droplet microarrays for single cell protein analysis. *Analyst* **139**, 5367–5374 (2014).
50. Heath, J. R., Ribas, A. & Mischel, P. S. Single cell analytic tools for drug discovery and development. *Nat Rev Drug Discov* **15**, 204–216 (2016).
51. Chaffer, C. L. & Weinberg, R. a. A Perspective on Cancer Cell Metastasis. *Science (80-. )*. **331**, 1559–1564 (2011).
52. Hsieh, J. C. & Wu, T. M. The Selection Strategy for Circulating Tumor Cells (CTCs) Isolation and Enumeration: Technical Features, Methods, and Clinical Applications. in *Tumor Metastasis* 145 (2016).
53. Massagué, J. & Obenauf, A. C. Metastatic colonization by circulating tumour cells.

- Nature* **529**, 298–306 (2016).
54. Zheng, X. *et al.* Epithelial-to-mesenchymal transition is dispensable for Metastasis but Induces Chemoresistance in Pancreatic Cancer. *Nature* **527**, (2015).
  55. Cristofanilli, M. *et al.* Circulating Tumor Cells, Disease Progression, and Survival in Metastatic Breast Cancer. *n engl j med* **351**, (2004).
  56. Yap, T. A., Lorente, D., Omlin, A., Olmos, D. & De Bono, J. S. Circulating Tumor Cells: A Multifunctional Biomarker. *Clin Cancer Res*; **20**, (2014).
  57. Alix-Panabières, C., Müller, V. & Pantel, K. Current status in human breast cancer micrometastasis. *Curr. Opin. Oncol.* **19**, 558–563 (2007).
  58. Nagrath, S. *et al.* Isolation of rare circulating tumour cells in cancer patients by microchip technology. *Nature* **450**, 1235–9 (2007).
  59. Pearl, M. L. *et al.* Treatment monitoring of patients with epithelial ovarian cancer using invasive circulating tumor cells (iCTCs). *Gynecol. Oncol.* **137**, 229–238 (2015).
  60. Zieglschmid, V., Hollmann, C. & Böcher, O. Detection of Disseminated Tumour cells in peripheral blood. *Crit. Rev. Clin. Lab. Sci.* **42**, 155–196 (2005).
  61. Alix-Panabières, C. & Pantel, K. Challenges in circulating tumour cell research. *Nat. Rev. Cancer* **14**, 623–631 (2014).
  62. Ashworth, T.R. (1869) A Case of Cancer in Which Cells Similar to Those in the Tumours Were Seen in the Blood after Death. *Med. J. Aust.* **14**, 146–147 (1869).
  63. Chambers, A. F., Groom, A. C. & MacDonald, I. C. Dissemination and growth of cancer cells in metastatic sites. *Nat. Rev. Cancer* **2**, 563–72 (2002).
  64. Nguyen, D. X., Bos, P. D. & Massagué, J. Metastasis: from dissemination to organ-specific colonization. *Nat. Rev. Cancer* **9**, 274–84 (2009).
  65. Fischer, K. R. *et al.* Epithelial-to-mesenchymal transition is not required for lung metastasis but contributes to chemoresistance. *Nature* **527**, 472–476 (2015).
  66. Thiery, J. P., Acloque, H., Huang, R. Y. J. & Nieto, M. A. Epithelial-Mesenchymal Transitions in Development and Disease. *Cell* **139**, 871–890 (2009).
  67. Dumont, N. *et al.* Sustained induction of epithelial to mesenchymal transition activates DNA methylation of genes silenced in basal-like breast cancers. *Proc. Natl. Acad. Sci. U. S. A.* **105**, 14867–72 (2008).
  68. Fidler, I. J. The pathogenesis of cancer metastasis: the ‘seed and soil’ hypothesis revisited. *Nat. Rev. Cancer* **3**, 453–458 (2003).
  69. Liang, W. & Ferrara, N. The Complex Role of Neutrophils in Tumor Angiogenesis and Metastasis. *Cancer Immunol. Res.* **4**, 83–91 (2016).
  70. Cameron, M. D. *et al.* Temporal progression of metastasis in lung: Cell survival, dormancy, and location dependence of metastatic inefficiency. *Cancer Res.* **60**, 2541–2546 (2000).
  71. Cho, H. *et al.* Microfluidic technologies for circulating tumor cell isolation. *Analyst*

- 143, 2936 (2018).
72. Yang, J. & Weinberg, R. A. Epithelial-Mesenchymal Transition: At the Crossroads of Development and Tumor Metastasis. *Dev. Cell* **14**, 818–829 (2008).
  73. Kolostova, K. *et al.* Isolation, primary culture, morphological and molecular characterization of circulating tumor cells in gynecological cancers. *Am. J. Transl. Res.* **7**, 1203–1213 (2015).
  74. Wang, R. *et al.* Cultured circulating tumor cells and their derived xenografts for personalized oncology. *Asian J. Urol.* (2016). doi:10.1016/j.ajur.2016.08.005
  75. Bast, R. C., Hennessy, B. & Mills, G. B. The biology of ovarian cancer: new opportunities for translation. *Nat Rev Cancer* **9**, 415–428 (2009).
  76. Danova, M., Torchio, M. & Mazzini, G. Isolation of rare circulating tumor cells in cancer patients: technical aspects and clinical implications. *Expert Rev. Mol. Diagn.* **11**, 473–485 (2011).
  77. Sequist, L. V., Nagrath, S., Toner, M., Haber, D. A. & Lynch, T. J. The CTC-chip an exciting new tool to detect circulating tumor cells in lung cancer patients. *J. Thorac. Oncol.* **4**, 281–283 (2009).
  78. Chalmers, J. J., Lustberg, M., Jatana, K. R. & Zborowski, M. Emerging Technologies for CTC Detection Based on Depletion of Normal Cells. *Recent Results Cancer Res.* **195**, 97–110 (2012).
  79. Alix-Panabie' Res, C., Riethdorf, S. & Pantel, K. Circulating Tumor Cells and Bone Marrow Micrometastasis. *Clin Cancer Res* **14**, (2008).
  80. Narayanamurthy, V. *et al.* Microfluidic hydrodynamic trapping for single cell analysis: mechanisms, methods and applications. *Anal. Methods* **9**, 3751–3772 (2017).
  81. Di Carlo, D., Aghdam, N. & Lee, L. P. Single-cell enzyme concentrations, kinetics, and inhibition analysis using high-density hydrodynamic cell isolation arrays. *Anal. Chem.* **78**, 4925–4930 (2006).
  82. Xu, X., Sarder, P., Li, Z. & Nehorai, A. Optimization of microfluidic microsphere-trap arrays. *Biomicrofluidics* **7**, 014112 (2013).
  83. Guan, A., Shenoy, A., Smith, R. & Li, Z. Streamline based design guideline for deterministic microfluidic hydrodynamic single cell traps. *Biomicrofluidics* **9**, (2015).
  84. MicroChem. *SU-8 2000 Permanent Epoxy Negative Photoresist.*
  85. Wojciechowski, J. C. *et al.* Capture and enrichment of CD34-positive haematopoietic stem and progenitor cells from blood circulation using P-selectin in an implantable device. *Br. J. Haematol.* **140**, 673–681 (2008).
  86. Hughes, A. D., Mattison, J., Powderly, J. D., Greene, B. T. & King, M. R. Rapid Isolation of Viable Circulating Tumor Cells from Patient Blood Samples. *J. Vis. Exp.* **64**, 4–7 (2012).
  87. Collin, M. & Kilian, M. Bacterial Modulation of Fc Effector Functions. in *Antibody Fc Linking Adaptive and Innate Immunity* 317–332 (Elsevier, 2014). doi:10.1016/B978-0-

12-394802-1.00018-2

88. Münz, M. *et al.* The carcinoma-associated antigen EpCAM upregulates c-myc and induces cell proliferation. *Oncogene* **23**, 5748–5758 (2004).
89. Biotec, M. *Isolation of mononuclear cells from human peripheral blood by density gradient centrifugation.* (2008).
90. Jaatinen, T. & Laine, J. Isolation of Mononuclear Cells from Human Cord Blood by Ficoll-Paque Density Gradient. *Curr. Protoc. Stem Cell Biol.* **1**, 1–4 (2007).
91. Jia, Y. *et al.* A Modified Ficoll-Paque Gradient Method for Isolating Mononuclear Cells from the Peripheral and Umbilical Cord Blood of Humans for Biobanks and Clinical Laboratories. *Biopreserv. Biobank.* **16**, (2018).
92. Tan, Y. S. & Lei, Y. L. Isolation of tumor-infiltrating lymphocytes by Ficoll-Paque density gradient centrifugation. in *Mouse Models of Innate Immunity: Methods and Protocols, Methods in Molecular Biology* 93–99 (1960). doi:10.1007/978-1-4939-9167-9\_8
93. Sciences, G. H. L. & Isolation. *Isolation of mononuclear cells Methodology and applications.* (2014).
94. Walker, J. M. *Immunogenetics Methods and Applications in Clinical Practice.* (Methods in Molecular Biology, 2012). doi:10.1007/978-1-61779-842-9
95. Biotend. *RBC Lysis Buffer (10X).* (2013).
96. Chernyshev, A. V. *et al.* Erythrocyte lysis in isotonic solution of ammonium chloride: Theoretical modeling and experimental verification. *J. Theor. Biol.* **251**, 93–107 (2008).
97. Ley, K. The role of selectins in inflammation and disease. *Trends Mol. Med.* **9**, 263–268 (2003).
98. Gout, S., Tremblay, P. L. & Huot, J. Selectins and selectin ligands in extravasation of cancer cells and organ selectivity of metastasis. *Clin. Exp. Metastasis* **25**, 335–344 (2008).
99. Thermo Electron Corporation. Accutase™ Cell Detachment Solution. (2005). Available at: [http://www.thermo.com.cn/Resources/200802/productPDF\\_26369.pdf](http://www.thermo.com.cn/Resources/200802/productPDF_26369.pdf). (Accessed: 21st September 2020)
100. Calnan, D. & Brunet, A. The FoxO code. *Oncogene* **27**, 2276–2288 (2008).
101. Tsai, K. L. *et al.* Crystal structure of the human FOXO3a-DBD/DNA complex suggests the effects of post-translational modification. *Nucleic Acids Res.* **35**, 6984–6994 (2007).
102. Hannenhalli, S. & Kaestner, K. H. The evolution of Fox genes and their role in development and disease. *Nat Rev Genet* **10**, 233–240 (2009).
103. Peng, S. Foxo in the immune system. *Oncogene* **27**, 2337–2344 (2008).
104. Coffey, P. J. & Burgering, B. M. T. Forkhead-box transcription factors and their role in

- the immune system. *Nat. Rev. Immunol.* **4**, 889–899 (2004).
105. Wang, M., Zhang, X., Zhao, H., Wang, Q. & Pan, Y. FoxO gene family evolution in vertebrates. *BMC Evol. Biol.* **9**, (2009).
  106. Obsil, T. & Obsilova, V. Structure/function relationships underlying regulation of FOXO transcription factors. *Oncogene* **27**, 2263–2275 (2008).
  107. Eijkelenboom, A. & Burgering, B. M. The forkhead box O (FOXO) family of transcription factors regulates diverse gene expression programmes and affects many cellular processes, including cell cycle regulation, cell survival and metabolism (reviewed in. *Nat. Rev. Mol. Cell Biol.* **14**, (2013).
  108. Eijkelenboom, A., Mokry, M., Smits, L. M., Nieuwenhuis, E. E. & Burgering, B. M. T. FOXO3 Selectively Amplifies Enhancer Activity to Establish Target Gene Regulation. *CellReports* **5**, 1664–1678 (2013).
  109. Dhawan, M., Wise, F. & Baemner, A. Development of a laser-induced cell lysis system Received: *Anal Bioanal Chem* **374**, 421–426 (2002).
  110. Chandradoss, S. D. *et al.* Surface Passivation for Single-molecule Protein Studies. *J. Vis. Exp* **86**, 1–8 (2014).
  111. Rasnik, I., Mckinney, S. A. & Ha, T. Surfaces and Orientations: Much to FRET about? *Acc. Chem. Res* **38**, 542–548 (2005).
  112. Invitrogen. *Avidin and NeutrAvidin™ Biotin-Binding Proteins and Conjugates.* (2009).
  113. Köhler, M. *et al.* pH-Dependent Deformations of the Energy Landscape of Avidin-like Proteins Investigated by Single Molecule Force Spectroscopy. *Molecules* **19**, 12531–12546 (2014).
  114. Salehi-Reyhani, A. L. I. TOOLS FOR SINGLE CELL PROTEOMICS. (2011).
  115. Wu, P. & Grainger, D. W. Comparison of hydroxylated print additives on antibody microarray performance. *J Proteome Res* **5**, 2956–2965 (2006).
  116. Olle, E. W. *et al.* Comparison of antibody array substrates and the use of glycerol to normalize spot morphology. *Exp. Mol. Pathol.* **79**, 206–209 (2005).
  117. Kang, H.-W. *et al.* A 3D bioprinting system to produce human-scale tissue constructs with structural integrity. *Nat. Biotechnol.* **34**, (2016).
  118. Fainerman, V. B., Miller, R., Wu, R. & Makievski, A. V. Adsorption Isotherm and Surface Tension Equation for a Surfactant with Changing Partial Molar Area. 1. Ideal Surface Layer. *J. Phys. Chem.* **100**, 7669–7675 (1996).
  119. Burgin, E. The design of a digital single-molecule detection platform, with direct application to single cell analysis. (2012).
  120. Rickman, D. S., Herbert, C. J. & Aggerbeck, L. P. Optimizing spotting solutions for increased reproducibility of cDNA microarrays. *Nucleic Acids Res.* **31**, e109 (2003).
  121. Armbruster, D. A. & Pry, T. Limit of Blank, Limit of Detection and Limit of Quantitation. *Clin Biochem Rev* **29**, (2008).

122. Boucher, J., Kleinridders, A. & Kahn, C. R. Insulin receptor signaling in normal and insulin-resistant states. *Cold Spring Harb. Perspect. Biol.* **6**, (2014).
123. Wang, Y. *et al.* FOXO transcription factors: their clinical significance and regulation. *Biomed Res. Int.* **2014**, 1–13 (2014).
124. Brent, M. M., Anand, R. & Marmorstein, R. Structural Basis for DNA Recognition by FoxO1 and Its Regulation by Posttranslational Modification. *Structure* **16**, 1407–1416 (2008).
125. Brunet, A. *et al.* Protein Kinase SGK Mediates Survival Signals by Phosphorylating the Forkhead Transcription Factor FKHRL1 (FOXO3a). **21**, 952–965 (2001).
126. Daitoku, H., Sakamaki, J. & Fukamizu, A. Regulation of FoxO transcription factors by acetylation and protein–protein interactions. *Biochim. Biophys. Acta* **1813**, 1954–1960 (2011).
127. Perrot, V. & Rechler, M. M. The Coactivator p300 Directly Acetylates the Forkhead Transcription Factor Foxo1 and Stimulates Foxo1-Induced Transcription. *Mol. Endocrinol.* **19**, 2283–2298 (2005).
128. Daitoku, H. *et al.* Silent information regulator 2 potentiates Foxo1-mediated transcription through its deacetylase activity. *PNAS* **101**, 10042–10047 (2004).
129. Motta, M. C. *et al.* Mammalian SIRT1 Represses Forkhead Transcription Factors. *Cell* **116**, 551–563 (2004).
130. Oteiza, A. & Mechti, N. Control of FoxO4 Activity and Cell Survival by TRIM22 Directs TLR3-Stimulated Cells Toward IFN Type I Gene Induction or Apoptosis. *J. Interferon Cytokine Res.* **35**, 859–874 (2015).
131. Van Der Horst, A. *et al.* FOXO4 transcriptional activity is regulated by monoubiquitination and USP7/HAUSP. *Nat. Cell Biol.* **8**, (2006).
132. Kong, D. & Yamori, T. ZSTK474 is an ATP-competitive inhibitor of class I phosphatidylinositol 3 kinase isoforms. *Cancer Sci.* **98**, 1638–1642 (2007).
133. Kong, D., Yaguchi, S. & Yamori, T. Effect of ZSTK474, a Novel Phosphatidylinositol 3-Kinase Inhibitor, on DNA-Dependent Protein Kinase. *Biol. Pharm. Bull.* **32(2)**, 297–300 (2009).
134. Link, W. *et al.* Chemical interrogation of FOXO3a nuclear translocation identifies potent and selective inhibitors of phosphoinositide 3-kinases. *J. Biol. Chem.* **284**, 28392–400 (2009).
135. Santo, E. E. *et al.* FOXO3a is a major target of inactivation by PI3K/AKT signaling in aggressive neuroblastoma. *Cancer Res.* **73**, 2189–98 (2013).
136. Boster. *RIPA Lysis Buffer*.
137. Miranti, C. K. Application of Cell Adhesion to Study Signaling Networks. in *Methods in Cell biology* (2002). doi:10.1895/wormbook.1.49.1
138. Anne Bergougoux, Mireille Claustres & Albertina De Sario. Nasal epithelial cells: a tool to study DNA methylation in airway diseases. *Epigenomics* **7**, 119–126 (2015).

139. Mercado, N., Ito, K. & Barnes, P. J. Accelerated ageing of the lung in COPD: new concepts. *Thorax* **70**, 482–489 (2015).
140. Hwang, J.-W. *et al.* FoxO3 deficiency leads to increased susceptibility to cigarette smoke-induced inflammation, airspace enlargement, and chronic obstructive pulmonary disease. *J. Immunol.* **187**, 987–998 (2011).
141. Taka, C. *et al.* SIRT1 and FOXO1 mRNA expression in PBMC correlates to physical activity in COPD patients. *Int. J. COPD* **12**, 3237–3244 (2017).
142. Zhang, X. *et al.* Similarities and differences between smoking-related gene expression in nasal and bronchial epithelium. *Physiol Genomics* **41**, 1–8 (2010).
143. Erbas, B. *et al.* Alternate methods of nasal epithelial cell sampling for airway genomic studies. *J. Allergy Clin. Immunol.* **136**, 1120-1123.e4 (2015).
144. Chronic obstructive pulmonary disease (COPD) statistics | British Lung Foundation. Available at: <https://statistics.blf.org.uk/copd>. (Accessed: 2nd May 2018)
145. Global Initiative for Chronic Obstructive Lung Disease. *Global Strategy for the diagnosis, Management, and Prevention of Chronic Obstructive Pulmonary disease*. (2017). doi:10.1164/rccm.201701-0218PP
146. Trevor T.Hansel, P. J. B. *An Atlas of CHRONIC OBSTRUCTIVE PULMONARY DISEASE*. (2004).
147. Tanner, R. & Primhak, M. Alpha-1 antitrypsin deficiency. *Arch Dis Child* **85**, 2–5 (2001).
148. Fattahi, F. *et al.* Atopy is a risk factor for respiratory symptoms in COPD patients: results from the EUROSCOP study. *Respir. Res.* **14**, 1–8 (2013).
149. Postma, D. S., Koppelman, G. H. & Meyers, D. A. *The Genetics of Atopy and Airway Hyperresponsiveness*. *Am J Respir Crit Care Med* **162**, (2000).
150. Salvi, S. S. & Barnes, P. J. Chronic obstructive pulmonary disease in non-smokers. *Lancet* **374**, 733–743 (2009).
151. Zanini, A. *et al.* Bronchial hyperresponsiveness, airway inflammation, and reversibility in patients with chronic obstructive pulmonary disease. *Int. J. COPD* **10**, 1155–1161 (2015).
152. Sandford, A., Weir, T. & Paré, P. Genetic risk factors for chronic obstructive pulmonary disease. *Eur Respir J* **10**, 1380–1391 (1997).
153. Rabe, K. F. & Watz, H. Chronic obstructive pulmonary disease. *Lancet* **389**, 1931–1940 (2017).
154. Salvi, S. S. & Barnes, P. J. Chronic obstructive pulmonary disease in non-smokers. *The Lancet* **374**, 733–743 (2009).
155. Boyce, J. A., Finkelman, F. & Shearer, W. T. Inflammatory mechanisms in patients with chronic obstructive pulmonary disease. *J. Allergy Clin. Immunol.* **138**, 16–27 (2016).

156. Wickens, A. P. Ageing and the free radical theory. *Respir. Physiol.* **128**, 379–391 (2001).
157. Boyce, J. A., Finkelman, F., Shearer, W. T. & Barnes, P. J. Mechanisms of allergic diseases Inflammatory mechanisms in patients with chronic obstructive pulmonary disease. *J. Allergy Clin. Immunol.* **138**, 16–27 (2016).
158. Fischer, B. M., Pavlisko, E. & Voynow, J. A. Pathogenic triad in COPD: oxidative stress, protease-antiprotease imbalance, and inflammation. *Int. J. COPD* **6**, 413–421 (2011).
159. Kim, V. & Criner, G. J. Chronic Bronchitis and Chronic Obstructive Pulmonary Disease. *Am J Respir Crit Care Med* **187**, 228–237 (2013).
160. van Agteren, J. E. M., Carson, K. V., Tiong, L. U. & Smith, B. J. Lung volume reduction surgery for diffuse emphysema. *Cochrane Database of Systematic Reviews* (2016). doi:10.1002/14651858.CD001001.pub3
161. Bakke, P. S. *et al.* Recommendations for epidemiological studies on COPD. *Eur. Respir. J.* **38**, 1261–1277 (2011).
162. Yao, H. *et al.* SIRT1 protects against emphysema via FOXO3-mediated reduction of premature senescence in mice. *J. Clin. Invest.* **122**, (2012).
163. Jochems, S. P. *et al.* Novel Analysis of Immune Cells from Nasal Microbiopsy Demonstrates Reliable, Reproducible Data for Immune Populations, and Superior Cytokine Detection Compared to Nasal Wash. *PLoS One* **12**, (2017).
164. Batista, C. M. A Bench to Bedside Investigation into Defective Innate Immunity in Chronic Obstructive Pulmonary Disease. (2017).
165. Thwaites, R. S. *et al.* Absorption of Nasal and Bronchial Fluids: Precision Sampling of the Human Respiratory Mucosa and Laboratory Processing of Samples. *J. Vis. Exp* **131**, 1–8 (2018).
166. Grant, L. R., Hammitt, L. L., Murdoch, D. R., O'Brien, K. L. & Scott, J. A. Procedures for collection of induced sputum specimens from children. *Clin. Infect. Dis.* **54**, (2012).
167. Hansel, T. T. *et al.* A Comprehensive Evaluation of Nasal and Bronchial Cytokines and Chemokines Following Experimental Rhinovirus Infection in Allergic Asthma: Increased Interferons (IFN- $\gamma$  and IFN- $\lambda$ ) and Type 2 Inflammation (IL-5 and IL-13). *EBioMedicine* **19**, 128–138 (2017).
168. Lü, F. X. & Esch, R. E. Novel nasal secretion collection method for the analysis of allergen specific antibodies and inflammatory biomarkers. *J. Immunol. Methods* **356**, 6–17 (2010).
169. Chawes, B. L. K. *et al.* A novel method for assessing unchallenged levels of mediators in nasal epithelial lining fluid. *Journal of Allergy and Clinical Immunology* **125**, (2010).
170. Brewington, J. J. *et al.* Brushed nasal epithelial cells are a surrogate for bronchial epithelial CFTR studies. *JCI Insight.* **3**, (2018).



171. Niehaus, M. D. *et al.* Lactoferrin and Eosinophilic Cationic Protein in Nasal Secretions of Patients with Experimental Rhinovirus Colds, Natural Colds, and Presumed Acute Community-Acquired Bacterial Sinusitis. *J. Clin. Microbiol.* **38**, 3100–3102 (2000).
172. Thwaites, R. S. *et al.* Nasosorption as a Minimally Invasive Sampling Procedure: Mucosal Viral Load and Inflammation in Primary RSV Bronchiolitis. *J. Infect. Dis.* **215**, 1240–1244 (2017).
173. Wai, A. K. C., Kwok, W. O., Chan, M. S. & Graham, C. A. Patients' perceptions of nasopharyngeal aspiration in the emergency department of a teaching hospital in Hong Kong. *Emerg Med J* **24**, 35–36 (2007).
174. Macfarlane, P., Denham, J. & Assous, J. RSV testing in bronchiolitis: which nasal sampling method is best? *Arch Dis Child* **90**, 634–635 (2005).
175. Alam, R., Sim, T. C., Hilsmeier, K. & Andrew Grant, J. Development of a new technique for recovery of cytokines from inflammatory sites in situ. *J. Immunol. Methods* **155**, 25–29 (1992).
176. Thwaites, R. S. *et al.* Reduced Nasal Viral Load and IFN Responses in Infants with Respiratory Syncytial Virus Bronchiolitis and Respiratory Failure. *Am J Respir Crit Care Med* Vol **198**, 1074–1084 (2018).
177. Riechelmann, H., Deutschle, T., Friemel, E., Gross, H.-J. & Bachem, M. Biological markers in nasal secretions. *Eur Respir J* **21**, 600–605 (2003).
178. Hunt Developmnts Ltd. *Nasosorption™ FX i.* (2018).
179. Katkov, I. L. & Mazur, P. Factors Affecting Yield and Survival of Cells When Suspensions Are Subjected to Centrifugation. *Cell Biochem. Biophys.* **31**, 231–245 (1999).
180. Kasprowicz, R., Suman, R. & O'Toole, P. Characterising live cell behaviour: Traditional label-free and quantitative phase imaging approaches. *Int. J. Biochem. Cell Biol.* **84**, 89–95 (2017).
181. Witten, I. H., Frank, E., Hall, M. A. & Pal, C. J. Data transformations. in *Data Mining* **69**, 285–334 (Elsevier, 2017).
182. Pizzichini, M. M. M. *et al.* Spontaneous and induced sputum to measure indices of airway inflammation in asthma. *Am. J. Respir. Crit. Care Med.* **154**, 866–869 (1996).
183. Bhowmik, A., Seemungal, T. A. R., Sapsford, R. J., Devalia, J. L. & Wedzicha, J. A. Comparison of spontaneous and induced sputum for investigation of airway inflammation in chronic obstructive pulmonary disease. *Thorax* **53**, 953–956 (1998).
184. Hogg, J. C. *et al.* The Nature of Small-Airway Obstruction in Chronic Obstructive Pulmonary Disease. *n engl j med* **350**, 2645–2653 (2004).
185. Dejean, A. S., Hedrick, S. M. & Kerdiles, Y. M. Highly specialized role of Forkhead box O transcription factors in the immune system. *Antioxid. Redox Signal.* **14**, 663–74 (2011).
186. Hansel, T. T. *et al.* A Comprehensive Evaluation of Nasal and Bronchial Cytokines

- and Chemokines Following Experimental Rhinovirus Infection in Allergic Asthma: Increased Interferons (IFN- $\gamma$  and IFN- $\lambda$ ) and Type 2 Inflammation (IL-5 and IL-13). *EBioMedicine* **19**, 128–138 (2017).
187. Esposito, S. *et al.* Collection by trained pediatricians or parents of mid-turbinate nasal flocked swabs for the detection of influenza viruses in childhood. *Viol. J.* **7**, 85 (2010).
  188. Rebuli, M. E., Speen, A. M., Clapp, P. W. & Jaspers, I. Novel applications for a noninvasive sampling method of the nasal mucosa. *Am J Physiol Lung Cell Mol Physiol* **312**, 288–296 (2017).
  189. Marx, V. A dream of single-cell proteomics. *Nat. Methods* **16**, 809–812 (2019).
  190. Konstantin Yakimchuk. Aptamers and Affimers. *Mater Methods* **5**, (2015).
  191. Lakhin, A. V, Tarantul, V. Z. & Gening, L. V. Aptamers: Problems, Solutions and Prospects. *Acta Naturae* **5**, 34–44 (2013).
  192. Bouchard, P. R., Hutabarat, R. M. & Thompson, K. M. Discovery and Development of Therapeutic Aptamers. *Annu. Rev. Pharmacol. Toxicol. is* **50**, 237–57 (2010).
  193. Gold, L. *et al.* Aptamer-Based Multiplexed Proteomic Technology for Biomarker Discovery. *PLoS One* **5**, (2010).
  194. Ozkumur, E. *et al.* Inertial Focusing for Tumor Antigen-Dependent and-Independent Sorting of Rare Circulating Tumor Cells. *Cancer Diagnostics* **5**, (2013).
  195. Parichehreh, V., Medepallai, K., Babbarwal, K. & Sethu, P. Microfluidic inertia enhanced phase partitioning for enriching nucleated cell populations in blood. **13**, 892 (2013).

# Appendix A: Volunteer recruitment

## Wording to be used to recruit volunteers in person

We are conducting a preliminary study involving the single cell analysis of nasal samples. We have approached you today because we would like for you to take part in this study. If you choose to volunteer, your involvement in this study will be straightforward and quick and will involve us collecting a nasal sample from your nasal cavity using a non-invasive technique called Nasosorption. In order to collect this sample, we will simply insert a small strip of absorbent material inside your nasal cavity and apply gentle pressure to the outside of your nose for 60s. This will take up the fluid inside your nose like blotting paper. After this, the material will be removed, and the sampling will be complete! This form of sampling has been shown to be non-invasive and cause minimal discomfort. Placing the paper into the nose can tickle and cause your eyes to water but again, this causes minimal discomfort and this technique has also been shown to be well tolerated in babies. Once we've obtained our sample, we intend to process them and analyse them within our microfluidic device in order to determine the protein copy number of two proteins of interest within single cells. We have also got a participant information sheet that describes the sampling and single cell analysis technique in more detail and will hopefully answer any questions you may have about the study and its purpose. Please feel free to ask any questions you may have which have not been answered in this information sheet. We hope you will be able to volunteer in our study. If you decide to volunteer, please get in contact either by email or telephone, both of which are provided on the information sheet we have just given to you. Thank you for your time.

# Appendix B: Consent forms

Joint Research  
Compliance Office

Imperial College  
London

ICRU  
Imperial Clinical  
Respiratory Research Unit

*Use participant label*  
Participant name:  
  
DOB:  
  
Number

## CONSENT FORM Healthy Volunteers

Title: -Single Cell Analysis by Multiplex of Mucosal Fluids (SAM)

Principal Investigator: Professor David Klug

Please Initial boxes

1.	I confirm that I have read and understand the Participant Information Sheet Version 3, dated 25/10/2018 for the above study and been given a copy to keep. I have had the opportunity to ask questions and have had these answered satisfactorily.	<input type="checkbox"/>
2.	I understand that my participation is voluntary, and that I am free to withdraw consent at any time, without giving any reason and without my medical care or legal rights being affected.	<input type="checkbox"/>
3.	I understand that sections of my medical notes and data collected during the study may be looked at by responsible individuals from Imperial College London or from regulatory authorities, where it is relevant to my taking part in this research. I give permission for these individuals to access my records.	<input type="checkbox"/>
4.	I agree to nasal samples being taken.	<input type="checkbox"/>
5.	I agree to the use of my nasal samples in this research project which may include the measurement of micro riboxynucleic acid (miRNA) and tumour circulating DNA. These samples will be retained for up to 10 years for this study.	<input type="checkbox"/>
6.	All samples will be fully anonymised and not be identifiable..	<input type="checkbox"/>
7.	I agree to take part in this study	<input type="checkbox"/>
8.	I would like to be contacted about future research studies based at Imperial College London	Y <input type="checkbox"/> N <input type="checkbox"/>

\_\_\_\_\_  
Name of Participant

\_\_\_\_\_  
Signature

\_\_\_\_\_  
Date

\_\_\_\_\_  
Name of Person taking consent  
(if different from study clinician)

\_\_\_\_\_  
Signature

\_\_\_\_\_  
Date

\_\_\_\_\_  
Name of the study clinician/Investigator

\_\_\_\_\_  
Signature

\_\_\_\_\_  
Date

# **Appendix C: Participant information sheet**

## **PARTICIPANT INFORMATION SHEET**

### **Healthy Volunteer**

**Study Number: XXXXXX**

**Full Title: Multiplexed single cell analysis of nasal fluids sampled by nasosorption from healthy volunteers.**

**Short Title: SAM (Single cell analysis by multiplex of mucosal fluids)**

**Principal Investigator: Professor David Klug**

**Reviewing body: Joint research compliance office (JRCO)**

You are being invited to take part in a research study. Before you decide whether to join the study it is important for you to understand why the research is being done and what it will involve. Please take time to read the following information carefully and discuss it with others if you wish.

We shall first tell you the purpose of this study and what will happen to you if you take part.

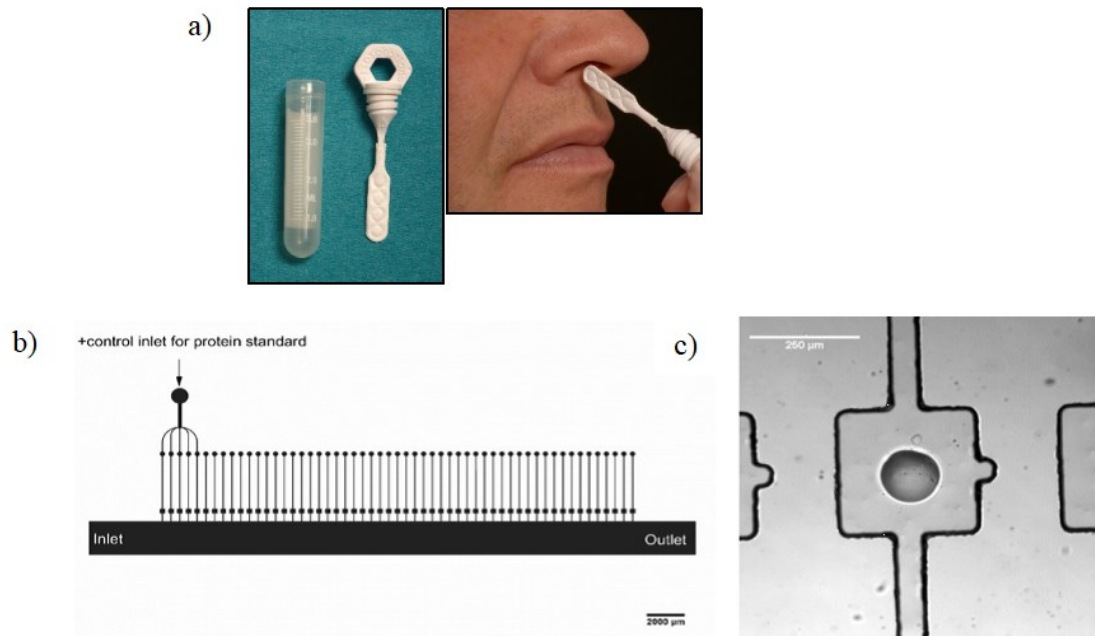
We will then give you more detailed information about the conduct of the study.

Please feel free to ask our staff any questions you may have which are not answered in this information sheet. If you decide to take part in the study you will be asked to sign a consent form and will receive a copy of this for your own records.

#### **What is the purpose of the study?**

The aim of this study is to develop methods for the study of single cells in the fluid that is present on the surface of the nasal passages (nostrils). This nasal fluid is collected by nasosorption (NS) that uses a soft swab to absorb

fluid directly from inside the nostril. The absorbent material consists of a Synthetic Absorptive Matrix (SAM), and this absorbs the nasal fluid that contains a few cells. In the laboratory the cells are then removed and studied as individual cells: by single cell analysis. This will enable us to study molecules within nasal cells from healthy people. In the future, we hope to compare results on cells from this study with cells from volunteers with diseases like asthma and cigarette smoking-related diseases.



**Why  
have I  
been**

**Figure 1** Nasal sample collection and single cell analysis using Microfluidic Antibody Capture (MAC) chip. **(a)** Nasosorption using Synthetic Absorptive Matrix (SAM). **(b)** Schematic diagram of the standard MAC chip used to analyse protein copy numbers within cells collected via SAMs. **(c)** Printed antibody spot in a 300 x 300 μm analysis chamber

**invited?**

You have been invited to take part in the study because you are a member of Imperial College. You will be assessed to determine if this study is suitable for you.

We also need participants to meet the criteria below. Please see the list of criteria below and make sure they are applicable to you.

1. Your age is 18-65 years
2. Your BMI is between 18 and 39
3. You have never smoked or you are an ex-smoker or you are a current smoker. If you are an ex-smoker, you will need to give the doctor details of how much you previously smoked so they can calculate your exposure to cigarette smoke.
4. Medical conditions: you either have no history of any medical conditions or allergy or only have a stable well controlled chronic condition that does not affect your lungs. Please discuss this with us if this applies to you.
5. Medications: You are not taking any anti-inflammatory drugs including steroids (in any form), statins, anti-histamines or anti-rheumatics. You are happy to stop over the counter medications for the duration of the study.
6. You should not have had a cold in the last 6 weeks.
7. Women of childbearing age should not be pregnant, planning to get pregnant or breast feeding (please see further information below).

If you do decide to take part you will be given this Participant Information Sheet to keep and be asked to sign a Consent Form.

### **Do I have to take part?**

You are under no obligation to take part in this study. If you decide not to take part (or if you change your mind and wish to withdraw at any point during the study) this will not affect the health care you receive now or in the future. The Investigator supervising the research, Professor David Klug, or Imperial College London (who is the sponsor for this study) may also stop the study or your participation in the study at any time, for any reason, without your consent. A reason will be given to you should this be necessary.

### **What will happen to me if I take part?**

You will be one of at least 20 healthy volunteers participating in this study. We will collect fluid from your nose for a maximum of 5 times on a single visit. The nasal sampling procedure is described below;

**Nasal lining fluid absorption (nasosorption):** We will use a small strip of absorbent material to soak up moisture from the inside surface of your nose. The absorbent material will be placed inside your nostril and left for 1 minute. This gently takes up fluid from your nose like blotting paper. Putting the paper into the nose can tickle and cause your eyes to water. However, this does not hurt and our method has been well tolerated in babies, children and adults. The paper absorbs fluid and many substances produced by the nasal cells, such as proteins. These can then be extracted from the paper and measured in the laboratory.

### **How will my samples be processed and stored?**

These samples will be stored anonymously, only identifiable by a sample number with no other personal information. Only the researcher will have the code to access them, and your details will be kept anonymous when we publish the outcomes of this study.

After the study has taken place, we will analyse all the samples in order to measure markers of inflammation. We may also look at the circulating tumour deoxyribonucleic acid (DNA) and messenger ribonucleic acid (mRNA) components of your samples to assess the proteins produced by cells. The analysis will be performed within Imperial College London. We may send samples outside the UK including both within and outside the European Union (EU). If so, samples will be sent fully anonymised as per the UK Data Protection Act and the sites will own a Human Tissue Authority license. Data protection laws outside the UK vary considerably however your samples will be fully anonymised before being sent for analysis.

### **What are the possible side effects of any procedures when taking part in this study?**

Inserting the nasal absorbent swab may tickle and be associated with mild discomfort but there are no long-term effects.

### **What are the possible benefits of taking part?**

The study is designed to determine the reproducibility of our methods and in order to check the reliability of our protocols. Thus the main comparison will be between your own samples taken at different times. It is not possible to deduce any healthcare or healthcare outcomes from the analysis of the data that we will collect from your samples.

### **What if something goes wrong?**

If you have any reaction to the sampling procedure we will want to know all about this immediately.

Please inform a member of the study team if you experience any discomfort during or after any procedures carried out as part of this study. Contact details are available on this document. The safety of our participants is our priority and we will take every precaution and action necessary to ensure your safety at all times. Imperial College London holds Public Liability (negligent harm) and Clinical Trial (non-negligent harm) insurance policies which apply to this trial. If you can demonstrate that you experienced serious and enduring harm as a result of your participation in this trial, you will be eligible to claim compensation without having to prove that Imperial College London is at fault. If the injury resulted from any procedure which is not part of the trial, Imperial College

Healthcare London will not be required to compensate you in this way. Your legal rights to claim compensation for injury where you can prove negligence are not affected.

Please contact the Principal Investigator if you would like further information about the insurance arrangements which apply to the trial.

### **What will I have to do?**

We would like you to adhere to the medication restrictions outlined above.

We would like you to contact us if you become unwell for any reason or have any health issues during the study, even if you don't think these are related to treatment.

### **Information for women of child-bearing age**

Pregnant and breast-feeding women may not participate in this study.

### **Am I paid for taking part in this study?**

We do not pay people specifically for taking part in the study. However, we will cover any costs for your travel, and you will be reimbursed for the time you donate to the study.

### **Will my taking part in this study be kept confidential?**

All information which is collected about you during the course of the research will be kept strictly confidential. Some parts of the data collected for the study may be looked at by the representatives of regulatory authorities and by authorised people to check that the study is being carried out correctly. Any information about you which leaves the department will have your name and address removed so that you cannot be recognised from it. The Investigator and designated hospital staff are the only people with access to the information linking this code to your name. You also have the right to see any information collected from you and to request the correction of any errors (if any) you may find. Procedures for handling, processing, storage and destruction of their data are compliant with the Data Protection Act 1998. Under the General data protection regulation (GDPR) laws, Imperial College London, as the sponsor for this study, is the controller of your personal data. We will be using information from you in order to undertake this study. This means that Imperial College London are responsible for looking after your information and using it properly. Imperial College London will keep identifiable information about you for 15 years after the study has finished in relation to data subject consent forms and primary research data.

Further information on Imperial College London's retention periods may be found at <https://www.imperial.ac.uk/media/imperial-college/administration-and-support-services/records-and-archives/public/RetentionSchedule.pdf>.

Your rights to access, change or move your information are limited, as we need to manage your information in specific ways in order for the research to be reliable and accurate. If you withdraw from the study, we will keep the information about you that we have already obtained. To safeguard your rights, we will use the minimum personally-identifiable information possible.

You can find out more about how we use your information from the Principle investigator of this study, Professor David Klug. This research does not affect your care/treatment and so there is no requirement to inform your GP of your participation.

As a university we use personally-identifiable information to conduct research to improve health, care and services. As a publicly-funded organisation, we have to ensure that it is in the public interest when we use personally-identifiable information from people who have agreed to take part in research. This means that when you agree to take part in a research study, we will use your data in the ways needed to conduct and analyse the research study.



Health and care research should serve the public interest, which means that we have to demonstrate that our research serves the interests of society as a whole. We do this by following the UK Policy Framework for Health and Social Care Research.

## INTERNATIONAL TRANSFERS

There may be a requirement to transfer information to countries outside the European Economic Area (for example, to a research partner). Where this information contains your personal data, Imperial College London will ensure that it is transferred in accordance with data protection legislation. If the data is transferred to a country which is not subject to a European Commission (EC) adequacy decision in respect of its data protection standards, Imperial College London will enter into a data sharing agreement with the recipient organisation that incorporates EC approved standard contractual clauses that safeguard how your personal data is processed.

## CONTACT US

If you wish to raise a complaint on how we have handled your personal data or if you want to find out more about how we use your information, please contact Imperial College London's Data Protection Officer via email at [dpo@imperial.ac.uk](mailto:dpo@imperial.ac.uk), via telephone on 020 7594 3502 and via post at Imperial College London, Data Protection Officer, Faculty Building Level 4, London SW7 2AZ.

If you are not satisfied with our response or believe we are processing your personal data in a way that is not lawful you can complain to the Information Commissioner's Office (ICO). The ICO does recommend that you seek to resolve matters with the data controller (us) first before involving the regulator.

### **What if I want to complain about any aspects of the study or staff involved?**

If you would like to complain about any aspects of the study or study staff, you can contact:

Professor David Klug  
Department of Chemistry  
Imperial College  
London, SW7 2AZ  
Email: [d.klug@imperial.ac.uk](mailto:d.klug@imperial.ac.uk)  
Telephone: 020 75945806

Imperial College London will keep your name, contact details and **personal information** confidential and will not pass this information. Imperial College London will use this information as needed, to contact you about the research study, and make sure that relevant information about the study is recorded for your care, and to oversee the quality of the study. Certain individuals from Imperial College London and regulatory organisations may look at your medical and research records to check the accuracy of the research study. Imperial College London will only receive information without any identifying information. The people who analyse the information will not be able to identify you and will not be able to find out your name, personal information or contact details.

When you agree to take part in a research study, the information about your health and care may be provided to researchers running other research studies in this organisation and in other organisations. These organisations may be universities, NHS organisations or companies involved in health and care research in this country or abroad. Your information will only be used by organisations and researchers to conduct research in accordance with the UK Policy Framework for Health and Social Care Research.

This information will not identify you and will not be combined with other information in a way that could identify you. The information will only be used for the purpose of health and care research, and cannot be used to contact you or to affect your care. It will not be used to make decisions about future services available to you, such as insurance.

Where there is a risk that you can be identified your data will only be used in research that has been independently reviewed by an ethics committee.

**What will happen to the results of the research study?**

The anonymous results will be analysed and, depending on the quality of the data collected, will form part of a publication in a scientific journal. We will be happy to produce, at your request, a straightforward overall summary of the results after the study has finished.

**Who is organising and funding the research?**

This study is funded by the Engineering and Physical Sciences Research Council (EPSRC) and sponsored by Imperial College London.

**Who has reviewed the study?**

This study was given a favourable ethical opinion by the Joint research compliance office (JRCO)

**Contact for Further Information**

If you have any queries, please do not hesitate to contact Professor David Klug.  
Professor David Klug  
Department of Chemistry, Imperial College London, SW7 2AZ  
Email: [d.klug@imperial.ac.uk](mailto:d.klug@imperial.ac.uk)  
Telephone: 020 75945806

You will be given a copy of the written information and signed Informed Consent form to keep.

*A copy of this written Participant Information Sheet and your signed Informed Consent form will be given to you to keep.*